

January 2015

High Pressure Micro-Scale Studies of Fast-Hydropyrolysis and Catalytic Hydrogenation of Biomass and Related Model Compounds

Harshavardhan Choudhari
Purdue University

Follow this and additional works at: https://docs.lib.purdue.edu/open_access_dissertations

Recommended Citation

Choudhari, Harshavardhan, "High Pressure Micro-Scale Studies of Fast-Hydropyrolysis and Catalytic Hydrogenation of Biomass and Related Model Compounds" (2015). *Open Access Dissertations*. 1178.
https://docs.lib.purdue.edu/open_access_dissertations/1178

This document has been made available through Purdue e-Pubs, a service of the Purdue University Libraries. Please contact epubs@purdue.edu for additional information.

**PURDUE UNIVERSITY
GRADUATE SCHOOL
Thesis/Dissertation Acceptance**

This is to certify that the thesis/dissertation prepared

By Harshavardhan J. Choudhari

Entitled

High Pressure Micro-Scale Studies of Fast-Hydropyrolysis and Catalytic Hydrogenation of Biomass and Related Model Compounds

For the degree of Doctor of Philosophy

Is approved by the final examining committee:

Fabio H. Ribeiro

Chair

Rakesh Agrawal

Co-chair

W. Nicholas Delgass

Co-chair

Hilkka Kenttämä

To the best of my knowledge and as understood by the student in the Thesis/Dissertation Agreement, Publication Delay, and Certification Disclaimer (Graduate School Form 32), this thesis/dissertation adheres to the provisions of Purdue University's "Policy of Integrity in Research" and the use of copyright material.

Approved by Major Professor(s): Fabio H. Ribeiro

Approved by: John A. Morgan

Head of the Departmental Graduate Program

5/13/2015

Date

HIGH PRESSURE MICRO-SCALE STUDIES OF FAST-HYDROLYSIS AND
CATALYTIC HYDROGENATION OF BIOMASS AND RELATED MODEL
COMPOUNDS

A Dissertation

Submitted to the Faculty

of

Purdue University

by

Harshavardhan J. Choudhari

In Partial Fulfillment of the

Requirements for the Degree

of

Doctor of Philosophy

August 2015

Purdue University

West Lafayette, Indiana

For my parents

ACKNOWLEDGEMENTS

I have been fortunate to work with three advisors, Prof. Fabio H. Ribeiro, Prof. Rakesh Agrawal, and Prof. W. Nicholas Delgass, and learn from them through their vast bank of knowledge and experience. Prof. Ribeiro's experimental prowess, and attention to detail, is something I hope to emulate now and even later in my life. I have always admired Prof. Agrawal for his extremely diverse skill set, constant striving for deep understanding of any field, and his ability to quickly grasp new concepts. His passion for research was always evident in every meeting I have been involved with him and has always inspired me during my stay at Purdue. Prof. Delgass' course introduced me to the world of catalysis through the lens of spectroscopy, and since then I have always enjoyed learning from him. Prof. Delgass' enthusiasm in teaching and research is very infectious, and his ability to put things in perspective has been very valuable towards problem solving. I am very grateful for the guidance and hope to effectively use the knowledge in the future. I would also like to thank Prof. Hilkka I. Kenttämäa for the valuable collaborations with her group, and suggestions as a part of my dissertation committee. The entire C3Bio center has been very supportive throughout the years towards promoting an atmosphere of teamwork and excellence. I would specially like to thank Dr. Maureen McCann, Carl Huetteman, Wendy Field, and Stephanie Bonebrake for facilitating these partnerships and research collaborations.

I would like to thank all the funding agencies which provided the resources for this research. The research was supported as part of the Center for Direct Catalytic Conversion of Biomass to Biofuels (C3Bio), an Energy Frontier Research Center funded by the U.S. Department of Energy (DOE), Office of Science, Basic Energy Sciences (BES), under Award# DE-SC0000997. Additionally, funding was provided by Air Force Office of Scientific Research (AFOSR) under Award# FA9550-08-1-0456 and FA9550-09-1-0494 and by National Science Foundation Emerging Frontiers in Research and Innovation (EFRI) under Award #0938033.

The entire catalysis group has been like a family to me and I am extremely grateful to each one of them for making this a new home for me. The senior students in the group, Dr. Bradley Fingland, Dr. Jorge Pazmino, Dr. Andrew Smeltz, Dr. Saurabh Chaugule, Dr. Vincent Kispersky, and Dr. Mayank Shekhar were very helpful in during the initial training and their guidance throughout the years has been valuable. The biomass group members both, past and present, Dr. Dhairya D. Mehta, Dr. Vinod Kumar Venkatakrishnan, Dr. Sara Yohe, John Degenstein, Dr. Andrew Smeltz, Dr. Dharik Mallapragada, Dr. Piotr Gawecki, Emre Gencer, Ian Smith, Taufik Ridha, and Richard Caulkins have been great colleagues. I thank you all for the being a part of the successes, and the many more failures, for being a sounding board for new ideas, for the innumerable discussions, for the late night report writing and for teaching me the value of working as a team. It was an enjoyable and at times frustrating experience to be a part of a project which was in its initial stages, and I would specially like to thank Dr. Sara Yohe, Dr. Dhariya D. Mehta and Dr. Dr. Vinod Kumar Venkatakrishnan for their suggestions

and help with the equipment construction and troubleshooting. To all the other past group members, Dr. Paul Dietrich, Dr. Shane Bates, Dr. Kaiwalya Sabnis, Dr. Damion Williams, Dr. Amir Gharachorlou, Dr. Fred Sollberger, Dr. Cem Akatay, Dr. Fernando Resende, Dr. Anuj Verma, Dr. Jun Wang and Dr. Zhenglong Li, thank you for being such great colleagues. I would also like to thank the current group members, Atish, John, Jamie, Yanran, Mike, Viktor, Han-Ting, McKay, Ian, Emre, Taufik, Richard, Arthur, Jonatan, Ishant, Cory, and Zhe, and wish them great success.

My flat mates, Dr. Dhairya D. Mehta, Dr. Karthikeyan Marimuthu, Dr. Krishnaraj Sambath, Sumeet Thete, and Ashish Vora, have been like a family to me. They have been very supportive through all the ups and downs, always bringing out the optimist perspective and providing encouragement. They have been instrumental in making my stay at Purdue memorable. A special mention for the entire co-rec loving group, Anirudh, Anshu, Atish, Dhairya, Karthik, Kaiwalya, Sumeet, Ashish, Krishna, Aniruddha, Vinod, and Parth. Playing squash, racquetball, walleyball, cricket, badminton etc. has always provided a refresher during the week. I have made great friends in Kaiwalya, Atish, Shankali, Anshu, Aniruddha, Anand, Chinmay, Gautham, Vishesh, Anirudh, Neelanjan, and Mahaprasad without whom life at Purdue would not have been as enjoyable for me. I will always cherish these memories.

Dr. Yury Zvinevich, is an integral part of the catalysis group and has been a savior for every student at some point of time during their PhD. I have always received a pertinent advice and prompt help from him, and I have learnt a lot about the approach to

troubleshooting from Yury. Deb Bowman has been very resourceful, efficient, kind and patient while dealing with the graduate students, and I would like to thank her for all the help during my graduate studies. I would also like to acknowledge the staff in the Purdue business office, Amy Hayden, Courtney Eddy, Jennifer Olinger, Amy Stanley, and Jill Meyers, for their support and always swiftly taking care of the administrative functions. Katherine Yater-Henke, Melissa Laguire, Karen Heide, Jason Davenport, Jeff Valley, and Larry Campbell, amongst others have been of a lot of help throughout my graduate life. Lastly, I would like to thank my parents, friends, and family back home in India for always encouraging me to pursue my dreams, and extending their unconditional support so I could complete graduate studies at Purdue University. My Fiancée, Dr. Niranjani Deshpande has steadfastly stood by me, being a source of love and strength, ever since I have known her. My parents, Madhuri Choudhari and Jayant Choudhari, have always been a source of inspiration for me, and I will be eternally grateful to them for everything that they have given me through their hard work, sacrifice, and everlasting love.

TABLE OF CONTENTS

	Page
LIST OF TABLES	xii
LIST OF FIGURES	xix
ABSTRACT	xxviii
CHAPTER 1. INTRODUCTION	1
1.1 Need for Alternate Sources of Energy	1
1.2 Biomass Conversion Processes	3
1.3 Lignocellulosic Biomass Structure.....	8
1.3.1 Cellulose and Hemicellulose	8
1.3.2 Lignin.....	9
1.4 Thesis Objectives	11
CHAPTER 2. REACTOR DESIGN AND EXPERIMENTAL METHODS.....	15
2.1 Introduction	15
2.2 Micro-scale semi-batch reactor with catalytic hydrodeoxygenation capability (Py-GC/MS system).....	17
2.3 GC column studies	23
2.3.1 Quantitative analysis of dimeric molecules from lignin pyrolysis	24
2.3.2 Quantitative analysis of dimeric molecules from cellulose pyrolysis	27
2.4 Conclusion.....	31
CHAPTER 3. FAST PYROLYSIS OF CELLULOSE	33
3.1 Introduction	33
3.2 Experimental Apparatus and Methods	36
3.2.1 Materials	36

	Page
3.2.2 Reactor description	36
3.2.3 Loading and reactor operation	37
3.2.4 Product identification and quantification.....	38
3.3 Results and Discussion.....	39
3.3.1 Effect of temperature	40
3.3.2 Effect of hydrogen as reactant gas.....	44
3.3.3 Quantitative detailed product distribution from cellulose	46
3.3.4 Pyrolysis of cellotriosan and cellobiosan	48
3.3.5 Effect of vapor phase residence time.....	52
3.4 Conclusion.....	56
CHAPTER 4. FAST PYROLYSIS OF GUAIACYL LIGNIN MODEL COMPOUNDS WITH B-O-4 LINKAGES: EFFECT OF CHAIN LENGTH AND VAPOR PHASE RESIDENCE TIME.....	
	58
4.1 Abstract	58
4.2 Introduction	59
4.3 Experimental Apparatus and Methods	63
4.3.1 Reactor description	63
4.3.2 Loading and reactor operation	64
4.3.3 Product identification and quantification.....	65
4.3.4 Model compound synthesis	65
4.4 Results	66
4.4.1 Quantitative analysis of dimeric molecules using GC/MS.....	66
4.4.2 Pyrolysis of Dimer 1	66
4.5 Pyrolysis of Trimer 2 , Tetramer 3 , Trimer 4 and Polymer 5	67
4.6 Discussion	71
4.6.1 Product distribution from lignin model compounds.....	71
4.6.2 Char formation.....	75
4.6.3 Effect of vapor phase residence time.....	77
4.6.4 Primary products of lignin pyrolysis	80

	Page
4.7 Conclusions	82
CHAPTER 5. CATALYTIC HYDRODEOXYGENATION OF MODEL	
COMPOUNDS	84
5.1 Introduction	84
5.2 Experimental methods.....	87
5.2.1 Catalyst preparation.....	87
5.2.2 Catalyst characterization.....	88
5.2.3 Micro-scale semi batch catalytic reactor (Py-GC/MS).....	88
5.2.4 Continuous, steady state, fixed bed catalytic reactor setup	91
5.3 Results and Discussion.....	92
5.3.1 Catalyst characterization.....	92
5.3.2 Reaction pathways and identified products	92
5.3.3 Role of Pt and Mo.....	95
5.3.4 Rate trends	103
5.3.5 Comparison between pulse catalytic studies and steady state catalytic studies	105
5.3.6 Pathway differences at different hydrogen pressures	107
5.3.7 Other model compounds.....	111
5.3.8 Pt/acidic support catalysts.....	113
5.3.9 Catalyst stability	116
5.3.10 M-Cresol hydrodeoxygenation.....	122
5.3.10.1 Motivation	122
5.3.10.2 Reaction pathways	122
5.3.11 Catalyst regeneration.....	128
5.4 Conclusion.....	133
CHAPTER 6. EFFECT OF HYDROGEN PRESSURE DURING	
HYDRODEOXYGENATION OF PYROLYSIS PRODUCTS FROM BIOMASS AND	
ITS INDIVIDUAL COMPONENTS.....	
6.1 Abstract	135

	Page
6.2 Introduction	136
6.3 Experimental methods.....	140
6.3.1 Materials	140
6.3.2 Catalyst preparation.....	141
6.3.3 Catalyst characterization.....	141
6.3.4 Reactor description	142
6.3.4.1 Lab-scale continuous flow cyclone type reactor	142
6.3.4.2 Micro-scale semi batch catalytic reactor (Py-GC/MS).....	142
6.4 Results	145
6.4.1 Hydrocarbon product distribution from HDO of biomass and related model polymers and compounds	145
6.4.2 Fast hydropyrolysis: effect of hydrogen pressure.....	146
6.4.3 Levoglucosan.....	147
6.4.4 Cellulose	148
6.4.5 Lignin model compounds	148
6.4.6 Xylan.....	149
6.4.7 PtMo series	150
6.4.8 Effect of hydrogen pressure.....	151
6.4.9 Cyclone reactor	153
6.5 Discussion	161
6.5.1 Role of Pt and Mo.....	161
6.5.2 Effect of hydrogen pressure.....	164
6.5.2.1 Yield of aromatic hydrocarbons	164
6.5.2.2 C-C bond scission.....	166
6.5.3 Comparison with lab-scale continuous flow cyclone type reactor	169
6.6 Conclusions	170
CHAPTER 7. SUMMARY AND FUTURE RECOMMENDATIONS	172
7.1 Summary	172
7.2 Future recommendations	177

	Page
7.2.1 C-C bond formation: Aldol condensation.....	177
7.2.2 Kinetics of phenol and methoxy deoxygenation at low hydrogen pressure	182
7.2.3 Fast pyrolysis studies with lignin model compounds and xylan polymer ...	182
LIST OF REFERENCES	184
APPENDICES	
Appendix A Supplementary information for Chapter 2.....	196
Appendix B Supplementary information for Chapter 3	198
Appendix C Supplementary information for Chapter 4	199
Appendix D Supplementary information for Chapter 5.....	204
Appendix E Supplementary information for Chapter 6	205
VITA.....	225

LIST OF TABLES

Table	Page
Table 2.1 List of the GC columns tested with the relevant parameters.	26
Table 2.2 Lumped pyrolysis products of dimer 1 as a function of the columns tested. ...	26
Table 2.3 Lumped pyrolysis products of tetramer 3 as a function of the columns tested.	27
Table 2.4 Lumped product distribution from GC injection (inlet temperature 330°C) of a solution of cellobiosan in water (20% by weight).	29
Table 2.5 Lumped product distribution from GC-MS and LC-MS analysis of the bio-oil obtained from the lab-scale continuous-flow millisecond residence time (70 ms) hydrolysis reactor.	30
Table 2.6 Comparison of abundance of major products (wt% of feed) from cellulose pyrolysis 500°C for two different GC columns used for analysis.	31
Table 3.1 Quantitative lumped pyrolysis product distribution (wt % of feed) produced from the pyrolysis-GC/MS reactor for pyrolysis of cellobiosan, cellotriosan, and cellulose.	50
Table 3.2 Quantitative detailed pyrolysis product distribution (wt % of feed) produced from the pyrolysis-GC/MS reactor for pyrolysis of cellotriosan and cellulose.	51
Table 3.3 Lumped product distribution from GC injection (inlet temperature 330°C) of a solution of cellobiosan in water (20% by weight).	52

Table	Page
Table 3.4 Relative abundance of selected ions from the products of fast pyrolysis of cellulose detected by mass spectrometry (negative ion mode with ionization by APCI with chloroform), as a function of the vapor phase residence time. m/z 359 - chloride adduct of cellobiosan, m/z 257 – chloride adduct of glucosylpyrano- β -glycolaldehyde.	55
Table 4.1 Quantified pyrolysis product distribution (Wt % of starting model compound) of various lignin model compounds.....	69
Table 4.2 Relative abundances of identified monomeric pyrolysis products normalized with respect to coniferyl alcohol.....	74
Table 5.1 List of the catalysts tested in the micro-scale semi-batch catalytic reactor (pyroprobe).	88
Table 5.2 Product selectivity from hydrodeoxygenation of dihydroeugenol over Pt-Mo bimetallic catalysts, studied at 300°C, and 25 bar hydrogen partial pressure.....	97
Table 5.3 Product selectivity from hydrodeoxygenation of dihydroeugenol over Pt-Mo bimetallic catalyst and a physical mixture of the Pt only and Mo only catalyst, studied at 300°C, and 25 bar hydrogen partial pressure.....	102
Table 5.4 Product selectivity from hydrodeoxygenation of dihydroeugenol over Pt-Mo bimetallic catalyst and a physical mixture of the Pt only and Mo only catalyst, studied at 300°C, and 1 bar hydrogen partial pressure.....	103
Table 5.5 Catalyst loading required to attain similar conversion over the Pt-Mo series of catalysts in the micro-scale semi-batch reactor, all other experimental conditions remaining constant.	105

Table	Page
Table 5.6 Comparison of product selectivity from hydrodeoxygenation of dihydroeugenol over the 5%Pt2.5%Mo/MWCNT catalyst, between the two reactors in similar conversion range. Catalyst studied at 300°C, and 1 bar hydrogen partial pressure.	107
Table 5.7 Product selectivity comparison from hydrodeoxygenation of dihydroeugenol over the 5%Pt2.5%Mo/MWCNT catalyst as a function of the hydrogen pressure, at temperature of 300°C.....	109
Table 5.8 Comparison of the ratio of yields of propylcyclohexane to that of propylbenzene from hydrodeoxygenation of dihydroeugenol over the 5%Pt2.5%Mo/MWCNT catalyst as a function of the hydrogen pressure, at temperature of 300°C, with the expected equilibrium ratio.	109
Table 5.9 Yield of hydrocarbon ring products from various lignin-derived model compounds over the 5%PtMo/MWCNT catalyst at 300°C and 25 bar hydrogen pressure.	112
Table 5.10 Product selectivity from hydrodeoxygenation of dihydroeugenol over various catalysts, studied at 300°C, and 25 bar hydrogen partial pressure.	115
Table 5.11 Reactor outlet stream composition from reaction of propylcyclohexane over various catalysts, studied at 300°C, and 25 bar hydrogen partial pressure.....	116
Table 5.12 Site time yield (STY) for dihydroeugenol consumption from hydrodeoxygenation of dihydroeugenol over Pt-Mo catalysts, studied at 300°C, and 1 bar hydrogen partial pressure.....	121
Table 5.13 Site time yield (STY) for primary product formation from hydrodeoxygenation of dihydroeugenol over 5%Pt/MWCNT and Pt-Mo catalysts, studied at 300°C, and 1 bar hydrogen partial pressure.....	121

Table	Page
Table 5.14 Site time yield (STY) for propylbenzene formation from hydrodeoxygenation of dihydroeugenol over 5%Pt/MWCNT and Pt-Mo catalysts, studied at 300°C, and 1 bar hydrogen partial pressure.....	121
Table 5.15 Site time yield (STY) for m-cresol consumption and primary product formation ,toluene and ring hydrogenation products (methylcyclohexanol + methylcylohexanone) during hydrodeoxygenation of m-cresol over the Pt-Mo catalysts, studied at 300°C, and 1 bar hydrogen partial pressure	128
Table 6.1 List of the catalysts tested in the micro-scale semi-batch catalytic reactor (pyroprobe)	141
Table 6.2 Lumped product distribution from different biomass and model feedstocks on a % carbon basis (experimental conditions: hydropyrolysis temperature – 500°C, Hydrodeoxygenation temperature – 300°C, hydrogen pressure – 25 bar)	153
Table 6.3 Lumped product distribution from hydrodeoxygenation of poplar and cellulose hydropyrolysis products on a % carbon basis from the Lab-scale continuous flow cyclone type reactor over the 5%Pt2.5%Mo/MWCNT catalyst (experimental conditions: hydropyrolysis temperature – ~480°C, Hydrodeoxygenation temperature – ~300°C) ..	161
Table 6.4 Observed ratio of aromatic to saturated cyclic hydrocarbons during hydrodeoxygenation of biomass hydropyrolysis products over 5%Pt 2.5%Mo/MWCNT at 300°C, and 1 bar hydrogen pressure.	169
Table 7.1 Product selectivity from aldol condensation of butanal over 2%Cu/TiO ₂ catalyst, as a function of hydrogen pressure in the conversion range of 80-88%, at a temperature of 300°C.....	179

Appendix Table	Page
Table C. 1 Predicted boiling point of the lignin model compounds – aim to show the relative volatility of the model compounds. Boiling point predicted via Joback fragmentation method modified by S.E. Stein. ¹⁹²	199
Table C. 2 Weight percentage of monomeric species based on the number of carbon atoms in the molecule.	200
Table C. 3 Elution time for dimer 1 for each of the different columns tested.	200
Table C. 4 Quantified lumped pyrolysis product distribution from coniferyl alcohol in wt% of the reactant.....	200
Table C. 5 Quantified pyrolysis product distribution from dimer 1 as a function of the vapor phase residence time in wt% of the reactant.....	203
Table C. 6 Quantified pyrolysis product distribution from polymer 5 as a function of the vapor phase residence time in wt% of the reactant.....	203
Table D. 1 Yield of products from the model compounds 4-isopropylcyclohexanol and 4-propylcyclohexanone over the 2.46%Mo/MWCNT catalyst at 300 °C and 350 PSIG hydrogen total pressure in the high-pressure pulse reactor.....	204
Table D. 2 Yield of products from the model compounds 4-isopropylcyclohexanol and 4-propylcyclohexanone over the 2.46%Mo/MWCNT catalyst at 300 °C and 25 PSIG helium total pressure in the high-pressure pulse reactor.....	204
Table E. 1 Compositional analysis of the biomass feedstocks, % wt (dry basis).	205
Table E. 2 Ultimate and proximate analysis of cellulose and biomass feedstocks.....	205
Table E. 3 Hydrocarbon products observed within the each hydrocarbon fraction classified on the basis of number of carbon atoms per molecule.	206

Appendix Table	Page
Table E. 4 Quantified pyrolysis product distribution from dimer 1 as a function of hydrogen pressure in wt% of the reactant.	206
Table E. 5 Quantified pyrolysis product distribution from polymer 2 as a function of hydrogen pressure in wt% of the reactant.	207
Table E. 6 Detailed product distribution from cellulose as a function of the Mo:Pt ratio of the catalysts tested quantified by carbon wt% of the reactant.	208
Table E. 7 Detailed product distribution from levoglucosan as a function of the Mo:Pt ratio of the catalysts tested quantified by carbon wt% of the reactant.	209
Table E. 8 CO uptake results obtained via chemisorption of the Pt-Mo series of bimetallic catalysts as a function of the Mo:Pt ratio.	210
Table E. 9 Detailed product distribution from cellulose as a function of the hydrogen pressure of the catalysts tested quantified by carbon wt% of the reactant.	211
Table E. 10 Detailed product distribution from levoglucosan as a function of the hydrogen pressure of the catalysts tested quantified by carbon wt% of the reactant.	212
Table E. 11 Detailed product distribution from xylan as a function of the hydrogen pressure of the catalysts tested quantified by carbon wt% of the reactant.	213
Table E. 12 Detailed product distribution from dimer 1 as a function of the hydrogen pressure of the catalysts tested quantified by carbon wt% of the reactant.	214
Table E. 13 Detailed product distribution from polymer 2 as a function of the hydrogen pressure of the catalysts tested quantified by carbon wt% of the reactant.	215
Table E. 14 Detailed product distribution from poplar as a function of the hydrogen pressure of the catalysts tested quantified by carbon wt% of the reactant.	216

Appendix Table	Page
Table E. 15 Detailed product distribution from pine as a function of the hydrogen pressure of the catalysts tested quantified by carbon wt% of the reactant.....	217
Table E. 16 Detailed product distribution from maize as a function of the hydrogen pressure of the catalysts tested quantified by carbon wt% of the reactant.....	218
Table E. 17 Percent of Pt monometallic, PtMo coordinated particles, and PtMo alloy particles as determined via STEM-EELS line-scans as a function of the Mo:Pt ratio (1:0.5, 1:1, and 1:2) for the series of PtMo /MWNCT catalysts.	219
Table E. 18 XPS Binding Energies and Component Percents for the Pt, Mo and PtMo catalysts.....	219
Table E. 19 Detailed product distribution from cellulose quantified by carbon wt% of the reactant.....	220
Table E. 20 Equilibrium ratio of aldehyde to alcohol at 300°C at two different hydrogen partial pressure conditions as estimated by ASPEN.	224
Table E. 21 Percentage contribution of different types of alkanes based on the structure towards the total hydrocarbon product distribution from fast hydrolysis and catalytic hydrodeoxygenation of cellulose and lignin polymer 2 at 1 bar hydrogen partial pressure and 300°C.	224

LIST OF FIGURES

Figure	Page
Figure 1.1 Share of total primary energy supply in 2012 ¹	2
Figure 1.2 Biomass conversion processes for production of liquid fuels. ⁹	5
Figure 1.3 The H ₂ Biooil Process. ²⁴	8
Figure 1.4 Cellulose chemical structure.....	9
Figure 1.5 Structural model of hemicellulose. ²⁹	9
Figure 1.6 Lignin monomer units, building blocks of lignin polymer.	10
Figure 1.7 Structural model of lignin. ¹²	11
Figure 2.1 Schematic of experimental setup (Py-GC/MS) for fast hydrolysis and catalytic hydrodeoxygenation studies with biomass during the sample loading phase. Red box indicates the heated zone (T=300°C).....	21
Figure 2.2 Schematic of experimental setup (Py-GC/MS) for fast hydrolysis and catalytic hydrodeoxygenation studies with biomass during the running phase. Red box indicates the heated zone (T=300°C).....	21
Figure 2.3 Pictorial representation of the internal components of a split/splitless inlet on a Agilent 7890A gas chromatographs with the modified flow patterns due to interfacing with the micro-scale semi-batch reactor system (also called Py-GC/MS system). Image adapted from an online source. ⁹ Split ratio calculation is shown below.	22

Figure	Page
Figure 2.4 Schematic for flow and pressure control for a electronically controlled split inlet. The mass flow sensor is used in a feedback control loop (red) to control total flow to the inlet, and is the electronic equivalent to a mechanical mass flow controller. A pressure sensor located on the septum purge line is used in a feedback control loop (green) with the backpressure controller on the split vent line to control inlet pressure. Image modified from the source. ⁹	23
Figure 3.1 Chemical structure of Cellobiosan and Cellotriosan	36
Figure 3.2 Product distribution from fast pyrolysis of cellulose as a function of pyrolysis temperature, grouped into categories: char, liquid (products expected to be a part of condensed bio-oil), and permanent gases (CO,CO ₂ , and methane).	43
Figure 3.3 Product distribution from the “liquid” fraction of fast pyrolysis of cellulose as a function of pyrolysis temperature, grouped into categories based on product structure.....	44
Figure 3.4 Product distribution from fast pyrolysis of cellulose as a function of the pyrolyzing gas (He, H ₂).	46
Figure 3.5 Relative abundance of selected ions from the products of fast pyrolysis of cellulose detected by mass spectrometry (negative ion mode with ionization by APCI with chloroform), as a function of the vapor phase residence time. m/z 359 - chloride adduct of cellobiosan, m/z 257 – chloride adduct of glucosylpyrano-β-glycolaldehyde. 56	56
Figure 4.1 Lignin model compounds (1-5) used in this study. Numbers inside the rings are for notation purposes only, relevant end groups are highlighted in blue.	66
Figure 4.2 Structures of the major products from pyrolysis of lignin model compounds.	70
Figure 4.3 Two pathways observed during pyrolysis of dimer 1	72

Figure	Page
Figure 4.4 Transformation of trimer 2 to potential products via pathway 1.....	75
Figure 4.5 Char yield as a function of the degree of polymerization of the lignin model compounds. Data point of Dp=3 is for trimer 2	77
Figure 4.6 Yield of products from pyrolysis of dimer 1 as a function of vapor phase residence time. dimer 1 (squares), Monomeric species (triangles), Coniferyl alcohol(circles), 2-methoxy-4-(2-(2-methoxyphenoxy)vinyl)phenol (diamonds).....	81
Figure 4.7 Yield of products from pyrolysis of polymer 5 as a function of vapor phase residence time. Dimeric species (circles), Monomeric species (triangles).....	82
Figure 5.1 Proposed major reaction pathway for high pressure (25 bar) vapor phase hydrodeoxygenation of dihydroeugenol (DHE) over the series of Pt-Mo bimetallic catalysts.....	94
Figure 5.2 Proposed major reaction pathways for vapor phase hydrodeoxygenation of dihydroeugenol (DHE) as a function of the hydrogen pressure over the series of 5%Pt2.5%Mo/MWCNT catalyst. Green-solid arrows indicate the major pathway at low hydrogen pressure (1 bar), while the Red-dotted arrows indicate the major pathway at high hydrogen pressure (25 bar). The Pt,Mo and Pt-Mo denotations above the arrows indicate the dominant role of that species for that step in the overall reaction pathway. Figure adapted from source. ³⁷	95
Figure 5.3 Product selectivity from hydrodeoxygenation of dihydroeugenol, as a function of the Pt:Mo ratio of the Pt-Mo bimetallic catalysts studied at 300°C, and 25 bar hydrogen partial pressure.....	98
Figure 5.4 Product selectivity ratio of propylcyclohexane to 4-propylcyclohexanol from hydrodeoxygenation of dihydroeugenol, as a function of the Pt:Mo ratio of the Pt-Mo bimetallic catalysts studied at 300°C, and 25 bar hydrogen partial pressure.....	98

Figure	Page
Figure 5.5 Yield of products from the model compounds, 4-isopropylcyclohexanol and 4-propylcyclohexanone, over the 2.46%Mo/MWCNT catalyst at 300 °C and 25 (350 psig) bar hydrogen pressure and 3 bar (30 psig) He pressure.....	100
Figure 5.6 Selectivity for propylcyclohexane and propylbenzene from hydrodeoxygenation of dihydroeugenol over the 5%Pt2.5%Mo/MWCNT catalyst, as a function of hydrogen pressure, at similar conversion (~100). Temperature of catalyst bed ~300°C.....	110
Figure 5.7 Conversion profile for dihydroeugenol as a function of time of operation over the 1.9%Pt1.2%Mo/SiO ₂ catalyst at 300°C and 1 bar hydrogen partial pressure.	117
Figure 5.8 WHSV plot for selectivity of propylbenzene versus DHE conversion on the 5%Pt2.5%Mo/MWCNT and the 1.9%Pt1.2%Mo/SiO ₂ catalyst, at 300°C, 1 bar hydrogen pressure in the conversion range of 10-80%.....	119
Figure 5.9 WHSV plot for selectivity of primary products, 4-propylphenol (circles), and 4-propylbenzene-1,2-diol (diamonds), versus DHE conversion on the 5%Pt2.5%Mo/MWCNT and the 1.9%Pt1.2%Mo/SiO ₂ catalyst, at 300°C, 1 bar hydrogen pressure in the conversion range of 10-80%.....	119
Figure 5.10 Proposed major reaction pathway for low hydrogen pressure (1 bar) vapor phase hydrodeoxygenation of m-cresol over the 5%Pt2.5%Mo/MWCNT catalyst.	125
Figure 5.11 WHSV plot for selectivity of major products versus m-cresol conversion on the 5%Pt2.5%Mo/MWCNT catalyst for the products, toluene (primary), methylcyclohexanol + methylcyclohexanone (primary) and methylcyclohexane (secondary), at 300°C, 1 bar hydrogen pressure in the conversion range of 5-100%.....	126

Figure	Page
Figure 5.12 Plot for ratio of products, methylcyclohexanone : methylcyclohexanol, as a function of m-cresol conversion on the 5%Pt2.5%Mo/MWCNT catalyst at 300°C, 1 bar hydrogen pressure in the conversion range of 5-100%.....	127
Figure 5.13 Plot for ratio of m-cresol : methylcyclohexanol, as a function of m-cresol conversion on the 5%Pt2.5%Mo/MWCNT catalyst at 300°C, 1 bar hydrogen pressure in the conversion range of 5-100%.	127
Figure 5.14 Conversion profile for m-cresol as a function of time of operation over the 5%Pt2.5%Mo/MWCNT catalyst at 300°C and 1 bar hydrogen partial pressure. Red – Fresh, reduced catalyst deactivation profile; Green – Deactivated catalyst was re-reduced at 450°C in hydrogen under standard conditions after 20 hours of operation; Yellow – Indicates first conversion data point on a new day of operation.....	131
Figure 5.15 Conversion profile for dihydroeugenol as a function of time of operation over the 1.9%Pt1.2%Mo/SiO ₂ catalyst at 300°C and 1 bar hydrogen partial pressure. Red – Fresh, reduced catalyst deactivation profile; Green – Deactivated catalyst was subjected to oxygen treatment at 300°C as described previously and then reduced at standard reduction procedure at 450°C; Blue - Deactivated catalyst was subjected to oxygen treatment at 350°C, as described previously, and then reduced at standard reduction procedure at 450°C; Yellow – Indicates first conversion data point on a new day of operation.	132
Figure 5.16 Conversion profile for m-cresol as a function of time of operation over the 1.9%Pt1.2%Mo/SiO ₂ catalyst at 300°C and 1 bar hydrogen partial pressure. Red – Fresh, reduced catalyst deactivation profile; Green – Deactivated catalyst was subjected to oxygen treatment at 300°C, as described previously, and then reduced at standard reduction procedure at 450°C; Yellow – Indicates first conversion data point on a new day of operation.	133

Figure	Page
Figure 6.1 Structures of lignin model compounds.....	140
Figure 6.2 Percentage carbon yield of product fractions from hydrodeoxygenation of levoglucosan as a function of the Mo:Pt ratio of the catalyst. (squares) C ₄₊ hydrocarbon fraction – liquid fuel range hydrocarbons, (circles) C ₆ hydrocarbon fraction.	154
Figure 6.3 Percentage carbon yield of product fractions from hydrodeoxygenation of fast hydrolysis products of cellulose as a function of the Mo:Pt ratio of the catalyst. (squares) C ₄₊ hydrocarbon fraction – liquid fuel range hydrocarbons, (circles) C ₆ hydrocarbon fraction.....	155
Figure 6.4 Percentage carbon yield of product fractions from hydrodeoxygenation of levoglucosan as a function of the hydrogen pressure over the 5%Pt2.5%Mo/MWCNT catalyst. (squares) C ₄₊ hydrocarbon fraction – liquid fuel range hydrocarbons, (circles) C ₆ hydrocarbon fraction.	156
Figure 6.5 Percentage carbon yield of product fractions from hydrodeoxygenation of fast hydrolysis products of cellulose as a function of the hydrogen pressure over the 5%Pt2.5%Mo/MWCNT catalyst. (squares) C ₄₊ hydrocarbon fraction – liquid fuel range hydrocarbons, (circles) C ₆ hydrocarbon fraction.	157
Figure 6.6 Percentage carbon yield of product fractions from hydrodeoxygenation of fast hydrolysis products of biomass model compounds/polymers as a function of the hydrogen pressure over the 5%Pt2.5%Mo/MWCNT catalyst. Indicates decrease in the corresponding hydrocarbon fraction from different components of biomass, illustrating increase in C-C scission with decrease in hydrogen pressure.....	158

Figure	Page
Figure 6.7 Percentage carbon yield of C ₄₊ hydrocarbon fraction from hydrodeoxygenation of fast hydropyrolysis products of Poplar (circles), Pine (triangles), Maize (Squares) as a function of the hydrogen pressure over the 5%Pt2.5%Mo/MWCNT catalyst.	159
Figure 6.8 Percentage carbon yield of aromatic hydrocarbon fraction from hydrodeoxygenation of fast hydropyrolysis products of Poplar (circles), Pine (triangles), Maize (Squares) as a function of the hydrogen pressure over the 5%Pt2.5%Mo/MWCNT catalyst.	160
Figure 7.1 Proposed major reaction pathways for vapor phase aldol condensation of butanal over the 2%Cu/TiO ₂ catalyst.....	180
Figure 7.2 GC chromatogram (FID) showing the hydrocarbon products from aldol condensation of glycolaldehyde over 2%Cu/TiO ₂ catalyst, at a temperature of 300°C.	180
Appendix Figure	
Figure A. 1 Schematic of the CDS pyroprobe 5200 high pressure reactor during the sample loading phase.	196
Figure A. 2 Schematic of the CDS pyroprobe 5200 high pressure reactor during the running phase.	197
Figure A. 3 Schematic of the CDS pyroprobe 5200 high pressure reactor during the sampling phase.....	197
Figure B. 1 GC chromatogram (Signal: FID) for direct injection of cellobiosan solution in water, with column 4, showing peaks for cellobiosan and levoglucosan.	198

Figure B. 2 GC chromatogram (Signal: FID) for analysis of cellulose pyrolysis products, with column 4, showing peaks for cellobiosan (minor), and levoglucosan. The lights were not resolved completely as shown by amalgamation of peaks in the initial (1-2 mins) part of the chromatogram. Cellulose pyrolysis conditions were, 500°C temperature, and the vapor phase residence time was ~0.5s. 198

Figure C. 1 Structure of lignin model compound Dimer **1** and predicted lignin fragment Dimer **6**. 199

Figure C. 2 Schematic of experimental setup (Py-GC/MS) for pyrolysis studies with Lignin model compounds. Red box indicates the heated zone (T=300°C). 200

Figure C. 3 Char yield and coniferyl alcohol fraction in the vapor phase pyrolysis products as a function of the degree of polymerization of the lignin model compounds. 202

Figure E. 1 Percentage carbon yield of liquid fuel range hydrocarbon fraction (C₄₊) from hydrodeoxygenation of cellulose pyrolysis products and levoglucosan as a function of the Mo:Pt ratio. (squares) cellulose, (circles) levoglucosan. (Triangles) Percent of PtMo bimetallic particles as determined via STEM-EELS line-scans as a function of the Mo:Pt ratio (1:0.5, 1:1, and 1:2) for the series of PtMo /MWNCT catalysts. 221

Figure E. 2 Percentage carbon yield of C₆ hydrocarbon fraction from hydrodeoxygenation of cellulose pyrolysis products and levoglucosan as a function of the Mo:Pt ratio. (squares) cellulose, (circles) levoglucosan. (Triangles) Percent of PtMo bimetallic particles as determined via STEM-EELS line-scans as a function of the Mo:Pt ratio (1:0.5, 1:1, and 1:2) for the series of PtMo /MWNCT catalysts. 222

Appendix Figure	Page
Figure E. 3 Percentage carbon yield of product fractions from hydrodeoxygenation of fast hydrolysis products of lignin model compound, dimer 1 as a function of the hydrogen pressure over the 5%Pt2.5%Mo/MWCNT catalyst. (squares) C ₇ hydrocarbon fraction, (circles) C ₈ hydrocarbon fraction, and (triangles) C ₉ hydrocarbon fraction.....	223
Figure E. 4 Percentage carbon yield of product fractions from hydrodeoxygenation of fast hydrolysis products of lignin model compound, polymer 2 as a function of the hydrogen pressure over the 5%Pt2.5%Mo/MWCNT catalyst. (diamonds) C ₆ hydrocarbon fraction, (squares) C ₇ hydrocarbon fraction, (circles) C ₈ hydrocarbon fraction, and (triangles) C ₉ hydrocarbon fraction.....	223

ABSTRACT

Choudhari, Harshavardhan J. Ph.D., Purdue University, August 2015. Micro-Scale Studies of Fast-Hydrolysis and Catalytic Hydrodeoxygenation of Biomass and Related Model Compounds. Major Professor: Fabio H. Riberio, Rakesh Agrawal, and W. Nicholas Delgass.

Biomass is a major source of renewable carbon which can be converted to hydrocarbon fuel with the aim of reducing the dependence on fossil based sources. Fast pyrolysis of biomass followed by catalytic hydrodeoxygenation of bio-oil is considered a promising biomass conversion route to produce drop in hydrocarbon fuels. The H₂Bioil process was proposed as an integrated high pressure fast hydrolysis and catalytic vapor phase hydrodeoxygenation (HDO) pathway for utilizing biomass to produce high energy density fuel. During fast hydrolysis biomass is rapidly heated to generate a complex mixture of compounds with high oxygen content (35-40 wt %). In the H₂Bioil process, hydrolysis vapors are immediately upgraded via a downstream catalytic reactor to reduce the oxygen content and produce a high energy density bio-oil.

In this dissertation, fast hydrolysis and inline catalytic hydrodeoxygenation studies were conducted in a micro pyrolyzer, with a unique modification, which allowed online sampling of biomass pyrolysis vapor products under high pressure hydrogen (up to 35 bar) directly into the gas chromatograph and mass spectrometer (GC-MS) for analysis. Identification and quantification of the entire range of vapor phase products from fast pyrolysis is essential to understand the governing mechanisms during pyrolysis as well as to design a suitable catalyst for downstream upgrading. Quantification of the pyrolysis and HDO products using the GC-MS accounted for > 90% of the starting mass from the cellulose, lignin, and biomass.

The structure of native lignin differs from that of extracted lignin and therefore, well characterized synthetic guaiacyl (G) lignin model oligomers and a polymer were used to investigate β -O-4 bond scission under fast pyrolysis conditions. The effect of degree of polymerization (Dp) on char formation and pathways for β -O-4 bond scission were also investigated, with the char yield increasing with increase in Dp. The major monomeric product observed from β -O-4 bond scission was coniferyl alcohol, along with the presence of a significant proportion of dimers (19-70 wt %) in the product distribution. Vapor phase residence time studies revealed that these lignin-derived oligomers underwent secondary reactions in the vapor phase to form monomers, which increased in abundance with an increase in the residence time. These results conclusively showed, for the first time, the presence of a significant proportion of dimers (>19%), and possibly oligomers, along with monomers amongst the primary products from lignin pyrolysis. Similar, results were observed with cellulose pyrolysis products resolving the debate in

literature about the nature of primary products from lignin and cellulose pyrolysis. Additionally, no deoxygenation was observed during cellulose and lignin fast pyrolysis experiments, in presence of hydrogen (up to 25bar), thereby showing the need for a downstream catalyst.

Model compound studies are important to develop an understanding of the reaction pathways and effect of catalyst composition on product distribution. Therefore, we began with a study of HDO of the cellulose and lignin based model compounds, levoglucosan, and dihydroeugenol, over a series of supported PtMo catalysts. Complete deoxygenation was obtained for both levoglucosan (~72% C₄₊ hydrocarbons) and dihydroeugenol (98% C₉ hydrocarbons) over a Pt-Mo/MWCNT catalyst at 100% conversion. Increasing the Mo:Pt (0:1-5:1) ratio was shown to favor the hydrodeoxygenation selectivity as well as decrease the extent of C-C bond cleavage, demonstrating the importance of Mo for oxygen removal. Reaction pathway studies were carried out with dihydroeugenol to demonstrate the role of Mo as an oxophilic promoter, which in conjunction with Pt improved the C-O bond scission selectivity. Based on these model compound studies, the 5%Pt2.5%Mo/MWCNT catalyst was tested to maximize C₄₊ hydrocarbon recovery from cellulose, xylan, lignin polymer and intact biomass.

Hydrodeoxygenation of biomass pyrolysis products (poplar, pine, and maize) over the 5%Pt2.5%Mo/MWCNT catalyst gave >69% carbon yield to hydrocarbons, with >41% yield to liquid fuel range (C₄₊) hydrocarbons, at 300°C and 25 bar hydrogen pressure. Hydrogen pressure played a critical role in determining the hydrocarbon product

distribution due to a significant impact on the degree of C-C scission. Decrease in the hydrogen pressure was shown to increase the degree of C-C scission, thereby decreasing the yield of liquid fuel range hydrocarbons by ~10 carbon wt %, within the pressure range of 1-25 bar. Studies with cellulose, xylan, and lignin polymer **2** showed that cellulose and xylan fraction contributed to a greater extent toward C-C scission than lignin, primarily due to the aromatic structure of the lignin pyrolysis products. Decrease in the hydrogen pressure also resulted in an increase in the yield of aromatic hydrocarbons (up to ~14 carbon wt % yield), which were chiefly derived from the lignin fraction of the biomass. Hydrogen pressure is a critical parameter, which can be tuned to control the hydrocarbon product distribution based on the composition of the biomass and maximize the value of products. These trends were replicated in the continuous-flow cyclone-type fast-hydrolysis (FHP) reactor with a downstream vapor-phase catalytic HDO reactor, demonstrating the capability of this micro-scale semi-batch reactor system to identify candidate catalysts via screening studies with a variety of biomass based feed stocks as well as model compounds.

CHAPTER 1. INTRODUCTION

1.1 Need for Alternate Sources of Energy

Energy, for any country is an indispensable commodity frequently indicating the level of prosperity. Energy is derived from a myriad of sources for human use, the majority of it being derived from fossil fuels. For United States of America, in 2012, ~83.9% of the total primary energy was derived from fossil based sources namely coal, oil and natural gas, while renewable sources accounted for a paltry 6.3% after nuclear energy (~10.8%) as shown in Figure 1.1.¹ Fast depleting fossil fuel resources, and concerns over the negative impact of excessive CO₂ emissions on the environment have forced us to explore alternate, renewable sources of energy, and imposed a need to efficiently manage the available carbon resources. Renewable carbon based fuels are necessary to reduce CO₂ emissions which are almost entirely from fossil fuels with alternative fuels contributing only 1% to the total CO₂ emissions.² The concept of “solar economy” summarizes the need for efficient utilization of the energy from the sun to meets all the needs of the human civilization, namely food, electricity, transportation, etc.³ The amount of solar energy available is in excess of the current rate of consumption, but it is currently inefficient to harness this energy in its primary form. The US transportation sector consumed ~28 % of the total energy consumption in 2013 and 90% of that was derived from petroleum based fuel.^{4,5} With US being the largest consumer of liquid transportation

fuel in the world at ~14 million barrels per day, there is a significant need and potential to replenish a significant fraction with renewable sources of energy.⁶ The transportation sector currently requires high energy density liquid fuel which is almost entirely obtained from fossil fuel sources. Therefore, there is a need to develop sustainable and renewable sources to produce liquid hydrocarbon fuel which can be readily integrated with the existing infrastructure for distribution. Batteries (electric vehicles), hydrogen fuel cells are known to have technical issues such as storage of low energy density fuel.⁷ Battery powered transportation would demand a network of charging stations and additional electricity, a significant portion of which is currently produced from fossil fuels, albeit more efficiently than direct consumption energy efficiency of a vehicle. Biofuels is one of the promising sources for production of high energy density fuel which can take advantage of the existing infrastructure of the petroleum industry.

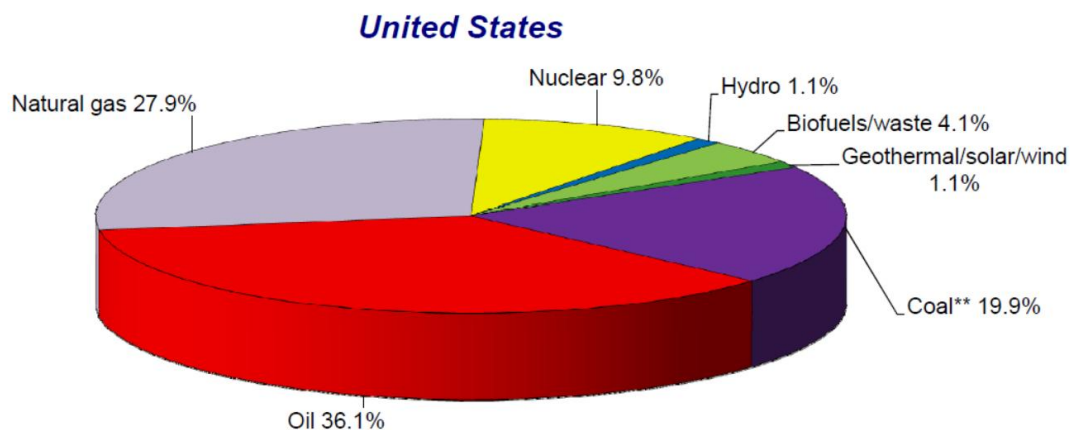


Figure 1.1 Share of total primary energy supply in 2012¹

1.2 Biomass Conversion Processes

Plants have evolved to utilize ~380 parts per million levels of CO₂ in the atmosphere and fix the carbon into the food chain in the form of carbohydrates, protein, lignin etc. Biomass is the only major source of renewable carbon, since CO₂ emissions from fuels can be claimed back to generate more fuels with future cycles of biomass. However, significant developmental work needs to be done to make current biomass conversion technologies commercially viable. Biomass conversion process can be broadly classified in to two categories: thermochemical conversion, and biological conversion.⁸ The biological route is mainly focused on making ethanol (and other alcohols) from sugar, while utilizing rest of the biomass for energy needs. The current EPA mandates for blending ethanol with gasoline and prospects for increasing the total biofuel based fraction of gasoline have encourage several oil corporations to invest in biological and enzymatic technologies for producing ethanol. However, purely increasing the capacity for ethanol production is not considered to be a feasible solution for replacement of petroleum based fuel. A primary reason being inability to blend ethanol beyond 10% by volume as well as low energy density value of ethanol compared to gasoline. Ethanol-enriched mixtures like E85 can be utilized by flexible fuel vehicles having specially designed engines.⁸ These limitations have developed a possibility of the biofuel contribution via ethanol reaching a “blend wall” in the near future, where in the total production of ethanol will exceed the amount that can be blend in gasoline at 10% by volume. These shortcomings have focused the research in the direction of developing technologies for direct production of liquid hydrocarbon fuel like molecules from

biomass. There are other developing technologies in the biological route like, making biodiesel from lipids extracted from plants. However, thermochemical technologies have an edge for direct production of hydrocarbon fuel from biomass.

The thermochemical route is very diverse with technologies involving pyrolysis, gasification, liquefaction, reforming etc.⁹⁻¹¹ Each of these technologies have certain pros and cons, with no clear winner and one can envision a future where an amalgamation of these technologies is used in a bio refinery to convert biomass to the most valuable concoction of products.¹²⁻¹⁵ Fast-pyrolysis of biomass followed by catalytic upgrading has been touted as a potentially economically attractive process for conversion of intact biomass to liquid fuel range hydrocarbons.¹⁶⁻¹⁸

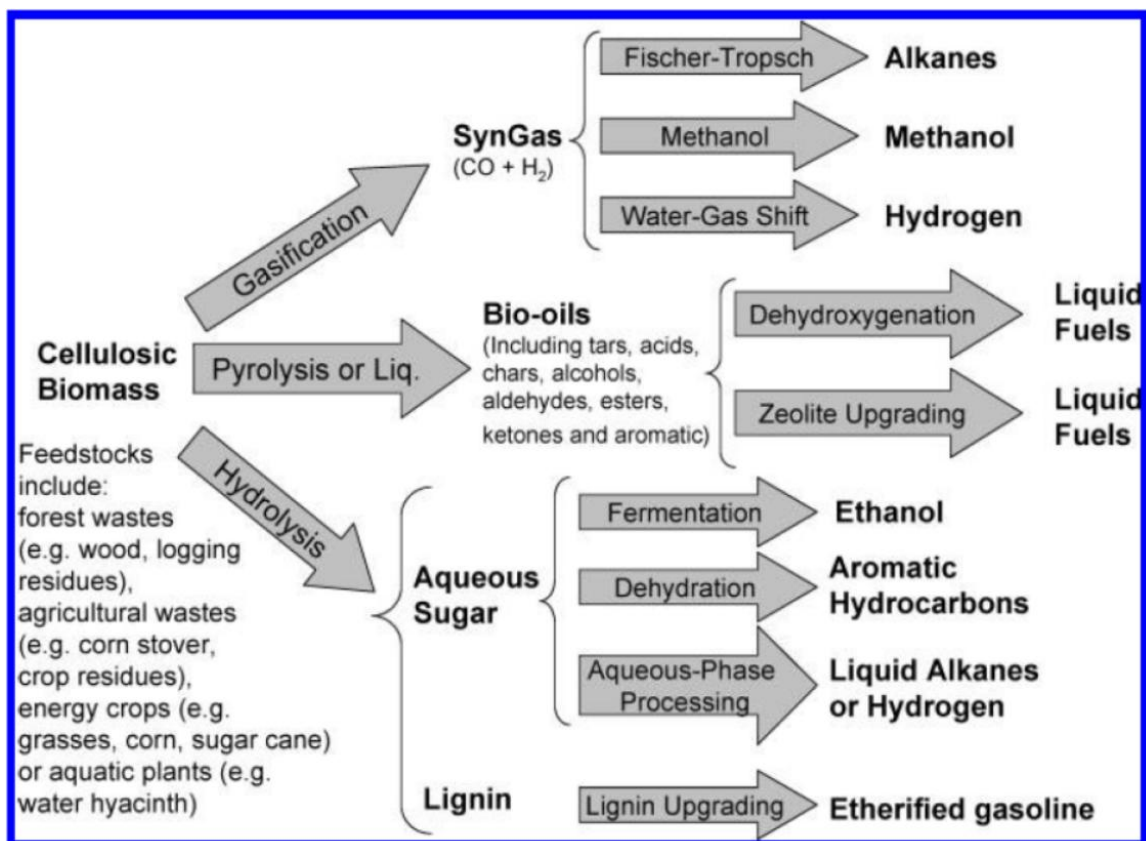


Figure 1.2 Biomass conversion processes for production of liquid fuels.⁹

Fast-pyrolysis involves heating the biomass at high temperature (400-600°C) in the absence of oxygen with fast heating rates (up to 1000°C.sec⁻¹) to depolymerize it into smaller molecules which can enter the vapor phase.^{19,20} These vapor phase compounds are then rapidly quenched to condense a liquid product called “bio-oil”. On the other hand, gasification occurs at higher temperatures (600-900°C) to produce syngas which can be subsequently converted to liquid fuels by the fischer-tropsch reaction. The energy density of lignocellulosic biomass is 16-19 MJ/kg, while that of petroleum is ~40 MJ/kg.⁷ This is primarily due to high oxygen content of biomass (35-60%).²¹ Typical crude biooil derived from fast pyrolysis of wood also has high oxygen content (30-45%) which

imparts it a low heating value (17 MJ/kg).²² Bio-oil is composed of ~25% water and balance polar organic oxygenates, and therefore reduction of oxygen content to <1% is necessary for utilizing it as a fuel for a vehicle. Furthermore, bio-oil is immiscible with hydrocarbons, corrosive, and chemically unstable creating hindrance for storage and transportation.²³ Bio-oil upgrading is studied extensively mainly utilizing hydrotreating technologies to remove oxygen with the aim of producing a refinery blend, however upgrading bio-oil comes with its own set of challenges like polymerization, reactor plugging, and catalyst coking. To overcome these obstacles, the H₂Bioil process was proposed as an integrated high pressure fast hydrolysis and catalytic vapor phase hydrodeoxygenation (HDO) pathway for conversion of biomass to produce high energy density fuel (Figure 1.3).^{16,24-27}

An ideal process for thermochemical conversion of biomass to biofuels would utilize every carbon available in the biomass for the fuel in an energy efficient manner. For such a process external hydrogen needs to be utilized to remove the oxygen in the form of water, which otherwise would be lost as CO, CO₂. The H₂CAR process was proposed wherein 100% of the biomass carbon was retained and H₂ from a carbon free source was utilized.⁷ The H₂CAR process utilized a gasifier and fischer-tropsch unit to convert biomass to liquid fuels. In search for a more efficient process, the H₂Bioil process was proposed which utilized fast hydrolysis and hydrodeoxygenation reactions in a single step, with H₂ from a carbon free source to make fuels.^{24,25} This process eliminated condensation of pyrolysis products to form bio-oil, followed by further deoxygenation steps at high temperature (200-300°C). The H₂Bioil process is versatile and can be

integrated with a coal gasifier or natural gas reformer to serve as a source of hot gas containing hydrogen. It has been shown that the H₂Bioil process has a higher carbon efficiency (~70%) and energy efficiency (~75%) over traditional biomass pyrolysis based processes and has the potential to produce 215 gge ton⁻¹ of liquid fuel annually.²⁴ Utilizing a thermochemical processes, such as H₂Bioil is advantageous since it is a biomass neutral process due to its ability to convert all the major components lignocellulosic biomass to hydrocarbons. As a result it does not feature in the food vs fuel debate since it is not dependent on sugar yield like the current corn and sugarcane feedstock based processes. Logistically, it will encounter the hurdle of economic harvesting and transportation of biomass, which is applicable for any biomass based process. Innovative solutions are required for tackling this issue, like making a mobile biomass to fuel unit which can have a reactor installed on a vehicle to increase the density of biomass by converting it to fuel on-site before transportation. Alternatively, construction of low capacity bio refineries with a catchment radius of ~150 miles have been proposed and would require low capital cost equipment for implementation. However, an efficient process with high carbon recovery will serve to alleviate some of these concerns and pave the path of commercial implementation of technology for production of renewable hydrocarbon fuel.

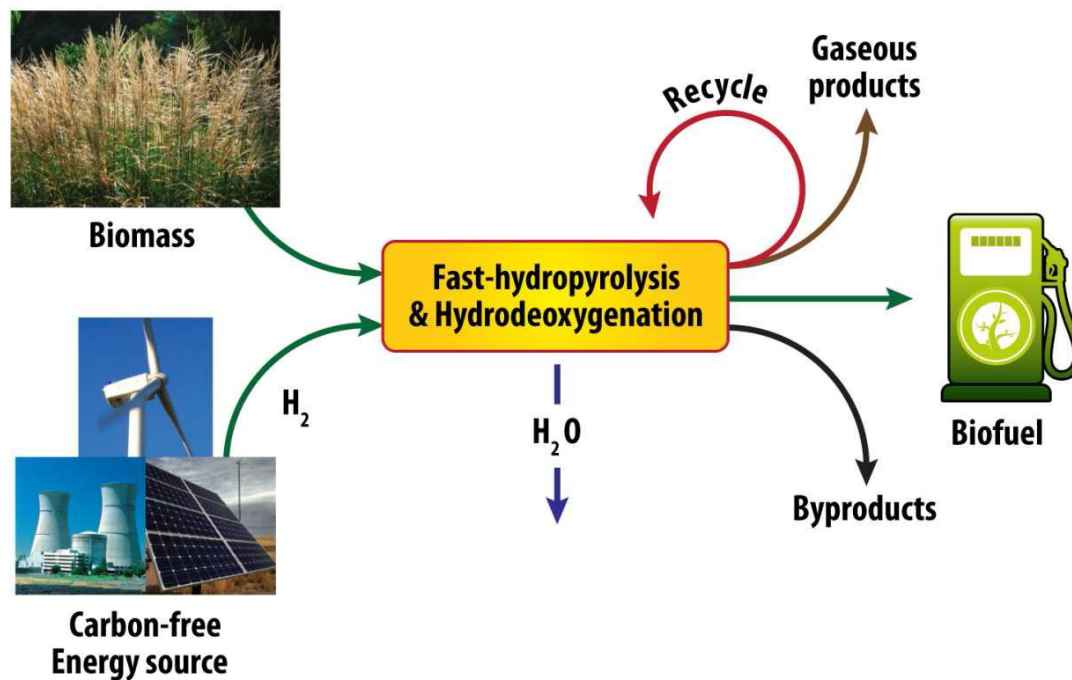


Figure 1.3 The H₂Bioil Process.²⁴

1.3 Lignocellulosic Biomass Structure

1.3.1 Cellulose and Hemicellulose

Cellulose is the most abundant naturally occurring polymer on the earth since it constitutes 30-50% of lignocellulosic biomass. Structurally, cellulose is a homo-polymer composed of glucose monomer units linked by glycosidic bonds (Figure 1.4). High abundance, uniform chemical structure and ease for extraction has resulted in cellulose being the most widely studied component of biomass for fast-pyrolysis. Unlike cellulose, hemicellulose (25-35% in woody biomass¹⁹) is a complex hetero-polymer, composed of several hexoses, pentoses and other minor components like hexuronic acids.²⁸ Variation in the proportion of monomeric units as well as structure (branched and linear) within different plant varieties make it extremely difficult to study hemicellulose. As a

compromise, xylan and other associated sugars (arabinose, mannose) are frequently used as surrogates for hemicellulose since they form the largest fraction of sugars that constitute hemicellulose (Figure 1.5).

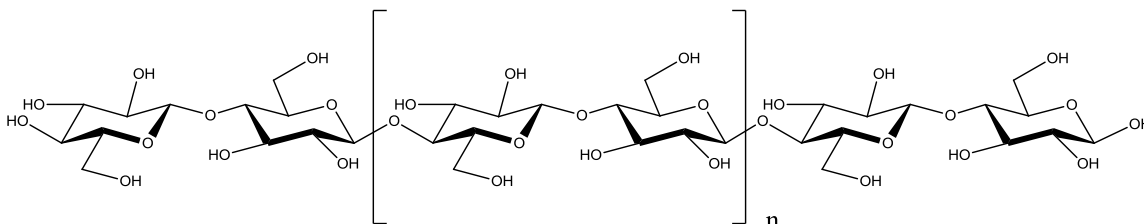


Figure 1.4 Cellulose chemical structure.

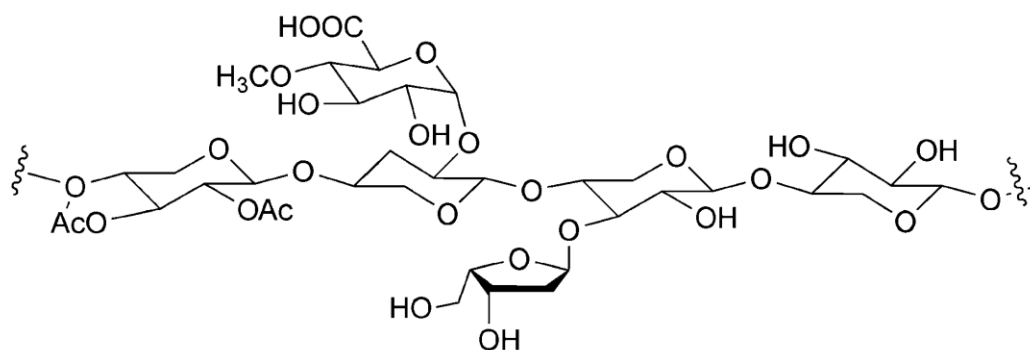


Figure 1.5 Structural model of hemicellulose.²⁹

1.3.2 Lignin

Lignin is embedded in the plant cell wall matrix along with cellulose and hemicellulose thereby having the potential to impact fast pyrolysis chemistry of the other components. Lignin is a complex highly cross-linked polymer which imparts strength and rigidity to the plant tissue. There are three major monomer units which form the building blocks of lignin; sinapyl alcohol, coniferyl alcohol, and p-coumaryl alcohol, and are connected by different types of linkages to form the cross linked polymer (Figure 1.6).^{19,30} G-lignin is a cross linked structure with coniferyl alcohol as the monomer, while S-lignin is a mostly

linear polymer of sinapyl alcohol units, because sinapyl alcohol cannot form a cross linked structure due to presence of methoxy groups in the ortho position with respect to the phenolic functional group (Figure 1.7). Lignin monomer units have high C/O ratio as compared to the sugar molecules and utilizing lignin (unlike certain sugar based processes) is critical for improving the overall carbon recovery from biomass. Lignin being a cross-linked polymer has a higher tendency to form char³¹ and hence, studying lignin depolymerization is important with the aim of maximizing the carbon yield by minimizing the amount of char formed. . It has been recently reported that it is possible to alter the relative ratios of the sub-units in the co-polymer in Arabidopsis by altering the expression (activity) of the enzymes which control the synthesis of the monomers.³² These opportunities for tailoring lignin polymer based on monomeric structure will potentially be valuable if the G-based and S-based polymers have different carbon recovery efficiencies.

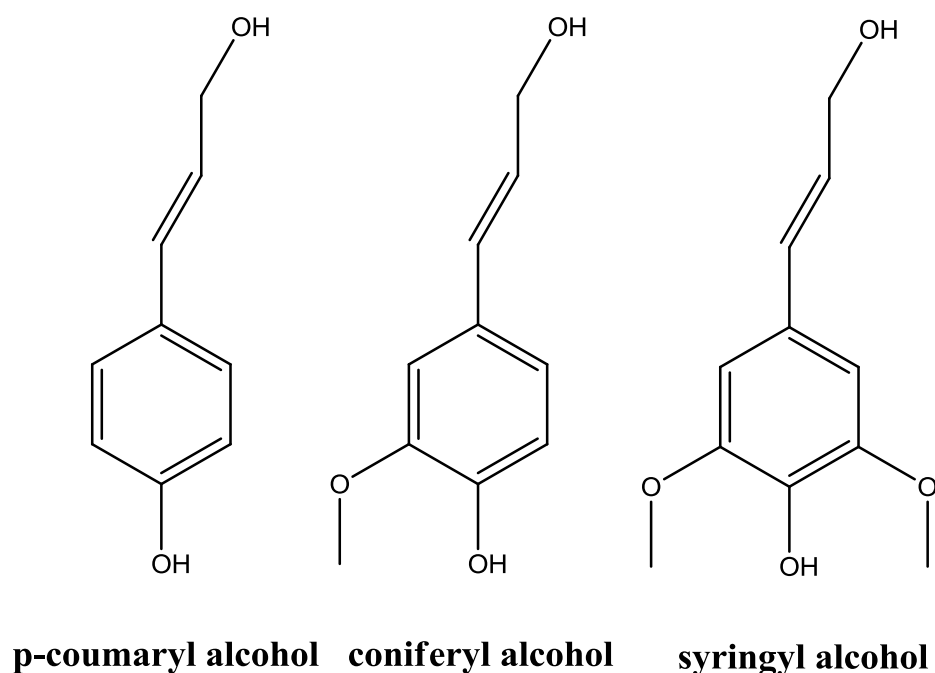


Figure 1.6 Lignin monomer units, building blocks of lignin polymer.

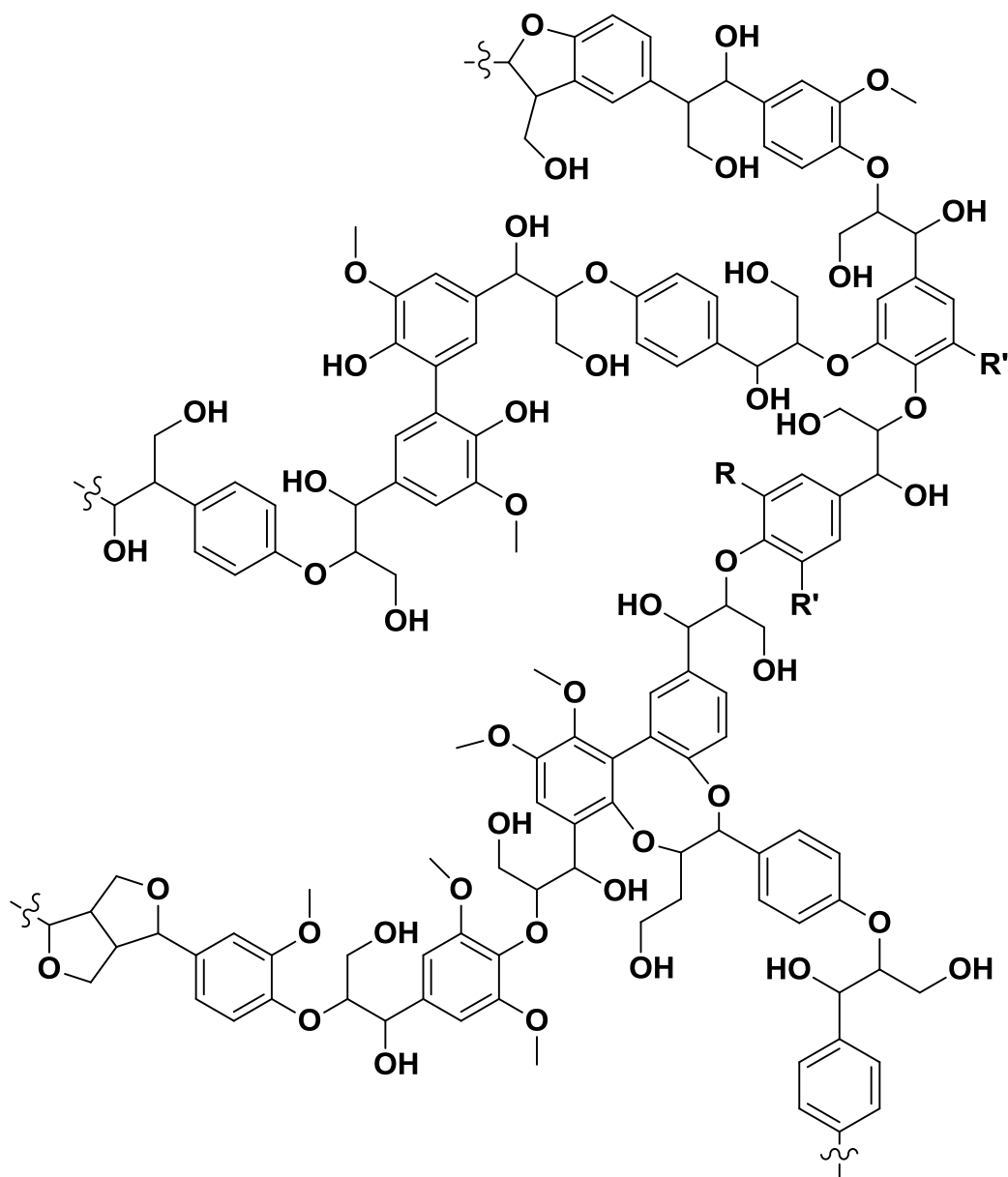


Figure 1.7 Structural model of lignin.¹²

1.4 Thesis Objectives

The main objective for this research was the experimental validation of the H₂Bioil process, which involved studying two main aspects, 1) hydrolysis of biomass, and 2) catalytic hydrodeoxygenation of the pyrolysis products. A primary goal was to design

and built a reactor system for enabling the testing of the different aspects of the process. Brief descriptions of the objectives for the projects that are a part of this dissertation are discussed below.

The biomass to liquid fuel conversion research group was at its initial stages and therefore the initial task was the construction of a pyrolysis reactor system capable of handling high hydrogen pressure and development of a suitable analytical capability for analysis of the products. A commercial pyrolysis unit equipped with a back pressure regulator for operation up to 35 bar pressure was acquired, and safety systems were installed for handling of hydrogen. However as reported in literature the overall mass balance for operation at high pressure was in the range of 30-50% which was unsuitable for completely understanding the product distribution.³³⁻³⁵ From that point onwards several modifications and iterations were made to increase the mass balance for operation at high pressure and a novel interfacing method was developed for achieving the target of >90% mass balance. Chapter 2 focusses on the details of the design and operation aspects of this newly designed reactor configuration. Inability of a GC-MS to quantitatively analyze dimeric species (due to low volatility and lack of GC column development in this particular area) from cellulose and lignin was identified as an important issue for incomplete mass balance, thereby necessitating use of multiple techniques. Liquid chromatography is suitable for higher molecular weight compounds, however has drawbacks preventing analysis of the entire spectrum of pyrolysis products. A combination of techniques would be required for analysis of biomass derived bio-oil.^{36,37} The idea was to identify parameters preventing the dimeric species from being analyzed

via gas chromatography and systematically improve column performance by minimizing the strong interactions between the GC column and dimeric species.

Fast-hydrolysis was traditionally studied for coal,³⁸ and the goal was to systematically study the effect of hydrogen pressure, temperature and other parameters for optimizing the pyrolysis conditions towards maximizing the yield of desired products. As the studies progressed, there arose a need to focus the attention towards a fundamental understanding of the underlying mechanisms during fast hydrolysis of biomass. Chapter 3 discusses cellulose pyrolysis studies in conjunction with model oligomers to identify an ideal surrogate for cellulose, and enable further mechanistic experimental and theoretical studies. Identical goals were chalked out for lignin pyrolysis as well, however the major hurdle was availability of pure native lignin feedstock. Unlike cellulose, lignin extraction processes resulted in significant modification of the structure rendering these feedstocks inadequate for representative pyrolytic and mechanistic studies. Synthetic lignin model oligomers and a polymer were synthesized by research collaborators which enabled quantitative pyrolysis studies in addition to fundamental mechanistic studies. The objective of these studies reported in Chapter 4 was to obtain a quantitative and representative pyrolysis product distribution from lignin fraction of the biomass. Additional goals involved identification of pathways of β -O-4 linkage scission and identify descriptors for char formation, which is considered a major source of carbon loss from the lignin fraction during pyrolysis of biomass.

Fast-hydrolysis of biomass did not lead to any significant deoxygenation in the absence of a catalyst. Therefore it became imperative to study catalytic hydrodeoxygenation of biomass pyrolysis products. Typically vapor phase catalytic hydrodeoxygenation was carried out at low hydrogen pressures and resulted in catalyst deactivation. The hypothesis was that high partial pressure of hydrogen will result in higher rate of hydrodeoxygenation and higher selectivity towards deoxygenation pathways. The goal for the micro-scale pulse studies involved catalyst screening to identify candidate catalysts with high selectivity for hydrodeoxygenation (minimum C-C bond scission), and then study their stability and kinetics with the continuous steady state fixed bed hydrodeoxygenation reactor. Additionally, reaction pathway studies in conjunction with catalyst characterization were necessary to identify catalyst descriptors to enable better catalyst design.

Hydrodeoxygenation studies in literature are performed primarily on model compounds and seldom extended to testing with pyrolysis products from intact biomass. The idea was to build an entire framework for testing catalysts from representative model compounds for lignin, cellulose to pyrolysis products from cellulose, hemicellulose, lignin and ultimately biomass. A systematic catalyst testing structure would result in a development of a robust catalyst which could handle the entire diversity of pyrolysis products from biomass to selective conversion to hydrocarbons. Chapters 5 and 6 focus on the results for catalytic hydrodeoxygenation of model compounds, and pyrolysis products from model polymers and biomass respectively.

CHAPTER 2. REACTOR DESIGN AND EXPERIMENTAL METHODS

2.1 Introduction

Fast pyrolysis of biomass is rapid heating of biomass to a high temperature (400-600°C) in an inert atmosphere so as to produce vapor phase products, which are subsequently condensed to a liquid product called bio-oil.²⁰ The vapor phase residence time is a crucial parameter and rapid quenching of the pyrolysis vapors (<2 sec) is important for curtailing undesired secondary reactions.²² The rapid heating and low residence time constraints associated with fast pyrolysis make the reactor design challenging. Several types of reactor designs have been tested in literature with fluidized bed, cyclone type and free fall reactor system being the most widely studied.^{11,20} A common problem associated with biomass pyrolysis studies is reactor and transfer tubing clogging due to char buildup. Elimination of cold zones and rapid heat transfer to prevent slow charring of biomass were of paramount importance during reactor design and operation.^{11,39}

Biomass fast-pyrolysis studies can be broadly classified on the basis of the type of reactor and the scale of operation into two categories, 1) Lab-scale continuous operation reactors and 2) Micro-scale batch/semi-batch reactors. The former category of reactors is widely used for testing reactor design parameters as well as carry out proof of concept demonstration studies. While the micro-scale reactors have the advantage of higher throughput facilitating fundamental studies related pyrolysis as well as used of model polymers which are not always available in larger quantities. In this study, we have used a commercial pyrolysis reactor system (CDS Pyroprobe 5200) and modified it to achieve the research objectives.

High pressure fast-hydrolypyrolysis required operational capability up to 35 bar pressure in presence of hydrogen resulting in introduction of safety systems for handling of hydrogen at such high pressure. While high pressure operational capability was available with the use of stainless steel reactors and connecting tubing, the major hurdle was absence of online analysis capable to providing high mass balance >90%. Effect of high pressure hydrogen on biomass pyrolysis was not widely studied and the existing studies had a low mass balance (20-50%).³³⁻³⁵ One of the objectives of the reactor design was developing an interfacing between the high pressure capable pyrolysis reactor and the GC-MS, which had a pressure limitation of 8 bar, thereby enabling online analysis of the pyrolysis products.

2.2 Micro-scale semi-batch reactor with catalytic hydrodeoxygenation capability (Py-GC/MS system)

A CDS pyroprobe 5200⁴⁰ capable of operation up to 35 bar pressure was used as the pyrolysis apparatus for carrying out the hydrolysis experiments with biomass. In the original setup the high pressure pyrolysis zone was interfaced with the GC-MS via a trap capable of adsorption of the pyrolysis products under room temperature conditions. The trap comprised of a polymer, Tenax-TATM, and was located downstream of the backpressure regulator (Figure A. 1). During the running phase (Figure A. 2), the pyrolysis vapors were carried to the trap by the reactant gas and the pyrolysis products were adsorbed on the trap, which was maintained at room temperature (25°C). During the sampling phase (Figure A. 3), the 8 port valve (MPV-1) was switched to have the GC carrier gas flush the trap, while simultaneously heating the trap up to 300°C. The desorbed vapors were carried to the GC inlet via the GC carrier gas through the heat traced transfer line tubing, where a suitable column in the GC-MS was used to analyze them. This setup enabled an effective separation of the high pressure pyrolysis reactor from the low pressure GC analysis carrier gas system. However, there were several drawbacks associated with this mode of operation primarily due to different adsorption affinities of the trap adsorbent for different molecules. Permanent gases namely CO, CO₂, methane, ethane, etc., as well as light oxygenates like methanol, and acetone, had very low adsorption affinity and were not observed in the GC-MS despite their presence in the pyrolysis product distribution. Additionally, certain other molecules were observed in less than stoichiometric proportions due to incomplete adsorption. On the other end of the

spectrum, heavy molecules like anhydrosugars, and possibly dimeric molecules, were permanently adsorbed on the trap solid phase due to low volatility. The pyrolysis was conducted at 500°C, while the trap was only heated to 300°C, resulting in some of the heavier molecules remaining on the trap and undergoing secondary reactions to form degradation products as well as char. Continuous operation over a period of 2-3 months required replacement of the trap due to loss in adsorption efficiency as well as visible char formation on the adsorbent. Additionally, operation at high pressure involved use of higher sccm flow rates of the reactant gases for maintaining consistent residence time of the vapor phase pyrolysis products in the pyrolysis zone, resulting in low concentration of the molecules in the vapors phase. The lower concentration of the molecules adversely affected the mass balance due to a lower degree of adsorption on the trap. All of these drawbacks resulted in incomplete mass balance (30-70%) as well as non-representative product distributions due to possible secondary reactions. A new analytical interfacing system with the GC-MS was designed to eliminate these flaws, and obtain a mass balance of >90% for all the reported experiments henceforth unless specified. Analytical challenges related to GC column method development were dealt with separately.

The redesigned interfacing system involved elimination of the adsorbent trap completely and a direct interfacing with the GC-MS. Figure 2.1 and Figure 2.2 shows the schematic of the redesigned system in the sample loading phase and running phase, respectively. The stream from the backpressure regulator was split into two parallel streams, one interfaced with the GC inlet via a heat traced transfer tubing, while the other was vented (vent 3). A needle valve was added on the vent line to control the flow rate to the GC

inlet. A relief valve was placed before the needle valve, on the vent line, to protect the GC inlet system from over pressurization in case of a failure of the backpressure regulator, and had a set point of 8 bar. The pressure in the lines after the backpressure regulator (up to the needle valve) was maintained by the proportioning valves of the GC inlet assembly (Figure 2.4), at the set point needed for normal column operation. The slipstream to the GC inlet was directly fed into the GC inlet liner via a modified needle assembly and augmented the GC inlet flow coming from the electronic pressure control module (mass flow controller – Figure 2.4) on the split/splitless inlet (Figure 2.3). Therefore, the actual flow rate through the inlet was higher than the actual set points on the GC. The GC column flow was not affected since that is governed by the pressure at the inlet (which was maintained at a constant value). However, the GC split flow which was used for calculation of the split ratio was different from the set point value due to extra flow from the reactor slip stream. As such the vent flow (vent 3) and the flow from the GC split vent were independently measured for each experiment and the split ratio was calculated using these flows. Figure 2.3 shows the flow scheme at the GC inlet with the calculation of the actual split ratio. The accurate calculation of the split ratio was very important for mass balance estimation due to high variation of the split ratio (50 to 800) depending on the experimental conditions.

Catalytic hydrodeoxygenation capability was incorporated through addition of a fixed bed reactor downstream of the pyrolysis zone. The catalyst bed was placed such that it was never exposed to air, which entered the pyrolysis zone during loading and unloading the sample. The temperature of the catalyst bed was accurately controlled via an

independent temperature control from the other tubing, which was enclosed in an oven and a thermocouple was placed in the catalyst bed for accurate temperature measurement. Introduction of the catalyst bed allowed for catalyst screening capability with operation up to 35 bar hydrogen pressure. The versatility of the micro-scale system was evident in the form of the multitude of feedstocks that could be utilized for testing catalysts. Model compounds, model polymers and intact biomass were pyrolyzed and passed over the catalyst bed and the products were accurately quantified. Reaction intermediates and model compounds which were only available in small quantities (not suitable for continuous $\text{g}\cdot\text{min}^{-1}$ scale studies) were studied for deciphering reaction pathways. Additionally, model compounds which were difficult to feed in larger scale reactors due to volatility limitations during evaporation (i.e. levoglucosan) were effectively tested over a pressure range of 1-25 bar. Therefore, the micro-scale reactor system was modified in a way to offer testing with the entire range of available feedstocks at up to 35 bar hydrogen pressure with greater than 90% mass balance.

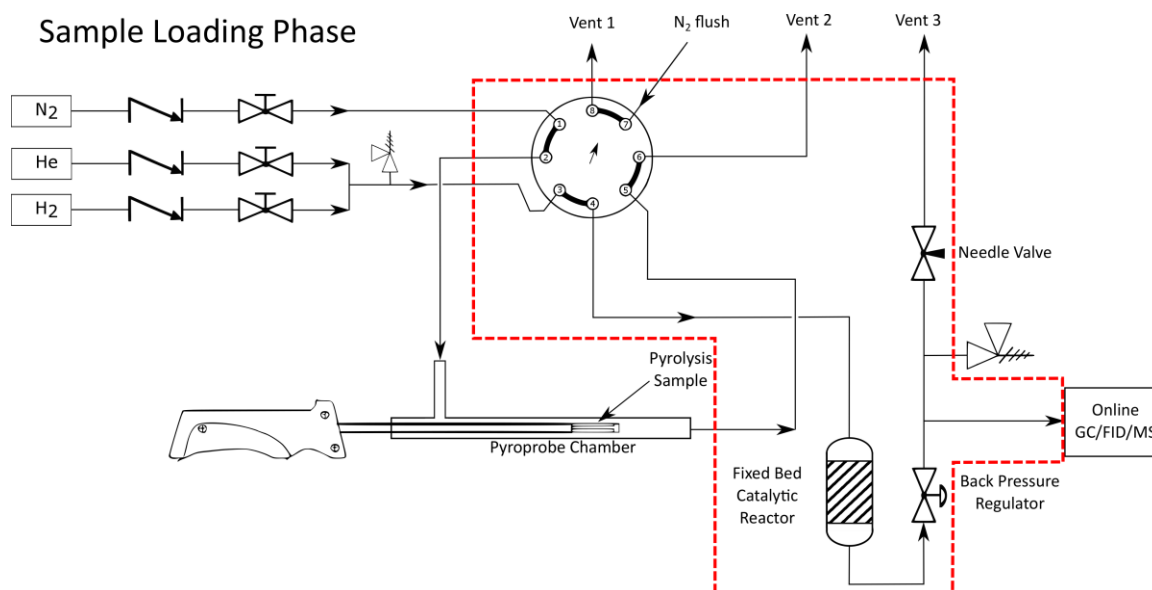


Figure 2.1 Schematic of experimental setup (Py-GC/MS) for fast hydrolysis and catalytic hydrodeoxygenation studies with biomass during the sample loading phase. Red box indicates the heated zone ($T=300^\circ C$).

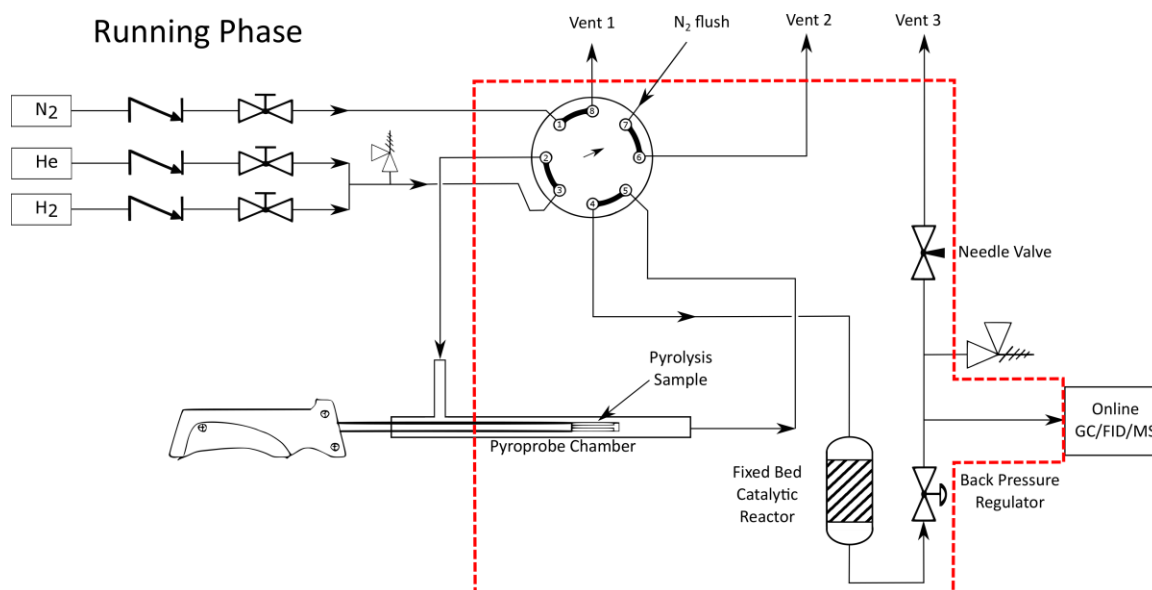


Figure 2.2 Schematic of experimental setup (Py-GC/MS) for fast hydrolysis and catalytic hydrodeoxygenation studies with biomass during the running phase. Red box indicates the heated zone ($T=300^\circ C$)

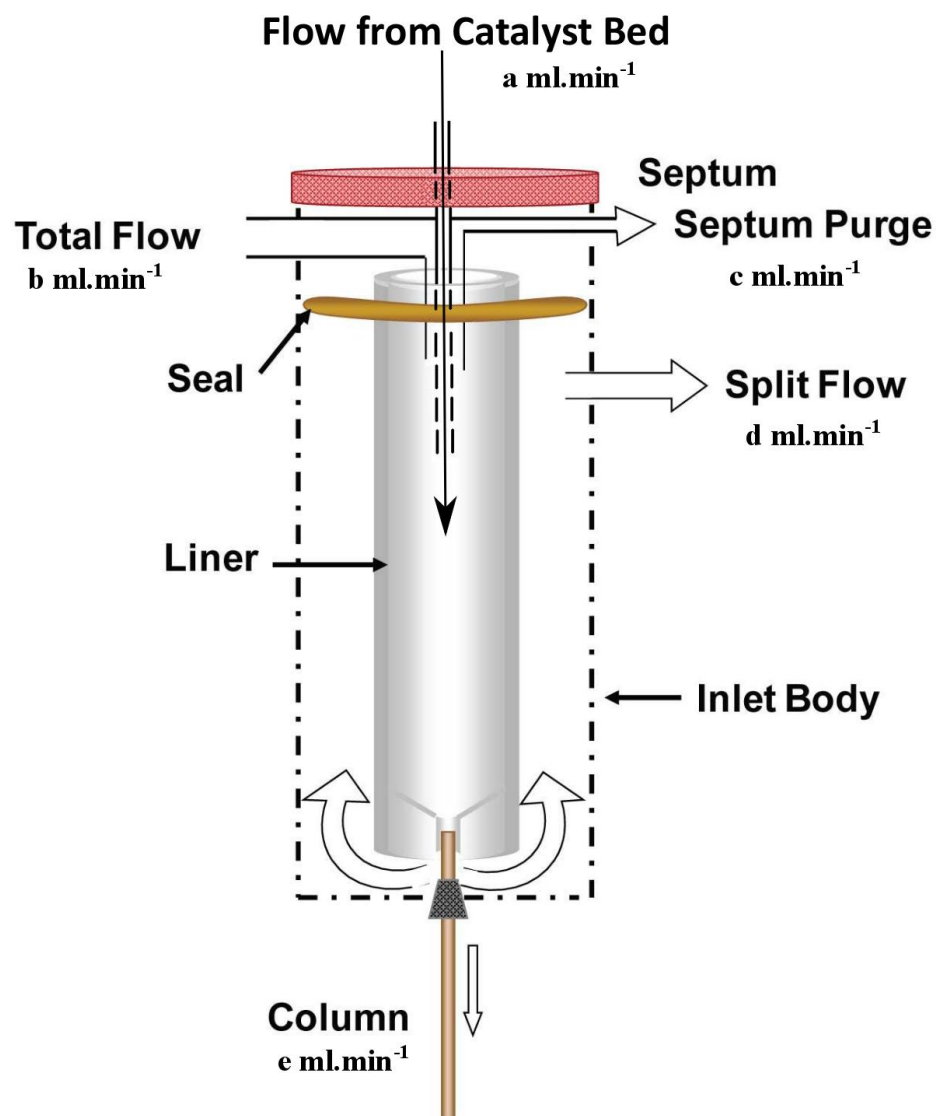


Figure 2.3 Pictorial representation of the internal components of a split/splitless inlet on a Agilent 7890A gas chromatographs with the modified flow patterns due to interfacing with the micro-scale semi-batch reactor system (also called Py-GC/MS system). Image adapted from an online source.⁴¹ Split ratio calculation is shown below.

$$\text{Split ratio} = \frac{a + d}{e}$$

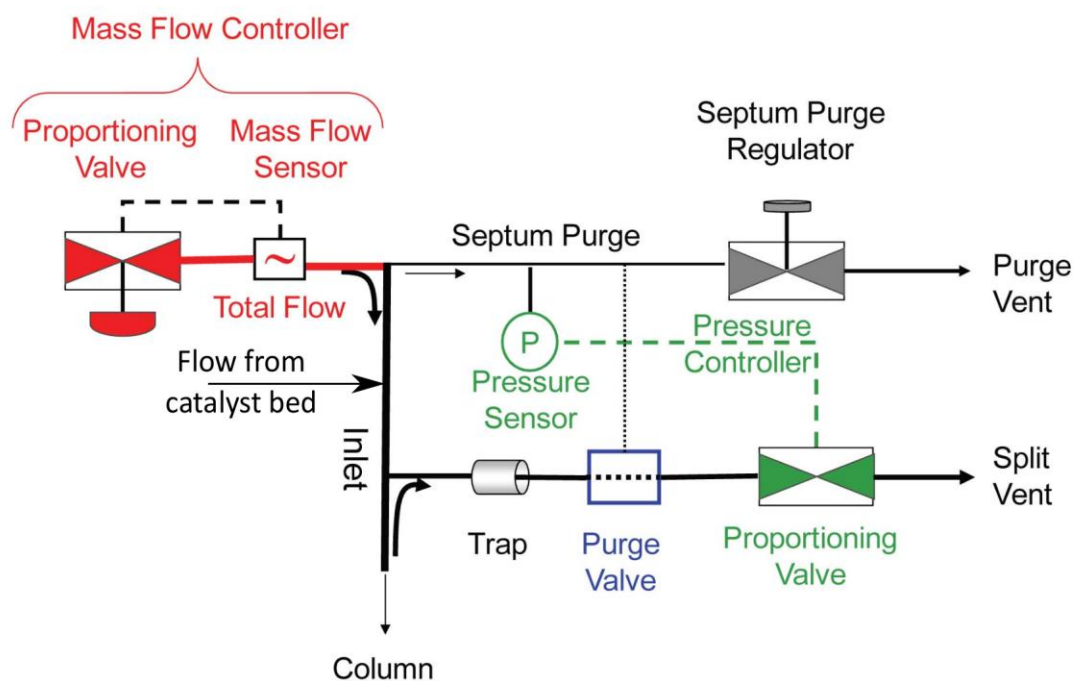


Figure 2.4 Schematic for flow and pressure control for a electronically controlled split inlet. The mass flow sensor is used in a feedback control loop (red) to control total flow to the inlet, and is the electronic equivalent to a mechanical mass flow controller. A pressure sensor located on the septum purge line is used in a feedback control loop (green) with the backpressure controller on the split vent line to control inlet pressure. Image modified from the source.⁴¹

2.3 GC column studies

Fast pyrolysis of biomass led to formation of a highly complex mixture of products which included primarily oxygen bearing organic molecules. The diversity of functional group along with the wide range of molecular weights of the observed species made analysis of the pyrolysis products a significant challenge. A single analytical method was not sufficient for analysis of the entire product distribution from pyrolysis of biomass or its individual constituents. Due to limitation of utilizing a single analytical technique (GC-

MS) for analysis of vapor phase pyrolysis products, significant strides were made to identify the shortcomings and develop solutions to increase the identification range and hence the mass balance. Selection of the GC column was very critical for quantitative analysis especially due to varying affinity of the various compounds for the solid phase in the GC columns. The choice of the solid phase, thickness of solid phase and length of the column were crucial parameters as was shown by studies performed with lignin model compounds and cellulose.

2.3.1 Quantitative analysis of dimeric molecules from lignin pyrolysis

Fast pyrolysis of the lignin component of the biomass is known to produce a distribution of molecules composed of monomeric, dimeric, and oligomeric depolymerization products. However, quantitative analysis of oligomers derived from lignin via GC-MS is considered to be a challenge due to their low volatility. Typically, liquid chromatography techniques (gel permeation chromatography, HPLC) have been used to identify and quantify the aforementioned oligomeric fraction of bio-oil.⁴² Liquid chromatography techniques are unsuitable for determining the accurate vapor phase product distribution due to secondary reactions accompanying condensation of the pyrolysis vapors.³⁷ Therefore, online analysis of vapor phase pyrolysis products is essential for understanding 1) the pathways governing depolymerisation of lignin during pyrolysis and 2) designing a downstream catalyst for direct vapor phase hydrodeoxygenation of the pyrolysis products.

In our efforts to develop a quantitative method of analysis of lignin derived dimeric species, we tested four different columns on the GC/MS (Table 2.1). Dimer **1** was chosen as a model dimer, and each column configuration was tested for online vapor phase analysis of its pyrolysis products. The observed product distribution has been divided into two major groups, namely monomeric products and dimer **1**. The overall mass balance for column 1 was ~40% with ~27% yield of monomeric products. For column 2, which has a lower solid phase thickness (0.25 μ m), the overall mass balance increased to ~72% with ~26% yield of monomeric products. We hypothesize that decreasing the solid phase thickness reduced the interactions of the dimeric molecules resulting in more molecules being able to elute out from the column. Column 3 did not have any solid phase and was unable to provide an adequate degree of resolution for the observed products, making identification and quantification very difficult. Column 4 was fabricated by using a fraction of the length from column 2 to reduce the total interactions with the solid phase while still retaining an adequate degree of resolution to delineate the observed peaks. The overall mass balance with column 4 was ~98% with 27% yield to monomeric products. From columns 1, 2 and 4 we observed an increase in the quantified amount of dimer **1** and other dimeric molecules, while the total amount of monomers remained constant. We conclude that increasing interactions with the solid phase can cause the dimeric species to get trapped in the column and hence not be detected. Table 2.2 shows the increase in the dimeric species observed when the total solid phase volume was decreased by two orders of magnitude from columns 1-4. It should also be noted that the dimeric species do not breakdown or degrade to form monomers, since the total amount of monomers observed over the different columns (each column having different elution times for dimer **1** –

Table C. 1) remained constant. Similar results were also obtained for the tetramer **3**, with an increase in the quantified dimeric species from column 1 to column 4 (Table 2.3). These results indicate that column 4 is suitable for quantitative analysis of lignin derived pyrolysis products comprised of monomers and dimers. This study has also demonstrated that one frequently used, commercially available configuration of GC column (Column 3) is not suitable for quantitative analysis of lignin derived dimeric species, since only a small proportion may be observed.

Table 2.1 List of the GC columns tested with the relevant parameters.

Column #	Column Name	Solid phase composition	Solid phase thickness / μm	Column Length / m	Column id / μm	Internal Surface area / mm^2	Solid phase volume / mm^3
Column 1	HP5	5PMPS	1.5	30	530	24892	37.4
Column 2	HP5-ms	5PMPS	0.25	30	320	15060	3.8
Column 3	Blank capillary	none	n/a	25	320	n/a	n/a
Column 4	HP5-ms	5PMPS	0.25	2.6	320	1285	0.3

Table 2.2 Lumped pyrolysis products of dimer **1** as a function of the columns tested.

Column #	Solid phase volume / mm^3	Dimer 1 / % wt of feed	Monomeric species / % wt of feed	Total mass balance / % wt of feed
Column 1	37.4	5.6	26.4	40.2
Column 2	3.8	39.4	26.3	72.0
Column 4	0.3	63.4	25.3	97.9

Table 2.3 Lumped pyrolysis products of tetramer **3** as a function of the columns tested.

Column #	Solid phase volume / mm ³	Dimeric species / % wt of feed	Monomeric species / % wt of feed	Total mass balance / % wt of feed
Column 1	37.4	3.6	42.8	68.7
Column 2	3.8	18.1	40.6	77.6
Column 4	0.3	30.9	41.5	94.4

2.3.2 Quantitative analysis of dimeric molecules from cellulose pyrolysis

From lignin pyrolysis studies it was evident that dimeric molecules from lignin pyrolysis could be quantitatively analyzed by the specially adapted column 4. Dimer **1** had a molecular weight of 320Da, and a molecular formula C₁₇H₂₀O₆ with three polar –OH groups and two methoxy groups. These groups are known to bind more strongly than other facets of the molecules with the solid phase in the columns having 5PMPS or analogous solid phases due to their polar nature. Other factors like overall molecular weight and volatility also play an important but secondary role in deciding the column characteristics. The dimeric species of interest from cellulose was cellobiosan (Figure 3.1), which had a molecular weight of 324 Da and a molecular formula C₁₂H₂₀O₁₀. Cellobiosan had a higher O/C ratio than dimer **1** along with six polar –OH groups and four ether linkages, making the molecule more susceptible to polar interactions with the column in addition to having a higher volatility. Additionally, direct injection of cellobiosan with column 2 resulted in observation of products only up to levoglucosan (~20 wt%) and lights. Cellobiosan was not observed even when the column was taken to the maximum operational temperature (280°C). This is in contrast to results with dimer **1** where dimer **1** was observed but in less than stoichiometric proportion. These results

confirmed the higher polarity and lower volatility of cellobiosan as compared to dimer 1 providing further hindrance of observation and quantification. Therefore, in an analogous experiment to dimer 1, cellobiosan solution was injected and column 4 was used for analysis. Cellobiosan was observed with ~32 wt% abundance along with degradation products, levoglucosan (~20 wt%) as shown in Table 2.4 Lumped product distribution from GC injection (inlet temperature 330°C) of a solution of cellobiosan in water (20% by weight).. The levoglucosan abundance was constant between column 2 and column 4 showing consistency within the experiments. It could be hypothesized that cellobiosan (like lignin derived dimeric molecules) did not decompose in the column but excessive interactions with the column solid phase resulted in cellobiosan remaining trapped in the column for time significantly greater than the analysis time. It could be possible that excessive interactions resulted in broadening of the cellobiosan peak to an extent that it was obscured into the GC baseline. The overall mass balance was ~94% thereby indicating that we had a near stoichiometric detection of molecules with molecular weight higher than levoglucosan (162 Da.). These experiments proved that decreasing the total molecular interactions with solid phase by reducing the length of the column facilitated observation and quantification of molecules previously thought “too heavy” for analysis via a GC-MS.

Column 4 was used for detection of cellulose pyrolysis products and cellobiosan was observed with ~1-3wt% abundance; however the entire mass balance quantification was difficult due to loss of resolution for the lights (C₁-C₄ oxygenates). This drawback could

be overcome by incorporating a cryo cooling feature in the GC-MS which would help in separation of the lights and detection of the entire range of molecules.

Table 2.4 Lumped product distribution from GC injection (inlet temperature 330°C) of a solution of cellobiosan in water (20% by weight).

Products	%wt of feed
Char*	15
Light oxygenates (C2-C4)	12.7
Dehydrated species (C5-C6)	6.5
Levoglucosan	20.2
Intermediates (>C6)	3.1
Anhydro-cellobiosan¹	4.3
Cellobiosan	32.5
Total	94.3

*estimated from cellobiosan solution (20% by wt) pyrolysis in quartz tube at 330°C, 1 – could not be conclusively identified and assumed to be anhydro-cellobiosan Py-MS studies with cellobiosan.

Cellobiosan injection in the gas chromatograph showed that cellobiosan did not evaporate cleaning, but decomposed to form levoglucosan and other lights. These results conclusively show that dimeric product from cellulose in bio-oil would break down during GC injections to form lights. Therefore, analysis of the bio-oil performed by a GC-MS will not be representative of the actual product distribution. This was demonstrated by carrying out analysis of the bio-oil obtained from the lab-scale continuous-flow millisecond residence time (70 ms) hydrolysis reactor, by LC-MS and GC-MS analytical techniques. The results, reported in Table 2.5, showed that the levoglucosan yield was higher with the GC-MS than with the LC-MS, which preserves the dimeric and monomeric structure. Cellobiosan and glucopyranosyl- β -glycolaldehyde were not observed since these studies were performed with the DB1701 column in which

dimeric molecules from cellulose pyrolysis could not be observed and therefore the overall mass balance was also lower than expected. However, these results showed that a GC-MS is not a suitable technique for analysis of bio-oil from cellulose and biomass by extension.

Table 2.5 Lumped product distribution from GC-MS and LC-MS analysis of the bio-oil obtained from the lab-scale continuous-flow millisecond residence time (70 ms) hydrolysis reactor.

Compound	LC-MS	GC-MS
Cellobiosan	9.9	0
Glucopyranosyl-β-glycolaldehyde	6.9	0
Levoglucosan	42.5	48.3
Glycolaldehyde	11.8	10.4
Other identified	11.9	16.2
% carbon accounted for	83	74.9

On the polarity scale, column DB1701 (60m X 250 μ m X 0.25 μ m) is more polar than HP-5ms (column 2) due to a difference in the solid phase composition, (14%-Cyanopropyl-phenyl)-methylpolysiloxane for DB1701, versus (5%-Phenyl)-methylpolysiloxane for the HP-5ms column. As a consequence the peak resolution was better on the DB1701 column when compared with HP-5ms, and was the initial column of choice of quantification of products from cellulose pyrolysis. However, comparison of the quantified data from the two columns for cellulose experiments showed a lower quantified yield for levoglucosan and other anhydrosugars with the DB1701 column (Table 2.6), which would be expected to have more polar groups than other lower molecular weight species being detected with the two columns. The total abundance for

other low molecular weight species were similar, however the overall mass balance was lower with DB 1701 column as compared to HP-5ms due to a relatively polar solid phase.

Table 2.6 Comparison of abundance of major products (wt% of feed) from cellulose pyrolysis 500°C for two different GC columns used for analysis.

Column	DB 1701	HP-5ms
Products		
Levoglucosan (+ isomers)	37.8	46.3
Glycolaldehyde	9.4	9.2
Other anhydrosugars	4.5	5.5
5-hydroxymethylfurfural	1.4	1.4
Methyl glyoxal	1.3	1.6
Furfural	0.5	0.4
1-hydroxy-2-propanone	0.5	0.3
DAGP	0.4	0.1
1,2-Cyclopentanedione	0.4	0.3
2-Propenal	0.3	n.d
Acetaldehyde	0.3	0.4
Overall mass balance	86.7	96

2.4 Conclusion

A micro-scale semi-batch reactor system was successfully modified from a commercial pyrolysis reactor system to incorporate online GC analysis at high pressure hydrogen conditions. This novel method of direct interfacing of a high pressure pulse reactor system with a GC-MS resulted in an increase in the overall mass balance to >90%. A fixed bed reactor was placed downstream of the pyrolysis zone for catalytic upgrading of pyrolysis products from various biomass related feedstocks. These capabilities were instrumental for pyrolysis studies as well as catalyst screening with a variety of

feedstocks like model compounds, reaction intermediates, biomass components, and intact biomass. Additionally, critical lessons in GC column selection were incorporated to modify GC columns to develop for the first time a quantitative analytical technique for analysis of lignin and cellulose derived dimeric species. These reactor and analytical modifications were critical for obtaining the results which have been reported in the subsequent chapters.

CHAPTER 3. FAST PYROLYSIS OF CELLULOSE

3.1 Introduction

Fast pyrolysis of lignocellulosic biomass, followed by catalytic upgrading is being regarded as promising thermochemical pathway for conversion of biomass to liquid fuel.⁴³ Biomass offers an abundant supply of carbon which can be renewably harvested and harnessing this carbon resource is extremely important for reducing the dependence on fossil based sources of fuel.²⁵ Fast pyrolysis involves rapid heating of biomass to a high temperature (~400-600°C) with the aim of depolymerizing biomass to produce vapor phase products which are condensed to obtain a complex mixture of compounds commonly referred to as bio-oil.²² Upgrading of bio-oil is essential for removal of oxygen (~30-40wt% of bio-oil) to increase the energy density by converting oxygenates to hydrocarbons which can be directly integrated within the existing transportation fuel infrastructure.^{19,44-46} The H₂Bioil process proposed direct vapor phase upgrading of the pyrolysis products via catalytic hydrodeoxygenation in presence of high pressure of hydrogen to eliminate the drawbacks associated with condensation of bio-oil.^{24-27,47} An accurate knowledge of the vapor phase product composition from biomass was essential for a rational catalyst design for effective upgrading of the pyrolysis vapors. On the other hand, knowledge of secondary reactions of the vapor phase pyrolysis products would be helpful for attaining control over the composition so as to tailor is for suitable upgrading

over a particular catalyst. Keeping the objectives in mind, cellulose and lignin pyrolysis studies were conducted and the nature of the primary products and the effect of vapor phase residence time on their transformations have been reported.

Cellulose has been the most extensively studied biopolymer⁴⁸ for understanding the underlying mechanism of pyrolysis and is aimed towards controlling the product distribution to minimum number of useful products or precursors to useful products. Cellulose depolymerization mechanisms have been investigated by using different types of theoretical modelling studies.⁴⁹ However, a majority of the studies have been based on weight loss profiles generated by thermogravimetric analysis (TGA) of cellulose.^{50,51} The heating rates used for these studies (max – $150^{\circ}\text{C}\cdot\text{min}^{-1}$) are insufficient to qualify for fast pyrolysis which typically have heating rate values greater than $100^{\circ}\text{C}\cdot\text{sec}^{-1}$.⁵²⁻⁵⁴ Additionally, lumped kinetic models which involve components like char, volatiles, tar and gas are unsuitable as they do not take into account the chemical reactions occurring during pyrolysis.⁵⁵⁻⁵⁹ Recently developed micro-kinetic models have been relatively successful at predicting the biooil composition from fast pyrolysis of glucose based carbohydrates.^{60,61} However, it is necessary to accurately to obtain the entire product distribution from cellulose/model compounds pyrolysis to verify as well as improve the model and develop a better understanding of the chemistry.^{62,63} Studies, both theoretical and experimental have been performed towards gaining a fundamental understanding of the reaction pathways during cellulose pyrolysis by studying surrogate molecules like cellobiose.^{62,64,65} Several sugars like cellobiose, cellotriose, cellotetraose, cellopentaose, and cellohexaose were investigated and the degree of polymerization (DP) was shown to

influence the product distribution with levoglucosan yield approaching that from cellulose with an increase in DP, thereby displaying the importance of the nature of the reducing end group during pyrolysis.⁶⁶ α -Cyclodextrin was observed as a suitable surrogate for cellulose with similar yields of products for thin film and powder pyrolysis however a high molecular weight renders it unsuitable for theoretical studies.⁶⁷ Based on these results cellobiosan and cellotriosan were investigated as surrogate molecules for cellulose, primarily due to absence of reducing end group chemistry while having a similar structure as that of cellulose.

The nature of primary products from cellulose pyrolysis has been debated in the literature with studies proposing formation of oligomeric products via secondary reactions of monomeric products.⁶⁸ Other studies propose simultaneous formation of oligomers, monomers and light oxygenates via depolymerization and subsequent volatilization of the fragments.⁶⁹⁻⁷³ Additionally, secondary reactions in the vapor phase have been shown to result in formation of light oxygenates.^{53,74,75} Condensation of vapor phase products may result in additional tertiary reactions in the liquid phase either during or after condensation, resulting in the bio-oil composition being different from that in the vapor phase.^{37,72,76} Presence of acids such as formic acid and acetic acid have been known to catalyze polymerization reactions amongst others.^{37,77} Therefore, online analysis of the vapor phase pyrolysis product distribution is important to avoid complications associated with condensation of bio-oil. Vapor phase product analysis was performed at different vapor phase residence time to study the nature of secondary reactions and also gain insight into the primary product distribution from cellulose pyrolysis.

3.2 Experimental Apparatus and Methods

3.2.1 Materials

The microcrystalline cellulose (50 μ m) used for all the experiments was purchased from Sigma-Aldrich. Cellobiosan (1,6-Anhydro- β -D-cellobiose) and Cellotriosan (1,6-Anhydro- β -D-cellobiose) was obtained from Carbosynth Limited.

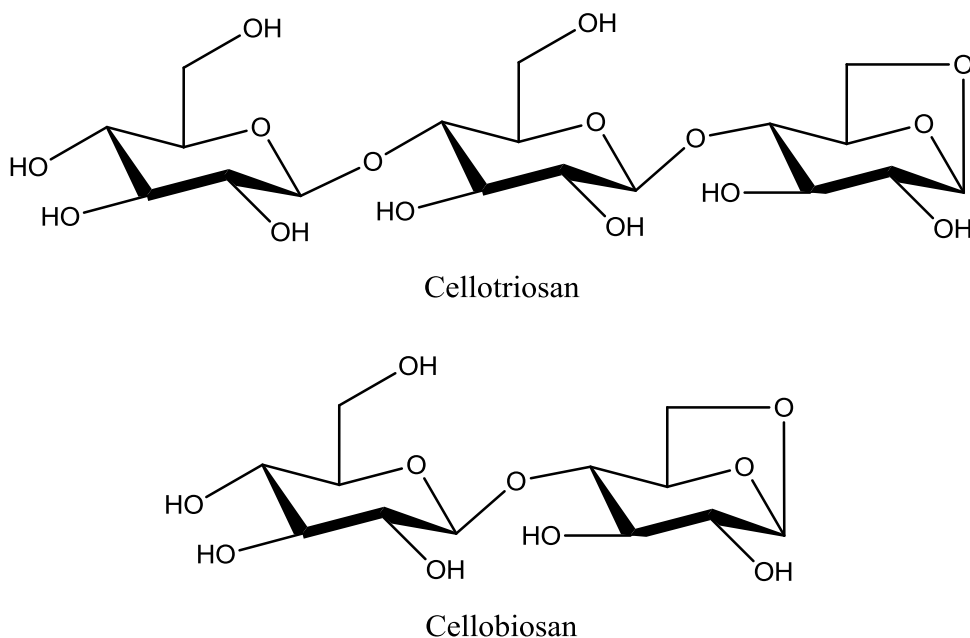


Figure 3.1 Chemical structure of Cellobiosan and Cellotriosan

3.2.2 Reactor description

Cellulose pyrolysis experiments were carried out using a Pyroprobe 5200 HP (CDS Analytical Inc.) connected to an online Gas Chromatograph (Agilent 7890A) equipped with a Flame ionization detector and a Mass Spectrometer (5975C) called the micro-scale semi-batch reactor (Py-GC/MS system). A resistively heated Pt coil was used as a heating source for pyrolysis of the lignin model compounds. A known weight of the reactant

sample was loaded in a quartz tube (0.15cm ID X 2.5cm length) which was subsequently placed in the annulus of the Pt coil. A heating rate of $1000^{\circ}\text{C s}^{-1}$ was used to attain a final temperature of 500°C during pyrolysis of the sample. The pyrolysis vapors were flushed out from the quartz tube by the carrier gas (He) and carried into the GC/MS. The GC was equipped with an HP-5ms column (solid phase – 5% diphenyl and 95% dimethylpolysiloaxane (5PMPS)) connected to a three way splitter with auxiliary gas input. The flow from the column was split to the FID and MS with synchronized peaks for quantification and identification, respectively.

The Py-MS system involved experiments with the direct interfacing of the Pyroprobe 5200 HP (CDS Analytical Inc.) with a linear quadrupole ion trap (LQIT) mass spectrometer and the detailed procedure is described here.^{62,63}

3.2.3 Loading and reactor operation

The sample (0.2-1 mg) was loaded in the quartz tube and the amount of sample was measured by weighing the quartz tube before and after the sample loading. No quartz wool was loaded in the quartz tube so that the carrier gas would flow through the tube and carry out the vapors efficiently. This was critical for accurate control of the vapor phase residence time after pyrolysis. The sample loading procedure was tested via carrier gas flow experiments to ensure that the sample was not dislodged by the flowing gas before pyrolysis.

After the sample was loaded, the quartz tube was placed inside the annulus of the Pt coil, which was mounted on a probe. The probe was then placed inside the pyrolysis chamber (Figure 2.1) and the air was flushed out using nitrogen. The 8 port valve was switched to introduce the reactant gas mixture (H_2 , balance He) and flush out the nitrogen, which subsequently pressurized the pyrolysis chamber to the desired operational pressure (Figure 2.2). The fixed bed reactor was kept empty for pyrolysis only experiments. The pyrolysis chamber was then heated by an external heater to a temperature of 300°C in ~ 10 s followed by the Pt coil being heated to a final temperature of 500°C at a heating rate of $1000^\circ\text{C}\cdot\text{s}^{-1}$. The pyrolysis vapors were carried out from the quartz tube to the GC-MS by heat traced tubing. The pressure was stepped down after the back pressure regulator so that it was within the acceptable range for the GC-MS (10-100 psi). Only a fraction of the flow was injected into the GC-MS to control the split ratio as well as protect the GC-MS from excessively high flow rates (>1 slpm) during the high pressure runs, while balance flow was vented. The split flow was controlled by a needle valve placed on the vent line. The split/splitless inlet of the GC was maintained at a temperature of 300°C and a split ratio in the range of 10:1 and 100:1 was used depending on the total pressure and flow rate through the fixed bed reactor. The actual split ratio was calculated by measuring the flow rates from the vent and GC split vent lines (Figure 2.3).

3.2.4 Product identification and quantification

The peaks observed in the gas chromatogram (FID) were quantified on the basis of calibrations made by using standard compounds. The identification of the observed products was performed by comparing the EI spectrum from the mass spectrometer to

those in the MS NIST (National Institute of Standards and Technology) database. CO and CO₂ were quantified by making calibrations with the major ion ($m/z=28$ for CO and $m/z=44$ for CO₂) in the mass spectrometer. The char analysis was performed by weighing the quartz tube after pyrolysis and obtaining the difference relative to the weight of the empty quartz tube. The overall mass balance was greater than 90% with the typical error in the product distributions being $\sim\pm 5\%$ based on duplicate experiments.

3.3 Results and Discussion

Investigation of the effect of various controlling parameters prevalent during fast pyrolysis provides valuable data and insight toward unraveling the dominant pathways by which cellulose unzips during pyrolysis. Temperature, heating rate, residence time, reactant gas, operation pressure, and mineral content have been proposed amongst others as important governing parameters for biomass pyrolysis. A systematic study of these parameters with respect to temperature, residence time and operation pressure was performed with the aim of understanding the product distribution, and developing suitable downstream catalysts for upgrading the product distribution from cellulose. The effect of heating rate was studied previously on the char formation from cellulose and it was observed that with an increase in the heating rate the amount of char formed decreased.⁷⁸ However, heating rate can be interpreted as a dynamic temperature based effect with different parts of the particle undergoing reactions at different temperatures for different period of time. Therefore, a prerequisite for the study with different heating rates was an understanding of the effect of temperature on the pyrolysis products from

cellulose, and hence the dominant pyrolysis pathways. It should be understood that a study of pyrolysis under purely isothermal temperature is nearly impossible due to intra-particle heat transfer limitations.^{74,79} In order to minimize the thermal lag, experiments were carried out extremely high heating rates ($1000^{\circ}\text{C}\cdot\text{s}^{-1}$) with the help of a resistively heated Pt coil. Additionally, a wide temperature range spanning $\sim 350^{\circ}\text{C}$ was used to study the effect of temperature on the products from cellulose pyrolysis.

3.3.1 Effect of temperature

Experiments were performed with cellulose and the pyrolysis vapors were analyzed via an online GC-MS-FID analyzer. The temperature was systematically varied within a temperature range of $350\text{-}700^{\circ}\text{C}$, which are considered the upper and lower bounds for pyrolysis.^{20,22} Cellulose pyrolysis yielded a highly complex mixture of products with >100 species being observed in the GC chromatogram. Therefore, these products were classified into different groups, based on the structure of the identified species, and the relative residence time as well as empirical formula for the unidentified species. A detailed pyrolysis product distribution from cellulose fast pyrolysis at 500°C , 1 bar pressure under inert conditions (He carrier gas) has been provided in Table 3.2.

Figure 3.2 shows the yield of char, liquid, and permanent gases from cellulose pyrolysis as a function of the pyrolysis temperature. The liquid fraction consisted of all the products detected in the GC-MS-FID analyzer, which would be collected as bio-oil in a continuous lab scale fast pyrolysis reactor system. Char was the residue left behind after pyrolysis while permanent gases consisted of methane, carbon monoxide (CO), and carbon dioxide (CO_2) which were quantified using the mass spectrometer. The amount of

char observed decreased substantially with an increase in the temperature from 350°C to 700°C from ~38% to ~5% thereby demonstrating the importance of choosing the correct pyrolysis temperature. On the contrary, the permanent gases increased in amount within the temperature range. The quantified liquid fraction increased up to 500°C and then slightly decreased at 700°C, indicating that for maximizing the liquid yield the operational temperature would have to be in the range of 500°C to 700°C. The products identified within the liquid fraction were sub-divided into three categories based on their origin and the number of carbon atoms per molecule. The first category labelled a “levoglucosan + isomers” consisted of levoglucosan, and other anhydrosugar molecules that were detected in the product distribution. The second category consisted of C₅-C₆ molecules, which were typically obtained by dehydration of the glucose based monomer in the cellulose polymer. The “dehydrated species” comprised of molecules like di-anhydrosugars, furfural, hydroxymethylfurfural (HMF), levoglucosenone, etc. The third category comprised of light oxygenates (C₂-C₄ range molecules) and was the undesired fraction from cellulose pyrolysis along with char and permanent gases. Light oxygenates were formed by C-C scission during pyrolysis and were a source of the less valuable light hydrocarbons (C₁-C₄) on hydrodeoxygenation. Figure 3.3 shows the variation in the product distribution within the liquid fraction in the temperature range of 350-700°C. The overall yield for C₅ and higher molecules was the highest at 500C temperature and decreases with an increase in temperature to 700°C. This was compensated by an increase in the light oxygenates and partly by an increase in the permanent gases. Therefore, an optimum temperature for obtaining the highest yield towards the liquid fraction with the least degree of C-C scission products was in the neighborhood of ~500°C. At 700°C, the

liquid product yield was comparable but with a higher proportion of light oxygenates which were formed by C-C scission as we approached the gasification regime temperature.^{20,75} Further experiments were performed in the temperature range of 480-580°C in the lab scale fast-hydrolysis cyclone type reactor system and have been reported here.⁶⁹ The narrower temperature range was used to obtain an optimum for the lab-scale reactor which had different hydrodynamic properties and hence heat transfer characteristics as compared to the micro-scale Py-GC/MS reactor system. Similar trends were observed in the lab-scale reactor with an increase in the light oxygenates with an increase in the temperature.⁶⁹ Cellulose hydro-pyrolysis experiments were also performed in the lab-scale continuous-flow millisecond residence time (70 millisecond) hydrolysis reactor, and while the product distribution was different from the other lab-scale reactor as well as the micro-scale pyrolysis reactor, the trends in the variation of the different category of products were identical.⁷⁰

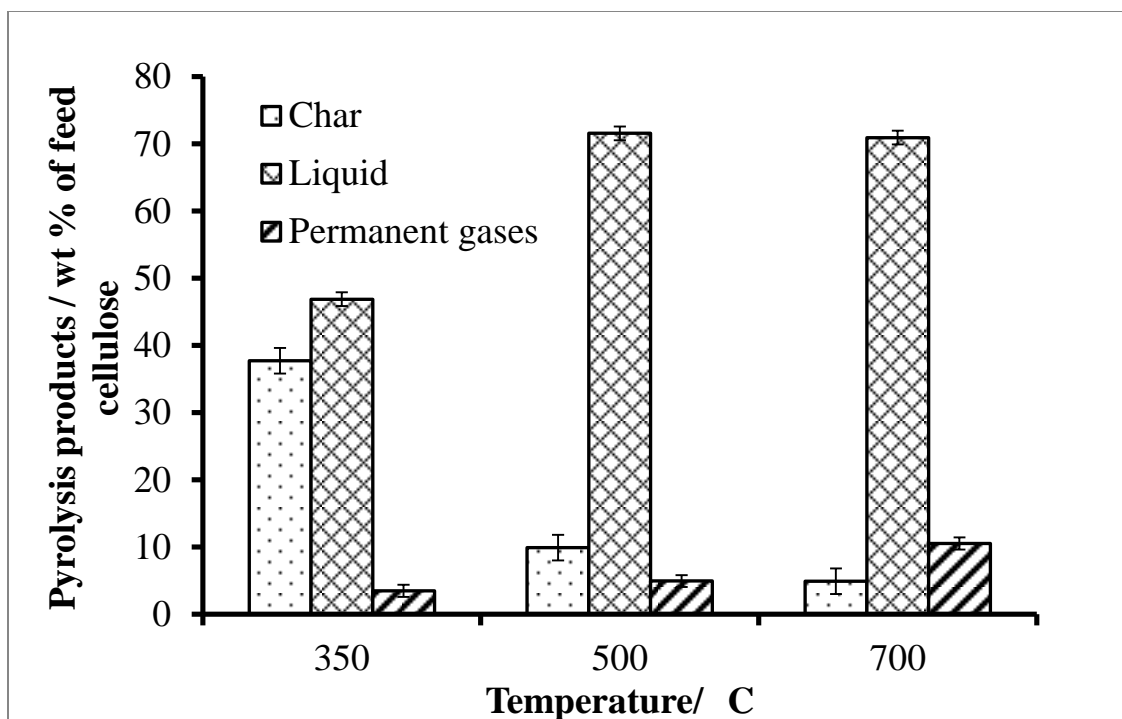


Figure 3.2 Product distribution from fast pyrolysis of cellulose as a function of pyrolysis temperature, grouped into categories: char, liquid (products expected to be a part of condensed bio-oil), and permanent gases (CO,CO₂, and methane).

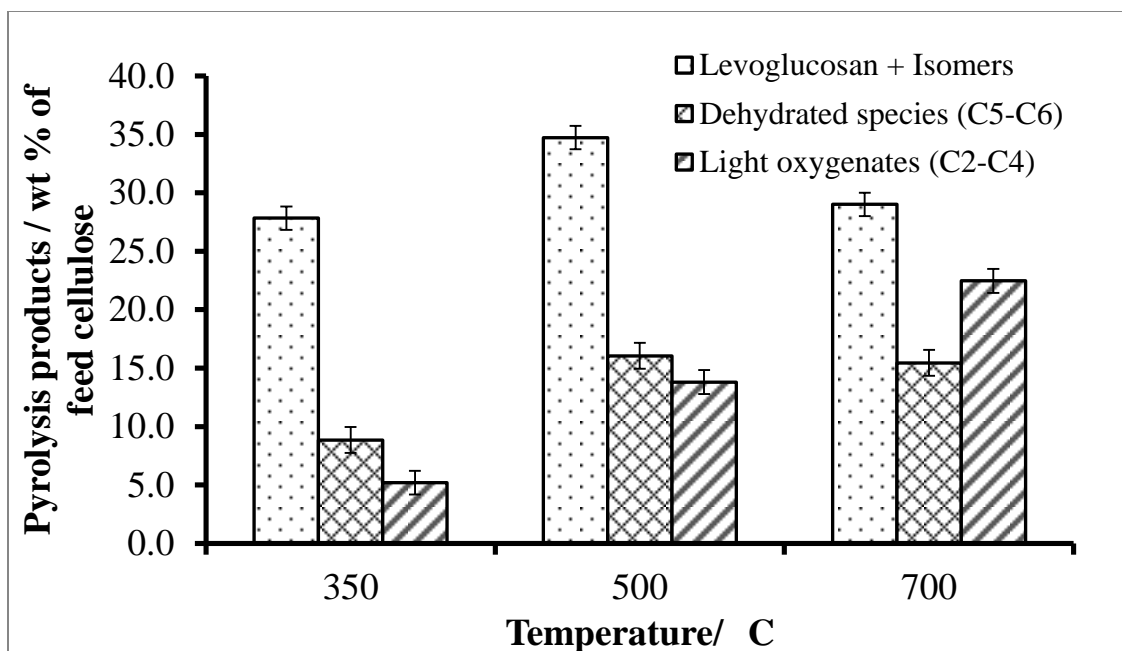


Figure 3.3 Product distribution from the “liquid” fraction of fast pyrolysis of cellulose as a function of pyrolysis temperature, grouped into categories based on product structure.

3.3.2 Effect of hydrogen as reactant gas

Pyrolysis of cellulose and biomass has been typically studied in an inert atmosphere (He, N₂), while the H₂Biooil process proposes an integrated fast-hydrolysis and hydrodeoxygenation step thereby requiring the pyrolysis to be carried out in the presence of hydrogen. To study the effect of hydrogen on the product distribution from cellulose pyrolysis, experiments were carried out in the micro-scale Py-GC/MS reactor system by using hydrogen as the carrier gas through the pyrolysis zone as well as the GC-MS. The product distribution obtained is represented within the five categories defined previously, namely, char, permanent gases, levoglucosan+isomers, dehydrated species, and light oxygenates. Figure 3.4 shows a direct comparison between the pyrolysis product distribution from cellulose in the presence of hydrogen and helium. The differences within

the product distribution were minor and could be attributed to experimental error. It was hypothesized that hydrogen gas does not influence any pathways during cellulose pyrolysis which could be due to presence of hydrogen as a gas and not in an activated form. Therefore, the mere presence of hydrogen during pyrolysis did not result in any observable deoxygenation of the cellulose pyrolysis products as compared to those with helium. Thus, it was imperative to have a catalyst which would activate hydrogen to achieve significant deoxygenation with the goal of producing hydrocarbons. To test the effect of high pressure hydrogen (up to 50 bar), experiments were carried out in the lab scale fast-hydrolysis cyclone type reactor system.⁶⁹ The results showed no discernable difference in the product distributions within experimental error, thereby demonstrating the need for a catalyst to facilitate deoxygenation in presence of hydrogen.

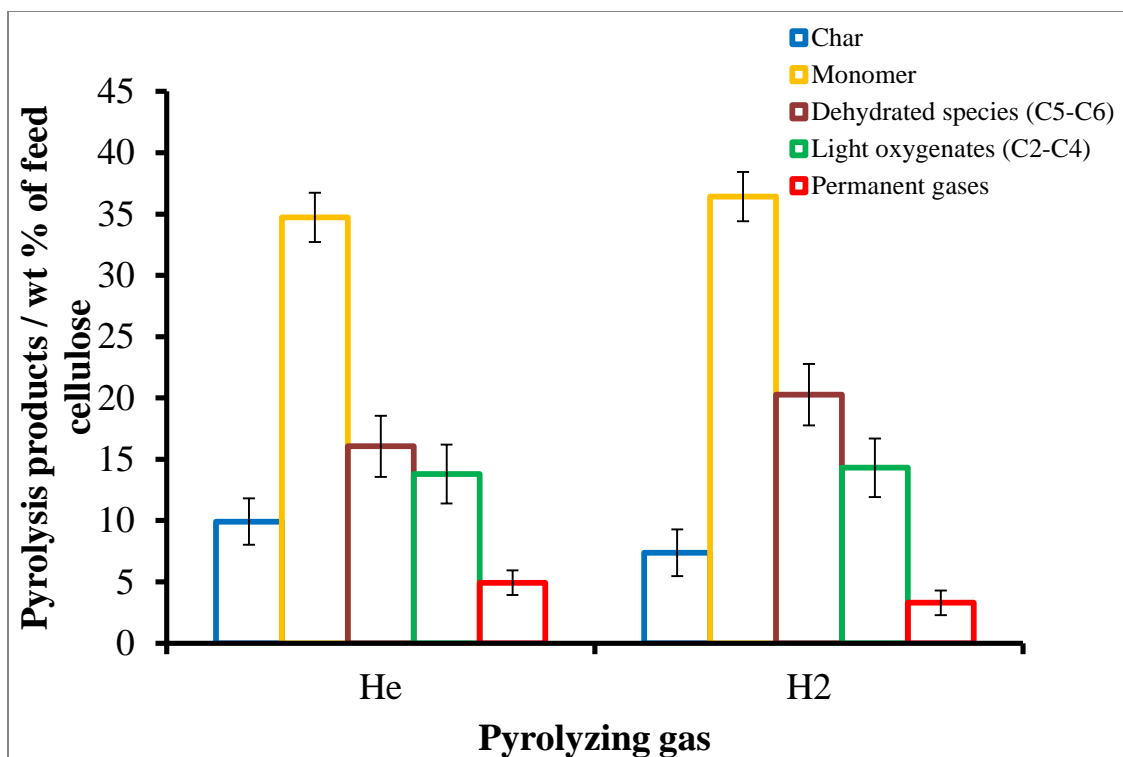


Figure 3.4 Product distribution from fast pyrolysis of cellulose as a function of the pyrolyzing gas (He, H₂).

3.3.3 Quantitative detailed product distribution from cellulose

Cellulose pyrolysis was carried out at 500°C at 1 bar pressure in inert atmosphere and the pyrolysis products were analyzed in the GC-MS-FID. The detailed pyrolysis product distribution has been provided in Table 3.2, showing an overall mass balance of 96±7 wt%. The major product observed was levoglucosan, accounting for ~44 wt% of the feed cellulose. The second most abundant product was glycolaldehyde ~9 wt% and accounted for a major portion of light oxygenates. Other anhydrosugars like 1,5-anhydro-4-deoxy-D-glycero-hex-1-en-3-ulose (ADGH), 1,4:3,6-dianhydro- α -d-glucopyranose (DAGP), 1,6-anhydroglucofuranose along with others made up for ~7.6 wt% of the product distribution. Numerous other identified and unidentified molecules with an abundance of

<1% combined to make up the remaining ~13 wt% of the product distribution which could be classified as bio-oil. ~11wt % of the cellulose was present in the form of char and ~6 wt% as permanent gases. The cellulose product distribution was comparable to those observed in literature^{67,71} with the abundances for levoglucosan and other molecules fluctuating by a large magnitude within literature. The variation in amount of levoglucosan amount from different sources in literature can be attributed to different types of reactor systems, which in spite of having the same pyrolysis temperature may have different actual heating rates which intern may depend on factors like reactor design, hydrodynamics, amount of sample pyrolyzed. For instance, in two comparable experiments, the cellulose was pyrolyzed as thin film versus as a powder in the same apparatus with drastically different product yields. Thin film pyrolysis which had a lower amount of sample had a lower levoglucosan yield (27%) as compared to powder cellulose pyrolysis (48%), while the glycolaldehyde yield from for thin film pyrolysis (7.9%) was higher than for powder pyrolysis (1.9%).⁶⁷ Intuitively, one would expect an opposite trend with the thin film having no heat and mass transfer gradients, resulting in lower degree of secondary reactions. It could be possible that different heat transfer regimes might promote various pathways and would require further investigation. Therefore, comparing results between different reactors may require an acute examination of heat transfer characteristics which in turn would depend on factors like nature of heat transfer, particle size amongst other previously listed factors. However, levoglucosan yield from powder cellulose pyrolysis is reported to be within a range of 40-58% and the results reported here are within the range observed in literature.

3.3.4 Pyrolysis of cellotriosan and cellobiosan

Cellulose is a polymer and has a molecular weight in excess of 10,000 Da., making highly non-ideal for exploring mechanistic options through controlled experimental studies or theoretical studies. As a consequence, several molecules having lower molecular weight have been investigated as surrogates in order to study the underlying mechanisms during pyrolysis. Glucose, cellobiose, cellotriose, cellotetraose, cellopentaose, and cellohexaose were investigated and the degree of polymerization was shown to influence the pyrolysis product distribution.⁶⁶ However, for the model compounds the levoglucosan yield was significantly lower than that for cellulose, with the levoglucosan yield increasing with an increase in the degree of polymerization and approaching towards that from cellulose. The reducing end group chemistry is thought to be responsible for lower yield of levoglucosan and conversely, the higher yield of lights. Theoretical studies have also shown the reducing end chemistry to be dominant for short chain molecules, unlike cellulose which has a very low proportion of the reducing end monomers.^{60,62} Cyclodextrin was observed as a suitable surrogate for cellulose with similar yields of products for thin film and powder pyrolysis, however its molecular weight is still too high for modelling studies. Therefore, in this study cellobiosan and cellotriosan (Figure 3.1) were investigated as surrogate molecules for cellulose partly due to their presence in minor quantity in the cellulose pyrolysis product distribution and also the absence of a reducing end thereby avoiding the drawbacks of previously studied model compounds in literature. Cellobiosan was observed with ~10 wt% yield in the lab-scale continuous-flow millisecond residence time (70 millisecond) hydrolysis reactor and could be considered as an intermediate during cellulose pyrolysis.⁷⁰ Cellotriosan was

also observed along with cellobiosan during low residence time (~150 ms) pyrolysis studies with direct analysis via a linear quadrupole ion trap (LQIT) mass spectrometer (Py-MS).⁸⁰

Cellobiosan, cellotriosan and cellulose were pyrolyzed at 500°C at 1 bar pressure in inert atmosphere and the pyrolysis products were analyzed in the GC-MS-FID. The lumped pyrolysis product distribution has been shown in Table 3.1. From the product distribution it can be observed that lumped product distributions were similar and the yield for levoglucosan + isomers was in the range of 45-52%. A striking difference was the yield of glycolaldehyde which was 2.4%, 6.6% and 9.2% for cellobiosan, cellotriosan and cellulose respectively. These differences could be attributed to a chain length effect, also suggesting two competing pathways, one for formation of levoglucosan (and anhydrosugars) and another for formation of glycolaldehyde (along with lights). Py-MS studies with cellulose have demonstrated the presence of intermediates which were precursors for glycolaldehyde formation with a greater relative abundance as compared to that with cellotriosan.⁸⁰ A competing pathway for formation of oligosaccharides from cellulose which in turn leads to formation of lights (and glycolaldehyde) from the reducing end was proposed by Degenstein et al.⁸⁰ The results reported here support this hypothesis since the amount of lights observed were the lowest for cellobiosan, and increased for cellotriosan and further more for cellulose. It should be kept in mind that for cellulose the amount of char formed was higher compared to cellotriosan and cellobiosan, thereby having a higher proportion of lights in the product distribution. Additionally, char formation was observed to a greater extent with oligosaccharides as compared to

corresponding anhydro-oligosaccharides,⁶⁶ lending correlational credibility to the proposed hypothesis which indicates that a higher proportion of oligosaccharides maybe formed from cellulose as compared to cellotriosan and cellobiosan. Nearly identical product distributions were obtained with cellotriosan and cellulose pyrolysis making cellotriosan an excellent surrogate capable of being used as a probe molecule for mechanistic studies (Table 3.2). Similar results were also obtained with the Py-MS system with cellulose, cellotriosan and cellopentosan having nearly identical mass spectrum.⁸⁰

Table 3.1 Quantitative lumped pyrolysis product distribution (wt % of feed) produced from the pyrolysis-GC/MS reactor for pyrolysis of cellobiosan, cellotriosan, and cellulose.

Product category	Cellobiosan	Cellotriosan	Cellulose
Char	5	5.8	10.5
Light oxygenates (C₂-C₄)	7.5	13.3	14.2
Dehydrated species (C₅-C₆)	23.2	16	14.5
Levoglucosan + isomers	51.1	46.5	46.3
Permanent gases	4.1	8.3	5.7
Water (assumed)	5	5	5
Total	95.8	94.8	96

Table 3.2 Quantitative detailed pyrolysis product distribution (wt % of feed) produced from the pyrolysis-GC/MS reactor for pyrolysis of cellotriosan and cellulose.

Compound	Cellotriosan	Cellulose
6 carbons		
levoglucosan	45 ± 2.9	44 ± 2.6
other anhydrosugars	4.5 ± 0.75	5.5 ± 0.35
1,6-anhydroglucofuranose	1.5 ± 0.37	2.6 ± 0.23
ADGH	1.6 ± 0.42	2.7 ± 0.23
5-hydroxymethylfurfural	1.4 ± 0.08	1.4 ± 0.07
levoglucosenone	0.22 ± 0.05	0.19 ± 0.06
DAGP	0.22 ± 0.05	0.14 ± 0.02
HMCP	0.13 ± 0.01	n.d.
5 carbons		
1,2-cyclopentanedione	0.59 ± 0.20	0.3 ± 0.01
furfural	0.37 ± 0.01	0.44 ± 0.06
2-methyl-furan	0.13 ± 0.04	0.08 ± 0
1,3-cyclopentadiene	0.08 ± 0.02	0.06 ± 0.01
3 and 4 carbons		
methylglyoxal	2.4 ± 0.48	1.6 ± 0.08
1-hydroxy-2-propanone	0.58 ± 0.20	0.26 ± 0.01
methyl vinyl ketone	0.48 ± 0.07	0.42 ± 0.02
DHHF	0.20 ± 0.03	0.23 ± 0.01
2-propenal	0.14 ± 0.02	n.d.
Light oxygenates		
glycolaldehyde	6.6 ± 0.5	9.2 ± 1.2
acetaldehyde and glyoxal	0.4 ± 0.12	0.4 ± 0.02
formaldehyde	0.25 ± 0.06	0.17 ± 0.03
Permanent gases		
methane	0.15 ± 0.04	0.15 ± 0.02
carbon monoxide	3.5 ± 0.28	2.1 ± 0.11
carbon dioxide	4.8 ± 0.57	3.6 ± 0.18
Other		
water (assumed)	5	5
char	5.8 ± 0.35	11 ± 1.2
unidentified and minor	9.0	5.5
Total	95 ± 7.6	96 ± 6.5

Abbreviations: n.d., not detected; ADGH, 1,5-anhydro-4-deoxy-D-glycero-hex-1-en-3-
ulose; DAGP, 1,4:3,6-dianhydro- α -d-glucopyranose; HMCP, 2-hydroxy-3-methyl-2-
cyclopenten-1-on; DHHF, dihydro-4-hydroxy-2(3H)-furanone.

Table 3.3 Lumped product distribution from GC injection (inlet temperature 330°C) of a solution of cellobiosan in water (20% by weight).

Cellobiosan Mass Balance	Wt %
Char*	15
Light oxygenates (C2-C4)	12.7
Dehydrated species (C5-C6)	6.5
Levoglucosan	20.2
Intermediates (>C6)	3.1
Anhydro-cellobiosan¹	4.3
Cellobiosan	32.5
Total	94.3

* estimated from cellobiosan solution pyrolysis in quartz tube at 330°C, 1 – could not be conclusively identified and assumed to be anhydro-cellobiosan Py-MS studies with cellobiosan.

3.3.5 Effect of vapor phase residence time

In order to develop a suitable catalyst for hydrodeoxygenation, it is very important to understand the vapor phase composition of the fast pyrolysis products of biomass. In this context, the vapor phase residence time between pyrolysis and catalytic hydrodeoxygenation becomes a critical parameter for tailoring the pyrolysis product distribution by promoting/mitigating the secondary reactions occurring in the vapor phase. However for the purposes of this study, investigation of vapor phase transformations were aimed at deciphering the primary vapor phase products from cellulose pyrolysis. As stated previously, utilizing a GC-MS to analyze bio-oil was not suitable since dimeric molecules could not be observed by using commercial columns. Additionally, dimeric species underwent transformation during vaporization in the GC inlet producing light molecules and making the observed chromatogram unrepresentative of actual bio-oil

composition. Concerns of secondary reactions during and after condensation also warrant a need for online analysis of the GC composition. As shown previously a novel method was developed for analysis of lignin and cellulose dimeric molecules (cellobiosan).

Cellobiosan was injected in the GC inlet (330°C) in solution form and the lumped product distribution obtained from the injections has been reported in Table 3.3. Due to the column dimensions the lights were bunched up together into an initial section of overlapping peaks, which made their identification and quantification nearly impossible (Figure B. 1). Only 32% of the cellobiosan was observed intact with other degradation products indicating that dimeric sugar molecules in the bio-oil cannot be efficiently analyzed via a GC-MS analytical system. A major degradation product observed was levoglucosan with ~20% abundance along with anhydro-cellobiosan (~5%). The amount of char formed was estimated with cellobiosan pyrolysis studies at identical temperature (330°C) with the Py-GC/MS system to be ~15%, and was substantially higher than that observed at 600°C (~5%). To the best of our knowledge, this is the first study to quantitatively observe cellobiosan with a GC-MS-FID system.

The effect of residence time on the pyrolysis products from cellulose was studied by varying the helium flow rate through the pyrolysis zone and the transfer line tubing carrying the products to the detector. These experiments were performed in the Py-GC-MS-FID and the Py-MS (LQIT) system and the results have been reported in Table 3.4. The mass spectrum had m/z abundances normalized to the highest abundance m/z (197) representing levoglucosan. The major products observed which had molecular weight

greater than levoglucosan and could be classified as dimeric molecules were m/z 359 and m/z 257. m/z 359 was a chloride adduct of cellobiosan, while m/z 257 represented glucosylpyrano- β -glycolaldehyde, which has been previously proposed and observed as an intermediate during pyrolysis of cellobiose.⁶² The abundance of these two compounds with respect to m/z 197 have been plotted as a function of residence time in Figure 3.5 and it showed a decrease in abundance of both the compounds indicating breakdown of those molecules to form lighter molecules, which may or may not be detected by the mass spec. These results demonstrated that vapor residence time had a significant impact on the product distribution from cellulose pyrolysis due to secondary reactions. If one were to extrapolate these abundances to time ≈ 0 s, it would provide a close approximation of the composition of the primary products from cellulose pyrolysis. Primary products are defined as the initial products to enter the vapor phase during pyrolysis. These primary products were comprised of dimeric species (cellobiosan, etc.) and possibly trimeric species which have been detected during previously reported experiments. It should be kept in mind that these abundances are not quantitative due to difference in ionization efficiency for different molecules, along with mass spectrometer parameters like tube lens voltage which were adjusted during experiments to provide adequate resolution of the heavier ions. For the purpose of all the residence time variation experiments all the other contributing factors remained constant to allow for accurate comparison. Quantitative experiments with Py-GC/MS system were also performed by varying in the residence time and cellobiosan was detected in the GC-MS with a yield of $\sim 3\%$ at the lowest residence time (~ 0.5 sec), the chromatogram is shown in Figure B. 2. The ratio of levoglucosan/cellobiosan increased with increase in residence time (14 to 38),

thereby supporting the results observed with the Py-MS system. However quantification of the lights was not possible due to numerous overlapping peaks, and for future studies a cryo cooling feature has been installed in the GC for resolution of the lights along with quantification of the entire product distribution up to dimeric species from cellulose pyrolysis product distribution. Lab-scale studies have also demonstrated these residence time effects with widely different yield for cellobiosan from the lab-scale continuous-flow millisecond residence time (70 millisecond) hydrolysis reactor (~10%) and the lab-scale continuous-flow cyclone type fast-hydrolysis reactor (~1%) which had a residence time of 2-5 seconds.

Table 3.4 Relative abundance of selected ions from the products of fast pyrolysis of cellulose detected by mass spectrometry (negative ion mode with ionization by APCI with chloroform), as a function of the vapor phase residence time. m/z 359 - chloride adduct of cellobiosan, m/z 257 – chloride adduct of glucosylpyrano- β -glycolaldehyde.

Flow rate / sccm	Vapor phase residence time / s	Relative abundance	
		m/z 359	m/z 257
60	1.7	23	10
160	0.6	45	19
350	0.3	69.5	43.5

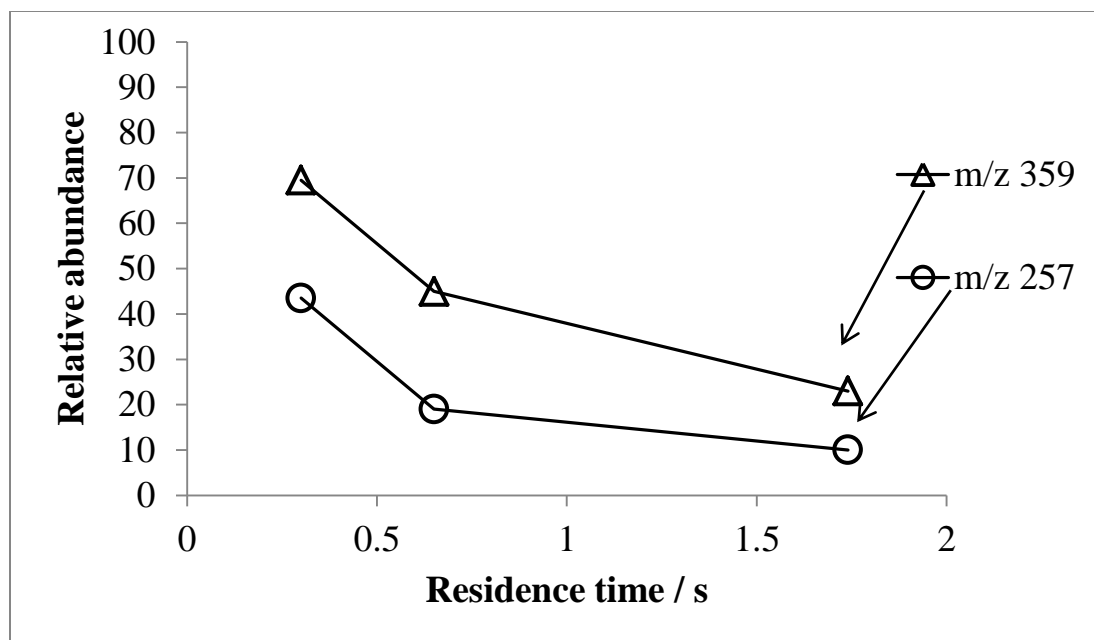


Figure 3.5 Relative abundance of selected ions from the products of fast pyrolysis of cellulose detected by mass spectrometry (negative ion mode with ionization by APCI with chloroform), as a function of the vapor phase residence time. m/z 359 - chloride adduct of cellobiosan, m/z 257 – chloride adduct of glucosylpyrano- β -glycolaldehyde.

3.4 Conclusion

Cellulose fast pyrolysis experiments were performed in the micro-scale pyrolysis GC-MS system with a mass balance of $96\pm 6\%$. Parametric studies were performed by first varying the pyrolysis temperature in the range of 350-700°C and an optimum pyrolysis temperature of $\sim 500^\circ\text{C}$ was obtained. The optimum temperature was such that the yield for “liquid” range molecules was maximized along with minimization of yield towards light oxygenates ($\text{C}_2\text{-C}_4$). Below 500°C, the yield toward char increased due to decrease in the net evaporation rates for molecules produced during pyrolysis, while at higher temperatures the yield for the undesired “light oxygenates” fraction increased due to increase C-C scission. Further studies on the lab scale with the fast-hydropyrolysis

cyclone type reactor system, and the continuous-flow millisecond residence time (70 milliseconds) hydrolysis reactor confirmed the observed trends. Presence of hydrogen as a reactant gas did not significantly alter the product distribution from cellulose pyrolysis when compared with that from inert gas, thereby suggesting that hydrogen activation was required for deoxygenation during the pyrolysis stage. Levoglucosan was the single most abundant product from cellulose pyrolysis with a yield of 44 wt%, while glycolaldehyde, which had a yield of ~9%, was second. Other products included anhydrosugars and a plethora of C₂-C₅ oxygenates. Minor quantity of dimeric molecules (~1-3%) were observed indicating that dimers were not very stable under pyrolysis conditions and underwent secondary reactions to transform to C₆ and lower oxygenate species. Residence time studies were performed with the Py-MS reactor system and showed a decrease in the relative proportion of m/z 359 (cellobiosan) and m/z 257 (glucosylpyrano-β-glycolaldehyde) with an increase in the residence time. Lab-scale studies were performed to verify these results with cellobiosan yield decreasing from ~10% to 1% with an increase in the residence time from 70ms to 3sec. Cellobiosan and cellotriosan were tested as surrogate molecules for mechanistic studies of cellulose pyrolysis. Cellotriosan was identified as a suitable candidate with minor variations in the pyrolysis product distribution when compared with cellulose. Collaboration between theoretical and experimental studies was used to predict mechanistic pathways prevalent during cellulose pyrolysis.

CHAPTER 4. FAST PYROLYSIS OF GUAIACYL LIGNIN MODEL COMPOUNDS WITH B-O-4 LINKAGES: EFFECT OF CHAIN LENGTH AND VAPOR PHASE RESIDENCE TIME

4.1 Abstract

The structure of native lignin differs from that of extracted lignin and therefore, well characterized synthetic guaiacyl (G) lignin model oligomers and a polymer were used to investigate β -O-4 bond scission under fast pyrolysis conditions. Identification and quantification of the entire range of vapor phase products from lignin pyrolysis is essential to understand the underlying mechanisms during pyrolysis as well as to design a suitable catalyst for downstream upgrading. To realize this goal, a new online GC/MS method was developed to enable quantitative analysis of greater than 90% of vapor phase lignin pyrolysis products, including dimeric molecules which were present in up to 70% yield. This new method enabled vapor phase residence time studies of lignin pyrolysis products, which showed the presence of a significant proportion of dimers (>19%), and oligomers, along with monomers amongst the primary products. The lignin-derived oligomers underwent secondary reactions in the vapor phase to form monomers, which increased in abundance with an increase in the residence time. Additionally, the effect of degree of polymerization (Dp) on char formation and pathways for β -O-4 bond scission were also investigated, with the char yield increasing with increase in Dp.

4.2 Introduction

Biomass is a major source of renewable carbon which can be converted to hydrocarbon fuel with the aim of reducing the dependence on fossil based sources. The CO₂ emissions from biomass-based renewable fuels can be considered to be part of a renewable cycle of carbon emissions. Fast pyrolysis followed by catalytic hydrodeoxygenation is considered a promising biomass conversion route to produce drop in hydrocarbon fuels.⁴³ Fast pyrolysis is the process of heating biomass to a high temperature (400-600°C), with high heating rates in the presence of inert and with a low vapor residence time before condensation of the bio-oil product.²² Typical crude bio-oil derived from fast pyrolysis of wood possesses a low energy density (17 MJ/kg), while that of petroleum is ~40 MJ/kg.^{22,43} This low energy density is primarily due to high oxygen content (35-40 wt%), and hence it is necessary to remove oxygen to <1% to produce a useful fuel. However, upgrading condensed bio-oil (via hydrotreating) has several drawbacks, including secondary reactions during revaporization of bio-oil leading to operational difficulties due to reactor plugging as well as catalyst coking.³⁹ To overcome these obstacles, the H₂Bioil process was proposed as an integrated high pressure fast hydrolysis and catalytic vapor phase hydrodeoxygenation (HDO) pathway for conversion of biomass to produce high energy density fuel.^{16,24-27} In order to develop a suitable catalyst for hydrodeoxygenation, it is very important to understand the vapor phase composition of the fast pyrolysis products of biomass. In this context, the vapor phase residence time between pyrolysis and catalytic hydrodeoxygenation becomes a critical parameter for tailoring the pyrolysis product distribution by promoting/mitigating the secondary

reactions occurring in the vapor phase. Neumann et al. have shown that presence of lignin dimeric species results in higher degree of coking over zeolites as compared to monomeric counterparts.⁸¹ In this study we have investigated the effect of vapor phase residence time on the product distribution from pyrolysis of model lignin oligomers.

Biomass is primarily composed of three types of polymers; cellulose, hemicellulose, and lignin, which are intertwined to make the structural framework of the plants. Although lignin only constitutes 10-30% of lignocellulosic biomass it accounts for 25-40% of the energy content of biomass, due in part to its higher C/O ratio than for cellulose and hemicellulose.⁸² Additionally, the presence of aromatic rings in the structural framework of the lignin polymer makes it a highly attractive source of a high-octane hydrocarbon fuel. Typically lignin is extracted from biomass by different types of processes, for example, the organosolv process.⁸³⁻⁸⁵ Numerous lignin pyrolysis studies have been performed with extracted lignin to study the effect of pyrolysis parameters on the product distribution. An increase in temperature was shown to decrease the amount of char left behind while increasing the yield of bio-oil.⁸⁶ The char yield from lignin pyrolysis was found to vary between 10-60% depending on the temperature and heating rate, while the yield of bio-oil was in the range of 20-60%.^{83,86-91} The products identified in the lignin pyrolysis bio-oils have a distribution of monomeric and oligomeric molecules. The formation of oligomers is a debated topic in literature with significant evidence for their formation by oligomerization of monomeric species in the condensed bio-oil.³⁷ However, in another study oligomeric molecules have been shown to be directly formed during pyrolysis of lignin and are proposed to be precursors to monomeric molecules.⁹² The

contribution of the oligomeric species to the initial vapor phase product distribution is unclear due to an absence of quantitative analytical tools for online analysis of oligomer-containing vapors. One of the objectives of this study is to understand the contribution of dimeric species to the initial product distribution via online GC/MS studies of pyrolysis of lignin model compounds.

In the literature, several studies have been published on pyrolysis of lignin where multiple analytical techniques were utilized due to the wide molecular weight range (50-2000 Da) of the detected products.^{37,88,92,93} It is clear that a single analytical technique is not capable of providing qualitative and quantitative results for condensed bio-oil. Common techniques used for identification of lignin pyrolysis products are GC/MS, MBMS (molecular beam mass spectrometry), FTIR, and mass spectrometry with an arsenal of different ionization methods.⁹⁴⁻⁹⁹ Amongst these, GC/MS is the most widely used tool for identification and quantification of monomeric products from lignin pyrolysis; whereas HPLC and GPC (liquid chromatography techniques) have been frequently used for analysis of oligomeric products in the bio-oil.^{37,42,92,97} Depending on the type of lignin pyrolyzed and the pyrolysis conditions, monomeric products may account for anywhere between 15 and 60 % of the product distribution.^{100,101} In a scenario where the amount of oligomers is >10%, GC/MS is not sufficient for quantitative analysis due to low volatility of oligomer molecules. Previously, Guillén and Ibargoitia¹⁰² have shown that lignin derived dimers can be qualitatively observed with GC-MS. However, there is a need to develop quantitative gas chromatography for lignin derived dimers since it would enable the analysis of a significant proportion of the vapor

phase product distribution. In the chapter 2, the development of a quantitative analytical technique (GC/MS) for analysis of the monomer and dimer fractions from lignin pyrolysis products was shown.

It is known that extracted lignin may undergo structural changes depending on the severity of the extraction process.^{85,103} Another shortcoming of extracted lignin is that it may have a higher proportion of impurities and mineral content, which has been shown to affect the product distribution and bio-oil yield.³⁶ As a result, synthetic model polymers have been previously employed for studying the pathways and mechanisms of lignin pyrolysis.^{100,104–109} Lignin is a heteropolymer with three major types of building blocks (coniferyl alcohol, sinapyl alcohol, and p-coumaryl alcohol) and at least 8 different types of linkages connecting the monomer units to form a cross linked polymer.⁸⁴ The β -O-4 linkage is the most abundant type of linkage and accounts for up to 50% of the linkages in softwood lignin. Therefore synthetic model dimers and polymers with β -O ether linkages have been studied widely to understand the bond cleavage pathways as well as mechanism. From previous studies it can be concluded that the mechanism of β -O ether bond cleavage is primarily dependent on two factors: 1) Substituents on the α and γ carbon atoms of the model compound, and 2) Temperature of pyrolysis. Jarvis et al.¹⁰⁴ have observed that below 1000°C the dominant reactions in cleavage of β -O ether bond are retro-ene and Maccoll reactions, while above 1000°C homolytic bond scission plays a prominent role as well.¹¹⁰ Huaming et al. have provided evidence based on theory and experiments for a dominant non-radical based mechanism for β -O-4 cleavage during pyrolysis at 600°C.¹¹¹ In another study with a model dimer, it was shown that the

presence of an –OH substituent on the γ carbon, modifies the β -O ether bond cleavage mechanism when compared with other substituents like –H.^{112,113} This indicates that choice of model compound also plays an important role in the governing mechanism for β -O ether bond scission, and the model compound should be an accurate structural representation of the natural lignin polymer. Therefore, in this study we have chosen synthetic model compounds with –OH substituent on the α and γ carbon atoms.

4.3 Experimental Apparatus and Methods

4.3.1 Reactor description

Lignin pyrolysis experiments were carried out using a Pyroprobe 5200 HP (CDS Analytical Inc.) connected to an online Gas Chromatograph (Agilent 7890A) equipped with a Flame ionization detector and a Mass Spectrometer (5975C). A resistively heated Pt coil was used as a heating source for pyrolysis of the lignin model compounds. A known weight of the reactant sample was loaded in a quartz tube (0.15cm ID X 2.5cm length) which was subsequently placed in the annulus of the Pt coil. A heating rate of $1000^{\circ}\text{C s}^{-1}$ was used to attain a final temperature of 500°C during pyrolysis of the sample. The pyrolysis vapors were flushed out from the quartz tube by the carrier gas (He) and carried into the GC/MS. The GC was equipped with an HP-5ms column (solid phase – 5% diphenyl and 95% dimethylpolysiloaxane (5PMPS)) connected to a three way splitter with auxiliary gas input. The flow from the column was split to the FID and MS with synchronized peaks for quantification and identification, respectively. Multiple columns with different dimensions (as shown in Table 2.1) were tested to obtain a suitable

configuration for quantitative analysis of lignin derived dimeric molecules. The details of the column selection procedure are provided in the results section.

4.3.2 Loading and reactor operation

The sample (0.2-1 mg) was coated on the inner surface of the quartz tube by application of mechanical force on the loaded sample via metallic tweezers and the amount of sample was measured by weighing the quartz tube before and after the sample loading. No quartz wool was loaded in the quartz tube so that the carrier gas would flow through the tube and carry out the vapors efficiently. This was critical for accurate control of the vapor phase residence time after pyrolysis. The sample loading procedure was tested via carrier gas flow experiments to ensure that the sample was firmly coated to the wall and was not dislodged by the flowing gas before pyrolysis.

After the sample was loaded, the quartz tube was placed inside the Pt coil, which is mounted on a probe. The probe was then placed inside the pyrolysis chamber (refer to Figure C. 2) and the air was flushed out using nitrogen. The valves were switched to introduce the carrier gas (He) and flush out the nitrogen. The pyrolysis chamber was then heated by an external heater to a temperature of 300°C in ~10 s to prevent condensation of pyrolysis vapors on the inner wall of the chamber. This was followed by the Pt coil being heated to a final temperature of 500°C at a heating rate of 1000°C s⁻¹. The pyrolysis vapors were carried out from the quartz tube, through the heat traced transfer tubing into the online GC-MS. The split/splitless inlet of the GC was maintained at a temperature of

300°C and a split ratio of 100:1 was used for the standard runs. For column 4, the oven was initially maintained at 33°C for 10 min, followed by a 10°C s⁻¹ ramp to 320°C. The final temperature was held for 10 min.

4.3.3 Product identification and quantification

The peaks observed in the gas chromatogram (FID) were quantified on the basis of calibrations made by using standard compounds. The identification of the observed products was performed by comparing the EI spectrum from the mass spectrometer to those in the MS NIST (National Institute of Standards and Technology) database. Some of the compounds which were not available in the database were identified by comparison with those from similar experiments performed with a pyrolysis-MS analytical technique. The char analysis was performed by weighing the quartz tube after pyrolysis and obtaining the difference relative to the weight of the empty quartz tube. The overall mass balance was greater than 90% with the typical error in the product distributions being $\sim\pm 5\%$ based on duplicate experiments.

4.3.4 Model compound synthesis

The lignin model compounds (Figure 4.1) used for pyrolysis in this study (with exception of Dimer 1) were synthesized at Purdue University. Dimer **1** (Guaiacylglycerol- β -guaiacyl ether, >97% purity) was obtained from TCI America. Trimer **2**, tetramer **3**, and trimer **4** were synthesized using the procedure outlined here.¹¹¹ Polymer **5** was synthesized by the procedure outlined by Kishimoto et al. and its structure was verified

by using NMR.¹¹⁴ For the synthesized molecules the structural conformity was tested by using ¹H-NMR and ¹³C-NMR studies.

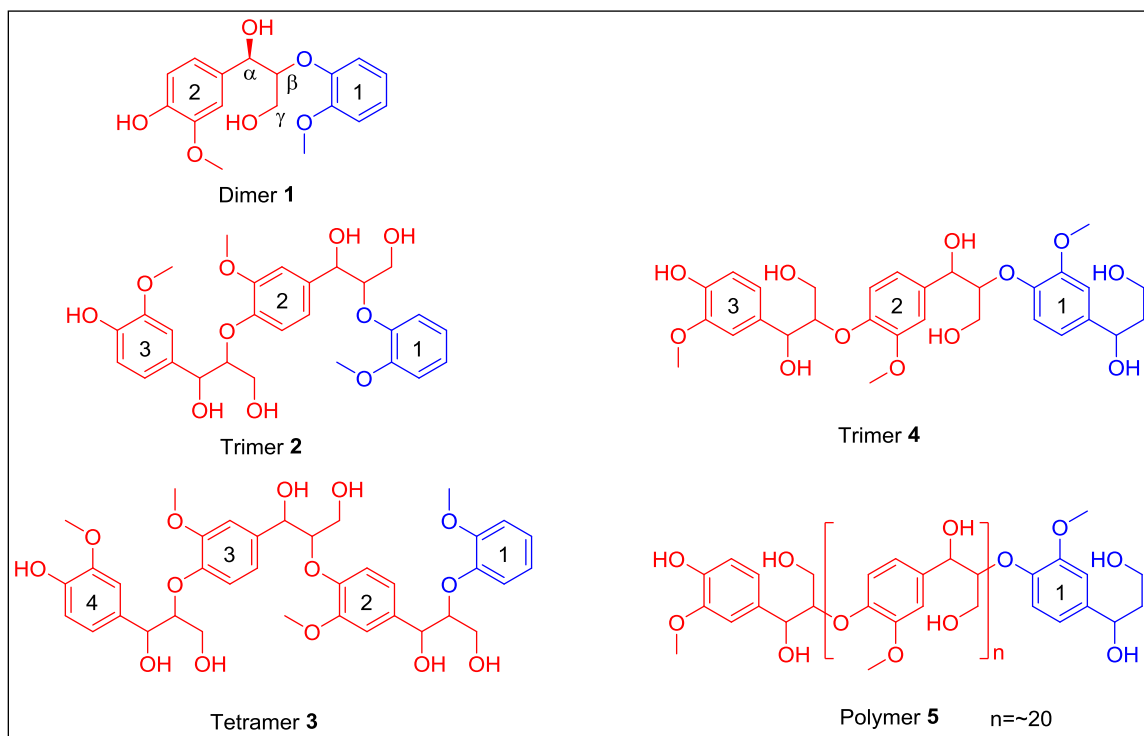


Figure 4.1 Lignin model compounds (**1-5**) used in this study. Numbers inside the rings are for notation purposes only, relevant end groups are highlighted in blue.

4.4 Results

4.4.1 Quantitative analysis of dimeric molecules using GC/MS

See Chapter 2.

4.4.2 Pyrolysis of Dimer 1

As shown in Table 2.2Table 4.1, the overall mass balance achieved during pyrolysis of dimer **1** was >97% when the column 4 was used for analysis of the products. The monomeric products accounted for 25.3 wt% of dimer **1** pyrolyzed. The detailed product

distribution of major identified molecules is provided in Table 4.1. The major monomeric products observed as a result of β -O-4 bond cleavage were guaiacol and coniferyl alcohol. Guaiacol was formed from the end group aromatic ring (blue aromatic ring in Figure 4.1), which does not have an alkyl substituent, with the expected ~12 wt% theoretical abundance, assuming that the moles of dimer **1** converted to monomers is equivalent to the total moles of guaiacol formed. However, since such end groups are not a significant part of the natural lignin polymer, guaiacol is not expected to be a major product from lignin pyrolysis. As a consequence, the high abundance of guaiacol can be considered as an artifact of the chosen model compound. Therefore, the major product from β -O-4 bond cleavage of dimer **1** was coniferyl alcohol. The dimeric products accounted for ~70% of the pyrolysis products of the dimer **1** model compound. It is also interesting to note that ~64 wt% of dimer **1** evaporated cleanly during pyrolysis, and was detected unaltered in the GC/MS.

4.5 Pyrolysis of Trimer **2**, Tetramer **3**, Trimer **4** and Polymer **5**

From the results in Table 4.1, it can be seen that similar monomeric products were observed for dimer **1**, trimer **2**, and tetramer **3**, with varying abundances. The varying proportions of the monomeric species can be attributed to, 1) varying proportion of guaiacyl end group (blue aromatic rings in Figure 4.1, Figure 4.2) varying degree of evaporation versus pyrolysis. It should be noted that for all the model compounds the major monomeric product observed was coniferyl alcohol. Among the dimeric products, only two molecules were identified (dimer **1** and 2-methoxy-4-(2-(2-

methoxyphenoxy)vinyl)phenol) due to lack of suitable matches in the NIST identification database for the other products. However, using MSⁿ experiments, dimeric molecular species which would also be expected to be a part of the pyrolysis product distribution here, have been identified. Dimer **1** was not detected from pyrolysis of trimer **4** and polymer **5** due to absence of the guaiacyl end group. However for all the model compounds, the abundance of the dimeric species was greater than or equal to 19 %, indicating that they made up a significant proportion of the vapor phase product distribution.

Table 4.1 Quantified pyrolysis product distribution (Wt % of starting model compound) of various lignin model compounds.

Compound	Dimer	Trimer	Tetramer	Trimer	Polymer
	1	2	3	4	5
Light Oxygenated Hydrocarbons (C₁-C₃)^(a)	1.8	8.9	7.0	7.3	7.4
Monomeric species^(b)					
Guaiacol (2-methoxy-phenol)	12.1	12.7	7.8	1.8	1.7
4-methoxy-4-methylphenol	n.d.	n.d.	0.1	0.2	0.5
3-methoxy-benzaldehyde	0.4	0.4	0.4	n.d.	n.d.
2-methoxy-4-vinylphenol	0.1	0.3	0.5	1.5	1.5
4-hydroxy-3-methoxybenzaldehyde	0.5	1.7	2.0	1.5	2.9
1-(4-hydroxy-3-methoxyphenyl)ethan-1-one	0.6	1.9	2.1	1.8	1.7
1-(4-hydroxy-3-methoxyphenyl)prop-2-en-1-one	1.5	3.5	3.8	3.2	2.5
4-(3-hydroxyprop-1-en-1-yl)-2-methoxyphenol	0.6	1.8	2.2	2.4	1.8
3-(4-hydroxy-3-methoxyphenyl)acrylaldehyde	0.3	0.9	0.9	1.6	1.1
Coniferyl alcohol (4-(3-hydroxyprop-1-en-1-yl)-2-methoxyphenol)	5.9	14.9	16.6	19.9	14.4
3-hydroxy-1-(4-hydroxy-3-methoxyphenyl)propan-1-one	1.8	1.6	1.3	0.7	0.4
<i>Other monomeric species</i>	1.7	2.0	3.8	9.9	10.4
Dimeric species^(b)					
Dimer 1	63.4	18.4	16.0	n.d.	n.d.
2-methoxy-4-(2-(2-methoxyphenoxy)vinyl)phenol	1.2	1.8	1.5	n.d.	n.d.
<i>Other dimeric species</i>	6.0	9.6	13.4	22.6	19.0
Char	n.d.	12.5	15.0	22.2	27.0
Total	97.9	92.9	94.4	96.7	92.3

(a) Composition - formaldehyde and residual solvents that were used during synthesis of model compounds.

(b) Structures for the monomeric and dimeric species are shown in Figure 4.2.

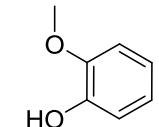
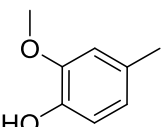
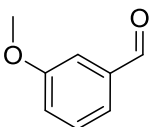
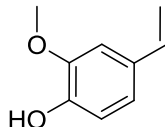
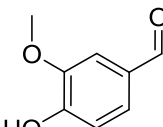
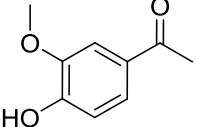
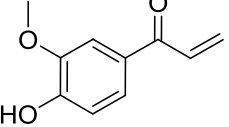
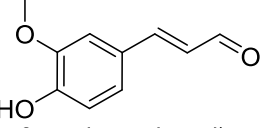
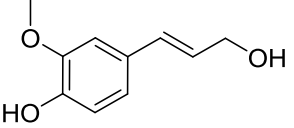
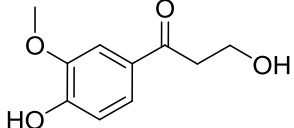
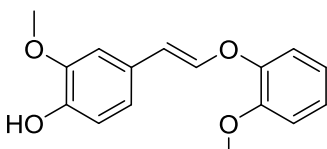
 2-methoxyphenol	 2-methoxy-4-methylphenol	 3-methoxybenzaldehyde
 2-methoxy-4-vinylphenol	 4-hydroxy-3-methoxybenzaldehyde	
 1-(4-hydroxy-3-methoxyphenyl)ethan-1-one	 1-(4-hydroxy-3-methoxyphenyl)prop-2-en-1-one	
 3-(4-hydroxy-3-methoxyphenyl)acrylaldehyde	 4-(3-hydroxyprop-1-en-1-yl)-2-methoxyphenol	
 3-hydroxy-1-(4-hydroxy-3-methoxyphenyl)propan-1-one		
 2-methoxy-4-(2-(2-methoxyphenoxy)vinyl)phenol		

Figure 4.2 Structures of the major products from pyrolysis of lignin model compounds.

4.6 Discussion

4.6.1 Product distribution from lignin model compounds

As discussed previously, a significant proportion (>60%) of the dimer **1** was detected intact after pyrolysis. A similar result was reported in literature by Kawamoto et al. with ~50% of dimer **1** evaporating under pyrolysis conditions.¹¹³ This result is a consequence of two competing phenomenon occurring while the model compound is being heated to the pyrolysis temperature, evaporation and structural change due to pyrolysis. The relative proportion of products obtained from evaporation and pyrolysis are primarily governed by the volatility of the reactant molecule, the heating rate, and temperature during pyrolysis. In this case, dimer **1** is not an ideal molecule to study the effect of pyrolysis parameters on the product distribution from lignin pyrolysis due to significant evaporation under fast pyrolysis conditions. However, studying pyrolysis of dimer **1** provided valuable information not only about the types of products that would be expected from pyrolysis of lignin, but also the reaction pathways. Two major reaction pathways were observed, 1) cleavage of the β -O-4 linkage to form guaiacol and coniferyl alcohol, 2) formaldehyde (γ elimination) and water loss. Studies by Kawamoto et al. have previously reported these two pathways during pyrolysis of dimer **1**.¹¹³ Pathway 1, which is the cleavage of the β -O-4 linkage was the major pathway for formation of monomeric species, while Pathway 2 was a minor pathway, which resulted in formation of the dimeric species, 2-methoxy-4-(2-(2-methoxyphenoxy)vinyl)phenol, as shown in Figure 4.3. In addition to these two pathways, we observed significant amounts of other monomeric products, which may have formed by alternate pathways as well as by

secondary transformations from coniferyl alcohol.¹¹⁵ All the major identified monomeric species have the characteristic phenolic and methoxy groups respectively at para and meta positions relative to the substituted alkyl chain as shown in Figure 4.2. Also, a major fraction (>85%) of the observed monomeric products (excluding guaiacol, from the end group) were composed of 10 carbon atoms, indicating a low degree of C-C bond scission during pyrolysis (Table C. 2). Monomeric products with 8 or 9 carbon atoms per molecule were observed due to carbon losses occurring from the substituted alkyl side chain.

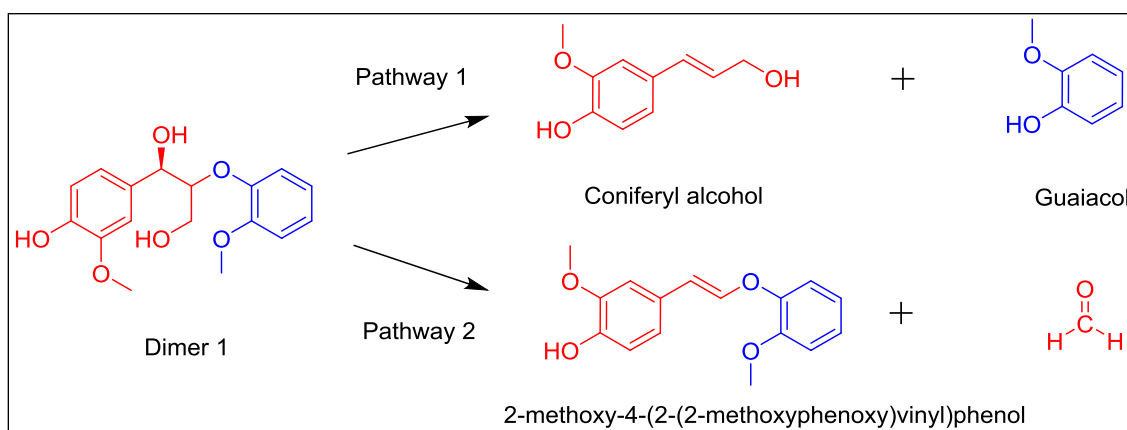


Figure 4.3 Two pathways observed during pyrolysis of dimer 1.

As stated earlier, the major monomeric product observed was coniferyl alcohol and had the highest absolute abundance for all the model compounds **1-5**. However, the absolute abundance varied for each of these compounds, primarily due to a change in the degree of polymerization, which resulted in a prominent guaiacyl end group effect (different relative proportion of guaiacol to monomeric fragments after β -O-4 bond scission). Additional causes include the extent of β -O-4 bond scission which was different for each

of the model compounds. One can hypothesize that the extent of β -O-4 bond scission is not only dependent on the volatility of the parent molecule but also the volatility of the molecular fragments formed during pyrolysis. For instance, if the β -O-4 linkage #1 in trimer **2** cleaves via pathway 1, it will produce a dimeric species dimer **6** and guaiacol (as shown in Figure 4.4). While with cleavage of β -O-4 linkage #2 it will produce dimer **1** and a monomeric product, coniferyl alcohol (Figure 4.4). The dimeric species with the guaiacyl end group (dimer **1**) will have a higher volatility compared to its counterpart (dimer **6**), in part due to its lower molecular weight (see Table C. 1 for estimated boiling points). Thus, there is a higher propensity for dimer **6** to undergo secondary reactions before being vaporized. This is evident from pyrolysis product distribution from trimer **2** in Table 4.1, where the total amount of dimer **1** observed is ~2 times that of the total amount of other dimeric species (the majority of which can be assumed to originate from cleavage of β -O-4 linkage #1). Furthermore model compounds trimer **4** and polymer **5** are devoid of the guaiacyl end group, which is reflected in a drastic decrease in the amount of guaiacol observed when compared with that for model compounds **1-3**. These differences make it difficult to directly compare the monomeric product distribution amongst the five model compounds. Therefore, to compare the monomeric product distribution, all the products were normalized by the absolute abundance (wt % of feed) of the major monomeric product, coniferyl alcohol. The results have been shown in Table 4.2. It is evident that the relative normalized proportion of all the major identified products (with the exception of 3-hydroxy-1-(4-hydroxy-3-methoxyphenyl)propan-1-one) is similar irrespective of the model compound **1-5** pyrolyzed. Guaiacol was formed in different proportions depending on the end group ratio (the ratio of blue to red rings from

Figure 4.1) for model compounds **1-3** and hence not included in Table 4.2. These results suggest that reactions occurring during β -O-4 bond scission are probably independent of the degree of polymerization, and that the nature of the end group (presence or absence of alkyl substituent on the guaiacyl end group) does not play a dominant role.

Table 4.2 Relative abundances of identified monomeric pyrolysis products normalized with respect to coniferyl alcohol.

Compound	Dimer	Trimer	Tetramer	Trimer	Polymer
	1	2	3	4	5
Monomeric species					
2-methoxy-4-vinylphenol	1.4	1.8	2.7	7.8	10.7
4-hydroxy-3-methoxybenzaldehyde	8.2	11.6	12.3	7.3	20.1
1-(4-hydroxy-3-methoxyphenyl)ethan-1-one	10.1	12.8	12.7	8.9	11.9
1-(4-hydroxy-3-methoxyphenyl)prop-2-en-1-one	25.9	23.4	22.7	16.3	17.0
4-(3-hydroxyprop-1-en-1-yl)-2-methoxyphenol	9.4	11.9	13.2	12.2	12.3
3-(4-hydroxy-3-methoxyphenyl)acrylaldehyde	5.9	5.8	5.4	8.0	7.7
Coniferyl alcohol (4-(3-hydroxyprop-1-en-1-yl)- 2-methoxyphenol)	100.0	100.0	100.0	100.0	100.0
3-hydroxy-1-(4-hydroxy-3- methoxyphenyl)propan-1-one	31.2	10.9	8.1	3.6	2.8

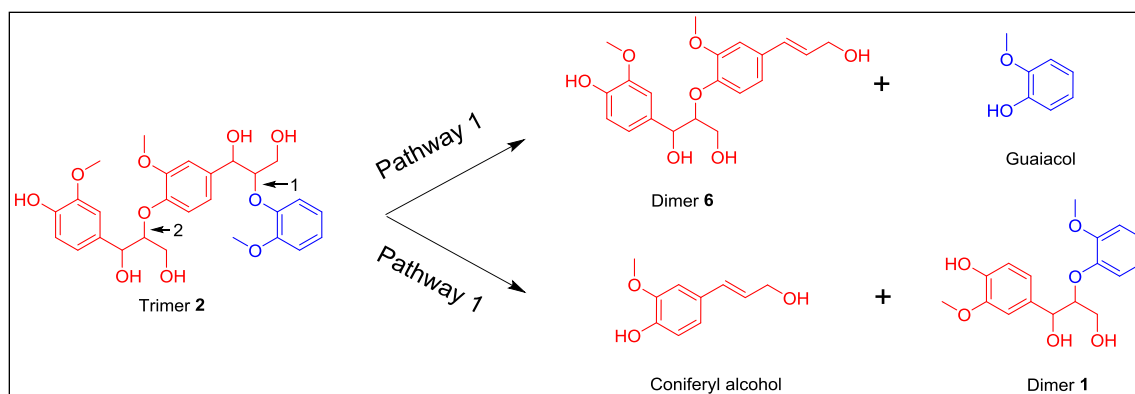


Figure 4.4 Transformation of trimer **2** to potential products via pathway 1.

4.6.2 Char formation

Char is the residue that is left behind during pyrolysis of biomass, and numerous studies have been carried out on char formation during pyrolysis of extracted lignin. Lignin is considered a significant contributor to char during biomass pyrolysis, and therefore it is necessary to understand the factors which influence char formation with the goal to increase the carbon yield. Here, we have systematically studied the amount of char formed as a function of the degree of polymerization by keeping all the other influencing parameters constant. Additionally, there was no influence of inorganic impurities on char formation since pure synthetic lignin oligomers have been used in this study. It was observed that the quantity of char formed increased with an increase in the degree of polymerization for model compounds **1,2,3,5** as shown in Figure 4.5. The degree of polymerization is indirectly linked to the volatility of the parent molecule as well as the number of bonds that need to be broken to form fragments, which have a rate of vaporization that is high relative to the rates of subsequent reactions. Therefore, it seems logical that char formation was proportional to the degree of polymerization of the lignin

model compounds. Kotake et al. have predicted a “polymer effect” which states that, the pyrolysis fragments tend to spend more time on the heated surface when more bonds are required to be broken, resulting in greater extent of char formation.¹¹⁶ A comparison of the char yields between trimer **2** (12.5%) and trimer **4** (22.2%) showed a notable increase in the amount of char formed for trimer **4**. In the case of trimer **4**, the end group has an alkyl substituent which results in an increase in the molecular weight and as well as the predicted boiling point of the compound when compared to trimer **2** (Table C. 1). Additionally, the monomers/dimers formed from the substituted end group as a result of β -O-4 bond cleavage have a lower volatility, as compared to those from trimer **2**. These factors could explain an increase in the amount of char formation, which progressively increases up to that produced by polymer **5** ($D_p = 20$).

An additional factor for char formation could be the concentration of coniferyl alcohol species at the pyrolysis surface. Studies have shown that when heated to temperature greater than 250°C, coniferyl alcohol undergoes polymerization reactions in addition to char formation, evaporation, and secondary reactions to form other monomeric species.¹¹⁵⁻¹¹⁸ On further investigation under pyrolysis conditions of 500°C, formation of dimeric molecules from coniferyl alcohol was observed along with formation of char, ~10% (Table C. 4). Only ~35% of the coniferyl alcohol evaporated intact, proving that it is an extremely reactive species and could be responsible for formation of char during pyrolysis of the model polymers. Condensation reactions have also been observed with lignin monomers having a α,β -unsaturated double bond ($C\alpha=C\beta$), which could be precursors for polymerization and eventual formation of char.¹¹⁷ The expected

concentration of coniferyl alcohol species and its oligomeric counterparts at the pyrolysis surface is also proportional to the degree of polymerization (Figure C. 3). Therefore polymerization of pyrolysis fragments (monomeric and oligomeric) with $C\alpha=C\beta$ could also result in formation of char which has been shown to possess a polyaromatic structure.⁸⁶

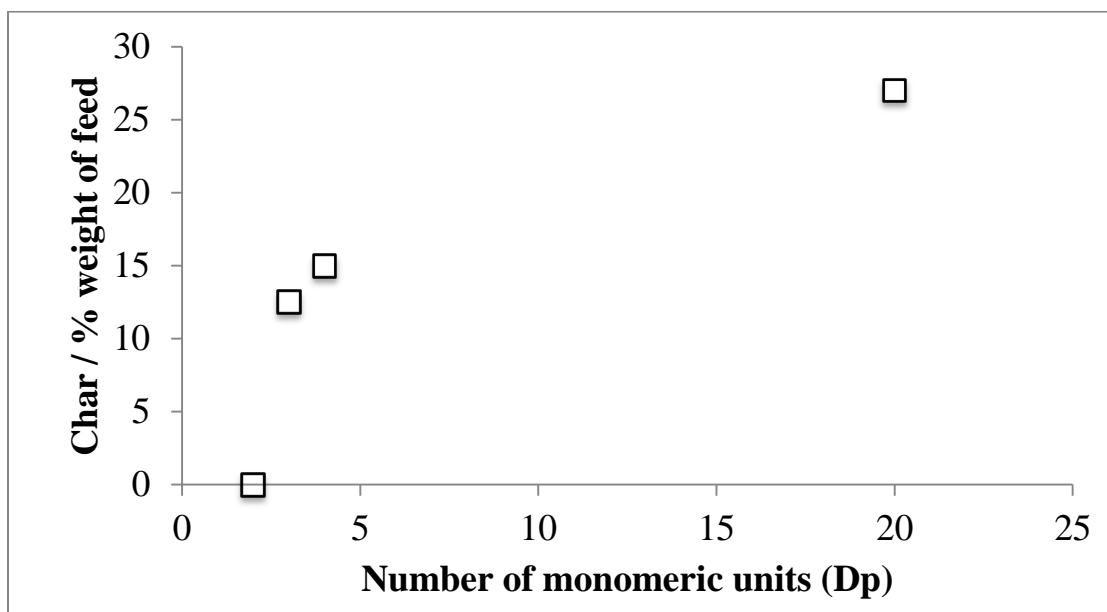


Figure 4.5 Char yield as a function of the degree of polymerization of the lignin model compounds. Data point of Dp=3 is for trimer **2**.

4.6.3 Effect of vapor phase residence time

Vapor phase residence time is considered to be a critical parameter in controlling the product distribution from fast pyrolysis of biomass. Previous studies have suggested that the primary products of lignin pyrolysis are monomeric compounds which subsequently undergo secondary reactions that lead to the formation of oligomers.^{37,97} There is evidence that these reactions occur during/after condensation of the pyrolysis vapors and

are aided by presence of acidic species in the bio-oil. However, it is unclear whether the oligomerization reactions also occur in the vapor phase. Hoekstra et al. performed vapor phase residence time studies on pyrolysis vapors from pine wood and observed a decrease in the yield of pyrolytic lignin (from bio-oil) with an increase in the residence time.³⁶ This result points towards a decrease in the average molecular weight of the product distribution from biomass, however there is little information on the composition of the pyrolytic lignin and the condensed bio-oil. In order to understand the nature of these secondary reactions, we performed lignin pyrolysis experiments at different vapor phase residence times by varying the gas flow rate through the pyrolysis zone. It should be noted that condensation was avoided by having online analysis GC/MS capability and fully heat-traced transfer lines. The residence times were calculated based on the gas flow rate and the estimated volume between the sample quartz tube and the GC column. The pyrolysis and analysis conditions were identical for these experiments and any change in the product distribution was attributed to a change in the vapor phase residence time.

These experiments were limited to the two model compounds, dimer **1** and polymer **5**, and the residence time was varied from 0.5 s to 3 s while maintaining the temperature of the entire post pyrolysis zone at 300°C. At the lowest residence time (0.5 s), the pyrolysis product distribution from dimer **1** was comprised of ~63% of the dimer **1**, and as the residence time was increased to 3 s the amount of dimer **1** observed went down to ~24 % (Figure 4.6). This was indicative of the dimer **1** undergoing secondary transformation to form other products in the vapor phase. The decrease in the dimer **1** abundance was simultaneously accompanied by an increase in the total monomeric products observed,

thereby providing evidence for β -O-4 bond scission in the vapor phase. The most abundant monomeric product observed was coniferyl alcohol and its yield increased with an increase in the residence time. 2-methoxy-4-(2-(2-methoxyphenoxy)vinyl)phenol (MW 272 Da.) also showed an increasing trend lending credence to the existence of a parallel pathway 2 for formation a dimeric species with a lower molecular weight than the parent species (MW 320 Da.). These results illustrate that the average molecular weight of the pyrolysis product distribution decreases with an increase in the vapor phase residence time and is attributed primarily to the β -O-4 bond scission.

Polymer **5** was also pyrolyzed under identical conditions to verify the observations from the residence time studies with dimer **1**. As stated previously, we were unable to identify the structures of dimeric species that were produced during pyrolysis of the polymer **5**. As a consequence, the entire product distribution in the dimer range has been lumped together. The total quantified dimeric products account for ~19% at the low residence time of 0.5 s and decrease to ~13.5% at a residence time of 1.6 s. The overall yield to the dimeric products is low compared to that from dimer **1** in part due to lower volatility of the dimeric products formed from the polymer as they are expected have a substituted alkyl side chain on both the aromatic rings (i.e. dimer **6**, Figure C. 1). These results indicate that the initial vapor phase products from pyrolysis are formed by thermal depolymerization of the lignin oligomers and are volatile enough to vaporize. These initial vapor phase products include monomers and dimers and possibly a minor fraction of trimers. The estimated boiling point for trimers is in excess of 690°C (Table C. 1) and hence trimers are expected to constitute only a minor fraction of the vapor phase under

our standard pyrolysis conditions (500°C). These products are then subjected to secondary reactions as they traverse through the heat traced tubing at 300°C before being quenched (33°C) at the inlet of the online GC-MS. As a consequence of these secondary reactions, the dimers and trimers breakdown to form monomers.

4.6.4 Primary products of lignin pyrolysis

There is no general consensus in the literature about the primary products of pyrolysis, which are generally regarded as either the first products to enter the vapor phase, or in a somewhat different interpretation, the major quantifiable products of pyrolysis. Analysis of these primary vapor phase products holds the key to understanding the pyrolysis pathways. In this study, both monomeric and dimeric species were observed at the lowest residence time of 0.5 s for lignin model compounds. These dimeric species undergo secondary reactions with an increase in the residence time. If one were to extrapolate this backwards, it would be prudent to say that the primary products of pyrolysis are comprised of monomers, dimers and possibly trimers. This is in agreement with results in literature from Zhou et al.,⁹² who observed oligomers as primary products in their wire mesh reactor with instant quenching of the vapors. These experiments were performed with organosolv lignin feedstock, under vacuum conditions and high heating rate of 8000°C.s⁻¹. Therefore, when addressing the issue of primary products it is important to acknowledge the role of nature of feedstock and pyrolysis conditions under which these products are detected. While oligomeric fragments are formed by depolymerization of lignin, their abundance in the vapor phase as primary products will depend on their volatility under the local temperature during pyrolysis. From this study, it can be

concluded that primary vapor phase products from lignin pyrolysis are a mixture of monomers and oligomers whose relative proportion is dependent on their structure and the pyrolysis conditions.

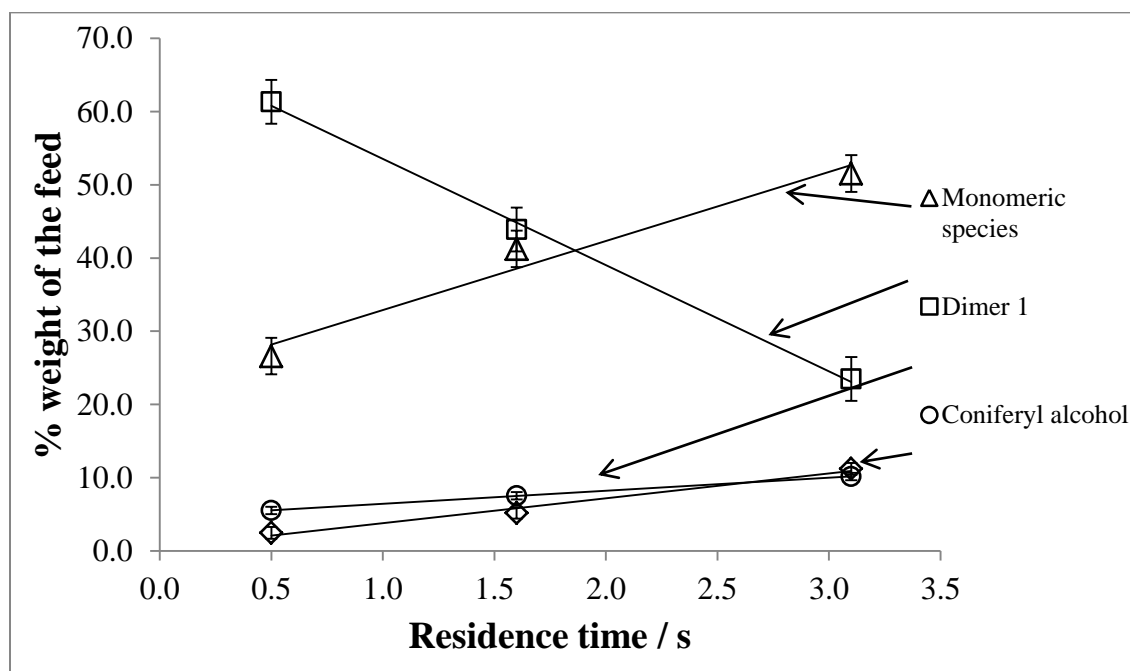


Figure 4.6 Yield of products from pyrolysis of dimer **1** as a function of vapor phase residence time. dimer **1** (squares), Monomeric species (triangles), Coniferyl alcohol(circles), 2-methoxy-4-(2-(2-methoxyphenoxy)vinyl)phenol (diamonds).

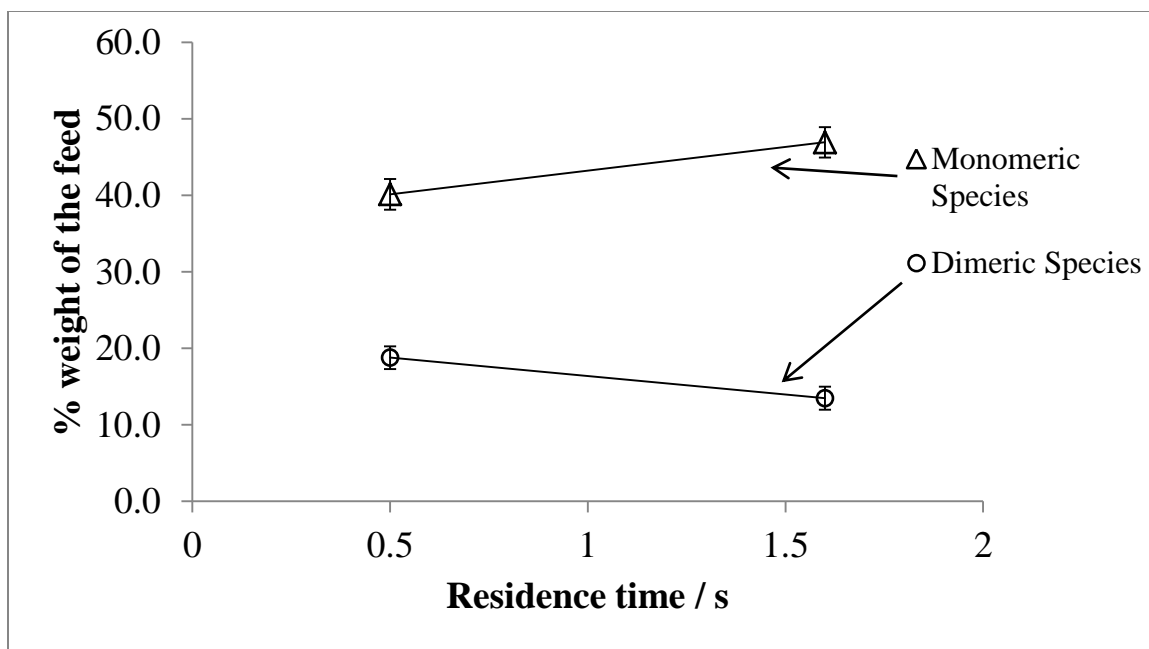


Figure 4.7 Yield of products from pyrolysis of polymer **5** as a function of vapor phase residence time. Dimeric species (circles), Monomeric species (triangles).

4.7 Conclusions

In this study, a new approach was developed for analysis of lignin derived dimeric species via an online GC/MS. Pyrolysis experiments were carried out with model lignin oligomers and a polymer with this approach to attain greater than 90% mass closure. This study provides quantitative results on pyrolysis of pure lignin model compounds with β -O-4 linkages to understand the underlying factors that govern the product distribution without the unwanted effects from impurities (inorganic, sugars and multiple poorly characterized reactants) which are generally present in extracted lignins. The major monomeric product observed from β -O-4 bond scission was coniferyl alcohol. A significant proportion of the pyrolysis products from all of the model compounds tested was dimeric species, with greater than 19% abundance. The relative ratios of major

monomeric compounds were similar for all the model compounds indicating that the nature of β -O-4 bond scission was independent of the degree of polymerization. The amount of char formed increased with the degree of polymerization highlighting the importance of the volatility and reactivity of the fragments formed during pyrolysis as governing factors in char formation. Additionally, vapor phase residence time was shown to have an important effect on the product distribution due to secondary reactions. An increase in the vapor phase residence time resulted in the dimeric species breaking down to form monomeric products thereby decreasing the average molecular weight of the product distribution. Vapor phase primary products from lignin pyrolysis were comprised of both monomeric and dimeric species (and possibly trimeric species) which underwent secondary (cracking/depolymerization) reactions in the vapor phase. These results can have important implications on the ability to tailor the vapor phase product distribution by modifying parameters like lignin structure (nature and number of linkages), temperature, and vapor phase residence time during lignin pyrolysis before the vapors are passed over a catalyst for hydrodeoxygenation. A systematic study with oligomers of guaiacyl (G) units connected via β -O-4 linkages (up to 50% of the linkages in lignin polymer) with -OH substituents at the α and γ carbon atoms was critical towards making this study relevant for towards development of the understanding of the dominant pathways during pyrolysis of native lignin. Similar studies with other lignin linkages (and potentially other monomeric units) would be beneficial for expansion of the knowledge base for pyrolysis of the natural lignin polymer.

CHAPTER 5. CATALYTIC HYDRODEOXYGENATION OF MODEL COMPOUNDS

5.1 Introduction

Lignocellulosic biomass is recognized a potential source of carbon for production of renewable hydrocarbon fuels and chemicals.^{22,119,120} There are multiple conversion processes that have been proposed for this transformation and involve depolymerization of biomass via chemical, thermochemical, enzymatic and biological means.^{8,10} Amongst these, very few processes focus on conversion of the lignin fraction of biomass to fuels and useful chemicals. Lignin constitutes 10-30% of lignocellulosic biomass and accounts for 25-40% of the energy content of biomass, due in part to its higher C/O ratio compared to cellulose and hemicellulose.⁸² Furthermore, the aromatic nature of the monomers forming the backbone of lignin render it as an important source for aromatic molecules which are valuable both a precursors for chemicals and gasoline range hydrocarbons (>100 RON).^{19,101,121} Fast-hydropyrolysis of biomass produces aromatic hydrocarbons bearing phenolic, methoxy function groups on the aromatic ring and other oxygen bearing functional groups on the alkyl side chain as discussed in Chapter 4. However, a downside of utilizing lignin for pyrolysis is that it produces substantially higher amount of char during pyrolysis as compared to cellulose and xylan. Thus, it is imperative to develop catalysts or pretreatment options which can potentially reduce char formation during lignin pyrolysis.

Recently developed processes claim to preferentially extract lignin from biomass via depolymerization and *insitu* catalytic treatment to selectively produce molecules like propylguaiacol and propylsyringol.^{12,122} Hydrodeoxygenation of lignin depolymerization products is essential for conversion to gasoline range hydrocarbons. Therefore, various catalytic systems were investigated for hydrodeoxygenation of phenolic and methoxy functional groups from lignin based model compounds, dihydroeugenol and m-cresol.

Hydrodeoxygenation of lignin based model compounds has been widely studied in literature for development of catalysts aimed at selective removal of phenolic and methoxy functional groups.^{84,123–125} A variety of supported noble metal catalysts in conjunction with an acidic function, either in the form of a support, a promoter or a solvent have been studied in liquid and vapor phase.^{126–130} Pt based catalysts have been extensively studied due to its strong hydrogenation function which is proposed to be essential for complete/partial ring hydrogenation prior to deoxygenation.^{131–133} PtMo bimetallic catalysts were shown to selectively promote C-O scission,^{134,135} while Mo in oxide and carbide form was also effective for hydrodeoxygenation of model compounds.^{136–139} The role Mo as an oxophilic promoter in conjunction with Pt has been investigated in this study, via a combination of pulse catalytic experiments and continuous steady state kinetic studies.

The pathways for deoxygenation of phenolic and methoxy groups have been proposed to be sensitive to hydrogen partial pressure, with studies spanning the hydrogen pressure range of 0.5 – 100 bar.^{131,140–145} A systematic study of variation of hydrogen pressure on

the PtMo bimetallic catalytic system showed that direct deoxygenation of phenol to form an aromatic hydrocarbon was the dominant pathway at low hydrogen pressure (1 bar), while at high hydrogen pressure (25 bar), sequential ring hydrogenation and dehydration occurred to give saturated hydrocarbons with high selectivity.^{70,146} On the flipside, lowering hydrogen pressure significantly affected the site time yield as it declined by an order of magnitude with decrease in the hydrogen pressure from 25 to 1 bar.¹⁴⁶ The product selectivity and reaction pathways studies at different hydrogen pressures in collaboration with the above reported results have been performed in the micro-scale semi-batch catalytic reactor. Conventionally, lignin model compounds HDO studies are focused on deoxygenation of the methoxy and phenolic moieties on the aromatic ring while entirely neglecting potential effects of the catalyst and reaction conditions on deoxygenation pathways and products from the substituted alkyl side chain. In this study, we will address the effects on the alkyl side chain via careful selection of the model compound as well as study of the hydrodeoxygenation of pyrolysis products from synthetic lignin polymer **5**. The model compound chosen as a surrogate for lignin pyrolysis products was dihydroeugenol, bearing the characteristic phenolic, methoxy and propyl side chain groups on the aromatic ring. Additional effects of hydrogen pressure and catalyst functionality on alkyl side chains bearing oxygen functional groups have been reported in Chapter 6.

5.2 Experimental methods

5.2.1 Catalyst preparation

The catalysts containing various proportions of platinum and molybdenum supported on multi-walled carbon nanotubes (MWCNT) have been used for this study (Table 5.1). The catalysts were prepared by incipient wetness impregnation method, and the detailed preparation procedure has been previously reported here.¹⁴⁶ The 1.9%Pt1.2%Mo/SiO₂ catalyst was synthesized by sequential impregnation and the detailed procedure for synthesis has been reported here.¹⁴⁷

For the 1% Pt/SiO₂-Al₂O₃ catalyst, 80 g of Davisil 135, SiO₂-Al₂O₃ (Aldrich) support was suspended in 300 ml of water, and concentrated NH₄OH was added until the pH was greater than 10. 1.6 g of the Pt precursor (Pt(NH₃)₄(NO₃)₂) was dissolved separately in 50 ml water and the pH was adjusted to a value of ~10 with conc. NH₄OH solution. The Pt precursor bearing solution was added quickly with stirring at room temperature. After 10 minutes, the solid was filtered and washed with water. The wet catalyst was dried overnight at 125°C and calcined by heating at 5°C.min⁻¹ to 500°C for 5 hours.

For the 1%Pt/KLTL catalyst, 100 g of K-LTL zeolite was NH₄NO₃ ion exchanged with a solution of 75 g NH₄OH in 500 mL H₂O, at 80°C, with stirring for 30 minutes. The sample was then filtered and washed with water. The sample was dried overnight at 125°C.

For the 1% Pt/H-USY catalyst, the support, H-USY zeolite (LZY-84) was obtained from UOP and calcined at 500°C for 3 hours. To 20g of zeolite support the Pt precursor solution (0.40 g Pt(NH₃)₄(NO₃)₂ dissolved in 15 ml water) was added by incipient wetness impregnation. The catalyst was dried overnight at 125°C and then calcined by heating at 2°C.min⁻¹ to 300°C for 3 hours.

Table 5.1 List of the catalysts tested in the micro-scale semi-batch catalytic reactor (pyroprobe).

Catalyst	Mo:Pt atomic ratio / moles:moles
5%Pt/MWCNT	0
5%Pt 1.2%Mo/MWCNT	0.5
5%Pt 2.46%Mo/MWCNT	1
2.5%Pt 2.46%Mo/MWCNT	2
2.46%Mo/MWCNT	∞

5.2.2 Catalyst characterization

Catalyst characterization techniques used were CO chemisorption, Transmission Electron Microscopy (TEM), Scanning Transmission Electron Microscopy (STEM), and Electron Energy Loss Spectroscopy (EELS), X-ray Absorption Spectroscopy (XAS), X-ray Photoelectron Spectroscopy (XPS). The details of these techniques, procedures and results have been reported here.¹⁴⁶

5.2.3 Micro-scale semi batch catalytic reactor (Py-GC/MS)

Fast-hydropyrolysis and catalytic hydrodeoxygenation experiments were carried out using a Pyroprobe 5200 HP (CDS Analytical Inc.), retrofitted with a downstream catalytic reactor and connected to an online Gas Chromatograph (Agilent 7890A)

equipped with a Flame ionization detector and a Mass Spectrometer (5975C). A resistively heated Pt coil was used as a heating source for evaporation of the model compounds (dihydroeugenol, m-cresol, etc). A known weight/volume of the reactant sample was loaded in a quartz tube (0.15cm ID X 2.5cm length), which was subsequently placed in the annulus of the Pt coil. A heating rate of $1000^{\circ}\text{C}\cdot\text{s}^{-1}$ was used to attain a final temperature which was required for the complete evaporation of the concerned model compound. The pyrolysis vapors were flushed out from the quartz tube by the reactant gas (H_2 , balance He) and passed over the catalyst bed on the way to the GC-MS. To obtain ideal evaporation conditions, experiments were performed to check for model compound decomposition with an empty fixed bed reactor and subsequent analysis via GC-MS. The GC was equipped with a DB1701 column (ID 0.25mm X 60m) for product separation, which was connected to a three way splitter with auxiliary gas input. The flow from the column was split to the FID and MS with synchronized peaks for quantification and identification, respectively. The system had two relief valves to prevent over pressurization of pyrolysis chamber and the fixed bed reactor assembly (set point 40 bar), and the GC-MS inlet assembly (set point 6.5 bar).

The solid reactant sample was loaded inside the quartz tube and the amount of sample was measured by weighing the quartz tube before and after the sample loading. For the liquid samples, a known volume of the sample was loaded via a $1\mu\text{l}$ syringe. After the sample was loaded, the quartz tube was placed inside the annulus of the Pt coil, which was mounted on a probe. The probe was then placed inside the pyrolysis chamber (Figure 2.1) and the air was flushed out using nitrogen. The 8 port valve was switched to

introduce the reactant gas mixture (H_2 , balance He) and flush out the nitrogen, which subsequently pressurized the pyrolysis chamber to the desired operational pressure. The fixed bed reactor was already heated to the desired operational temperature (300°C) and pressurized with the flowing reactant gas mixture before the sample loading procedure. At no point during the sample loading and running phases was the pre-reduced catalyst exposed to air. The pyrolysis chamber was then heated by an external heater to a temperature of 300°C in ~ 10 s followed by the Pt coil being heated to a desired final temperature at a heating rate of $1000^\circ\text{C}\cdot\text{s}^{-1}$. The pyrolysis vapors were carried out from the quartz tube to the catalyst bed by heat traced tubing. The pressure was stepped down after the back pressure regulator so that it was within the acceptable range for the GC-MS (10-100 psi). Only a fraction of the flow was injected into the GC-MS to control the split ratio as well as protect the GC-MS from excessively high flow rates (>1 slpm) during the high pressure runs, while balance flow was vented. The split flow was controlled by a needle valve placed on the vent line. The split/splitless inlet of the GC was maintained at a temperature of 300°C and a split ratio in the range of 10:1 and 100:1 was used depending on the total pressure and flow rate through the fixed bed reactor. The actual split ratio was calculated by measuring the flow rates from the vent and GC split vent lines (Figure 2.3). The catalyst was reduced *insitu* before the reaction, by loading into the reactor and using a 2 hour ramp to 450°C (400°C for 5%Pt/MWCNT catalyst) from room temperature, at 1 bar pressure, in 50-100 sccm H_2 flow.

The peaks observed in the gas chromatogram (FID) were identified by comparing the EI spectrum from the mass spectrometer to those in the MS NIST (National Institute of

Standards and Technology) database. These products were quantified on the basis of calibrations made by using available standard compounds. CO and CO₂ were quantified by making calibrations with the major ion (m/z=28 for CO and m/z=44 for CO₂) in the mass spectrometer.

5.2.4 Continuous, steady state, fixed bed catalytic reactor setup

The detailed description, schematic, and reactor operation have been previously reported here.¹⁴⁶ The weight hourly space velocity was defined as ($WHSV = \frac{\text{gram dihydroeugenol fed}}{\text{gram catalyst} \cdot \text{h}}$)

for 5%Pt-2.5%Mo/MWCNT catalyst was varied in the range of 1.6-82 h⁻¹ to span the conversion range from 10-99.99%. Dihydroeugenol (or m-cresol) conversion was

estimated by $X = \frac{\text{moles of dihydroeugenol reacted}}{\text{moles of dihydroeugenol fed}} \cdot 100\%$ and ring-product selectivity was

defined as $S_{\text{ring}} = \frac{\text{moles of ring product}}{\text{moles of dihydroeugenol reacted}} \cdot 100\%$. Overall Site time yields (STYs)

were estimated as $STY_{\text{Pt}} = \frac{X \cdot \text{moles of DHE fed}}{\text{moles of Pt} \cdot \text{s}}$, product STYs as

$STY_{\text{Pt}} = \frac{X \cdot S_{\text{ring}} \cdot \text{moles of DHE fed}}{\text{moles of Pt} \cdot \text{s}}$. For comparing rates between Pt-Mo catalysts the STYs

were normalized by total moles of CO chemisorbed per gram of catalyst instead of moles

of Pt and were calculated as $STY_{\text{COchemi}} = \frac{X \cdot S_{\text{ring}} \cdot \text{moles of DHE fed}}{\text{moles CO chemisorbed per gm catalyst} \cdot \text{s}}$.^{70,146}

5.3 Results and Discussion

5.3.1 Catalyst characterization

Catalyst characterization techniques (STEM-EELS, XPS, XAS and CO chemisorption) were used to study the changes in the catalyst structure, with change in Mo loading, in the PtMo bimetallic catalysts. CO chemisorption results showed that the CO uptake per gram of the catalyst decreased with an increase in the Mo loading, indicating decrease in surface Pt (Table E. 8). Particle size analysis was performed on the TEM/STEM images from the bimetallic catalysts, to obtain the percentage of Pt only and Pt-Mo bimetallic particles. The results show an increase in the percentage of the PtMo bimetallic particles with an increase in the Mo loading relative to Pt (Table E. 17). XAS results confirmed the presence of Pt-Mo co-ordination under reduced conditions indicating formation of Pt-Mo alloy in the bimetallic catalyst. Additionally, the presence of multiple oxidation states of Mo was determined from XPS studies with identification of Mo^0 , Mo^0 carbide-like species, and Mo-oxide (4^+ and 6^+) phases (Table E. 18). The detailed characterization results on the series of Pt-Mo bimetallic catalysts have been reported in elsewhere.¹⁴⁶

5.3.2 Reaction pathways and identified products

Hydrodeoxygenation of dihydroeugenol focused on deoxygenation of phenolic and methoxy oxygen groups without carbon loss from the alkyl side chain. Preliminary testing with the continuous, steady state, fixed bed catalytic reactor showed promising hydrodeoxygenation selectivity with the Pt-Mo bimetallic catalyst. Space velocity studies were carried out to determine the reaction pathways by classifying products as primary,

secondary, and tertiary based on their selectivity profiles with conversion.¹⁴⁶ Previous studies have shown that the major reaction pathway was dependent on the hydrogen partial pressure. Figure 5.1 shows the dominant pathway for hydrodeoxygenation on bimetallic Pt-Mo catalysts at 25 bar hydrogen partial pressure based on the space velocity studies. The primary products are methoxy cleavage and ring hydrogenation products, 4-propyl phenol and 2-methoxy-4-propylcyclohexanol. These can intern undergo ring hydrogenation and methoxy cleavage to yield 4-propylcyclohexanol. Minor intermediate products like 4-propylcyclohexanone are observed and are products of dehydrogenation of the alcohol group over the catalyst, however they do not undergo direct deoxygenation as shown previously. 4-propylcyclohexanol then underwent dehydration to form propylcyclohexene which was readily hydrogenated to form propylcyclohexane. At ~100% conversion, > 97% yield to propylcyclohexane was obtained with the 5%Pt 2.5%Mo/MWCNT catalyst with both the continuous steady state fixed bed catalytic reactor and the micro-scale semi-batch catalytic reactor. The methoxy group was lost primarily in the form of methanol which was detected intact and at higher conversions underwent transformation to form methane, CO and CO₂. The methoxy group dexoygenation contributed to an irreversible carbon loss yielding a C₉ hydrocarbon as the final product. Methoxy group carbon loss occurred through two major pathways C_{sp2}-O scission or C_{sp3}-O scission, resulting in formation of methanol and methane respectively. At high hydrogen pressure C_{sp2}-O scission was the dominant pathway, while at low hydrogen pressure (1 bar), both the pathways had comparable selectivity. This was corroborated by observation of an equivalent amount of 4-propylbenzene-1,2-diol from C_{sp3}-O scission pathway. Additional studies reported here⁷⁰ at 1 bar hydrogen pressure

showed that the dominant pathway was different from that at high pressure (25 bar) as shown in Figure 5.2.

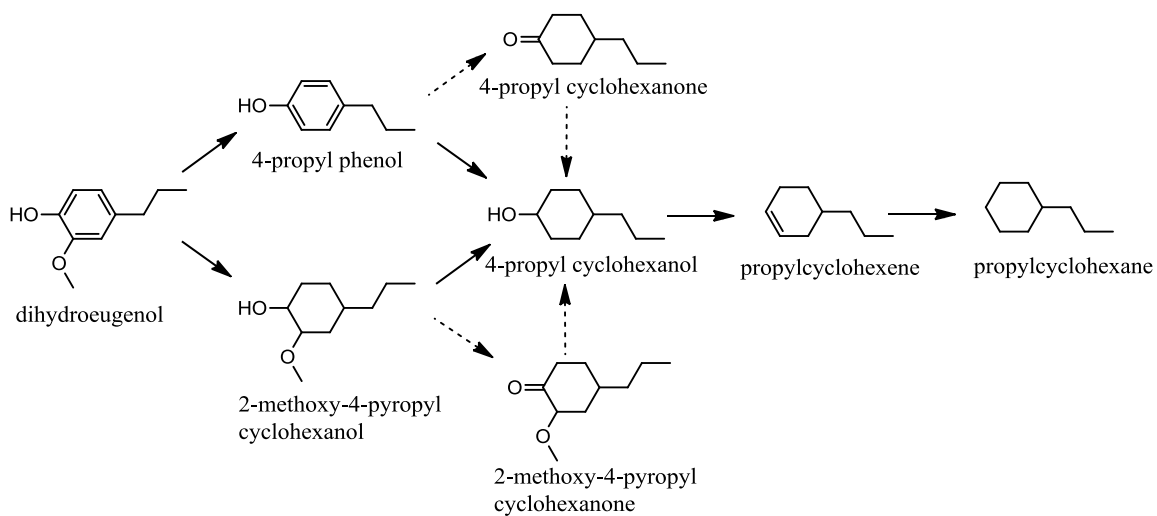


Figure 5.1 Proposed major reaction pathway for high pressure (25 bar) vapor phase hydrodeoxygenation of dihydroeugenol (DHE) over the series of Pt-Mo bimetallic catalysts.

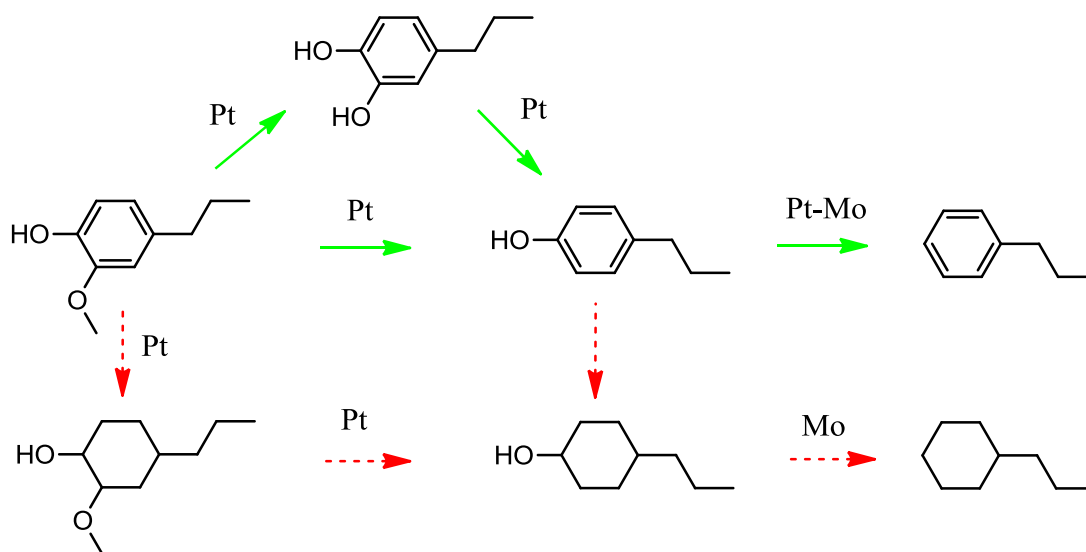


Figure 5.2 Proposed major reaction pathways for vapor phase hydrodeoxygenation of dihydroeugenol (DHE) as a function of the hydrogen pressure over the series of 5%Pt2.5%Mo/MWCNT catalyst. Green-solid arrows indicate the major pathway at low hydrogen pressure (1 bar), while the Red-dotted arrows indicate the major pathway at high hydrogen pressure (25 bar). The Pt,Mo and Pt-Mo denotations above the arrows indicate the dominant role of that species for that step in the overall reaction pathway. Figure adapted from source.⁷⁰

5.3.3 Role of Pt and Mo

In order to decipher the role of Pt and Mo in the 5%Pt2.5%Mo/MWCNT catalyst, a series of catalysts with varying proportions of Pt and Mo were prepared. Table 5.1 shows the different catalysts that were prepared and tested with dihydroeugenol under the reaction conditions of 25 bar hydrogen partial pressure and 300°C catalyst temperature. Previous studies with the 5%Pt/MWCNT showed that the major product was 4-propylcyclohexanol with a minor yield of propylcyclohexane. Pt alone was able to catalyze the cleavage of C_{sp^2} -O bond in the methoxy linkage; however it was unable to selectively deoxygenate the phenolic -OH linkage. Addition of Mo to the Pt resulted in

increase in the selectivity of the final deoxygenated product propylcyclohexane. All the catalysts were tested in the conversion range of 40-45 % to enable a fair comparison between the product selectivity as shown in Table 5.2 and Figure 5.3. A mid conversion range was chosen to show the trends in the deoxygenation of the phenolic –OH group which is the tertiary step in the pathway and not prominent at low conversion (10-15%). The selectivity for propylcyclohexane increase drastically from ~16% for 5%Pt/MWCNT to ~55% for 5%Pt1.25%Mo/MWCNT catalyst within a conversion range of 40-45%, and continued to rise with an increase in the Mo content relative to Pt. These results indicated that Mo played a dominant role during deoxygenation of 4-propylcyclohexanol to propylcyclohexane. For the 2.5%Mo/MWCNT catalyst, the yield towards deoxygenated hydrocarbons (propylcyclohexane, propylcyclohexene and propyl benzene) was ~47% down from ~67% for the 2.5%Pt2.5%Mo/MWCNT catalyst. There was also a corresponding increase in the yield of 4-propylphenol selectivity from ~6% for the 2.5%Pt2.5%Mo/MWCNT catalyst to ~39% for the 2.5%Mo/MWCNT catalyst. When comparing the two aforementioned catalysts it should be kept in mind that the absence of Pt in results in a serious loss in the ring hydrogenation ability of the 2.5%Mo/MWCNT catalyst which is demonstrated by a sudden increase in the selectivity of 4-propyl phenol and propylbenzene. Additionally, an accumulation of 4-propylphenol on the 2.5%Mo/MWCNT also showed that it did not readily deoxygenate over the catalyst and probably ring hydrogenation was required to deoxygenate the phenolic –OH group over Mo. In order to accurately represent the role of Mo in the overall pathway we needed to look at the ratio of propylcyclohexane/total hydrocarbon yield to the 4-propylcyclohexanol ratio. As shown in Figure 5.4, the ratio increased with an increase in

the Mo content and was the highest for the Mo only catalyst. These results show that the intermediate 4-propylcyclohexanol was consumed more readily with increasing Mo content.

Table 5.2 Product selectivity from hydrodeoxygenation of dihydroeugenol over Pt-Mo bimetallic catalysts, studied at 300°C, and 25 bar hydrogen partial pressure.

Catalyst	5%Pt/ MWCNT	5%Pt1.2%Mo /MWCNT	5%Pt2.5%M o/ MWCNT	2.5%Pt2.5% Mo/MWCNT	2.5%Mo/ MWCNT
Conversion / %	44.8	44.6	40.7	39.4	40.77
Product Selectivity / %					
<i>Propylcyclohexane</i>	16.5	56.5	65.0	65.8	35.5*
<i>Propylbenzene</i>	0.2	0.7	1.0	1.1	10.9
<i>4-propylcyclohexanol</i>	37.2	10.5	10.1	11.0	5.4
<i>4-propylcyclohexanone</i>	1.2	0.4	1.2	1.2	1.4
<i>4-propylphenol</i>	3.0	7.6	5.4	5.5	39.0
<i>2-methoxy-4-propyl- cyclohexanol</i>	26.1	14.1	10.6	8.2	1.3
<i>Other Products</i>	15.9	10.1	6.7	7.1	6.5

* 28.4% selectivity to propylcyclohexane + 7.1% selectivity to propylcyclohexene

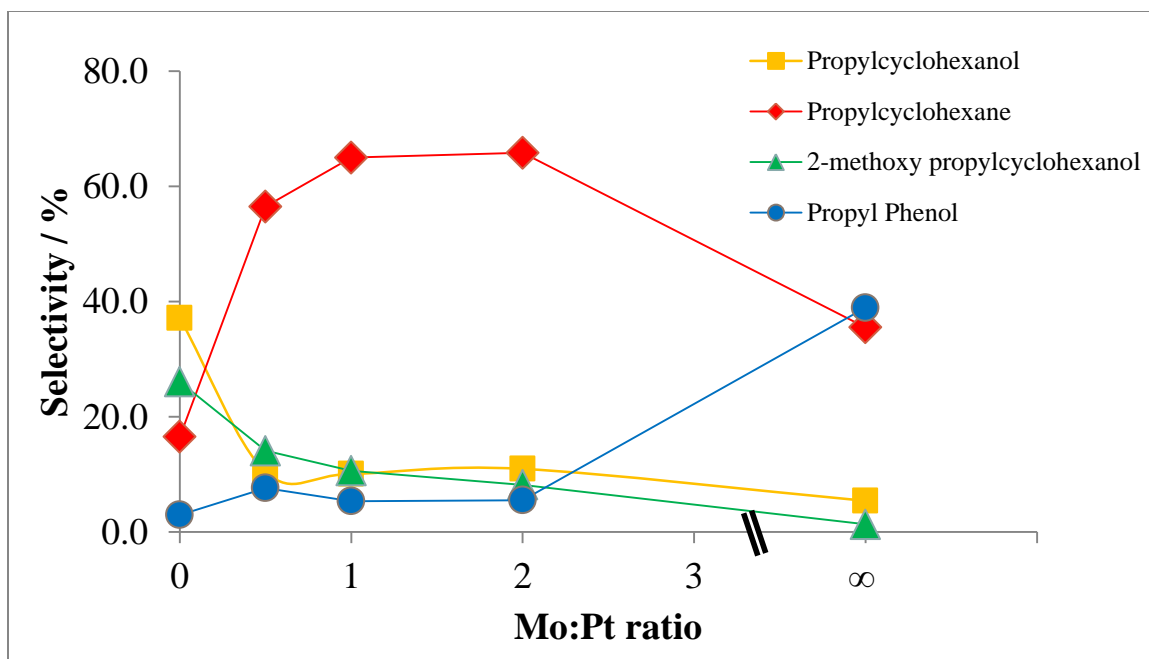


Figure 5.3 Product selectivity from hydrodeoxygenation of dihydroeugenol, as a function of the Pt:Mo ratio of the Pt-Mo bimetallic catalysts studied at 300°C, and 25 bar hydrogen partial pressure.

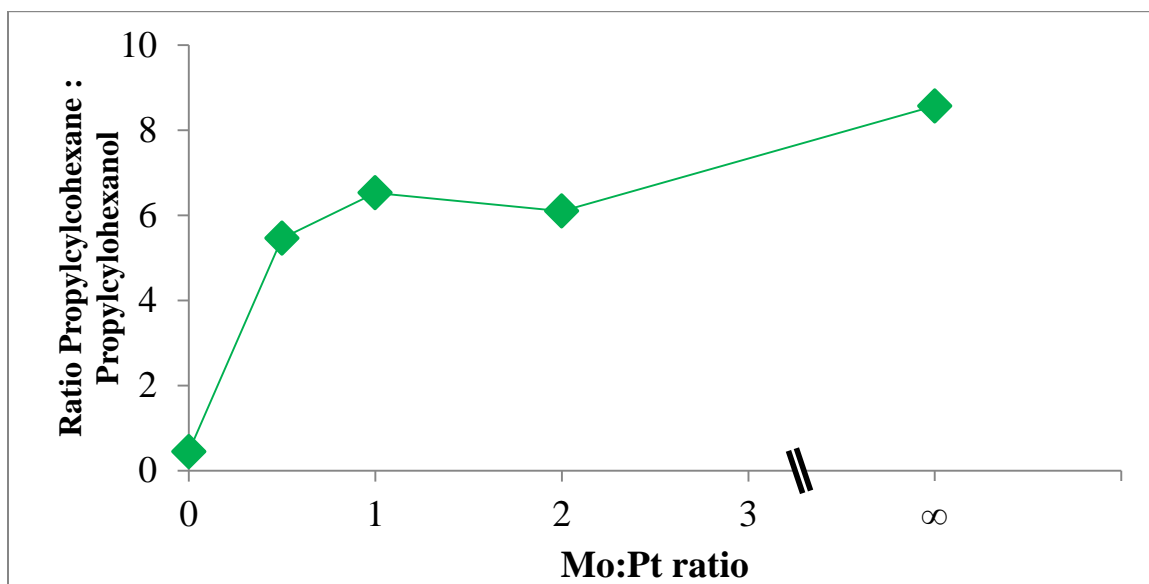


Figure 5.4 Product selectivity ratio of propylcyclohexane to 4-propylcyclohexanol from hydrodeoxygenation of dihydroeugenol, as a function of the Pt:Mo ratio of the Pt-Mo bimetallic catalysts studied at 300°C, and 25 bar hydrogen partial pressure.

Further experiments were performed to show that Mo was capable of carrying out dehydration of 4-propylcyclohexanol by feeding 4-isopropylcyclohexanol and 4-propylcyclohexanone as reactant molecules. Experiments were performed over the 2.5%Mo/MWCNT catalyst at 300°C at 25 bar hydrogen pressure and in absence of hydrogen. At 25 bar, both molecules were converted to hydrocarbons with >90% selectivity towards the saturated hydrocarbon. Minor observed products were intermediate (iso/n)-propylcyclohexene and (iso/n)-propylbenzene. These results showed that the reduced 2.5%Mo/MWCNT catalyst was capable of deoxygenation of the –OH group after ring saturation in presence of hydrogen (Figure 5.5). However when the reactant gas was switched from H₂ to He the major product from 4-isopropylcyclohexanol was isopropylcyclohexene which was the expected product as a result of dehydration reaction. 4-propylcyclohexanone however did not show major conversion with ~97% passing over the catalyst unreacted, with a minor yield of dehydration products. These experiments showed that the Mo species in the 2.5%Mo/MWCNT catalyst were responsible for the dehydration of the alkylcyclohexanol species.

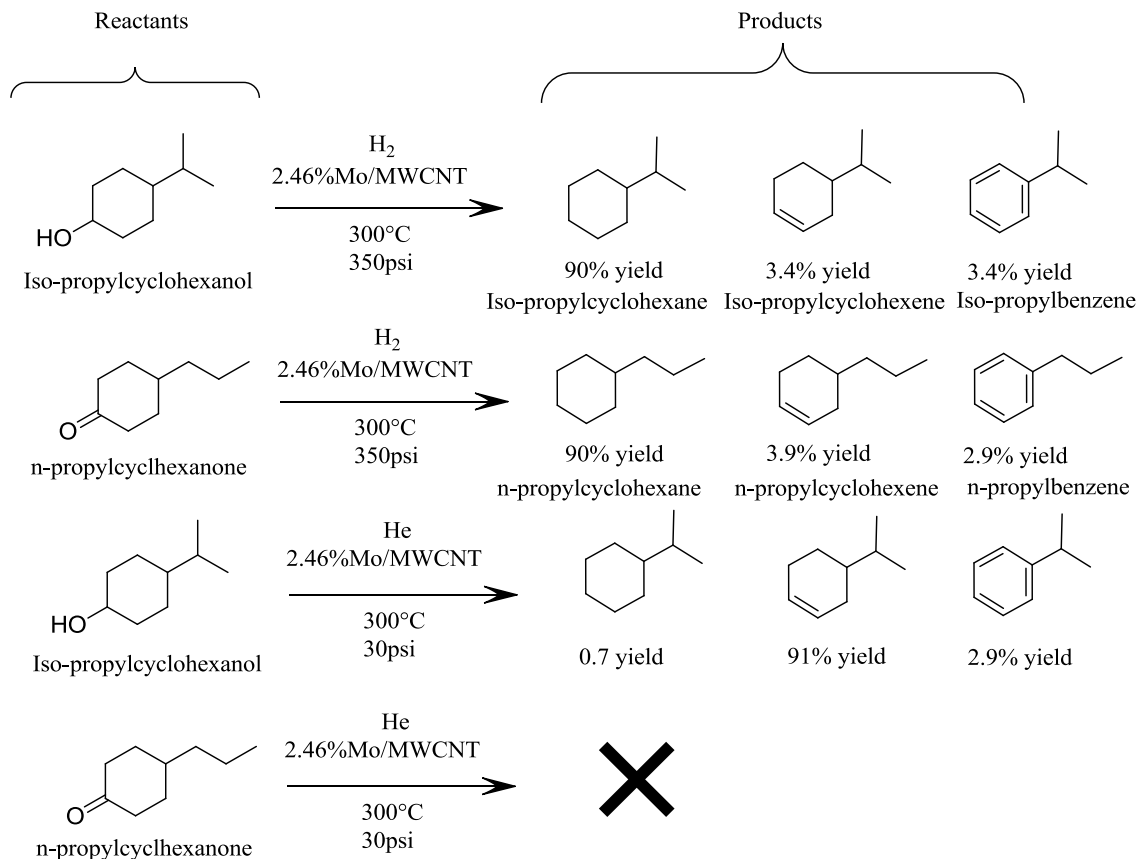


Figure 5.5 Yield of products from the model compounds, 4-isopropylcyclohexanol and 4-propylcyclohexanone, over the 2.46% Mo/MWCNT catalyst at 300 °C and 25 (350 psig) bar hydrogen pressure and 3 bar (30 psig) He pressure.

As stated previously, XAS studies have shown the presence of multiple oxidation states of Mo which was confirmed with XPS studies via identification of Mo^0 , Mo^0 carbide-like species, and Mo-oxide (4^+ and 6^+) phases. These species were observed in different proportions depending on the Mo:Pt ratio in the catalyst, with the Pt abundance affecting the proportion of the reduced Mo phases. While PtMo bimetallic alloy system could be responsible for deoxygenation, its exact role is unclear from the experiments performed thus far. In literature, partially oxidized oxophilic metal oxide species (MoO_x) have been shown to produce brønsted/strong acid sites which promote C-O scission via dehydration

hydrogenation of biomass derived oxygenates.^{134,148,149} These observations are in line with the results from model compounds studies on the 2.5%Mo/MWCNT catalyst.

In summary, Pt primarily catalyzes the cleavage of methoxy group and ring hydrogenation and other hydrogenation steps in the overall hydrodeoxygenation pathway. While Mo is responsible for dehydration of the ring hydrogenated alkylcyclohexanol intermediate, although methoxy group cleavage can occur over Mo, reaction rate studies on the continuous, steady state, fixed bed catalytic reactor have shown that Pt plays a dominant role for methoxy cleavage.⁷⁰ This was shown by the two orders of magnitude rate difference between methoxy group scission products over the 5%Pt/MWCNT and 2%Pt5%Mo/MWCNT catalyst.

Pt and Mo play distinct roles in the reaction pathway with stable intermediate species which can shuttle across distant Pt and Mo sites on the catalyst. Therefore, one can anticipate a physical mixture of Pt/MWCNT and Mo/MWCNT catalyst to exhibit the same level of performance as a bimetallic catalyst with the same Mo:Pt ratio. Table 5.3 and Table 5.4 show the results from dihydroeugenol HDO with the physical mixture of 5%Pt/MWCNT and 2.5%Mo/MWCNT catalyst. The selectivity for propylcyclohexane decreased to ~84% from 97% for the corresponding bimetallic catalyst. There was an increase in the selectivity to C₈ and C₇ hydrocarbons which are formed as a result of carbon loss from the alkyl side chain via C-C scission. C-C scission products were observed to a higher extent over the 5%Pt/MWCNT catalyst and their proportion decreased with increase in the Mo content of the bimetallic catalyst. Therefore, presence

of Mo in close proximity to Pt or in the form of an alloy with Pt reduces the side reactions which can result in carbon loss via undesired C-C scission reactions. C-C scission products were also observed in high selectivity over the 20%Mo/MWCNT catalyst in the continuous, steady state, fixed bed catalytic reactor at 1 bar hydrogen partial pressure and 300°C, a phenomenon observed with strong acidic sites. Therefore an optimum amount of Mo serves to temper the C-C scission activity of monometallic Pt while preferentially increasing the selectivity for hydrodeoxygenation by playing the role of an oxophilic promoter. The synergy between Pt and Mo is responsible for mitigating C-C scission and was observed to a greater extent during hydrodeoxygenation of cellulose pyrolysis products.

Table 5.3 Product selectivity from hydrodeoxygenation of dihydroeugenol over Pt-Mo bimetallic catalyst and a physical mixture of the Pt only and Mo only catalyst, studied at 300°C, and 25 bar hydrogen partial pressure.

Catalyst	5%Pt 2.5%Mo/MWCNT	5% Pt/MWCNT, 2.5%Mo/MWCNT physical mixture
Conversion / %	100.0	99.8
Product Selectivity / %		
<i>Propylcyclohexane</i>	97.7	83.8
<i>Propylbenzene</i>	0.5	0.6
<i>Propylcyclopentane</i>	0.4	3.8
<i>Methyl propyl cyclopentane</i>	0.0	0.7
<i>C₇ hydrocarbons</i>	0.0	6.5
<i>C₈ hydrocarbons</i>	0.0	3.1
<i>Other Products</i>	1.5	1.4

Table 5.4 Product selectivity from hydrodeoxygenation of dihydroeugenol over Pt-Mo bimetallic catalyst and a physical mixture of the Pt only and Mo only catalyst, studied at 300°C, and 1 bar hydrogen partial pressure.

Catalyst	5%Pt 2.5%Mo/MWCNT	5% Pt/MWCNT, 2.5%Mo/MWCNT physical mixture
Conversion / %	98.8	98.4
Product Selectivity / %		
<i>Propylcyclohexane</i>	0.8	1.3
<i>Propylbenzene</i>	74.2	18.8
<i>Propyl phenol</i>	19.6	44.2
<i>other oxygenates</i>	1.3	6.0
<i>C₇ hydrocarbons</i>	1.4	19.2
<i>C₈ hydrocarbons</i>	1.0	7.8
<i>Other Products</i>	1.7	2.7

5.3.4 Rate trends

Mo played an important role as an oxophilic promoter for augmenting the hydrodeoxygenation selectivity towards propylcyclohexane. However Mo by itself was incapable of effectively deoxygenating the phenolic –OH group at 25 bar hydrogen pressure primarily due to absence of ring hydrogenation capability. Therefore both Pt and Mo were needed for deoxygenation, however in order to find the optimum blend of Pt and Mo it was required to study the reaction rates. Reaction rates could not be measured in the micro-scale semi-batch catalytic reactor due to the reactant being a pulse passing over the catalyst. However, the amount of catalyst needed to attain the same level of conversion (40-45%) could be used as an indicator for the relative rate trends with the different catalysts. Table 5.5 shows the amount of catalyst loaded and it demonstrates that increasing the Mo content resulted in requirement of higher loading of catalyst despite a higher degree of secondary and tertiary reactions with increase in Mo loading relative to

Pt. It is interesting to note the stark difference in the amount of loading between the Pt only and the Mo only catalyst indicating that Mo by itself has low reactivity for the primary and secondary steps in the reaction pathway. Reaction rates were also measured for all the catalysts except 2.5%Mo/MWCNT in the continuous, steady state, fixed bed catalytic reactor, in a low conversion range (8-15%) and have been reported here.¹⁴⁶ Since the reaction rate was not measured under true differential conditions they will be referred to as site time yield (STY). The STY_{molPt} decreased with an increase in the Mo loading with that for 2%Pt5%Mo/MWCNT being two orders of magnitude lower than 5%Pt/MWCNT. CO chemisorption results are indicative of decrease in the total surface Pt with increase in the Mo loading. The STY trends can be attributed to a decrease in the surface Pt, as the STY at low conversion is primarily due to methoxy cleavage and ring hydrogenation reactions, both of which are dominant over Pt sites. Therefore, an optimum Pt and Mo ratio would be a balance between the STY and HDO product selectivity required for complete deoxygenation with minimum degree of side reactions like C-C scission. Additional considerations during hydrodeoxygenation of cellulose and hemicellulose pyrolysis products need to be taken into account and these have been discussed in Chapter 6.

Table 5.5 Catalyst loading required to attain similar conversion over the Pt-Mo series of catalysts in the micro-scale semi-batch reactor, all other experimental conditions remaining constant.

Catalyst	Loading / mg
5%Pt/MWCNT	0.5
5%Pt1.25%Mo/MWCNT	0.6
5%Pt2.5%Mo/MWCNT	0.64
2.5%Pt2.5%Mo/MWCNT	1
2.5%Mo/MWCNT	9

5.3.5 Comparison between pulse catalytic studies and steady state catalytic studies

Pulse catalytic studies serve as an important tool, which enable quick screening of catalysts as well as a variety of feedstocks. They provide valuable information about reaction pathways via study of reaction intermediates which are difficult to feed/study in steady state reactor. However, pulse catalytic studies report initial conversion and cannot be effectively used to gauge catalyst deactivation and measure reaction rate, thereby making it imperative to carry out these studies in tandem with steady state studies. Table 5.6 shows a direct comparison of the product selectivity between micro-scale semi-batch catalytic reactor and the continuous steady state fixed bed catalytic reactor in the mid conversion range and at complete conversion. The product selectivity is comparable under complete conversion conditions while in the mid-conversion range it is widely different. These differences can be due to a contribution of various factors like pulse nature of feed, hydrogen coverage, and catalyst deactivation. During the initial waxing part, and the later waning part of the pulse, the primary products formed insitu encounter fresh catalytic sites and continue to react further, resulting the product distribution being skewed towards the secondary and tertiary products along the pathway. When this is

compared with steady state operation, the continuous flow of the reactant does not leave as high an abundance of empty/fresh sites along the pathway especially at low/mid conversions, resulting in lower conversion of the primary products to secondary and tertiary products. At complete conversion, for both cases primary products encounter higher proportion of empty catalytic sites as they pass through the catalyst bed due since all of the reactant molecules are converted to products in the initial portion of the bed. This explains the similar selectivity at high conversion (100%), since the primary products are formed initially encounter more catalyst to go further along the pathway in both systems. The catalyst can be assumed to have a higher coverage of hydrogen in pulse catalytic studies due to non-competitive adsorption before and after the brief pulse exposure. Higher hydrogen coverage could result in preferential conversion towards pathways which have a higher hydrogen order. This effect is not very prominent during hydrodeoxygenation of dihydroeugenol due to absence of a prominent competing pathway with no or little hydrogen dependence. This effect was evident during hydrodeoxygenation of levoglucosan, and cellulose pyrolysis products with the extent C-C scission occurring to a lower extent with the pulse catalytic studies when compared with the steady state conditions.

Table 5.6 Comparison of product selectivity from hydrodeoxygenation of dihydroeugenol over the 5%Pt2.5%Mo/MWCNT catalyst, between the two reactors in similar conversion range. Catalyst studied at 300°C, and 1 bar hydrogen partial pressure.

Type of reactor	Micro-scale semi-batch reactor		Continuous steady state reactor	
Catalyst	5%Pt2.5%Mo/MWCNT		5%Pt2.5%Mo/MWCNT	
Conversion / %	40.7	100.0	56.4	100.0
Product Selectivity / %				
Propylcyclohexane	65.0	95.5	18.1	97.4
Propylbenzene	1.0	1.4	2.0	0.2
4-propylcyclohexanol	10.1	0.9	23.0	0.0
4-propylcyclohexanone	1.2	0.0	3.6	0.0
4-propylphenol	5.4	0.0	12.8	0.0
2-methoxy-4-propyl-cyclohexanol	10.6	0.0	23.4	0.0
Other Products	6.7	2.3	17.1	2.4

5.3.6 Pathway differences at different hydrogen pressures

Hydrogen was a key factor is governing the product distribution from hydrodeoxygenation of dihydroeugenol, with the major product being propylcyclohexane. At 25 bar, ring hydrogenation is favored and the equilibrium is heavily skewed in favor of propylcyclohexane with only a minor fraction of propylbenzene being observed (Table 5.7). Keeping in line with the objective of producing gasoline range hydrocarbons from lignin the role of hydrogen pressure was investigated to increase the yield towards aromatic hydrocarbons. Aromatic hydrocarbons have a octane number in excess of 100 (RON) while their saturated counterparts are in the range of ~60-70. The hydrogen pressure was decreased from 25 bar to 1 bar and correspondingly the yield of propyl benzene increased from ~0.5% to ~91.5% (Figure 5.6). The 5%Pt2.5%Mo/MWCNT catalyst was effective in deoxygenation of the dihydroeugenol to propyl benzene with a high selectivity. At intermediate hydrogen pressures the distribution of propylbenzene and propylcyclohexane within an order of

magnitude of their estimated thermodynamic equilibrium ratios (Table 5.8). Pulse catalytic studies demonstrated a promising product distribution from the 5%Pt 2.5%Mo/MWCNT catalyst at 1 bar hydrogen pressure, leading to further experiments with the continuous steady state fixed bed catalytic reactor. The objective of these experiments was primarily to demonstrate the catalyst stability at 1 bar hydrogen partial pressure over a time scale of 30-50 hours. Previous studies have shown that catalysts used for hydrodeoxygenation show continuous deactivation and high hydrogen partial pressure has been used to mitigate coking on the catalysts. Studies by Mehta et al. demonstrated the stability of the catalyst at 1 bar hydrogen pressure, thereby establishing the feasibility of this catalyst as an effective candidate for hydrodeoxygenation of lignin pyrolysis products.⁷⁰ Additionally, it was discovered that the dominant pathways for phenolic -OH group deoxygenation were different at 25 bar and 1 bar hydrogen partial pressure. As stated before, at 25 bar hydrogen pressure the dominant pathway was methoxy cleavage and ring hydrogenation to form propylcyclohexanol followed by dehydration of the -OH group to form the saturated hydrocarbon. However at low hydrogen pressure (1bar) the dominant pathway was direct deoxygenation of the phenolic -OH to yield propylbenzene.⁷⁰ At intermediate hydrogen pressure of 7 bar intermediates from both pathways were observed thereby showing a relative rate dependence of the two pathways on the hydrogen partial pressure. The mechanism of direct deoxygenation of the phenolic -OH is widely debated in the literature with two major proposed pathways, 1) Direct C-O hydrogenolysis and 2) Partial hydrogenation of the aromatic ring followed by dehydration to restore the ring aromaticity.^{133,150} Both these pathways would produce highly reactive intermediates, which are also extremely difficult to observe under reaction

conditions. Isotopic labeling studies could be proposed to differentiate between the two pathways provided H/D scrambling can be prevented over the catalyst.

Table 5.7 Product selectivity comparison from hydrodeoxygenation of dihydroeugenol over the 5%Pt2.5%Mo/MWCNT catalyst as a function of the hydrogen pressure, at temperature of 300°C.

Partial Pressure of hydrogen /bar	25	7	2.4	1
Conversion / %	100.0	100.0	100.0	99.9
Product Selectivity / %				
<i>Propylcyclohexane</i>	97.7	88.5	34.9	3.5
<i>Propylbenzene</i>	0.5	9.2	61.2	91.5
<i>Propylcyclopentane</i>	0.4	0.6	1.9	1.0
<i>Methylcyclopentane</i>	0.1	0.2	0.2	0.0
<i>Other Products</i>	1.4	1.5	1.8	4.0

Table 5.8 Comparison of the ratio of yields of propylcyclohexane to that of propylbenzene from hydrodeoxygenation of dihydroeugenol over the 5%Pt2.5%Mo/MWCNT catalyst as a function of the hydrogen pressure, at temperature of 300°C, with the expected equilibrium ratio.

Partial Pressure of hydrogen /bar	1	2.4	7	25
Ratio –				
Propylcyclohexane:Propylbenzene				
Experimental	199.4	9.6	0.57	0.038
Equilibrium - Literature^(a)	199.9	6.1	0.18	0.013
Equilibrium - ASPEN^(b)	475.6	14.4	0.42	0.030

(a) – Ratio estimated from equilibrium constants obtained from literature¹⁵¹

(b) – Estimated via theoretical calculation from ASPEN

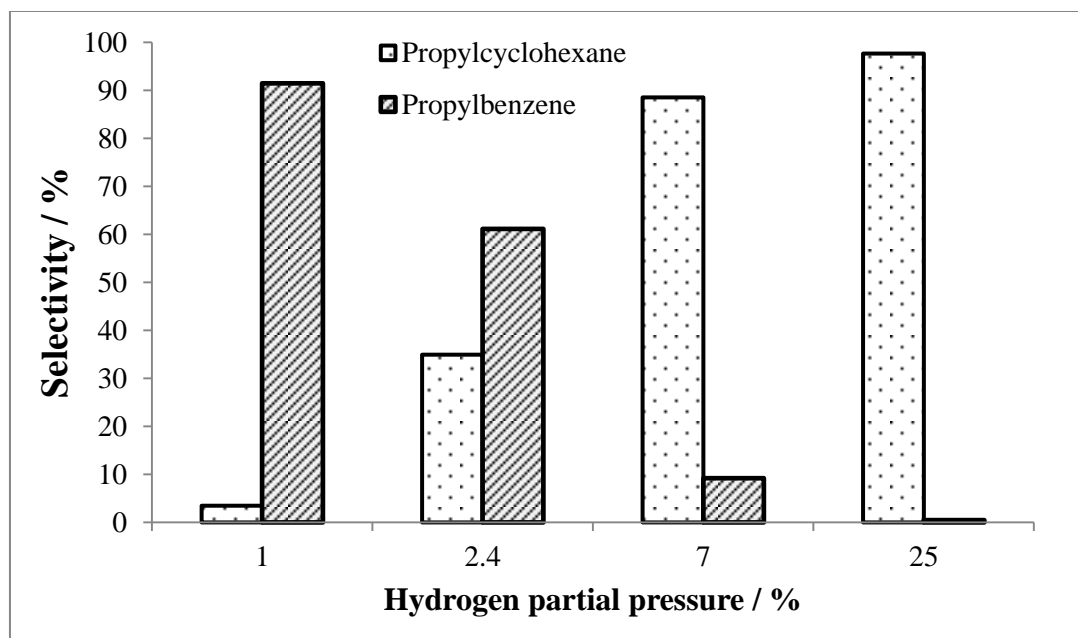


Figure 5.6 Selectivity for propylcyclohexane and propylbenzene from hydrodeoxygenation of dihydroeugenol over the 5%Pt2.5%Mo/MWCNT catalyst, as a function of hydrogen pressure, at similar conversion (~100). Temperature of catalyst bed ~300°C.

Studies with the continuous steady state fixed bed catalytic reactor showed that both Pt and Mo function were required for hydrodeoxygenation of the phenolic -OH group at 1 bar hydrogen pressure. Both 5%Pt/MWCNT, and 20%Mo/MWCNT catalyst had very low selectivity to propylbenzene when compared with the 5%Pt2.5%Mo/MWCNT catalyst.⁷⁰ Further experiments were performed with a physical mixture of 5%Pt/MWCNT and 2.5%Mo/MWCNT catalyst and the showed a significantly low selectivity to propylbenzene (~19%) when compared with the 5%Pt2.5%Mo/MWCNT catalyst (~75%) at ~98% conversion. These results showed Pt and Mo in close proximity (as in the bimetallic catalyst) were responsible for deoxygenation of the phenolic -OH group from 4-propylphenol to yield propylbenzene. As shown before, the primary pathway (at 1 bar hydrogen partial pressure) for phenolic -OH deoxygenation was a

direct deoxygenation pathway with potentially short lived reactive intermediate species and hence required PtMo bimetallic sites or Pt and partially oxidized MoO_x species in close proximity for effective deoxygenation. Additionally, for the physical mixture a substantial selectivity to C-C cleavage products (~27%) was observed which was characteristic of independent Pt and MoO_x functions. It is also interesting to note that the selectivity to C-C scission products was higher at 1 bar hydrogen pressure (~27% with ~98% selectivity to hydrocarbons) when compared with that at 25 bar hydrogen pressure (~13% with ~47% selectivity to hydrocarbons) further indicating the importance of the synergy between Pt and Mo especially at low hydrogen pressure conditions.

5.3.7 Other model compounds

Various lignin-derived oxygenated model compounds were tested with the 5%Pt2.5%Mo/MWCNT catalyst in the high-pressure pulse reactor to gain insight into the effect of aromatic ring functional groups on extent of deoxygenation. The compounds tested in addition to dihydroeugenol were propylsyringol (2,6-dimethoxy-4-propylphenol), 4-propylphenol, 4-propylanisole, and 2-methoxyphenol (guaiacol). Table 5.9 shows the yield of products obtained from the model compounds at 100% conversion. Regardless of the oxygen side group present, greater than 98% yield to the corresponding saturated hydrocarbon was obtained for all the compounds studied.

Table 5.9 Yield of hydrocarbon ring products from various lignin-derived model compounds over the 5%PtMo/MWCNT catalyst at 300°C and 25 bar hydrogen pressure.

Model Compounds						
Products	Propyl cyclohexane	4-propyl phenol	4-propyl anisole	Propyl syringol	Guaiacol ^a	Products^a
Propylcyclohexane	99.3	99.2	99.0	97.4	98.4	cyclohexane*
Propylbenzene	0.4	0.3	0.3	0.7	0.0	benzene*
Propylcyclopentane	0.0	0.2	0.2	0.3	0.0	cyclopentane*
Methyl-propyl cyclopentane	0.0	0.0	0.0	0.0	0.4	Methyl cyclopentane*
Other Products	0.3	0.3	0.5	1.6	1.2	

^a Indicates products from hydrodeoxygenation of Guaiacol.

Propylcyclohexane was also reacted to determine the impact of dehydrogenation and isomerization reactions of the final hydrocarbon products. Propylcyclohexane did undergo dehydrogenation to form 0.4% propylbenzene, which was very similar to the calculated thermodynamic equilibrium between the aromatic (99.8%) and saturated ring (0.2%) compounds at the same temperature and pressure. Additionally, propylcyclohexane did not isomerize to form either propylcyclopentane or methyl-propylcyclopentane.

All of the lignin-derived oxygenated model compounds tested, including dihydroeugenol (2-methoxy-4-propylphenol), propylsyringol (2,6-dimethoxy-4-propylphenol), 4-propylphenol, 4-propylanisole, and 2-methoxy phenol (guaiacol) were converted in yields greater than 98% to the corresponding saturated hydrocarbon. This suggests that all of these oxygenated compounds followed the same reaction pathway on the PtMo bimetallic catalyst: hydrogenation of the aromatic ring and cleavage of the methoxy group, followed by dehydration of the alcohol functionality to form water and the corresponding alkene,

which was then hydrogenated to form the final alkane product. The formation of the final hydrocarbon product was not affected by the presence of an additional methoxy group (propylsyringol), absence of a methoxy group (4-propylphenol), presence of only a methoxy oxygen group (4-propylanisole), or absence of the propyl side group (guaiacol).

5.3.8 Pt/acidic support catalysts

Numerous studies have reported the existence of a ring hydrogenation, dehydration pathway for deoxygenation of lignin derived phenolic model compounds. A variety of supported noble metal catalysts in conjunction with an acidic function, either in the form of a support, a promoter or a solvent have been studied with reasonable success. However, as stated before the effect of acidic function on the fate of the alkyl side is not well established. Pt/acidic support catalysts, 1%Pt/SiO₂Al₂O₃, 1%Pt/KLTL, and 1%Pt/HUSY were tested at 25 bar hydrogen pressure and 300°C temperature with dihydroeugenol to compare with the PtMo catalyst series. Table 5.10 shows the selectivity towards hydrocarbon products at near complete conversion of dihydroeugenol. It can be observed that the selectivity for propylcyclohexane from all the Pt/acidic support catalysts was less than that from 5%Pt2.5%Mo/MWCNT catalyst. For the 1%Pt/HUSY catalyst, propylcyclohexane selectivity was ~39% with an overall selectivity of ~81% to C₉ hydrocarbons. Numerous structural isomers of propylcyclohexane were observed due to rearrangement of the alkyl side chain from a linear propyl segment to various combination is ethyl-methyl, trimethyl segments in additions to ring isomerization to five membered ring products. A significant fraction of the hydrocarbon product distribution was in the form of C₆-C₈ hydrocarbons due to the rampant C-C scission as a result of

cracking reactions from the alkyl side chain. It is important to note that with an increase in the DHE conversion the selectivity towards isomerization and cracking products increased while that for propylcyclohexane decreased. This indicated that propylcyclohexane formed from deoxygenation of DHE further underwent transformation to form quaternary products unlike PtMo bimetallic system where the hydrocarbons did not react further over the catalyst (Table 5.11). The propylcyclohexane selectivity was higher for the other two catalysts, with 1%Pt/SiO₂Al₂O₃ having a selectivity of ~89% with a few ring isomerization products (propyl cyclopentane, methyl propyl cyclopentane) occupying the remaining 11%. It would be interesting to study the underlying cause for the difference in behavior of the three Pt/acidic support catalysts, by studying the nature of acidic sites, strength of acidic sites, their relative distribution and also Pt:acidic site ratio. It would yield valuable information for tailoring the product distribution according to the requirements. It is clear that amongst the catalysts tested PtMo bimetallic system has the highest selectivity towards a single C₉ product, propyl cyclohexane, with the least propensity to undergo C-C scission reaction resulting in loss of carbon as light hydrocarbons.

Propylcyclohexane was also reacted on the 5%Pt2.5%Mo/MWCNT catalyst to determine the impact of ring/side chain isomerization reactions of the final hydrocarbon products. Propylcyclohexane did undergo dehydrogenation to form 0.4% propylbenzene, which was very similar to the calculated thermodynamic equilibrium between the aromatic (99.8%) and saturated ring (0.2%) compounds at the same temperature and pressure. Additionally, propylcyclohexane did not isomerize to form either propyl cyclopentane or

methyl propyl cyclopentane and there was no loss of carbon from the alkyl side chain. Similar results were observed on the 1%Pt//SiO₂Al₂O₃ catalyst with ~0.4% selectivity to ring isomerization product propyl cyclopentane (C₈) with loss of one carbon. Severe cracking and isomerization reactions were observed over 1%Pt/KLTL, and 1%Pt/HUSY catalysts with only 83% and 70% propylcyclohexane being detected intact. These results are concurrent with those observed during DHE hydrodeoxygenation which shows that selectivity to propylcyclohexane decreased with increase in DHE conversion at the cost of increasing selectivity to isomerization products (other C₉ hydrocarbons) and cracking products (C₆-C₈ hydrocarbons).

Table 5.10 Product selectivity from hydrodeoxygenation of dihydroeugenol over various catalysts, studied at 300°C, and 25 bar hydrogen partial pressure.

Catalyst	5%Pt 2.5%Mo/ MWCNT	1%Pt/ SiO ₂ Al ₂ O ₃	1% Pt/ KLTL	1% Pt/ HUSY	1% Pt/ HUSY	1% Pt/ HUSY
Conversion / %	100.0	99.8	100.0	96.4	99.1	100.0
Product Selectivity / %						
<i>Propylcyclohexane</i>	97.7	88.4	65.6	51.3	43.5	38.5
<i>Propylbenzene</i>	0.5	2.5	1.1	1.3	1.0	0.5
<i>Propylcyclopentane</i>	0.4	2.9	4.0	0.0	0.0	0.0
<i>Methyl propyl cyclopentane</i>	0.0	3.4	3.0	0.0	0.0	0.0
<i>C6</i>	0.0	0.0	4.6	3.9	7.4	6.7
<i>C7</i>	0.0	0.0	2.8	4.3	5.2	4.3
<i>C8</i>	0.0	0.0	2.1	4.0	4.0	4.6
<i>C9</i>	0.0	0.5	13.2	29.2	34.3	41.9
<i>C10</i>	0.0	1.1	2.5	3.9	3.9	3.5
<i>Other Products</i>	1.5	1.2	1.1	2.0	0.4	0.0

Table 5.11 Reactor outlet stream composition from reaction of propylcyclohexane over various catalysts, studied at 300°C, and 25 bar hydrogen partial pressure.

Catalyst	5%Pt 2.5%Mo/ MWCNT	1%Pt/ SiO ₂ Al ₂ O ₃	1% Pt/ KLTL	1% Pt/ HUSY
Reactor outlet stream %				
<i>Propylcyclohexane</i>	99.3	99.0	82.8	70.2
<i>Propylbenzene</i>	0.4	0.4	0.2	0.1
<i>Propylcyclopentane</i>	0.0	0.4	0.7	0.0
<i>Methyl propyl cyclopentane</i>	0.0	0.1	3.2	0.0
<i>C6</i>	0.0	0.0	2.6	0.0
<i>C7</i>	0.0	0.0	0.8	0.0
<i>C8</i>	0.0	0.0	0.0	1.2
<i>C9</i>	0.0	0.0	9.4	27.4
<i>C10</i>	0.0	0.0	0.2	0.3
<i>Other Products</i>	0.4	0.2	0.0	0.7

5.3.9 Catalyst stability

Catalyst stability studies were performed in the continuous, steady state fixed bed catalytic reactor for the initial 25-30 hours of operation before changing conditions for space velocity studies. Figure 5.7 shows the conversion profile for dihydroeugenol hydrodeoxygenation at 1 bar hydrogen partial pressure as a function of time. After an initial period of deactivation the conversion approached a stable range with less than 5% decrease in the conversion value within consecutive runs, however to truly determine the catalyst stability it would be necessary to have data over >100 hours of operation. Additionally, these studies were carried out over a model compound, while during HDO of biomass pyrolysis product one could expect a myriad of compounds to cause catalyst deactivation. Studies in the literature have shown coking to be one of the major reasons for catalyst deactivation during hydrodeoxygenation of bio-oil. The objective of this part

of the study was to study the possibility of catalyst regeneration with the PtMo bimetallic system with the overall goal of developing a robust catalytic system for hydrodeoxygenation.

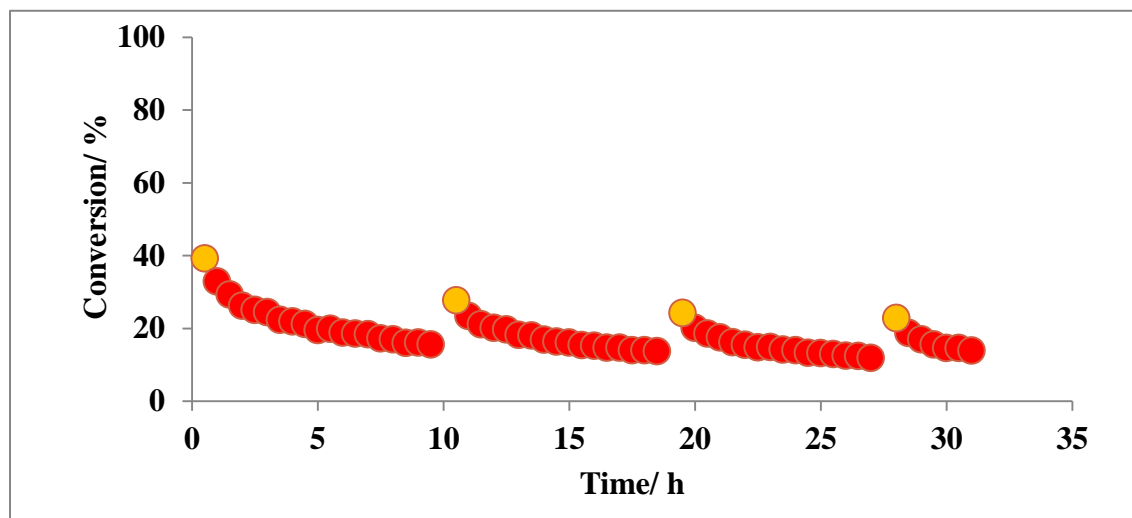


Figure 5.7 Conversion profile for dihydroeugenol as a function of time of operation over the 1.9%Pt1.2%Mo/SiO₂ catalyst at 300°C and 1 bar hydrogen partial pressure.

Multi walled carbon nanotubes (MWCNT) which was used as the catalyst support has a major drawback as it cannot be used for regeneration of the catalyst in presence of gaseous oxygen, due to possibility of combustion of the support. Therefore, SiO₂ was chosen as a support due to its inert nature for the relevant reactions. A 1.9%Pt1.2%Mo/SiO₂ catalyst was synthesized using the procedure outline previously in the document (section 5.1) and had a Mo:Pt atomic ratio of 1:1.2, rendering it suitable for comparison with the 5%Pt2.5%Mo/MWCNT catalyst (Mo:Pt atomic ratio; 1:1). An identical reduction procedure was followed for the 1.9%Pt1.2%Mo/SiO₂ catalyst and experiments at both 25 bar and 1 bar hydrogen partial pressure were performed. Figure

5.7 shows the conversion profile as a function of time with catalyst stabilization after an initial period of deactivation. The spike in conversion was a result of partial regeneration of catalytic activity as DHE flow was stopped overnight, while the catalyst bed was continuously flushed with 50sccm hydrogen.

The dominant reaction pathway for hydrodeoxygenation of dihydroeugenol at 1 bar hydrogen pressure is shown in Figure 5.2 with propylbenzene being major hydrocarbon product. Figure 5.8 shows the selectivity for propylbenzene as a function of conversion within a range of 10-80% for 1.9%Pt1.2%Mo/SiO₂ and 5%Pt2.5%Mo/MWCNT catalysts. The selectivity trend for propyl benzene is comparable amongst both the catalysts, with a slightly higher selectivity for the 1.9%Pt1.2%Mo/SiO₂ catalyst in the conversion range of 10-40%. In the low conversion range (10-25%) the methoxy cleavage products have high selectivity (~80-90%) and are the primary products as shown in the reaction pathway. The combined selectivity for the methoxy cleavage products also follows similar trends and is within a close range of $\pm 2\%$ for both the catalysts. However, the selectivity of the two methoxy cleavage products, 4-propyl phenol and 4-propylbenzene-1,2-diol is significantly different for the MWCNT and silica supported catalysts as shown in Figure 5.9. The selectivity for 4-propylbenzene-1,2-diol is higher for the MWCNT supported catalysts while the silica supported catalyst has a higher selectivity towards 4-propylphenol. It should be kept in mind that 4-propylphenol is both a primary product from DHE (C_{sp2}-O cleavage) and a secondary product from 4-propylbenzene-1,2-diol, thereby making it difficult to delineate the actual rates/selectivity for the primary pathway for C_{sp2}-O scission vs C_{sp3}-O scission.

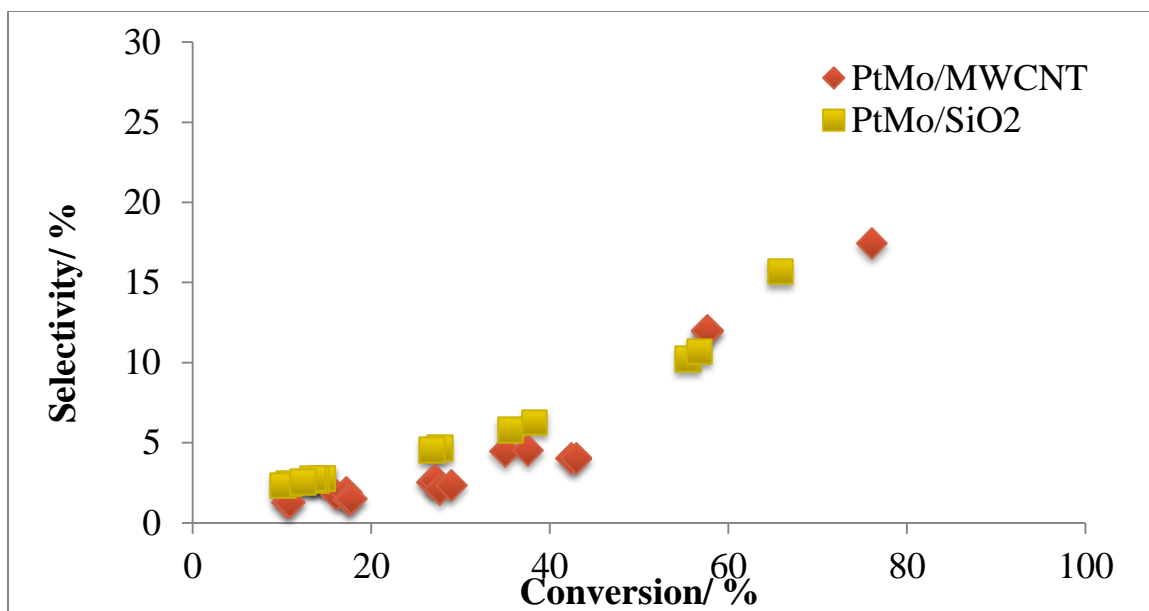


Figure 5.8 WHSV plot for selectivity of propylbenzene versus DHE conversion on the 5%Pt2.5%Mo/MWCNT and the 1.9%Pt1.2%Mo/SiO₂ catalyst, at 300°C, 1 bar hydrogen pressure in the conversion range of 10-80%

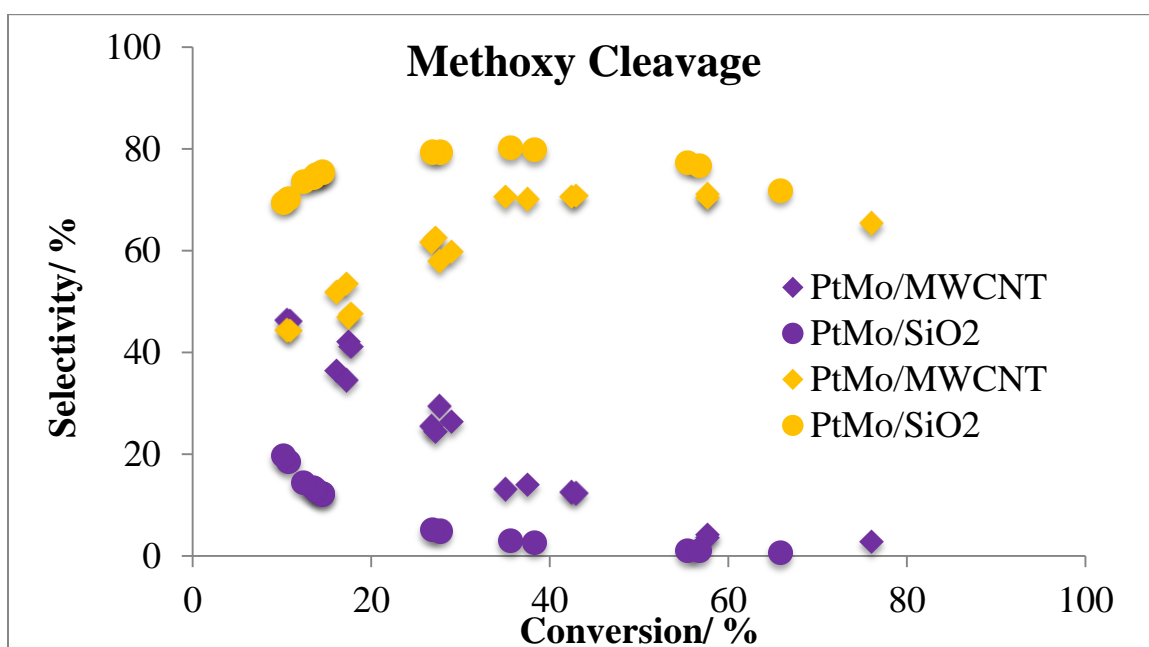


Figure 5.9 WHSV plot for selectivity of primary products, 4-propylphenol (circles), and 4-propylbenzene-1,2-diol (diamonds), versus DHE conversion on the 5%Pt2.5%Mo/MWCNT and the 1.9%Pt1.2%Mo/SiO₂ catalyst, at 300°C, 1 bar hydrogen pressure in the conversion range of 10-80%

The site time yield (STY) normalized by total surface CO chemisorption sites for the dihydroeugenol consumption were calculated for both the catalysts with the assumption that the active sites for the primary pathways were those titrated by CO. Previously, it was shown that methoxy cleavage was the dominant reaction at low conversions and Pt sites were primarily responsible for the chemical transformation thereby partly justifying the assumption.⁷⁰ The overall $STY_{CO\ chemi}$ for DHE consumption were similar for both the PtMo bimetallic catalysts on the different supports. The major difference between the two catalysts was the difference between the ratio of the STY for 4-propylbenzene-1,2-diol and 4-propyl phenol which was ~ 1 for 5%Pt2.5%Mo/MWCNT catalyst and ~ 0.3 for the 1.9%Pt1.2%Mo/SiO₂ catalyst. It was interesting to note that the ratio was ~ 1.9 for the 5%Pt/MWCNT catalyst under the same reaction conditions. Therefore, the addition of Mo to Pt may have modified the pathway to promote C_{sp2}-O scission to form 4-propylphenol, alternatively it may favor the conversion of 4-propylbenzene-1,2-diol to 4-propylphenol thereby decreasing aforementioned ratio in a similar conversion range. STEM/EELS characterization of 5%Pt2.5%Mo/MWCNT catalyst have shown the presence of Pt only (23%) and PtMo bimetallic particles (77%) and the difference in the ratio between the two PtMo bimetallic catalysts could be a result of a different distribution of Pt only and PtMo bimetallic particles, since the Mo:Pt atomic ratio for the MWCNT catalyst is 1:1, while that for SiO₂ support is 1.2:1. The STY yield for the phenolic deoxygenation to propylbenzene was 3 times higher for the SiO₂ supported catalyst and could be partly attributed to a higher Mo:Pt ratio. From a direct comparison between the two catalysts it can be concluded that changing the support from MWCNT to SiO₂ did not qualitatively and quantitatively affect the overall rate and

hydrodeoxygenation selectivity. Therefore, the silica supported catalyst could be used as a substitute for the 5%Pt2.5%Mo/MWCNT for further catalyst regeneration studies.

Table 5.12 Site time yield (STY) for dihydroeugenol consumption from hydrodeoxygenation of dihydroeugenol over Pt-Mo catalysts, studied at 300°C, and 1 bar hydrogen partial pressure.

Catalyst	Conversion /%	STY _{COchemi} /10 ⁻¹ .moles(CO chemisorption sites.sec) ⁻¹
5%Pt 2.5%Mo/MWCNT	10.91	7.1
1.9%Pt 1.2%Mo/SiO₂	10.81	10.4

Table 5.13 Site time yield (STY) for primary product formation from hydrodeoxygenation of dihydroeugenol over 5%Pt/MWCNT and Pt-Mo catalysts, studied at 300°C, and 1 bar hydrogen partial pressure.

Catalyst	Conversion /%	STY _{COchemi} /10 ⁻¹ .moles(surface CO chemisorption sites.sec) ⁻¹		
		Propyl phenol	Propyl benenediol	Ratio (benenediol/phenol)
5%Pt /MWCNT	23.05	1.4	2.6	1.9
5%Pt2.5%Mo/MWCNT	10.91	3.2	3.3	1.0
1.9%Pt1.2%Mo /SiO₂	10.81	8.9	2.4	0.3

Table 5.14 Site time yield (STY) for propylbenzene formation from hydrodeoxygenation of dihydroeugenol over 5%Pt/MWCNT and Pt-Mo catalysts, studied at 300°C, and 1 bar hydrogen partial pressure.

Catalyst	Conversion	STY _{COchemi} /10 ⁻² .moles(surface CO chemisorption sites.sec) ⁻¹
5%Pt2.5%Mo/MWCNT	10.91	0.91
1.9%Pt 1.2%Mo/SiO₂	10.81	3.11

5.3.10 M-Cresol hydrodeoxygenation

5.3.10.1 Motivation

Dihydroeugenol was chosen as a model compound due to presence of key defining functional groups on pyrolysis products from lignin – methoxy group, phenolic group, alkyl side chain. However, the major drawback of studying kinetics of dihydroeugenol hydrodeoxygenation was the difference in reactivity of the two functional groups. Methoxy cleavage was favored at low conversion always preceded phenol hydrodeoxygenation, thereby providing kinetic data from methoxy group scission. As a consequence, m-Cresol was chosen as a model compound for studying the kinetics of phenolic –OH hydrodeoxygenation. Previously, m-cresol hydrodeoxygenation has been studied at low hydrogen pressure (0.5-2 bar) over supported Pt, Ni-Fe catalysts.^{129,132,133,150}

5.3.10.2 Reaction pathways

The space velocity was varied to evaluate the reaction pathway for m-cresol hydrodeoxygenation over the 5%Pt2.5%Mo/MWCNT catalyst at 1 bar hydrogen partial pressure and 300°C temperature. Two main reaction classes were identified: hydrogenation of the aromatic ring, and hydrodeoxygenation. The products formed by aromatic ring hydrogenation without any oxygen removal were methylcyclohexane and methylcyclohexanone, while the hydrodeoxygenation products included toluene, methylcyclohexane and methylcyclohexene (Figure 5.10). Water was formed as a byproduct of hydrodeoxygenation of the phenolic group. Figure 5.11 shows the plots of

selectivity of the identified major products versus m-cresol conversion which enabled the determination of the primary, secondary and tertiary products in the reaction pathway.

The primary products observed were toluene, methylcyclohexanol and methylcyclohexanone with toluene having ~40% selectivity at ~5% conversion. This shows the existence of a direct deoxygenation pathway for phenolic oxygen over the 5%Pt2.5%Mo/MWCNT catalyst which is in agreement with the studies on dihydroeugenol. Methylcyclohexanol was a product of aromatic ring hydrogenation of m-cresol and readily underwent dehydrogenation to form methylcyclohexanone. The selectivity towards methylcyclohexanone was as high as 35% at ~5% conversion, while that for methylcyclohexanol was ~10%. It is interesting to note that the ratio of methylcyclohexanone : methylcyclohexanol was constant over the entire conversion range (~3.5-4) and was indicative of existence of any equilibrium between the two species (Figure 5.12). Resasco et al. have proposed a three way equilibrium between m-cresol, methyl cyclohexanol, and methylcyclohexanone over Pt/SiO₂ catalyst, however it was not observed over the PtMo bimetallic catalytic system, over the entire conversion range. The ratio between m-cresol and methylcyclohexanol changed with space velocity prior to ~20% conversion after which it assumed a constant value (Figure 5.13). Expectedly, a similar trend was observed between m-cresol and methylcyclohexanone, thereby confirming the existence of a rapid equilibrium of methylcyclohexanol and methylcyclohexanone with m-cresol after ~20% conversion. These studies did not confirm an existence of a direct conversion pathway between m-cresol and methylcyclohexanone as has been reported in literature.

The major secondary product was methylcyclohexane and was formed via dehydration of methylcyclohexanol followed by hydrogenation of the intermediate, methylcyclohexene. The selectivity for methylcyclohexane gradually increased with increase in conversion and was accompanied by concurrent decrease in the selectivity of ring hydrogenated oxygenates. From previous studies we have shown that alkylcyclohexanone needed to go through an alkylcyclohexanol intermediate before it underwent dehydration over the Mo sites. As such methylcyclohexanone can be regarded as a reservoir for rapid production of methylcyclohexanol as soon as it is consumed by the dehydration reaction due to existence of equilibrium between the two species over the entire conversion range. Methylcyclohexane was further consumed to toluene, thereby making toluene both, a primary and tertiary product from m-cresol. At ~99.96% conversion, toluene had a selectivity of 93.6% and methylcyclohexane had a selectivity of 5.7% thereby showing the capability of the catalyst for deoxygenation with high selectivity to the major product toluene.

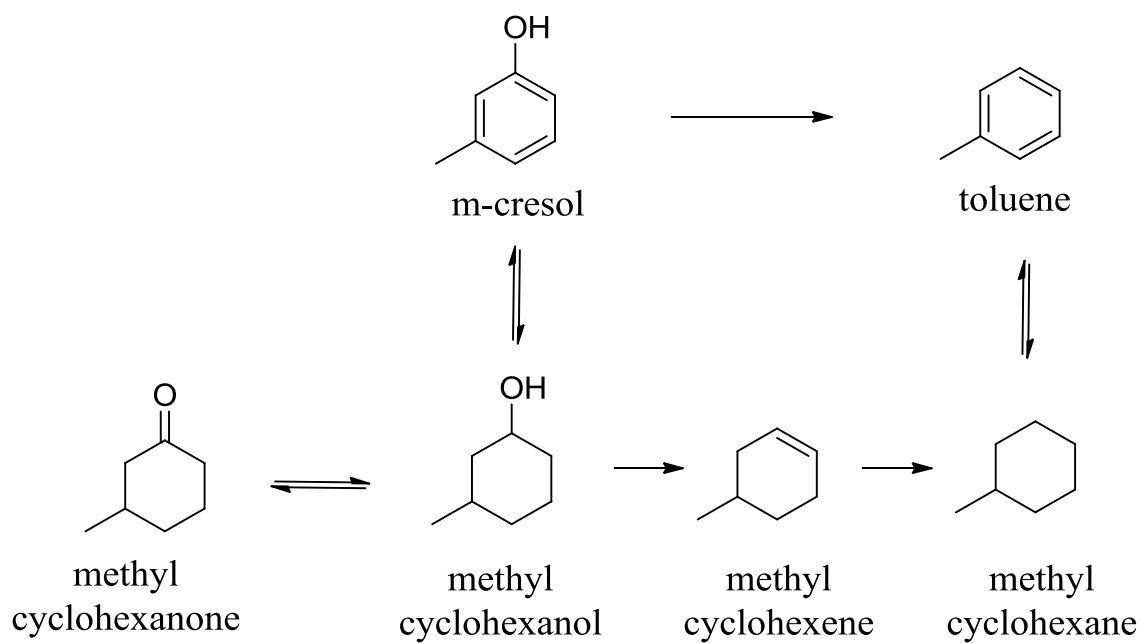


Figure 5.10 Proposed major reaction pathway for low hydrogen pressure (1 bar) vapor phase hydrodeoxygenation of m-cresol over the 5%Pt2.5%Mo/MWCNT catalyst.

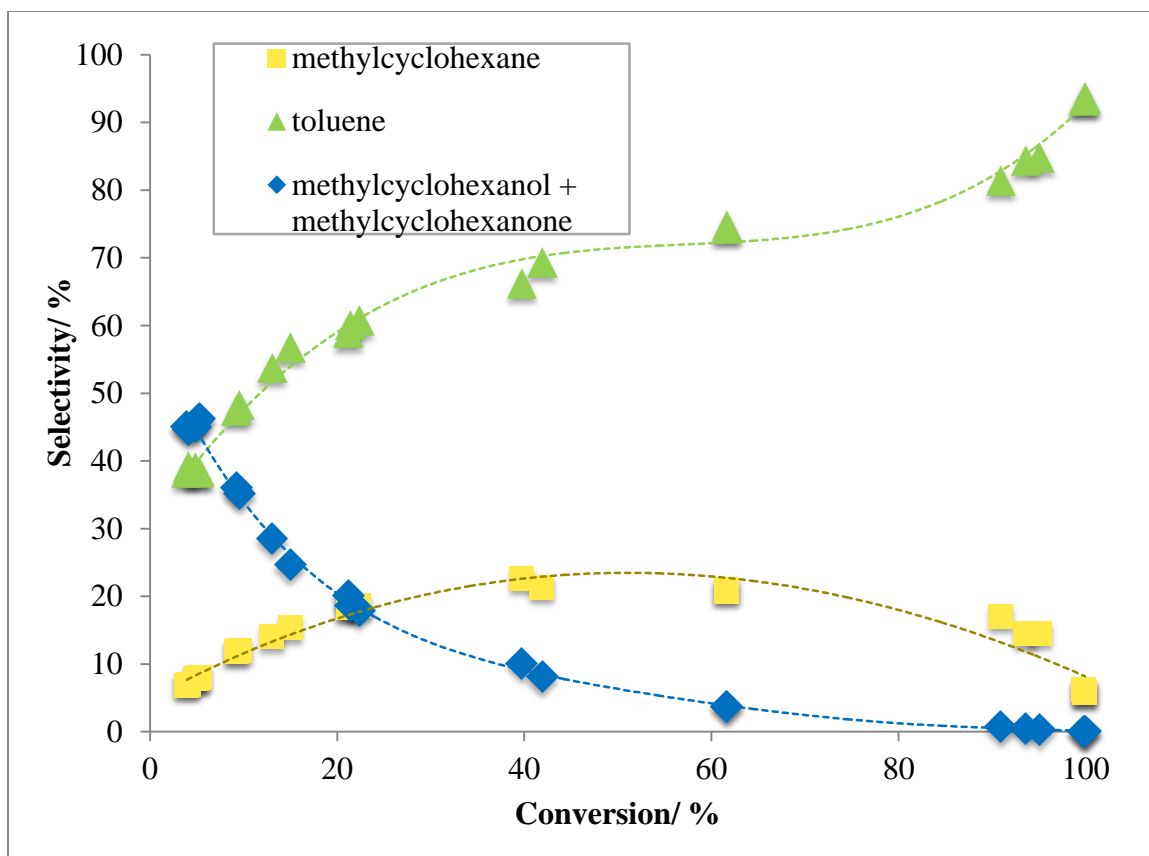


Figure 5.11 WHSV plot for selectivity of major products versus m-cresol conversion on the 5%Pt2.5%Mo/MWCNT catalyst for the products, toluene (primary), methylcyclohexanol + methylcyclohexanone (primary) and methylcyclohexane (secondary), at 300°C, 1 bar hydrogen pressure in the conversion range of 5-100%.

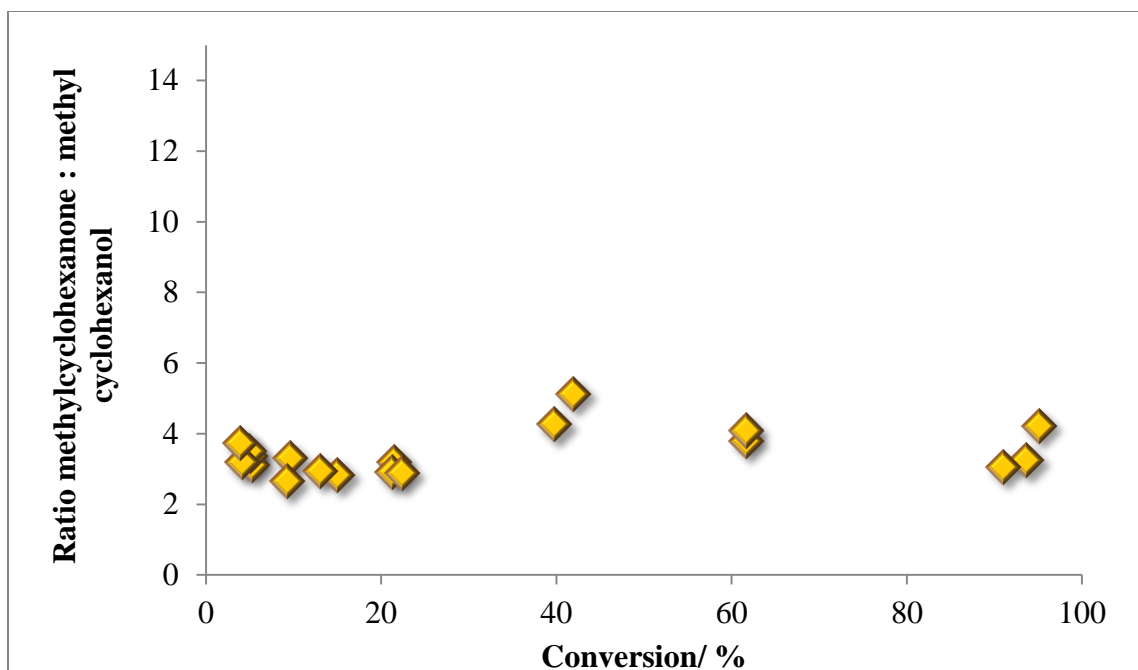


Figure 5.12 Plot for ratio of products, methylcyclohexanone : methylcyclohexanol, as a function of m-cresol conversion on the 5%Pt2.5%Mo/MWCNT catalyst at 300°C, 1 bar hydrogen pressure in the conversion range of 5-100%.

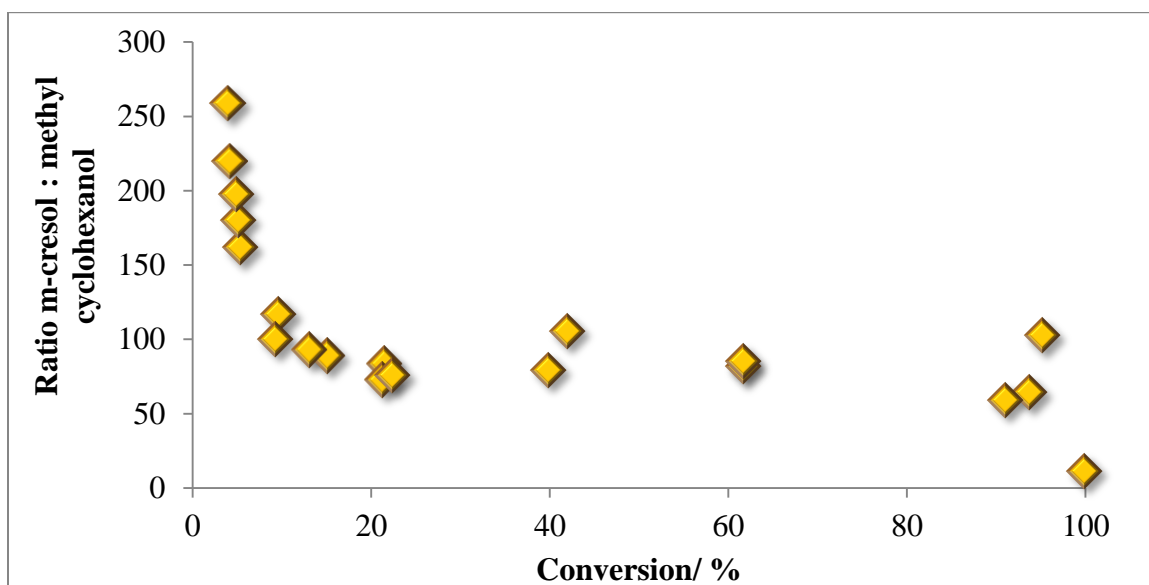


Figure 5.13 Plot for ratio of m-cresol : methylcyclohexanol, as a function of m-cresol conversion on the 5%Pt2.5%Mo/MWCNT catalyst at 300°C, 1 bar hydrogen pressure in the conversion range of 5-100%.

The STY for cresol conversion, toluene formation and ring hydrogenation products for 5%Pt2.5%Mo/MWCNT and 1.9%Pt1.2%Mo/SiO₂ catalysts at ~5% conversion have been reported in Table 5.12. The STYs for cresol conversion are comparable over the two catalysts are comparable with a higher STY for toluene formation over the 1.9%Pt1.2%Mo/SiO₂ catalyst. A parallel can be drawn between a similar trend observed over the 1.9%Pt1.2%Mo/SiO₂ catalysts for methoxy cleavage pathway during dihydroeugenol with higher selectivity to the 4-propylphenol as compared to 5%Pt2.5%Mo/MWCNT. Both phenomenon could be explained on the basis of a higher atomic Mo:Pt ratio for the 1.9%Pt1.2%Mo/SiO₂ catalyst as explained previously.

Table 5.15 Site time yield (STY) for m-cresol consumption and primary product formation ,toluene and ring hydrogenation products (methylcyclohexanol + methylcyclohexanone) during hydrodeoxygenation of m-cresol over the Pt-Mo catalysts, studied at 300°C, and 1 bar hydrogen partial pressure

Catalyst	Conversion	STY _{Pt} / mol.(mol of Pt) ⁻¹ .s ⁻¹		
		m-Cresol	toluene	ring hydrogenation
PtMo/MWCN	5.06	0.031	0.012	0.014
T				
PtMo/SiO₂	4.91	0.031	0.014	0.012

Catalyst	Conversion	STY _{COchemi} / mol.(mol of CO chemisorption sites) ⁻¹ .s ⁻¹		
		m-Cresol	toluene	ring hydrogenation
PtMo/MWCN	5.06	0.39	0.15	0.18
T				
PtMo/SiO₂	4.91	0.39	0.18	0.15

5.3.11 Catalyst regeneration

Preliminary catalyst regeneration studies focused on developing a strategy to restore the initial catalyst activity after a run time of at least 3 days (~25-30 hours). The leading

causes for catalyst deactivation are nanoparticle sintering, coking, poisoning etc.^{152–155} Catalyst characterization studies have shown that there is no change in the Pt particle size distribution between the fresh and the used catalyst within the specified error range. Catalyst coking has been previously observed during hydrodeoxygenation of biomass pyrolysis products and generally requires high temperature oxygen treatment to regenerate the catalyst. Accumulation of carbonaceous species has also been proposed to be the cause for catalyst deactivation during hydrodeoxygenation of furfural over Mo₂C catalysts.¹⁵⁶ Regeneration in 1 bar hydrogen at 570K for ~1hr was shown to completely restore the conversion and selectivity of the catalyst. Partial regeneration of catalyst activity was observed due to overnight flow of hydrogen in absence of reactant, m-Cresol (Figure 5.14). Reduction of the deactivated catalyst in hydrogen at 450°C for 2 hours was insufficient to restore the catalyst activity to its initial level (Figure 5.14). However, it could be used to partially regenerate the catalyst after continuous operation.

Oxygen treatment has been used previously to burn off carbonaceous species off the catalyst as a means to regenerate the catalyst. The deactivated catalyst was heated to a final temperature (250°C, 300°C, 350°C, and 450°C) in 10% v/v oxygen in balance helium in 2 hours and was held at the final temperature for 1 hour, followed by a cool down to room temperature. The catalyst was then reduced in hydrogen according to the standard reduction procedure for PtMo bimetallic catalysts, outlined previously. The reduced catalyst was then tested with the model compound (DHE/m-Cresol) and the activity was compared with the fresh, reduced catalyst. As shown in Figure 5.15, oxygen treatment resulted in further catalyst deactivation with DHE. The regeneration treatment

at 300°C decreased the overall $STY_{\text{per mole Pt}}$ to 0.015 moles.s⁻¹, as compared to 0.09 moles.s⁻¹ for the reduced only catalyst. Increasing the final temperature of the oxygen treatment resulted in further decrease in the overall STY. Therefore for the 1.9%Pt1.2%Mo/SiO₂ catalyst, oxygen treatment was not an option for catalyst regeneration. Curiously, a similar oxygen treatment with m-cresol as reactant (final temperature = 300°C) resulted in partial regeneration of the catalyst activity as shown in Figure 5.16. It has been shown before that STY_{DHE} measures the catalyst activity for methoxy group deoxygenation, while $STY_{\text{m-Cresol}}$ measures the catalyst activity for phenolic -OH deoxygenation. Therefore, it could be proposed that the active sites for these two steps are different over the catalyst and oxygen treatment resulted in preferential modification of the active site for methoxy group cleavage. Further characterization studies need to be done to understand the change in the catalyst structure to explain the observed results.

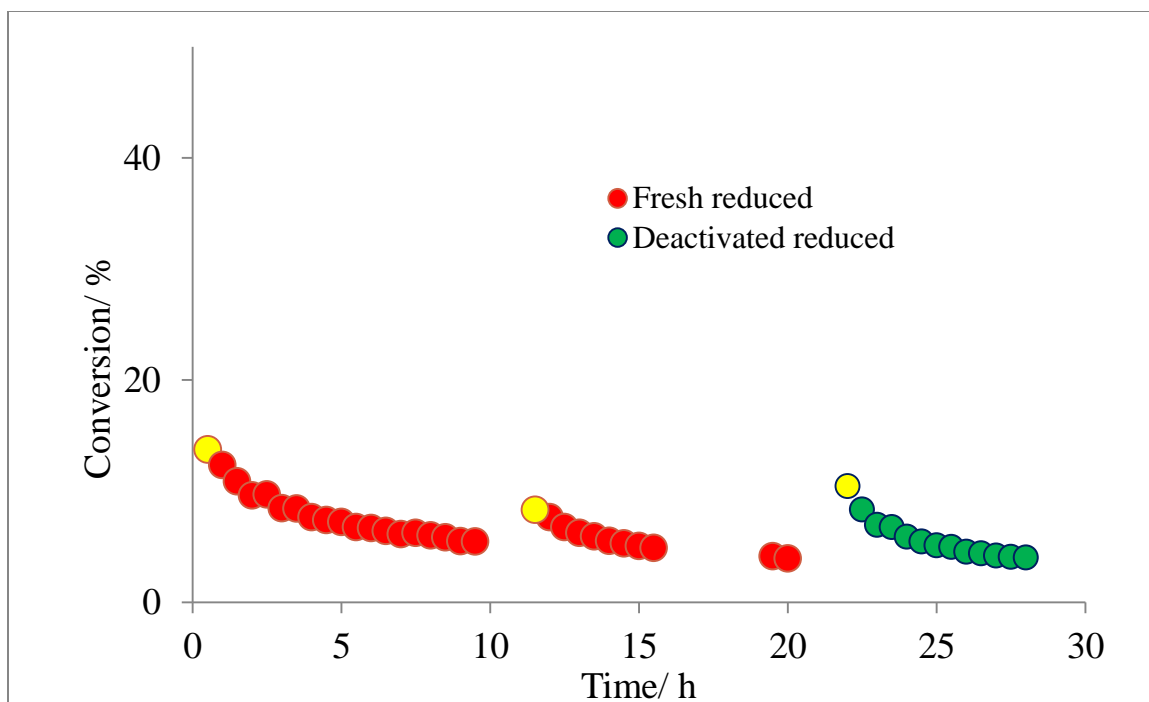


Figure 5.14 Conversion profile for m-cresol as a function of time of operation over the 5%Pt2.5%Mo/MWCNT catalyst at 300°C and 1 bar hydrogen partial pressure. Red – Fresh, reduced catalyst deactivation profile; Green – Deactivated catalyst was re-reduced at 450°C in hydrogen under standard conditions after 20 hours of operation; Yellow – Indicates first conversion data point on a new day of operation.

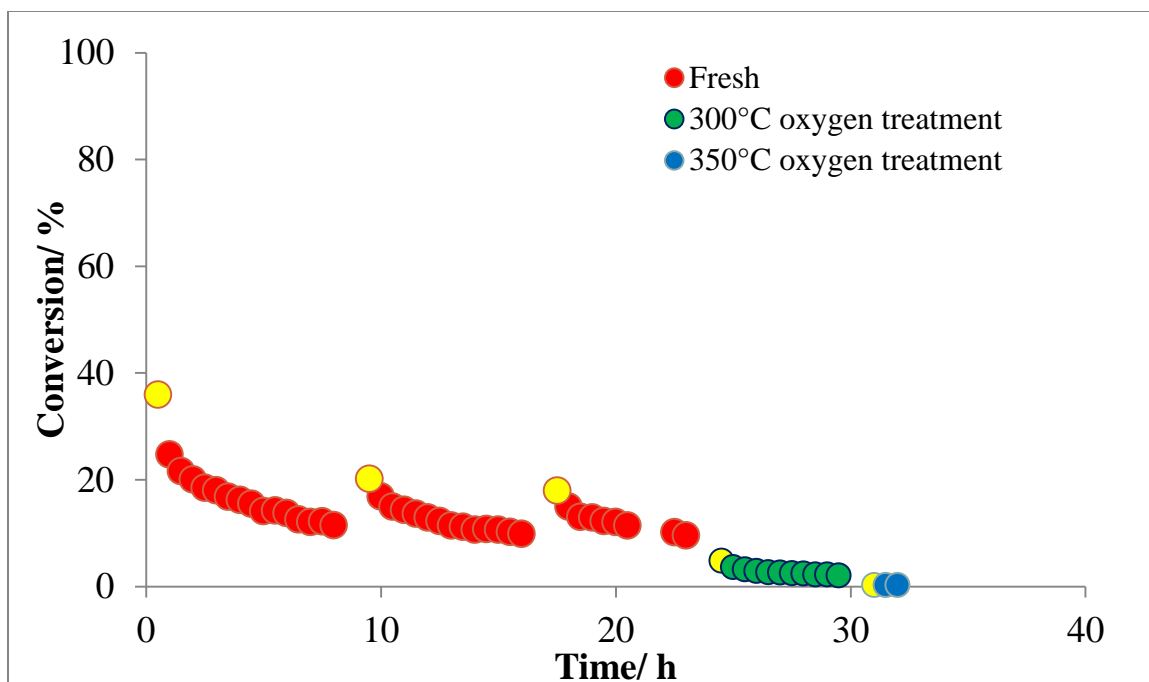


Figure 5.15 Conversion profile for dihydroeugenol as a function of time of operation over the 1.9%Pt1.2%Mo/SiO₂ catalyst at 300°C and 1 bar hydrogen partial pressure. Red – Fresh, reduced catalyst deactivation profile; Green – Deactivated catalyst was subjected to oxygen treatment at 300°C as described previously and then reduced at standard reduction procedure at 450°C; Blue - Deactivated catalyst was subjected to oxygen treatment at 350°C, as described previously, and then reduced at standard reduction procedure at 450°C; Yellow – Indicates first conversion data point on a new day of operation.

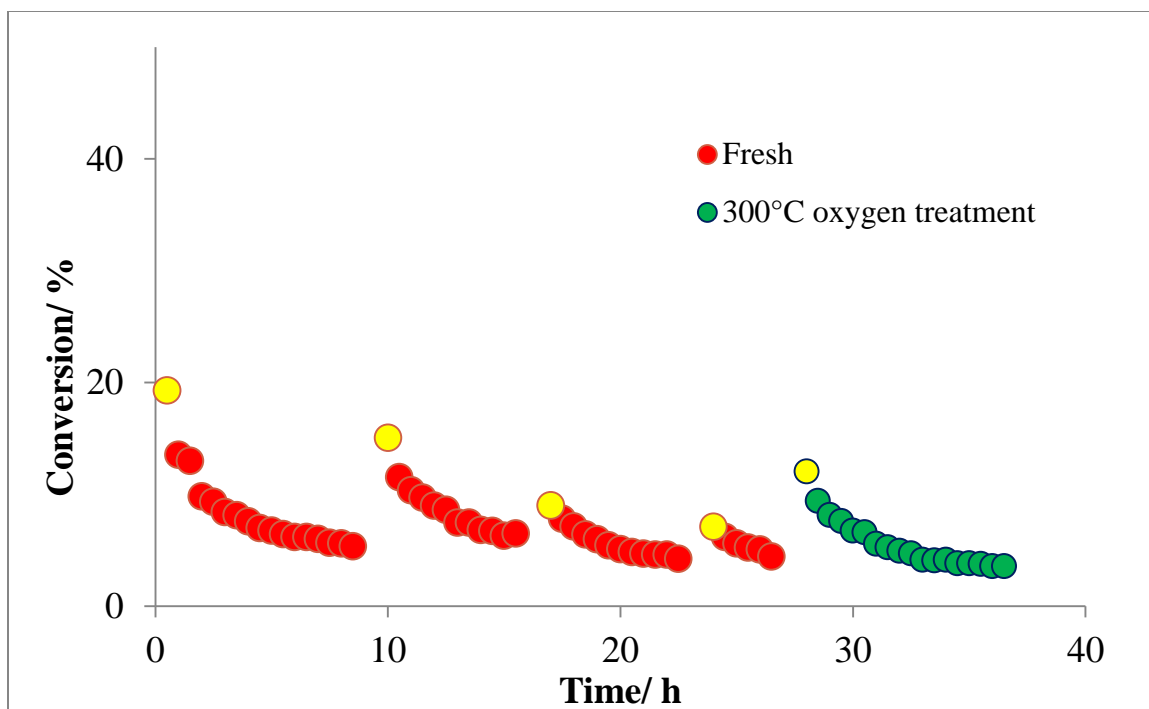


Figure 5.16 Conversion profile for m-cresol as a function of time of operation over the 1.9%Pt1.2%Mo/SiO₂ catalyst at 300°C and 1 bar hydrogen partial pressure. Red – Fresh, reduced catalyst deactivation profile; Green – Deactivated catalyst was subjected to oxygen treatment at 300°C, as described previously, and then reduced at standard reduction procedure at 450°C; Yellow – Indicates first conversion data point on a new day of operation.

5.4 Conclusion

Pt based catalysts were studied for hydrodeoxygenation of lignin model compounds, dihydroerugenol and m-cresol. Pt promoted with oxophilic promoter Mo was shown to have high selectivity for producing hydrocarbons from dihydroerugenol with ~97% yield to propylcyclohexane at 25 bar hydrogen partial pressure and ~92% yield to propyl benzene at 1 bar hydrogen partial pressure. The role of Pt and Mo in the reaction pathway was investigated by varying the relative atomic ratio of Pt and Mo. An increase in the Mo content was shown to promote the selectivity for the final deoxygenation step to product

propyl cyclohexane at 25 bar hydrogen pressure. Experiments with reaction intermediates were performed on the Mo only catalyst which showed that Mo phases were responsible for dehydration of the phenolic –OH after ring hydrogenation. However despite playing distinct roles in the reaction pathway, Pt and Mo were required in conjunction for production of C₉ hydrocarbons with high selectivity, with a physical mixture of the Pt only and Mo only catalysts resulting in decrease in the selectivity. Pt on acidic supports (silica alumina, HUSY) were studied and showed C-C scission of the propyl side chain form C₇-C₈ hydrocarbons, concurrently decreasing the selectivity towards C₉ hydrocarbons. Catalyst stability and regeneration studies were performed on the PtMo bimetallic catalyst supported on silica. Catalyst stability and reaction pathway studies showed no effect of support when it was changed from MWCNT to silica. Regeneration attempts with molecular oxygen treatment up to 450°C were unsuccessful and resulted in a decrease in the site time yield for dihydroeugenol and partial regeneration for m-cresol. Additional catalyst characterization studies will be required for understanding the change in the catalyst structure with oxygen treatment. However, it can be concluded that high temperature oxygen treatment did not result in catalyst regeneration. Additionally, m-cresol hydrodeoxygenation was studied and demonstrated a direct deoxygenation pathway for phenolic –OH hydrodeoxygenation at 1 bar hydrogen partial pressure, which are in agreement with previous studies with dihydroeugenol.

CHAPTER 6. EFFECT OF HYDROGEN PRESSURE DURING HYDRODEOXYGENATION OF PYROLYSIS PRODUCTS FROM BIOMASS AND ITS INDIVIDUAL COMPONENTS

6.1 Abstract

Pulse catalytic studies were used to investigate the effect of hydrogen pressure (1-25 bar) during hydrodeoxygenation (HDO) of pyrolysis products from biomass (poplar, pine, maize) and model compounds (cellulose, xylan, lignin) over Pt-Mo bimetallic catalysts at 300°C. The Pt-Mo ratio was varied to ascertain the role of Mo as an oxophilic promoter for increasing the yield towards HDO products. Hydrogen pressure, in the range of 1-25 bar, was found to be a critical factor for governing the hydrocarbon product distribution due to an increase in C-C scission at low hydrogen pressures, which resulted in a decrease in the yield of liquid fuel range (C₄₊) hydrocarbons. A decrease in the hydrogen pressure resulted in an increase in the yield of aromatic hydrocarbons, derived primarily from the lignin fraction of biomass. The results from the pulse reactor were verified in a continuous-flow fast-hydrolysis and catalytic hydrodeoxygenation reactor system with cellulose and poplar as feedstocks.

6.2 Introduction

Lignocellulosic biomass is an abundant source of renewable carbon, which can be harnessed for conversion to liquid hydrocarbon fuels to reduce the dependence on fossil based sources of fuel.^{7,13,25} Fast pyrolysis followed by in-line hydrodeoxygenation is considered a feasible process for conversion of biomass to liquid hydrocarbon fuel with potential to be economically viable.^{16,24} The condensed liquid product from fast pyrolysis of biomass, called bio-oil, is a highly complex mixture of oxygenates with energy content similar to that of the biomass.^{22,43} Therefore, it is necessary to upgrade the bio-oil by catalytic hydrodeoxygenation, which generally poses major challenges such as catalyst coking, undesired secondary reactions (i.e polymerization), and reactor plugging.^{39,157,158} To overcome these challenges, the H₂Bioil process proposes an integrated, high pressure fast hydrolysis followed by a vapor phase hydrodeoxygenation step to avoid undesired secondary reactions that take place during condensation of bio-oil.^{24,26,27,37} Presence of high pressure hydrogen was shown to mitigate catalyst coking^{154,159} during hydrotreating processes at the same time leading to higher hydrodeoxygenation rates.^{70,146} However, the systematic data on the effect of hydrogen pressure needed to optimize the process is not yet available. To fill this need, this chapter presents the effect of hydrogen pressure on hydrodeoxygenation product yields for model compounds as well as biomass pyrolysis products.

Among the biomass conversion pathways involving fast pyrolysis and subsequent vapor phase hydrodeoxygenation, there are two major distinctions depending on the location of

the catalyst relative to the pyrolysis zone; *in situ* and *ex situ*.^{157,160} For *in situ*, also known as catalytic pyrolysis, the catalyst is placed in the pyrolysis zone thereby minimizing the residence time between pyrolysis and deoxygenation. Several studies have reported using zeolites as candidate catalysts for catalytic pyrolysis with the aim of producing aromatic hydrocarbons from lignocellulosic biomass.^{160,161} HZSM-5 was reported to have the highest yield towards aromatic hydrocarbons (~35%), but was accompanied by formation of substantial quantity of coke (20-40% carbon yield) on the catalyst, necessitating frequent catalyst regeneration for continuous process operation.¹⁶²⁻¹⁶⁵ Another drawback of catalytic pyrolysis is lack of independent temperature control of the catalyst from that of pyrolysis. On the contrary, *ex situ* catalytic hydrodeoxygenation allows for the catalyst to be placed downstream of the pyrolysis zone, with an independent control over the catalyst as well as the pyrolysis temperature, both of which have been shown to play an important role in governing the product distribution.^{69,70,166}

The major challenge for hydrodeoxygenation of biomass pyrolysis products is development of catalysts which are stable, and selective despite the large diversity of molecules that need to be processed. The literature on deoxygenation studies of model compounds covers conversion of cellulose/hemicellulose derived oxygenates (furfural, HMF, glycolaldehyde, etc) and lignin derived oxygenates (guaiacol, dihydroeugenol, m-cresol, etc). Lignin derived molecules have an aromatic backbone bearing primarily phenolic and methoxy groups, in addition to a substituted alkyl chain, usually in the para position with respect to the phenolic oxygen.⁸⁴ Hydrodeoxygenation studies on lignin model compounds have been focused on developing active, stable and selective catalysts

for deoxygenation of the phenolic and methoxy functional groups.⁹⁸ A variety of supported noble metal catalysts in conjunction with an acidic function, either in the form of a support, a promoter or a solvent have been studied with success.¹²⁶⁻¹³⁰ Hydrogen pressure was proven to be a critical parameter for not only controlling the final product distribution but also the dominant pathways of deoxygenation of these lignin derived molecules.⁷⁰ However, the effect of these catalysts on deoxygenation of the substituted propyl side chain has not been widely studied, mostly because of the choice of model compounds like guaiacol, m-cresol, and dihydroeugenol. It is imperative to stem any carbon loss from the alkyl side chain thereby maximizing the yield towards C₉ aromatic hydrocarbons. The most desirable products from hydrodeoxygenation of lignin pyrolysis products are aromatic hydrocarbons, with the objective to produce gasoline range molecules, as they have a higher octane number than their saturated counterparts.

There have been several interesting studies for conversion of cellulose and cellulose derived molecules to alkanes in the liquid phase with hydrogenation and acid chemistry being utilized for selective hydrodeoxygenation.¹⁶⁷⁻¹⁷⁰ However, most of the liquid phase processes are multi-stage, requiring prior extraction of cellulose/hemicellulose from the biomass. A major challenge during hydrodeoxygenation of sugar-derived molecules is selective C-O scission without C-C scission, which results in the decrease in molecular weight of final products as well as reduction in the overall carbon efficiency.¹⁷¹ In the literature, furfural has been studied as a model compound to identify catalyst descriptors for minimizing C-C scission via decarbonylation reactions.^{70,172} Previous studies have effectively utilized bimetallic chemistry to modify the electronic properties of the

hydrogenating metals (Pd,Ni,Pt) with oxophilic promoters (Cu,Fe,Mo) for suppressing carbon loss via the decarbonylation pathway.^{173,174} In other studies, Mo alloyed with Pt was shown to selectively promote C-O scission,^{134,135} while Mo in oxide and carbide form was also effective for hydrodeoxygenation of model compounds.¹³⁶⁻¹³⁹ In this study, we have extended the vapor phase model compound studies towards hydrodeoxygenation of pyrolysis products from cellulose, lignin and intact biomass, in order to understand the role of Pt and Mo in governing the final hydrocarbon product yields. Recently published studies from our group have shown that a Pt-Mo bimetallic catalyst was effective in producing ~73% carbon recovery from cellulose and ~54% from poplar in the form of hydrocarbons in a $\text{g}\cdot\text{min}^{-1}$ scale continuous fast hydrolysis and vapor phase catalytic hydrodeoxygenation reactor.¹⁶⁶ Others have reportedly used a combination of catalytic hydrolysis and downstream hydrodeoxygenation to produce hydrocarbons with proprietary catalysts.^{175,176} In this chapter, we have explored the effect of hydrogen partial pressure on hydrodeoxygenation of pyrolysis products from different components for biomass over the PtMo bimetallic catalyst system and its importance for controlling aromaticity and C-O versus C-C bond scission.

6.3 Experimental methods

6.3.1 Materials

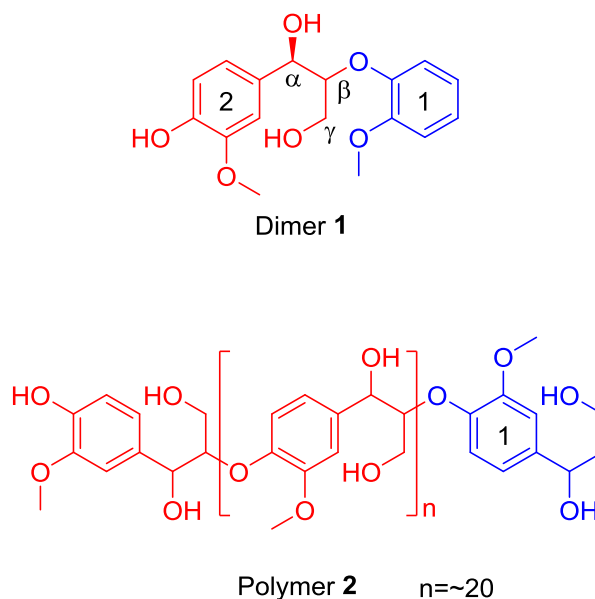


Figure 6.1 Structures of lignin model compounds.

The microcrystalline cellulose (50 μ m) used for all the experiments was purchased from Sigma-Aldrich. Xylan (min 95% purity) was obtained from Carbosynth Limited, while the lignin model compound, dimer **1** was purchased from TCI America. The other lignin model compound, polymer **2** was synthesized by the procedure outlined by Kishimoto et al. and its structure was verified by using $^1\text{H-NMR}$ and $^{13}\text{C-NMR}$ studies.¹¹⁴ The poplar and pine feedstocks (<80 mesh) were obtained from National Renewable Energy Laboratory (NREL). The maize feedstock (B73) was obtained as a part of collaborate research effort in the Energy Frontier Research Center, C3Bio.¹⁷⁷ All the biomass samples were milled to less than 270 mesh (0.053mm) to eliminate mass transfer

limitations due to particles size effects. The results of compositional analysis of biomass have been reported in Table E. 1.

6.3.2 Catalyst preparation

Five catalysts containing various proportions of platinum and molybdenum supported on multi-walled carbon nanotubes (MWCNT) have been used for this study (Table 6.1). The catalysts were prepared by incipient wetness impregnation method, and the detailed preparation procedure has been previously reported.¹⁴⁶

Table 6.1 List of the catalysts tested in the micro-scale semi-batch catalytic reactor (pyroprobe)

Catalyst	Mo:Pt atomic ratio / moles:moles
5%Pt/MWCNT	0
5%Pt 1.2%Mo/MWCNT	0.5
5%Pt 2.46%Mo/MWCNT	1
2.5%Pt 2.46%Mo/MWCNT	2
2.46%Mo/MWCNT	∞

6.3.3 Catalyst characterization

Catalyst characterization techniques used were CO chemisorption, Transmission Electron Microscopy (TEM), Scanning Transmission Electron Microscopy (STEM), and Electron Energy Loss Spectroscopy (EELS), X-ray Absorption Spectroscopy(XAS), X-ray Photoelectron Spectroscopy(XPS). The details of these techniques, procedures and results have been reported previously.¹⁴⁶

6.3.4 Reactor description

6.3.4.1 Lab-scale continuous flow cyclone type reactor

The lab-scale, high-pressure, continuous-flow fast-hydropyrolysis and vapor-phase catalytic hydrodeoxygenation (HDO) reactor was used to carry out continuous studies with $\sim 0.1 \text{ gm}\cdot\text{min}^{-1}$ flow rate of cellulose and poplar. The reactor served to perform proof of concept studies and verification of the results from the micro-scale semi-batch catalytic reactor. A detailed description of the reactor has been reported previously.^{69,166}

6.3.4.2 Micro-scale semi batch catalytic reactor (Py-GC/MS)

Fast-hydropyrolysis and catalytic hydrodeoxygenation experiments were carried out using a Pyroprobe 5200 HP (CDS Analytical Inc.), retrofitted with a downstream catalytic reactor and connected to an online gas chromatograph (Agilent 7890A) equipped with a Flame ionization detector and a mass spectrometer (5975C). A resistively heated Pt coil was used as a heating source for pyrolysis/evaporation of the model compounds (levoglucosan), model polymers (cellulose, dimer **1**, polymer **2**) and intact biomass. A known weight of the reactant sample was loaded in a quartz tube (0.15cm ID X 2.5cm length), which was subsequently placed in the annulus of the Pt coil. A heating rate of $1000^\circ\text{C}\cdot\text{s}^{-1}$ was used to attain a final temperature of 500°C during pyrolysis/evaporation of the sample. The pyrolysis vapors were flushed out from the quartz tube by the reactant gas (H_2 , balance He) and passed over the catalyst bed on the way to the GC-MS. For pyrolysis only experiments, no catalyst was loaded in the fixed bed reactor. The GC was equipped for hydrocarbon separation with a GS-GasPro column

(ID 0.32mm X 5m), which was connected to a three way splitter with auxiliary gas input. The flow from the column was split to the FID and MS with synchronized peaks for quantification and identification, respectively. The system had two relief valves to prevent over pressurization of pyrolysis chamber and the fixed bed reactor assembly (set point 40 bar), and the GC-MS inlet assembly (set point 6.5 bar).

The pyrolysis sample (0.2-1 mg) was loaded inside the quartz tube in front of a plug of quartz wool and the amount of sample was measured by weighing the quartz tube before and after the sample loading. The sample loading procedure was tested via reactant gas flow and pressure variation (1 bar to 25 bar) experiments to ensure that the sample was not dislodged from the quartz tube before pyrolysis.

After the sample was loaded, the quartz tube was placed inside the annulus of the Pt coil, which was mounted on a probe. The probe was then placed inside the pyrolysis chamber (Figure 2.1) and the air was flushed out using nitrogen. The 8 port valve was switched to introduce the pressurized reactant gas mixture (H_2 , balance He) and flush out the nitrogen, which resulted in the pyrolysis chamber being pressurized to the desired operational pressure. The placement of the fixed bed reactor ensured that at no point during the sample loading and running phases was the pre-reduced catalyst exposed to air. The pyrolysis chamber was then heated by an external heater to a temperature of $300^\circ C$ in ~ 10 s followed by the Pt coil being heated to a final temperature of $500^\circ C$ at a heating rate of $1000^\circ C \cdot s^{-1}$ to start the run. The pyrolysis vapors were carried out from the quartz tube to the catalyst bed through heat traced tubing. The pressure was stepped down after

the back pressure regulator so that it was within the acceptable range for the GC-MS (10-100 psi). Only a fraction of the flow was injected into the GC-MS to control the split ratio as well as protect the GC-MS from excessively high flow rates (>1 slpm) during the high pressure runs. The balance flow was vented. The split flow was controlled by a needle valve placed on the vent line. The split/splitless inlet of the GC was maintained at a temperature of 300°C and a split ratio in the range of 10:1 and 100:1 was used depending on the total pressure and flow rate through the fixed bed reactor. The actual split ratio was calculated by measuring the flow rates in the vent and GC split vent lines (Figure 2.3). During a typical run, the GC oven was initially maintained at 35°C for 5 min, followed by a $10^{\circ}\text{C s}^{-1}$ ramp to 300°C and held at the final temperature for 20 min.

The peaks observed in the gas chromatogram (FID) comprised of C_1 - C_{10} hydrocarbons which were identified by comparing the EI spectrum from the mass spectrometer to those in the MS NIST (National Institute of Standards and Technology) database. These products were quantified on the basis of calibrations made by using available standard compounds. CO and CO_2 were quantified by making calibrations with the major ion ($m/z=28$ for CO and $m/z=44$ for CO_2) in the mass spectrometer. The char analysis was obtained by weighing the quartz tube, before (quartz wool + sample) and after (quartz wool + char residue) pyrolysis and obtaining the difference from the weight of the quartz tube with quartz wool only. All the product quantification has been reported in the form of carbon yield percentage of the feed biomass. The percentage of carbon in the biomass was estimated by ultimate analysis, performed by Hazen Research Inc (Table E. 2), while

the percentage of carbon in the char was obtained from the lab-scale continuous flow cyclone type reactor was estimated by Galbraith Laboratories, Inc.

The products from hydrodeoxygenation of biomass pyrolysis vapors included hydrocarbons, and permanent gases (CO and CO₂). No oxygenates were detected in the product stream, and a total carbon balance of 95±5% indicated near complete hydrodeoxygenation of the pyrolysis products. Previous experiments with the same catalyst on cellulose and poplar pyrolysis products in a continuous fast hydrolysis, hydrodeoxygenation reactor have found no detectable coke formation on the catalyst (5%Pt 2.5%Mo/MWCNT) with steady operation up to 1 hour at a biomass feed rate of ~0.1 gm.min⁻¹.¹⁶⁶

6.4 Results

6.4.1 Hydrocarbon product distribution from HDO of biomass and related model

polymers and compounds

The products obtained from fast hydrolysis and hydrodeoxygenation of biomass and biomass model compounds comprised of char, CO, CO₂, and C₁ through C₁₀ hydrocarbons. Preliminary hydrodeoxygenation studies with levoglucosan over the 5%Pt 2.5%Mo/MWCNT at 50-80% conversion resulted in formation of >100 molecular intermediates making identification and analysis a significant challenge. Therefore for all the reported experiments, the catalyst loadings were sufficiently high such that there was no detectable yield of oxygenated species after hydrodeoxygenation. The only exceptions

were experiments for hydrodeoxygenation of cellulose pyrolysis products with Pt/MWCNT, where oxygenated species were detected. The observed hydrocarbons have been grouped in fractions depending on the number of carbon atoms per molecule, for instance C₁-C₃, C₄₊ etc. The detailed product composition of these fractions is available in Table E. 3. The grouping categorizes C₄₊ hydrocarbons as liquid fuel range molecules, which is consistent with other studies in literature.^{166,175,176} Additionally, these categories were an indication of the extent of C-C bond scission prevalent during hydrodeoxygenation of pyrolysis molecules and a higher yield of C₁-C₃ fraction implied a higher degree of C-C bond scission, which was considered undesirable. Hydrocarbons (propyl benzene, propylcyclohexane) were passed over the 5%Pt 2.5% Mo/MWCNT catalyst under standard experimental conditions to test their reactivity over the catalyst. Hydrocarbons were detected intact in the GC-MS and did not react to give any other products. Therefore, it was concluded that any C-C scission occurred during hydrodeoxygenation, and any hydrocarbons formed subsequently, passed through the catalyst bed with any loss of carbon. This assured that excess loading of the catalyst was unlikely to affect the product distribution after complete hydrodeoxygenation of the pyrolysis products from the various feedstocks.

6.4.2 Fast hydropyrolysis: effect of hydrogen pressure

Studies by Venkatakrishnan et al. have shown that pyrolysis of cellulose in the presence of hydrogen (up to 25 bar pressure) does not significantly alter the pyrolysis product distribution at 480°C when compared with that under inert conditions (He).⁶⁹ As shown by Mehta et al.,⁷⁰ during cellulose hydropyrolysis the products retain the same oxygen

content as that in cellulose, and no significant deoxygenation takes place in the presence of high pressure hydrogen. Hence, downstream catalytic hydrogenation is critical for removing majority of the oxygen content to produce hydrocarbons for fuel applications. In the case of pure levoglucosan, it was observed to have evaporated cleanly without any detectable byproducts under standard pyrolysis conditions, and was obtained with >95% mass balance in the GC-MS. The results for fast pyrolysis of lignin model compounds (dimer **1** and polymer **5**) have been reported in Chapter 4. Pyrolysis of lignin model compounds under elevated hydrogen pressure (25 bar) had no significant effect on the pyrolysis product distribution when compared with pyrolysis under inert conditions (He, 1 bar) as shown in Table E. 4 and Table E. 5. Therefore, it was assumed that the pyrolysis product distribution from cellulose, lignin model compounds, and by extension biomass is independent of the hydrogen pressure during pyrolysis. Consequently, any variations in the hydrocarbon product distribution, as a result of systematic variation in the hydrogen pressure were attributed to downstream catalysis.

6.4.3 Levoglucosan

Levoglucosan was chosen as a model compound for hydrodeoxygenation of cellulose derived molecules since it is the most abundant product from cellulose pyrolysis.^{69,71} Levoglucosan was passed over the 5%Pt 2.5%Mo/MWCNT catalyst at 300°C at 25 bar hydrogen pressure, and the lumped hydrocarbon product distribution is shown in Table 6.2. The total carbon yield of hydrocarbons was ~94%, while that for the fuel range hydrocarbons (C₄₊) was ~72%. The carbon yield toward C₆ hydrocarbons was ~47% and was obtained by complete deoxygenation of levoglucosan without any C-C scission

during hydrodeoxygenation. No char was detected in the quartz tube during evaporation of levoglucosan during any of the experiments.

6.4.4 Cellulose

Cellulose pyrolysis vapors were passed over the 5%Pt 2.5%Mo/MWCNT catalyst at 300°C at 25 bar hydrogen pressure and the lumped hydrocarbon product distribution is shown in Table 6.2. The total carbon yield of hydrocarbons was ~74%, while that for the fuel range hydrocarbons (C₄₊) was ~50%. The carbon yield toward C₆ hydrocarbon fraction was ~23%, and was lower than that for levoglucosan partly due loss of carbon in the form of char (~17%) and partly due to C-C bond scission during pyrolysis. A minor fraction of the hydrocarbon comprised of C₇ and higher hydrocarbons, with a cumulative carbon yield of ~7%. The overall carbon balance including char, CO, CO₂, and hydrocarbons was ~94%, indicating close to complete deoxygenation of cellulose pyrolysis products.

6.4.5 Lignin model compounds

The structures of lignin model compounds, dimer **1** and polymer **2** are shown in Figure 6.1. Both model compounds are composed of guaiacyl lignin monomers connected by β-O-4 linkage, which is the most abundant linkage in the lignin polymer.⁸⁴ Pyrolysis products from the aforementioned lignin model compounds were passed over the 5%Pt 2.5%Mo/MWCNT catalyst at 300°C at 25 bar hydrogen pressure, and the lumped hydrocarbon product distribution is shown in Table 6.2. The major hydrocarbon products observed were cyclohexane (C₆), methylcyclohexane (C₇), ethylcyclohexane (C₈), and

propylcyclohexane (C₉). Without any C-C scission, propyl cyclohexane (C₉) was the expected major product from hydrodeoxygenation of lignin pyrolysis products on the basis of model compound studies with dihydroeugenol. For dimer **1**, the C₆ fraction carbon yield (36%) was primarily from the guaiacyl end group of the molecule and is similar to the theoretical estimation of ~35% (carbon yield of benzene from ring #1 of dimer **1** as shown in Figure 6.1). The C₇-C₉ hydrocarbon yield was obtained from ring 2 of dimer **1**, with the alkyl chain exhibiting carbon loss due to C-C scission. For lignin polymer **2**, the yield of C₆ hydrocarbons was substantially lower (~5%) due to presence of an end group with a substituted propyl side chain (ring 1 from Figure 6.1). Carbon loss from the alkyl side chain as a result of pyrolysis was estimated to account for 15-20% of the products in the monomer fraction. However, C₇ and C₈ hydrocarbons accounted for greater than 50% of the C₇-C₉ hydrocarbon fraction thereby indicating C-C scission from the alkyl side chain during hydrodeoxygenation as well.

6.4.6 Xylan

The pyrolysis vapors from xylan were passed over the 5%Pt 2.5%Mo/MWCNT catalyst at 300°C at 25 bar hydrogen pressure and the lumped hydrocarbon product distribution is shown in Table 6.2. The total carbon yield of hydrocarbons was ~78%, while that for the fuel range hydrocarbons (C₄₊) was ~50%. The C₅ hydrocarbon fraction had the highest yield analogous to the C₆ hydrocarbon yield from cellulose since the starting polymer was made up of C₅ sugar monomers. Additionally, a minor fraction of the hydrocarbon comprised of C₇ and higher hydrocarbons with a cumulative carbon yield of ~10%. While

a part of the C₇ could be derived from lignin-related impurities associated with the xylan sample.

6.4.7 PtMo series

In order to understand the role of Pt and Mo during hydrodeoxygenation, studies were performed with Pt only, Mo only and bimetallic PtMo catalysts having varying ratios of Pt and Mo. The summary of the various catalysts tested has been given in Table 6.1. For the 5% Pt/MWCNT catalyst, the total carbon yield towards hydrocarbons from levoglucosan HDO was ~43%, while that from cellulose was ~27%. Additionally, the total carbon balance from cellulose was ~75%, indicating a presence of partially deoxygenated species. The column used for hydrocarbon analysis was unable to detect these oxygenates, however their presence was confirmed by carrying out identical experiments with a column compatible with oxygenates. For all the other catalysts a total carbon balance of >90% was observed and additional experiments were performed to ensure that no oxygenates were detected. The detailed hydrocarbon product distribution over the Pt only, Mo only and PtMo bimetallic catalysts have been provided in Table E. 6 and Table E. 7. The yield to fuel range hydrocarbons (C₄₊) was observed to increase with an increase in the Mo content relative to the Pt (Figure 6.2 and Figure 6.3Figure 6.2), with 2.5%Mo/MWCNT having the highest yield towards fuel range hydrocarbons for both, levoglucosan (~76%) and cellulose (~55%). This was indicative of lower degree of C-C scission with increasing Mo: Pt atomic ratio in the catalyst.

6.4.8 Effect of hydrogen pressure

The effect of hydrogen pressure on the hydrodeoxygenation product yields was studied on the 5%Pt 2.5%Mo/MWCNT with the biomass model compounds, and three different varieties of biomass (hardwood - poplar, softwood - pine, and grass - maize). The reaction rates could not be measured from these screening studies since only a pulse of the reactant molecules was passed over the catalyst, therefore reaction rates from model compounds studies were invoked as benchmarks. Previously, the reaction rates for hydrodeoxygenation of model compounds (furfural and dihydroeugenol) were obtained over a range of Pt-Mo bimetallic catalysts at elevated hydrogen pressures (25 bar). For both the model compounds, it was shown that the rate normalized by total moles of Pt decreased with an increase in the amount of Mo promoter, with at least 2 orders of magnitude difference in the STY between the 5%Pt/MWCNT and 2%Pt 4.9%Mo/MWCNT (Pt:Mo ratio = 1:5) catalyst.^{70,146} Additionally, previously reported experiments showed that both Pt and Mo were needed for hydrodeoxygenation of the phenol moiety from the lignin pyrolysis products. Therefore, as compromise between opposing rate and selectivity (for C₄₊ hydrocarbons) trends, the 5%Pt 2.5%Mo/MWCNT catalyst was chosen as an optimum for testing with biomass pyrolysis products.

The hydrogen pressure during fast hydrolysis and hydrodeoxygenation was varied within the range of 1 to 25 bar. For lignin model compounds, a decrease in the hydrogen pressure was accompanied by an increase in the yield of aromatic hydrocarbons as shown in Figure 6.8. The increased proportion of aromatic hydrocarbons at lower hydrogen pressures indicated a lower degree of ring hydrogenation. This expected result is in

agreement with recently reported hydrodeoxygenation studies of dihydroeugenol (lignin model compound) over the Pt-Mo bimetallic catalyst at different hydrogen pressures. During hydrodeoxygenation of levoglucosan, xylan and cellulose hydrolysis products, the total carbon yield of the liquid fuel range hydrocarbon fraction (C_{4+}) decreased with a decrease in the hydrogen pressure and was indicative of an increase in the C-C scission activity during hydrodeoxygenation. Total yield of the C_6 fraction from levoglucosan and cellulose, and C_5 fraction from xylan also exhibited the same trend as shown in Figure 6.4, Figure 6.5, and Figure 6.6. A corresponding result was also obtained with lignin model compounds as the total yield of the C_9 fraction decreased (C-C scission of the alkyl side chain) with decrease in the hydrogen pressure (Figure 6.6).

Three biomass samples derived from poplar, pine, and maize were pyrolyzed at 500°C, and the pyrolysis vapors were deoxygenated over the 5%Pt 2.5%Mo/MWCNT catalyst at 300°C (Table 6.2). As shown for previously analyzed substrates, the hydrogen pressure was a critical factor governing the liquid fuel range hydrocarbon yield from various components of biomass as well as the yield to aromatics from the lignin fraction. Figure 6.7 shows that for all the biomass samples tested, the C_{4+} hydrocarbon yield decreased with a decrease in the hydrogen pressure. For instance, the C_{4+} hydrocarbon yield from poplar decreased from ~44% at 25 bar to ~31% at 1 bar hydrogen pressure. Also, the yield to aromatic hydrocarbons increased with a decrease in the partial pressure of hydrogen as depicted in Figure 6.8. The overall carbon balance for all biomass samples tested was greater than 90% indicating that all the major products and pathways for conversion were represented by these results. The detailed hydrocarbon product

distribution as a function of hydrogen pressure, for all the feedstocks is reported in Table E. 9, Table E. 10, Table E. 11, Table E. 12, Table E. 13, Table E. 14, Table E. 15, and Table E. 16.

6.4.9 Cyclone reactor

A proof of concept study for the H₂Bioil process was performed in a continuous cyclone-type fast-hydropyrolysis (FHP) reactor with a downstream vapor-phase catalytic HDO reactor and the product distribution from cellulose and poplar with 5%Pt 2.5%Mo/MWCNT catalyst at 300°C at 25 bar hydrogen pressure have been previously reported.¹⁶⁶ Further experiments were performed at 2.5 bar hydrogen pressure, and the comparison is presented in Table 6.3. The liquid fuel range hydrocarbon yield decreased with hydrogen pressure (25 bar to 2.5 bar) for both cellulose (55% to 41%) and poplar (32% to 23%), thereby validating the trends observed from the micro-scale semi-batch catalytic reactor.

Table 6.2 Lumped product distribution from different biomass and model feedstocks on a % carbon basis (experimental conditions: hydropyrolysis temperature – 500°C, Hydrodeoxygenation temperature – 300°C, hydrogen pressure – 25 bar)

	Model compounds / polymers					Biomass		
	Levogluconan	Cellulose	Xylan	Lignin dimer 1	Lignin polymer 2	Poplar	Pine	Maize
CO	1.8	2.7	7.1	0.6	1.6	1.8	4.0	2.2
CO₂	0.4	0.5	1.4	n/a	0.3	n/a	n/a	n/a
Hydrocarbons								
C ₁ -C ₃ range	20.6	24.2	28.1	15.7	12.0	26.8	26.9	20.3
C ₄ + range	72.1	50.0	49.9	82.1	48.2	44.4	42.0	43.7
Char	n.d	17.0	18.0	n.d	32.0	26.0	25.5	31.5
Total	94.8	94.4	104.5	98.4	94.0	99.1	98.3	97.7

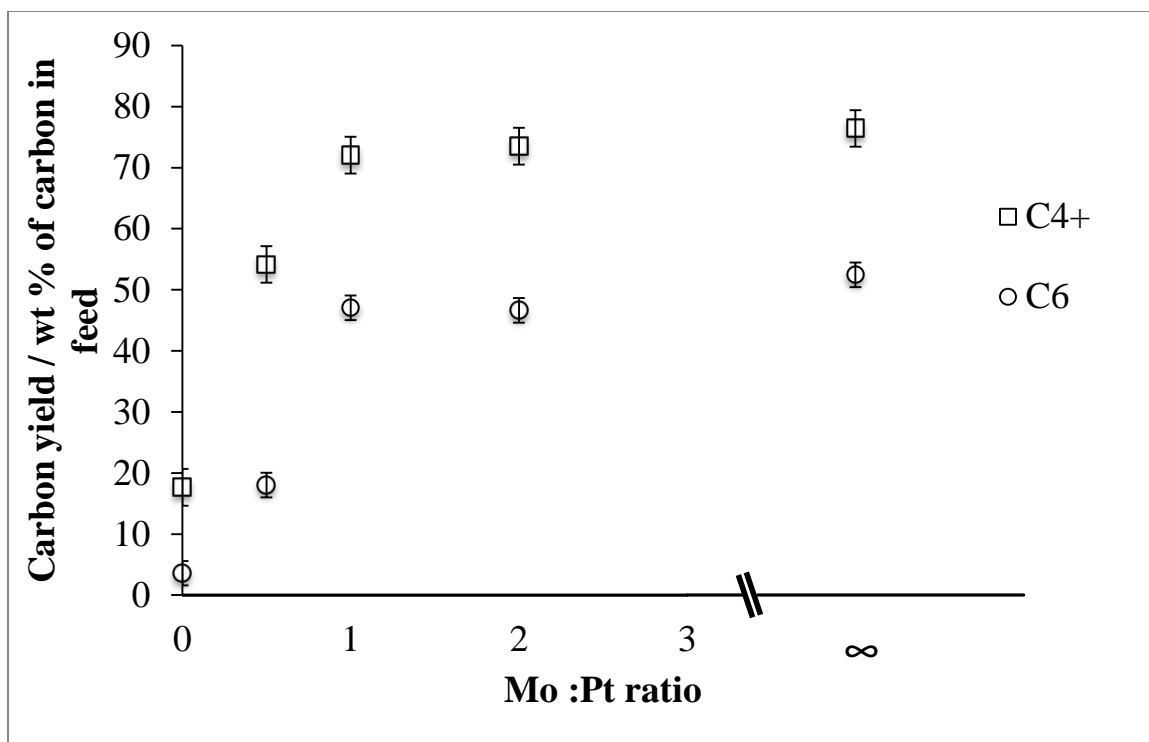


Figure 6.2 Percentage carbon yield of product fractions from hydrodeoxygenation of levoglucosan as a function of the Mo:Pt ratio of the catalyst. (squares) C₄₊ hydrocarbon fraction – liquid fuel range hydrocarbons, (circles) C₆ hydrocarbon fraction.

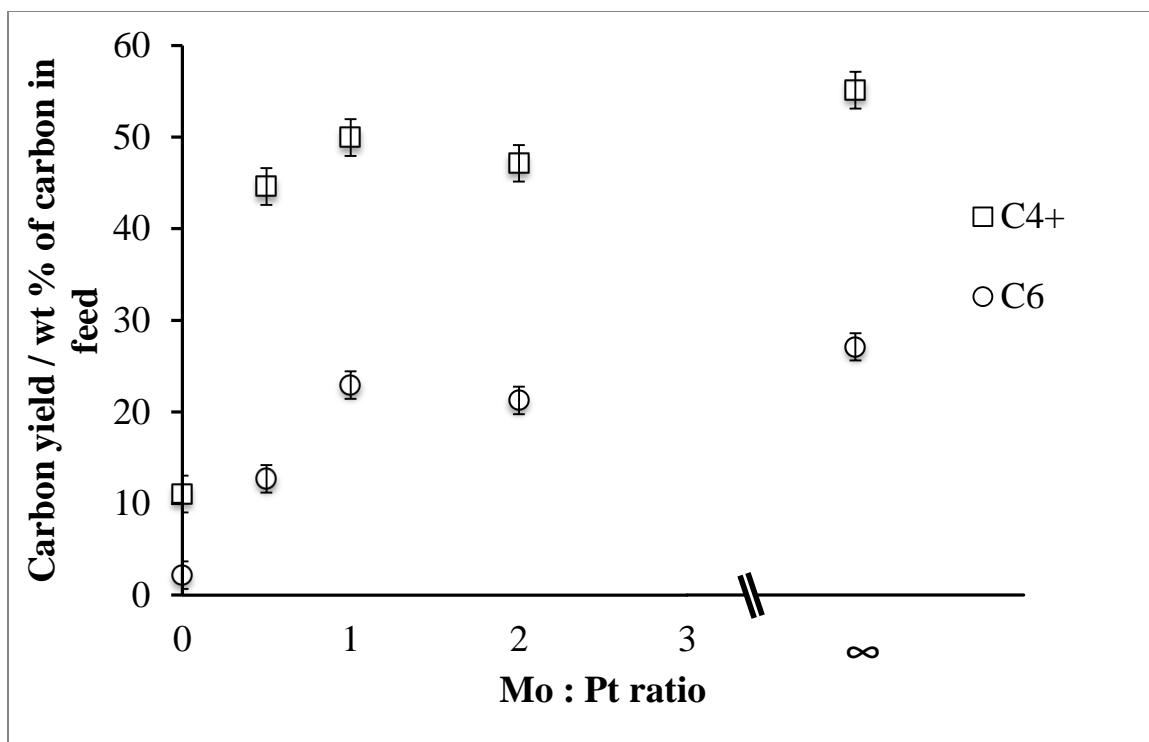


Figure 6.3 Percentage carbon yield of product fractions from hydrodeoxygenation of fast hydrolysis products of cellulose as a function of the Mo:Pt ratio of the catalyst. (squares) C₄₊ hydrocarbon fraction – liquid fuel range hydrocarbons, (circles) C₆ hydrocarbon fraction.

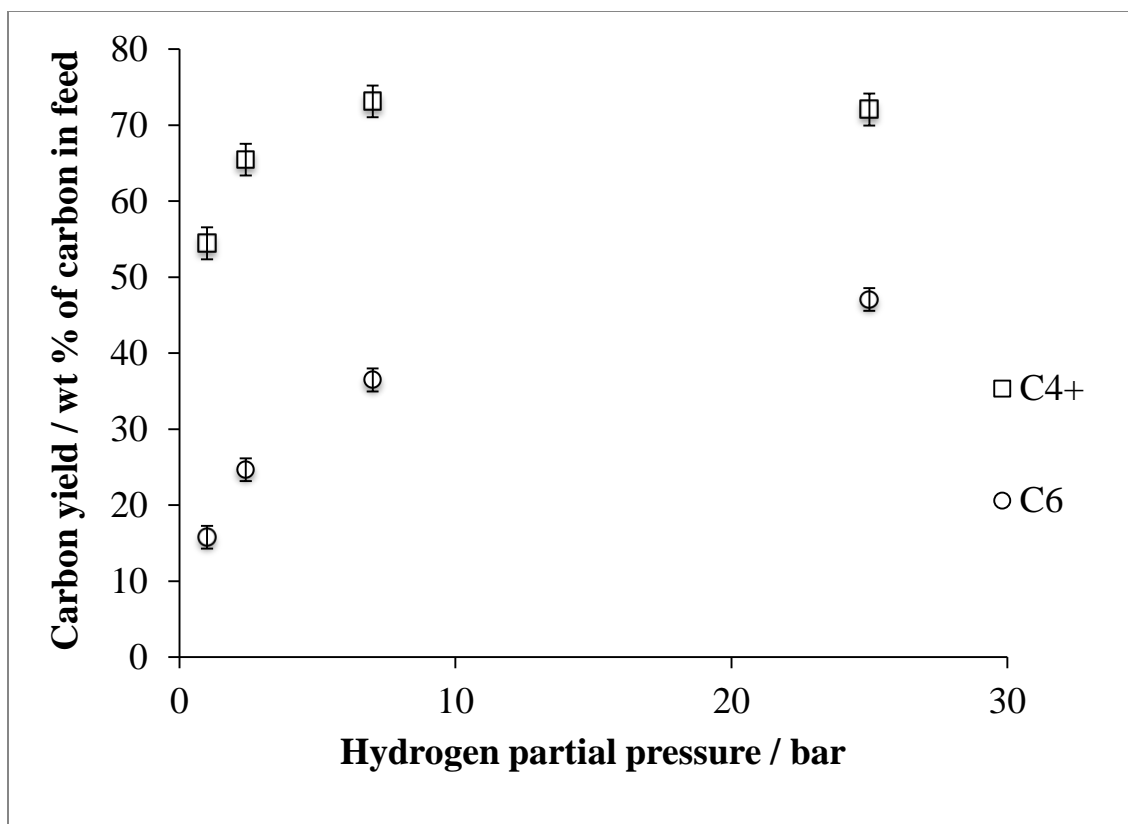


Figure 6.4 Percentage carbon yield of product fractions from hydrodeoxygenation of levoglucosan as a function of the hydrogen pressure over the 5%Pt2.5%Mo/MWCNT catalyst. (squares) C₄₊ hydrocarbon fraction – liquid fuel range hydrocarbons, (circles) C₆ hydrocarbon fraction.

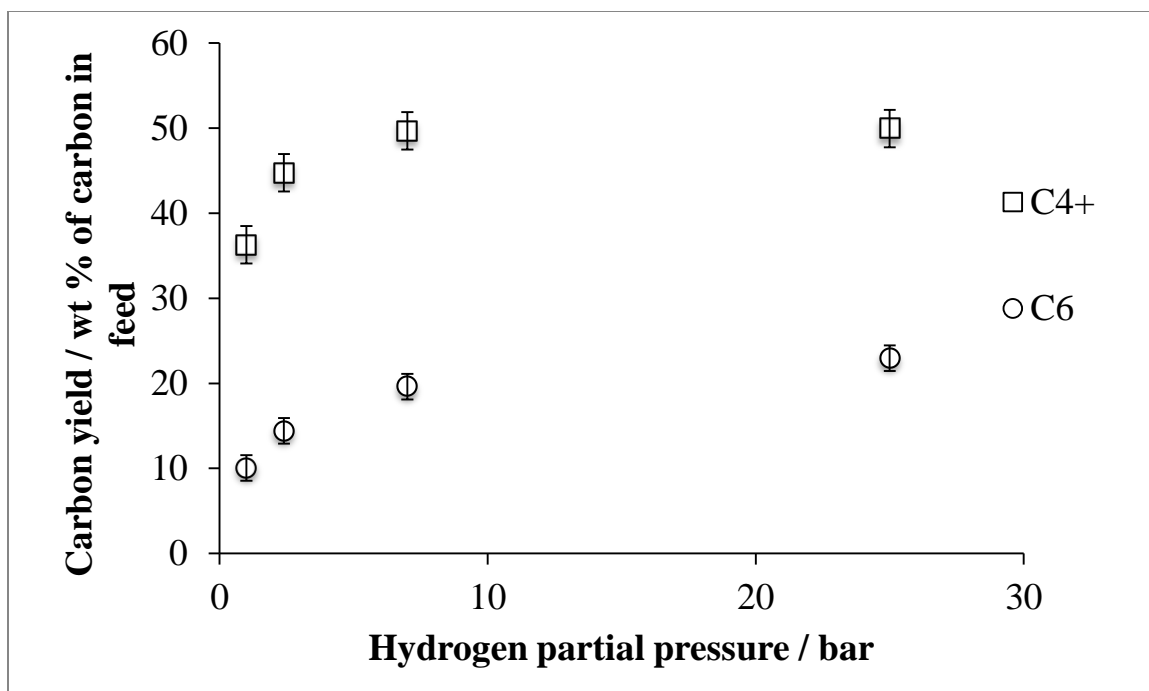


Figure 6.5 Percentage carbon yield of product fractions from hydrodeoxygenation of fast hydrolysis products of cellulose as a function of the hydrogen pressure over the 5%Pt2.5%Mo/MWCNT catalyst. (squares) C₄₊ hydrocarbon fraction – liquid fuel range hydrocarbons, (circles) C₆ hydrocarbon fraction.

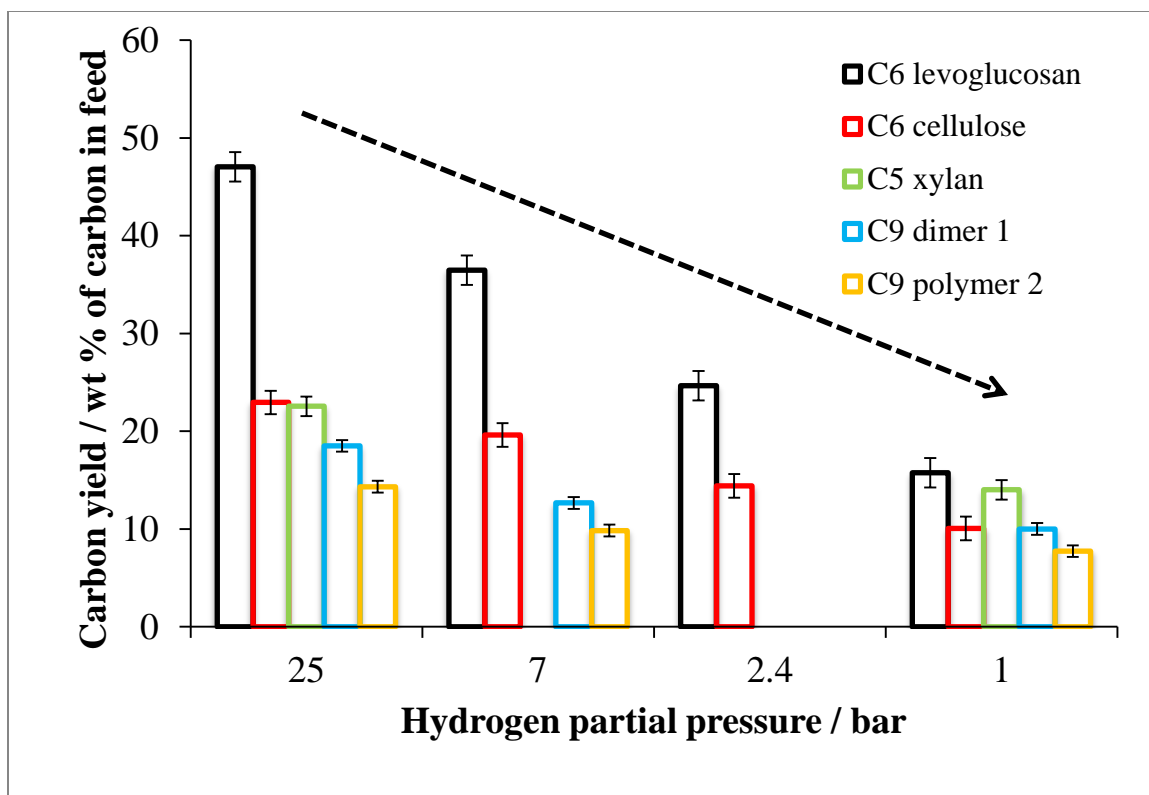


Figure 6.6 Percentage carbon yield of product fractions from hydrodeoxygenation of fast hydrolysis products of biomass model compounds/polymers as a function of the hydrogen pressure over the 5%Pt2.5%Mo/MWCNT catalyst. Indicates decrease in the corresponding hydrocarbon fraction from different components of biomass, illustrating increase in C-C scission with decrease in hydrogen pressure.

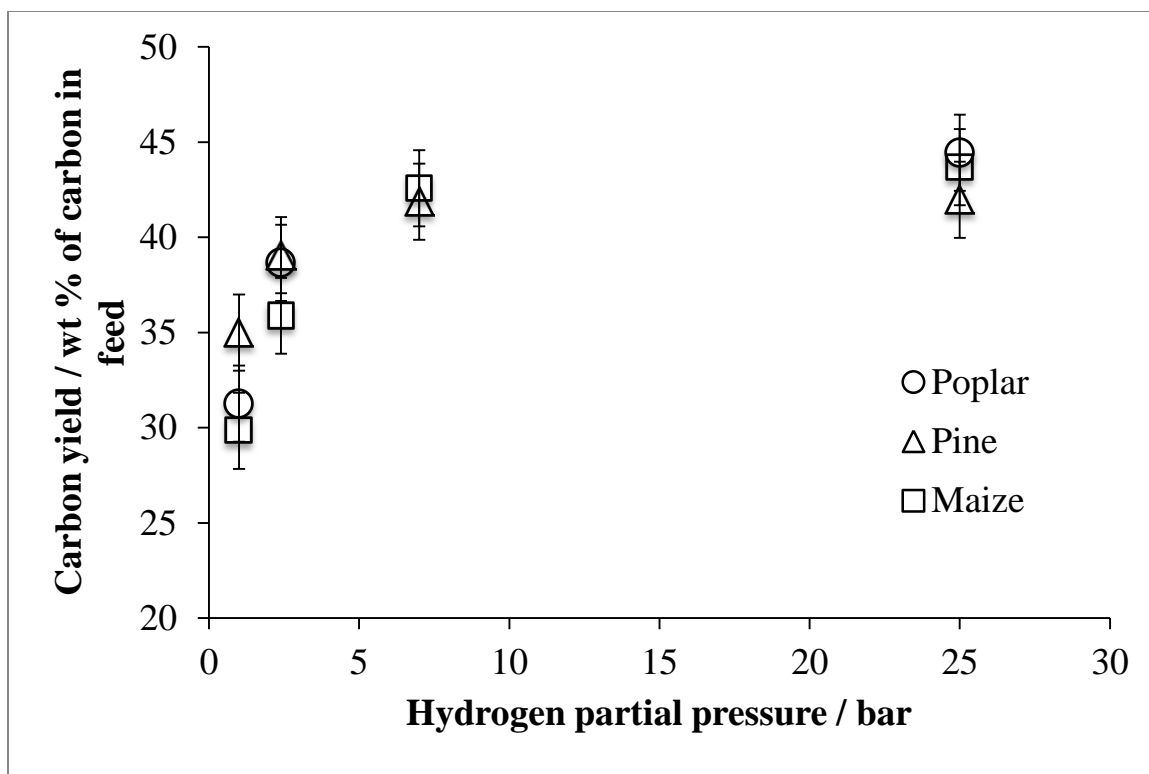


Figure 6.7 Percentage carbon yield of C₄₊ hydrocarbon fraction from hydrodeoxygenation of fast hydrolysis products of Poplar (circles), Pine (triangles), Maize (Squares) as a function of the hydrogen pressure over the 5%Pt2.5%Mo/MWCNT catalyst.

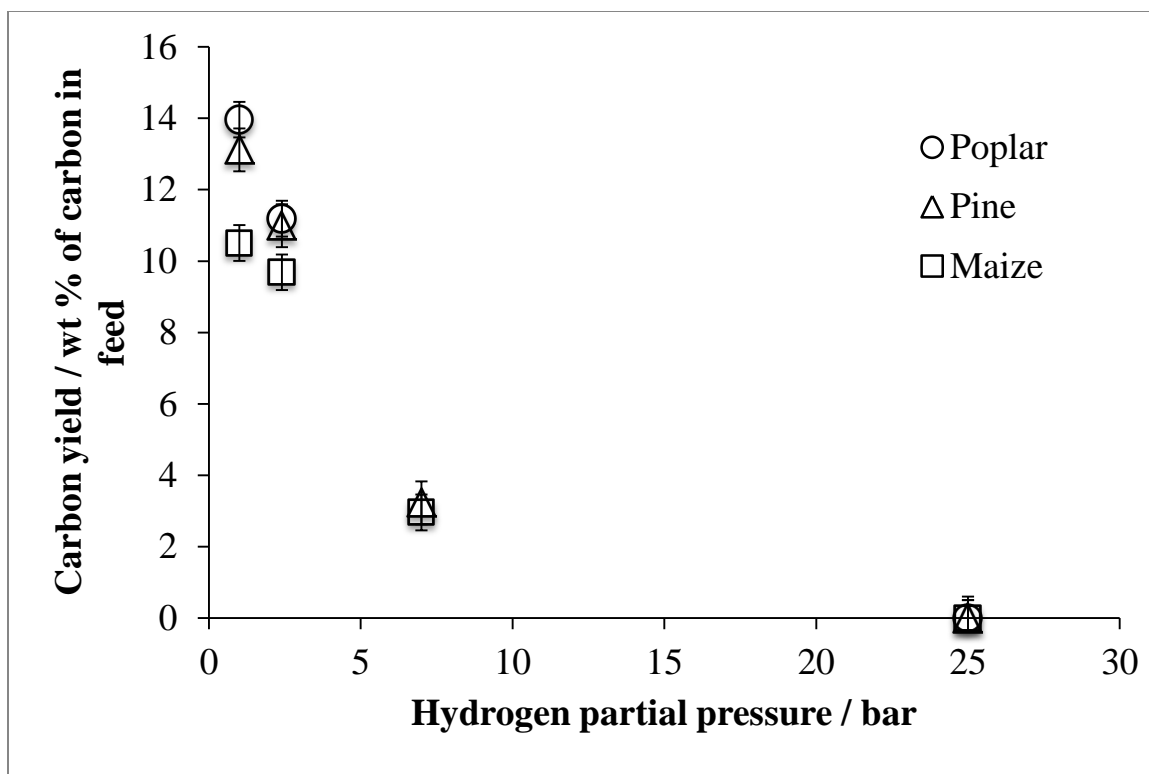


Figure 6.8 Percentage carbon yield of aromatic hydrocarbon fraction from hydrodeoxygenation of fast hydrolysis products of Poplar (circles), Pine (triangles), Maize (Squares) as a function of the hydrogen pressure over the 5%Pt2.5%Mo/MWCNT catalyst.

Table 6.3 Lumped product distribution from hydrodeoxygenation of poplar and cellulose hydropyrolysis products on a % carbon basis from the Lab-scale continuous flow cyclone type reactor over the 5%Pt2.5%Mo/MWCNT catalyst (experimental conditions: hydropyrolysis temperature – ~480°C, Hydrodeoxygenation temperature – ~300°C)

	Cellulose		Poplar	
	25	2.5	25	2.5
Hydrogen pressure / bar				
Products yields / % carbon of feed				
CO	15.6	28.2	9.6	19.3
CO₂	2.0	6.3	2.7	6.0
Hydrocarbons				
C1-C3 range	17.6	15.2	21.7	12.1
C4+ range	55.0	40.9	32.1	23.1
Char	3.0	4.6	28.5	29.8
Total	93.2	95.2	94.6	90.3
Aromatics	n.d	2.3	n.d	8.6

6.5 Discussion

6.5.1 Role of Pt and Mo

Catalyst characterization techniques (STEM-EELS, XPS, XAS and CO chemisorption) were used to study the changes in the catalyst structure, with change in Mo loading, in the Pt-Mo bimetallic catalysts. CO chemisorption results showed that the CO uptake per gram of the catalyst decreased with an increase in the Mo loading, indicating decrease in surface Pt. Particle size analysis was performed on the TEM/STEM images from the bimetallic catalysts, to obtain the percentage of Pt only and Pt-Mo bimetallic particles. The results show an increase in the percentage of the Pt-Mo bimetallic particles with an increase in the Mo loading relative to Pt (Table E. 17). XAS results confirmed the presence of Pt-Mo co-ordination under reduced conditions indicating formation of Pt-Mo

alloy in the bimetallic catalyst. Additionally, the presence of multiple oxidation states of Mo was determined from XPS studies with identification of Mo^0 (as a Pt_xMo_y alloy phase(s) or isolated Mo monometallic nanoparticles), molybdenum carbide-like phase, and Mo-oxide (4^+ and 6^+) phases (Table E. 18). The detailed characterization results on the series of Pt-Mo bimetallic catalysts have been reported in elsewhere.¹⁴⁶

Hydrocarbon product distributions from hydrodeoxygenation of cellulose and levoglucosan indicated a varying degree of C-C scission products, over the Pt only, Mo only and Pt-Mo bimetallic catalysts. Figure 6.2 and Figure 6.3 show an increase in the C_{4+} hydrocarbon yield with an increase in the Mo:Pt atomic ratio for both cellulose and levoglucosan. This was accompanied by a corresponding decrease in the $\text{C}_1\text{-C}_3$ species, which included CO, CO_2 and $\text{C}_1\text{-C}_3$ hydrocarbons. It is interesting to note that the increase in the C_{4+} hydrocarbon yield also corresponds closely to the increase in the percentage of the Pt-Mo bimetallic particles observed via STEM-EELS characterization (Figure E. 1) Decarbonylation of carbonyl species has been identified as one of the pathways for C-C bond scission, and has been studied in literature using furfural as the model compound. Mehta et al. have shown that addition of Mo as a promoter to Pt resulted in significant reduction in selectivity for the decarbonylation pathway during vapor phase hydrodeoxygenation of furfural.⁷⁰ Hydrodeoxygenation studies with other alloy systems (Ni-Fe, Pd-Cu) have also observed a lower degree of decarbonylation compared to the monometallic catalysts (Pd,Ni) and attribute it to modification of the electronic properties of the hydrogenating metal (Ni,Pd) by the promoter.^{173,174} Furthermore, DFT studies indicate a modification of the adsorption characteristics of

furfural on the catalyst surface as a result of alloying, which is responsible promotion of hydrogenation of the carbonyl functional group.¹⁷³ Thus we propose that one contribution to C-O bond scission is that Mo, being an oxophilic species could modify the electronic properties of Pt, which affect the adsorption properties of the pyrolysis oxygenates and selectively promotes C-O scission reactions. Competing C-C scission (via direct C-C hydrogenolysis),¹⁷⁸ and C-O scission reactions have been observed during aqueous phase reforming of primary, secondary alcohols, and polyols over Pt based catalysts.¹³⁴ Dietrich et al. have shown that the PtMo bimetallic catalyst had higher selectivity for C-O scission reactions as compared to Pt during aqueous phase reforming of glycerol.¹³⁴ Furthermore, partially oxidized oxophilic metal oxide species (MoO_x) have been shown to produce Brønsted acid sites which promote C-O scission via dehydration hydrogenation of biomass derived oxygenates.^{148,149} Therefore, in addition to PtMo bimetallic species, partially oxidized species Mo species, which were observed during XPS characterization can play an important role in enhancing the C-O scission activity. The selectivity to C_{4+} hydrocarbons is governed by the ratio of C-O and C-C scission rates, however, and it is potentially the synergy between the Pt, Mo^0 and MoO_x species in the bimetallic catalyst which is important for further reduction of the C-C scission. This conclusion is supported by the enhanced C-C scission during HDO of cellulose over physical mixture of equal quantity of 5%Pt/MWCNT and 2.5%Mo/MWCNT catalysts, when compared with 5%Pt2.5%Mo/MWCNT (Table E. 19). For Mo:Pt atomic ratio 0 to 2, the proportion of bimetallic Pt-Mo particles, estimated by STEM-EELS increased (Table E. 17), along with partially oxidized Mo oxide species (Table E. 18). Therefore, addition of Mo as a

promoter to Pt catalyst has been shown to inhibit C-C scission pathways, thereby increasing the selectivity towards deoxygenation products.

The role of Pt and Mo for hydrodeoxygenation of lignin model compound, dihydroeugenol was previously studied in detail by Yohe et al. and Mehta et al. Their results indicated that both Pt and Mo are required for removal of the phenolic oxygen from the lignin model compound, while the methoxy group deoxygenation was observed over the monometallic Pt catalyst as well. In this case, Mo, used an oxophilic promoter played a critical role in conjunction with Pt for hydrodeoxygenation of the phenolic oxygen.

6.5.2 Effect of hydrogen pressure

6.5.2.1 Yield of aromatic hydrocarbons

Results from hydrodeoxygenation of biomass pyrolysis products indicated that hydrogen pressure played a critical role in not only in governing the hydrocarbon product distribution, but also the total yield to liquid fuel range products. In the results section, it was shown that the yield of the aromatic hydrocarbon fraction from lignin model polymers and biomass was a also strong function of the hydrogen pressure. For lignin polymer **2**, at the lowest pressure (1 bar), the carbon yield for aromatic hydrocarbons was ~40% with the total carbon yield to C₆₊ hydrocarbon fraction being 46%, and progressively decreased with increase in hydrogen pressure, approaching zero at 25 bar (Table E. 13). Similar trends were observed for dimer **1**, poplar, pine, and maize as well

with higher selectivity towards aromatic products at lower hydrogen pressures (Table E. 12, Table E. 14, Table E. 15, Table E. 16, and Figure 6.8). These results are in agreement with previously published studies, showing high selectivity for aromatic hydrocarbons (93% at 99.9% conversion) during hydrodeoxygenation of dihydroeugenol at low hydrogen partial pressure (1 bar). Reaction pathway studies have shown that direct deoxygenation of phenol to form an aromatic hydrocarbon was the dominant pathway at low hydrogen pressure (1 bar), while at high hydrogen pressure (25 bar), sequential ring hydrogenation and dehydration occurred to give saturated hydrocarbons with high selectivity. On the other hand, lowering hydrogen pressure significantly affected the site time yield lowering it by an order of magnitude with decrease in the hydrogen pressure from 25 to 1 bar.

Minor yields (<3%) of aromatic hydrocarbons (C₆-C₉) were obtained during hydrodeoxygenation of levoglucosan, cellulose and xylan pyrolysis products at low hydrogen pressure (1 bar). The low yield was not surprising due to the lack of C-C linked rings or aromaticity in the starting compounds. Hydrodeoxygenation of the pyrolysis products from cellulose primarily resulted in formation of linear hydrocarbons with the maximum length equal to the number of carbon atoms in the monomer (Table E. 19). On the other hand, 80% of the hydrocarbons from lignin polymer **2** were cycloalkanes and aromatic hydrocarbons along with of the 20% aliphatic hydrocarbons, 17% of which were in the C₁-C₄ range and were obtained from methoxy group deoxygenation as well as C-C scission of the alkyl side chain. This implies that a major fraction of the aromatic

hydrocarbons produced from HDO of biomass pyrolysis products was derived from the lignin fraction of the biomass.

It is interesting to note, however, that the ratio of the aromatic hydrocarbons to their saturated counterparts was dependent on the length of the alkyl side chain. An increase in the molecular weight of the alkyl side chain tilted the balance towards a higher ratio of aromatic compounds to the saturated counterparts, as shown in Table 6.3. These ratios were compared to theoretically estimated values for equilibrium ratio for C_6 to C_9 hydrocarbons at 300°C (Table 6.3). Therefore, it can be concluded that reducing the carbon loss from the alkyl side chain of the lignin pyrolysis products can promote the overall yield of aromatic hydrocarbons.

6.5.2.2 C-C bond scission

The advantage of vapor phase hydrodeoxygenation of biomass, specifically lignin pyrolysis products at low hydrogen pressure (1 bar) was to produce aromatic hydrocarbons with high selectivity. However, a casualty from decreasing the hydrogen pressure was an increased degree of C-C scission as shown by a decreasing yield of C_{4+} hydrocarbons from HDO of levoglucosan, cellulose, xylan and biomass pyrolysis products. In case the of levoglucosan, and the majority of cellulose pyrolysis products, hexane (C_6 hydrocarbons) was expected to be the product of complete HDO without any C-C scission or formation reactions. However, the C_6 hydrocarbon yield for levoglucosan was less than stoichiometric and decreased further with a decrease in the hydrogen

pressure. A similar trend, but more severe trend was observed with cellulose as well, and was indicative of a higher degree of C-C bond scission occurring at lower hydrogen pressures.

As stated previously, decarbonylation has been reported as one of the C-C scission pathways during hydrodeoxygenation of furfural on supported metal catalysts. Mehta et al. have shown that the selectivity of decarbonylation products from furfural decreases significantly with increase in the hydrogen pressure (from 1 bar to 19 bar), with a corresponding increase in the selectivity towards hydrogenation products.⁷⁰ Huber et al. have also reported an increased selectivity to higher carbon number alkanes (i.e. decreased C-C scission) with increasing hydrogen partial pressure (up to 40 bar) during aqueous phase reforming of sorbitol over supported Pt catalysts.¹⁷⁹ Furthermore, at low hydrogen pressure (1 bar), dehydrogenation of alcoholic functional groups is preferred (Table E. 20), resulting in formation of aldehydes, which can subsequently undergo decarbonylation. Therefore, lowering the hydrogen pressure can result in buildup of a higher concentration of species that are prone to decarbonylation, which could further contribute towards increased C-C scission. These trends support the results observed here which show that C-C scission is enhanced at lower hydrogen pressure. Thus, we conclude that increasing the hydrogen pressure can be an effective strategy for raising the carbon yield towards liquid fuel range hydrocarbons.

The extent of C-C scission was observed to a larger extent for during HDO of cellulose and xylan hydropyrolysis products (~14-16% decrease in C₄₊ hydrocarbon yield) as

compared to polymer **2** (~2-3% decrease in C₄₊ hydrocarbon yield), and was primarily due to aromatic make up of lignin pyrolysis products. For the lignin pyrolysis products, there was no observable loss of carbon from the aromatic ring and only the alkyl side chain was susceptible to the loss of carbon via C-C hydrogenolysis (Table E. 21). This was evident from the decrease in the C₉ hydrocarbon fraction with decrease in hydrogen pressure from both dimer **1** and polymer **2**, and a subsequent increase in the C₇ and C₈ fraction (Figure E. 3 and Figure E. 4). As stated previously, experiments with propyl cyclohexane and propyl benzene over the 5%Pt 2.5%Mo/MWCNT catalyst revealed no cracking products, with the propyl side chain remaining intact. Therefore, it can be concluded that any C-C scission observed from alkyl side chain was a result of presence oxygen bearing functional groups, and the C-C scission occurred during hydrodeoxygenation. The hydrodeoxygenation pathways for the oxygen functional groups on the alkyl side chain can be considered similar to those for levoglucosan and cellulose pyrolysis products.

Hydrodeoxygenation studies are typically focused on developing suitable catalysts for hydrodeoxygenation of lignin model compounds which, either lack alkyl side chains or have saturated alkyl side chains (i.e guaiacol, m-cresol, dihydroeugenol). On the contrary, majority of the lignin pyrolysis products have oxygen functional groups on the alkyl side chains. As a result, it is very important to understand the effect that these catalysts have on C-C scission on the alkyl side chain while studying HDO activity for phenolic and methoxy groups. Thus, hydrogen pressure was a critical factor in governing the mechanism of phenolic oxygen removal and as shown in this study also had an impact on

the degree of carbon loss from the alkyl side chain. Therefore, for determining a suitable catalyst, and operating conditions, it is necessary to assess the effects of the parameters on hydrodeoxygenation of the pyrolysis products from individual components of biomass (cellulose, hemicellulose, lignin).

Table 6.4 Observed ratio of aromatic to saturated cyclic hydrocarbons during hydrodeoxygenation of biomass hydropyrolysis products over 5%Pt 2.5%Mo/MWCNT at 300°C, and 1 bar hydrogen pressure.

Biomass	Poplar	Pine	Maize Stover	Theoretical*
Hydrocarbons				
C6	3.6	3.0	2.6	5.2
C7	6.0	6.0	4.4	10.9
C8	10.3	9.9	8.0	24.0
C9	18.2	14.5	12.6	32.9

* Estimated via theoretical calculations using ASPEN.

6.5.3 Comparison with lab-scale continuous flow cyclone type reactor

Experiments were performed at two hydrogen pressures (25 bar and 2.5 bar) with two feedstocks (cellulose, poplar) in a continuous cyclone-type fast-hydropyrolysis (FHP) reactor with a downstream vapor-phase catalytic HDO reactor. The results showed a decrease in the liquid fuel range hydrocarbon yield with a decrease in the hydrogen pressure, thereby confirming the trends observed in the pulse catalytic studies with the micro-scale reactor. Additionally, low hydrogen pressure (2.5 bar) resulted in an increased yield of aromatic hydrocarbons from the lignin fraction of the poplar as compared to 25 bar hydrogen pressure. There is a difference in the yields of liquid fuel range hydrocarbon fraction from the two reactors, for both cellulose and poplar. It should be kept in mind that while the pyrolysis temperature is within ~480-550°C for both the

reactors, there can be differences in the pyrolysis product distribution as indicated by the difference in the char yield for cellulose (3% vs 17%). In case of the micro-scale semi-batch catalytic reactor, a pulse of the pyrolysis products was passed over the catalyst and the initial product yields were measured. Therefore, unlike the lab-scale continuous flow cyclone type reactor the catalyst did not undergo initial deactivation. Additional differences like local concentration of reactant molecules, hydrogen coverage and effective heating rate could also contribute to these variations in behavior.

6.6 Conclusions

In this study a micro-scale semi-batch catalytic reactor with an online GC-MS was developed to be capable of operation at high pressure hydrogen (up to 35 bar) in order to screen catalysts and examine the effect of hydrogen pressure on hydrodeoxygenation of the pyrolysis products from biomass and its individual components, with greater than 90% carbon balance. The hydrocarbon product distribution was investigated to evaluate the relative degree of C-C scission prevalent during the hydrodeoxygenation reactions. Mo was used as an oxophilic promoter for Pt, and increasing the Mo content (or Mo:Pt atomic ratio) was shown to decrease the C-C scission activity of the catalyst. 5%Pt2.5%Mo/MWCNT was used as a candidate catalyst for hydrodeoxygenation of biomass pyrolysis products (poplar, pine, and maize), providing >69% carbon yield to hydrocarbons, with >41% yield to liquid fuel range (C₄₊) hydrocarbons, at 300°C and 25 bar hydrogen pressure. Hydrogen pressure played a critical role in determining the hydrocarbon product distribution due to a significant impact on the degree of C-C

scission. Decrease in the hydrogen pressure was shown to increase the degree of C-C scission, thereby decreasing the yield of liquid fuel range hydrocarbons by ~10 carbon wt % within the pressure range of 1-25 bar. Studies with cellulose, xylan and lignin polymer **2** showed that cellulose and xylan fraction contributed to a greater extent toward C-C scission than lignin, primarily due to the aromatic structure of the lignin pyrolysis products. Decreased hydrogen pressure also resulted in an increase in the yield of aromatic hydrocarbons, which were chiefly derived from the lignin fraction of the biomass. Hydrogen pressure variation experiments with lignin model compounds, dimer **1** and polymer **2**, showed an increased yield to aromatic hydrocarbons simultaneously accompanied by increased C-C scission from the alkyl side chain with a decrease in the hydrogen pressure from 25 to 1 bar. Additionally, the ratio of aromatic to saturated cyclic hydrocarbons increased with increase in the length of the alkyl side chain indicating the importance of curbing C-C scission for increasing the yield of aromatic hydrocarbons. Experiments were also performed with a continuous-flow cyclone-type fast-hydropyrolysis (FHP) reactor with a downstream vapor-phase catalytic HDO reactor to confirm the trends observed with the micro-scale studies. The yield of liquid fuel range hydrocarbons decreased with decrease in hydrogen pressure for both, poplar and cellulose. Additionally, ~9% yield of aromatic hydrocarbons was obtained with poplar at 2.5 bar hydrogen pressure thereby, validating the results obtained with the micro reactor and establishing the feasibility of the Pt-Mo bimetallic catalyst for continuous operation with biomass pyrolysis products. Hydrogen pressure is a critical parameter, which can be tuned to control the hydrocarbon product distribution based on the composition of the biomass and maximize the value of the products.

CHAPTER 7. SUMMARY AND FUTURE RECOMMENDATIONS

7.1 Summary

The studies reported in this dissertation focused on developing an understanding for fast-hydrolysis of two biomass components, cellulose and lignin, as well as catalytic hydrodeoxygenation of biomass pyrolysis products over Pt based catalysts. A substantial effort was employed in developing the tools for enabling these studies, especially to overcome the mass balance limitations associated with high pressure pyrolysis studies. A high pressure (up to 35 bar) micro-scale semi-batch reactor was successfully interfaced with a low pressure (up to 7 bar) online gas chromatograph and resulted in an increase in the overall mass balance to >90%. Additionally, for the first time, a quantitative analytical technique for analysis of lignin and cellulose derived dimeric species via a GC-MS was developed by modifying commercially available GC columns. This eliminated the need to use of multiple techniques for analysis of >90% of the pyrolysis product distribution from biomass and enabled vapor phase residence times studies which were important for understanding the nature of secondary reactions during pyrolysis.

Cellulose fast pyrolysis experiments were performed in the micro-scale pyrolysis GC-MS system with a mass balance of $96\pm 6\%$ (Chapter 3). Levoglucosan was observed to be the major product from fast pyrolysis of cellulose with ~ 44 wt% yield, while glycolaldehyde which had a yield of $\sim 9\%$ was second. Parametric studies showed that temperature played a critical role in determining the product distribution, with $\sim 500^\circ\text{C}$ being an optimum temperature for maximizing the yield of “liquid” range products with minimum C-C bond scission. Vapor phase residence time studies in collaboration with other reactor systems showed the presence of higher proportion (~ 10 - 15 wt%) dimeric species (cellobiosan, glucosylpyrano- β -glycolaldehyde) at low residence time (70-100ms). Increasing the residence time resulted in breakdown of these species contributing ~ 1 - 3 wt% at higher residence times (2-3s).

Quantitative results on pyrolysis of pure lignin model compounds with β -O-4 linkages were essential to know the underlying factors that govern the product distribution without the unwanted effects from impurities (inorganic, sugars and multiple poorly characterized reactants) which are generally present in extracted lignins. For the first time, a direct vapor phase analysis of the entire range of products (monomeric and dimeric species) from lignin pyrolysis was performed with greater than >90 wt% mass balance, with the dimeric species accounting for at least ~ 19 wt% of the product distribution. Degree of polymerization (Dp) did not have an observable effect on the nature of β -O-4 scission products however there was a significant effect on the amount of char formed, which increased with an increase in Dp. Evidence was obtained, via vapor phase residence time studies, to show that the primary products from lignin pyrolysis comprised of both

monomeric and dimeric species with the possibility of having oligomeric species in minor quantities. These results are important in the light of the current debate in literature on the nature of primary products from lignin pyrolysis and their secondary vapor phase transformations. An online vapor phase analysis capability proved to be an excellent tool to study these secondary reactions, showing unequivocally the breakdown of dimeric species to form monomers and lights with an increase in the vapor phase residence time. This study of G-lignin model oligomers with β -O-4 linkages was relevant to understanding the overall picture of lignin pyrolysis since β -O-4 linkages are the most abundant (up to 50%) linkage in the lignin polymer. Additionally, the extra methoxy group on the S-lignin monomers is not expected to have an impact on the nature of β -O-4 scission. However, further studies need to be done to study these effects along with incorporating the study of other types of linkages present in the lignin polymer.

The presence of hydrogen (up to 25bar) did not result in any significant deoxygenation during the pyrolysis stage for either cellulose or lignin. Thus, the presence of catalyst was essential, either in the pyrolysis zone or downstream to remove oxygen and upgrade the pyrolysis product to target molecules. A series of collaborative studies, and lessons from literature, culminated into fruitful results with the Pt-Mo bimetallic catalytic system supported on the multi-walled carbon nanotubes. A series of Pt-Mo catalyst with varying Pt and Mo ratios were investigated to find an optimal composition as well understand the role of the contributing metals to the reaction pathways. A two pronged approach was used to studying biomass derived pyrolysis products by studying model compounds (dihydroeugenol, m-cresol, levoglucosan, etc.) and then applying those results to

cellulose, lignin and biomass pyrolysis products. The model compounds were studied to establish the reactions pathways for hydrodeoxygenation and understand the role of Pt and Mo in the individual reaction steps (Chapter 5). Pt was shown to primarily provide the hydrogenation function, while Mo phases provided the hydrodeoxygenation function through pathways like dehydration of –OH function groups. Increasing the Mo content relative to Pt was shown to increase the selectivity for deoxygenation products for lignin model compounds and decrease in the C-C bond scission for cellulose and hemicellulose pyrolysis products. Although Pt and Mo played distinct roles, the synergy between Pt and Mo species on the bimetallic catalyst was critical for increasing the selectivity for phenol deoxygenation at low hydrogen pressure and decreasing the C-C scission during hydrodeoxygenation of cellulose pyrolysis products (Chapter 5 and 6).

The 5%Pt2.5%Mo/MWCNT catalyst was tested as the candidate catalyst for hydrodeoxygenation of biomass pyrolysis products (poplar, pine, and maize), providing >69% carbon yield to hydrocarbons, with >41% yield to liquid fuel range (C_{4+}) hydrocarbons, at 300°C and 25 bar hydrogen pressure. Hydrogen pressure did not have any impact on the pyrolysis product distribution, however it was influential in governing the yield of hydrocarbons as well as the hydrocarbon product distribution. Decrease in the hydrogen pressure was shown to increase the degree of C-C bond scission, thereby decreasing the yield of liquid fuel range hydrocarbons by ~10 carbon wt% within the pressure range of 1-25bar. Pyrolysis products from cellulose and xylan fraction from biomass were shown to be more susceptible to C-C bond scission as compared to those from lignin. In contrast, a decrease in the hydrogen pressure resulted in increase in the

yield of aromatic hydrocarbons, primarily from the lignin fraction of the biomass. Lignin model compound studies (dihydroeugenol, m-cresol) in partnership with previous studies in our group showed the existence of a direct deoxygenation pathway for phenolic –OH group resulting in high yield (~93%) of aromatic hydrocarbons at 1bar hydrogen partial pressure. Therefore, hydrogen partial pressure was an important lever for manipulating the product distribution from biomass pyrolysis products. Additional recommendations were made to increase the carbon recovery towards liquid fuel range hydrocarbons from biomass during the experimental implementation of the H₂Bioil process.

The thesis objective of studying all aspects of the H₂Bioil process resulted in development of a versatile tool capable to testing all kinds of feedstocks from model compounds to intact biomass. This was coupled with the ability to study fundamental aspects of fast pyrolysis and catalytic hydrodeoxygenation in a single reactor system, currently unprecedented in the literature. Finally, a complete platform was developed by integrating the micro-scale semi-batch reactor system with other continuous steady state reactor systems, designed, and built by other group members for studying all aspects of a chosen catalytic system; from catalyst screening studies, kinetic studies, and regeneration studies with model compounds to lab-scale testing with biomass pyrolysis products.

7.2 Future recommendations

7.2.1 C-C bond formation: Aldol condensation

The hydrocarbon product distribution from biomass was comprised of a substantial proportion of lights (C_1 - C_3) as well as permanent gases (CO and CO_2). The contribution of higher than C_6 hydrocarbons was primarily from the lignin fraction of the biomass due to its aromatic structure. Cellulose and hemicellulose pyrolysis products tend to form hydrocarbons which have 6 or less carbon atoms per molecule since they are built from C_6 and C_5 sugar based monomers. Therefore, in order to increase the yield of long chain hydrocarbons it would be necessary to form C-C bonds especially from the pyrolysis products from cellulose and hemicellulose, which tend to undergo a higher degree of C-C scission and make light hydrocarbons. Amongst the different processes for formation of C-C bonds, the two relevant processes are aldol condensation, and alkene oligomerization. Alkene oligomerization processes suffer from coking as well as low selectivity for higher carbon number hydrocarbons. Therefore, aldol condensation can be used as a promising pathway for formation of C-C bonds. There are numerous studies in literature for vapor phase aldol condensation with various metal oxide catalysts with the aim of producing long chain hydrocarbons.¹⁸⁰⁻¹⁸⁷ As a preliminary study, a 2%Cu/TiO₂ catalyst was prepared and tested on the micro-scale semi-batch reactor for the aldol condensation reaction. Butanal was used as a feed molecule due to its relatively high boiling point (72°C), which allowed it to be fed with relatively low losses during the loading procedure. Two main pathways were observed as shown in Figure 7.1. The first was the hydrodeoxygenation pathway which resulted in formation of butane and butene, through

a butanol intermediate, and was the undesired pathway. The second competing pathway was aldol condensation followed by hydrogenation (and further HDO) which resulted in formation of C_8 , C_{12} and higher molecular weight hydrocarbons and oxygenates. The major C_8 oxygenates observed were 2-ethylhexanal and 2-ethylhexenal, which had the precise branched structure expected from aldol condensation products. The selectivity of all the classes of products has been reported in Table 7.1. At 3 bar hydrogen partial pressure the total selectivity to C_4 hydrocarbons was ~18%. As the hydrogen pressure was decreased systematically to 0.5 bar, the selectivity decreased to ~2% nearly shutting down the pure HDO pathway. This was primarily due to a lower degree of hydrogenation of butanal to butanol, which was the intermediate for formation of C_4 hydrocarbons. Therefore, it was concluded that operation at low hydrogen pressure was necessary to effectively shut down the pure hydrodeoxygenation pathway and boost the selectivity for the aldol condensation followed by subsequent hydrodeoxygenation pathway.

Testing with butanal gave way to testing with cellulose and biomass relevant molecules namely, glycolaldehyde and levoglucosan, which are the two most abundant products from cellulose pyrolysis. These molecules were tested along with preliminary testing of butanol, 1,2-propanediol, 1,3-propanediol and glycerol. All the molecules showed aldol condensation activity at low hydrogen pressure. However since these were preliminary pulse catalytic studies, the overall mass balance for these studies was low. It is possible that the molecules bind strongly to the catalyst and do not desorb completely and due to excess loading of the catalyst as well as low hydrogen pressure the mass balance is less than stoichiometric. However, even at less than 70 wt% mass balance a significant

proportion (85%) of aldol products were present amongst the observed products. Figure 7.2 shows the GC chromatogram from aldol condensation of glycolaldehyde, and shows a significant proportion of C₄₊ hydrocarbons. These results demonstrate that light oxygenates like glycolaldehyde (C₂) can be successfully converted to higher hydrocarbons through the aldol condensation pathway. However, reaction rate, catalyst stability, and deactivation studies over this catalyst are required to be performed to establish it as a candidate for testing with cellulose pyrolysis products in the lab scale cyclone type FHP and catalytic hydrodeoxygenation reactor.

Table 7.1 Product selectivity from aldol condensation of butanal over 2%Cu/TiO₂ catalyst, as a function of hydrogen pressure in the conversion range of 80-88%, at a temperature of 300°C.

Hydrogen partial pressure /bar	3	1	0.5
Conversion / %	88.2	82.9	80.0
Selectivity / %			
Butane + butene	18.4	7.2	2.0
C₈ hydrocarbons	36.5	22.9	15.5
2-ethyl hexanal/hexenal	17.5	24.7	28.7
C₁₂ hydrocarbons	12.4	17.9	17.7
C₁₂ oxygenates	10.7	17.9	27.2
C₁₂₊	4.6	9.9	9.4
Total Aldol products	81	93	98

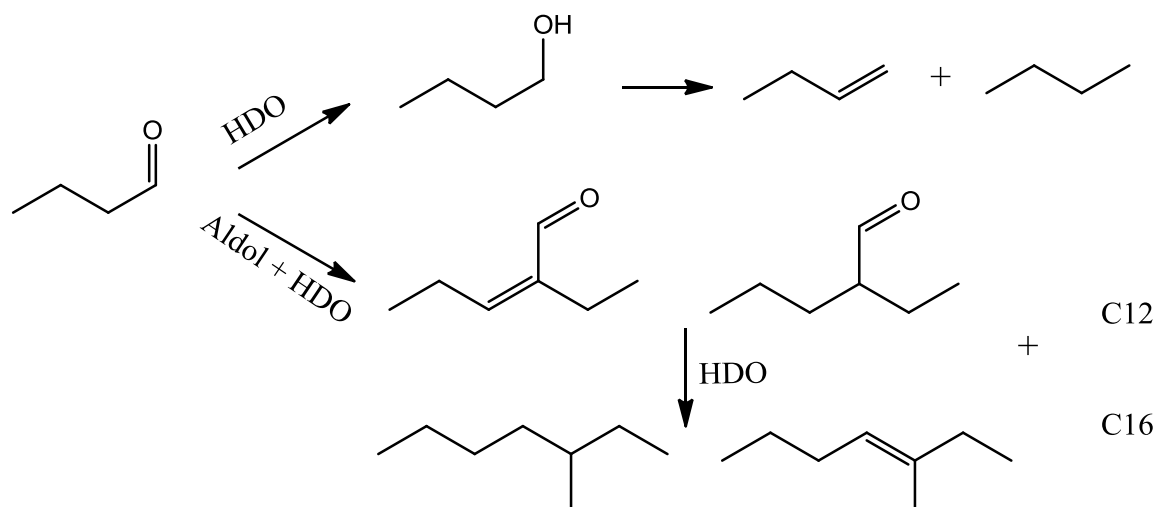


Figure 7.1 Proposed major reaction pathways for vapor phase aldol condensation of butanal over the 2%Cu/TiO₂ catalyst.

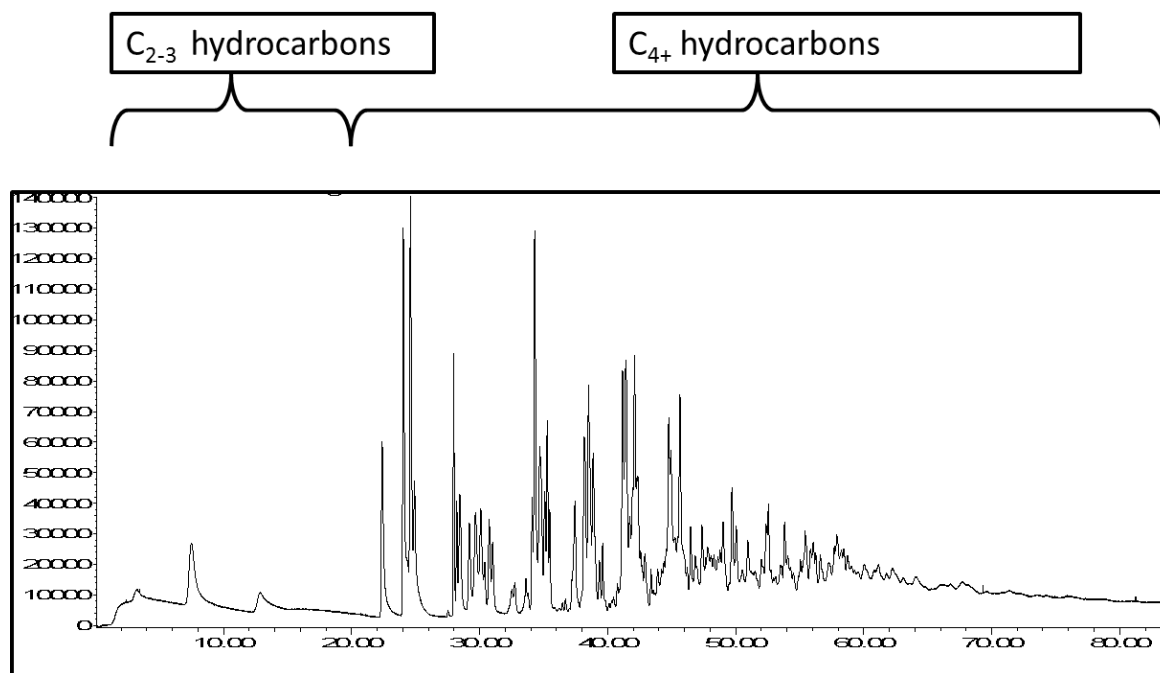


Figure 7.2 GC chromatogram (FID) showing the hydrocarbon products from aldol condensation of glycolaldehyde over 2%Cu/TiO₂ catalyst, at a temperature of 300°C.

Opportunity exists in this field for studying molecules like glycolaldehyde which have an –OH group on the α carbon atom. This study would be relevant for sugar based molecules which tend to have multiple –OH groups that need to be dehydrogenated to form an aldehyde or ketone before being converted via aldol condensation. Low hydrogen pressure is known to favor formation of aldehydes/ketones from alcohol functional groups, and a study at low hydrogen pressure would favor aldol condensation due to *insitu* formation of aldehydes from alcohols. Additional studies could be conducted with molecules like 1,2-propanediol, 1,3-propanediol to study the effect of adjacent –OH groups on aldol condensation activity and selectivity. Furthermore, deactivation and regeneration studies will need to be done, since titania (P25) in absence of Cu has been shown to have significant deactivation during aldol condensation.¹⁸⁸ Other catalytic systems like Ru/TiO₂, ceria-zirconia mixed oxides, aluminophosphates, and zeolites have been tested, and insights can be drawn from these studies to design better catalysts from aldol condensation of sugar derived molecules.^{183,184,189–191} An important parameter is the selection of the correct metallic function to go with the metal oxide support. Cu does not show any C-C bond scission activity, however is due to its weak hydrogenation function it is not suitable for HDO of lignin derived molecules. On the other hand Pt based catalysts will show substantial C-C bond scission activity, but will be good for lignin compound HDO. Therefore, an ideal catalyst would be something that has both the desired properties of Cu and Pt, and a bimetallic catalyst (for e.g. Pt-Sn, Pt-Mo, Pd-Cu, Ni-Fe, Rh-Re), which curbs the C-C scission activity of the hydrogenating metal, supported on titania (or other metal oxide active for aldol condensation) may be an ideal candidate for carrying out aldol condensation in conjunction with HDO.

7.2.2 Kinetics of phenol and methoxy deoxygenation at low hydrogen pressure

Preliminary results at low hydrogen pressure with the model compound m-cresol have been reported in Chapter 5. Further studies with the Pt-Mo series of bimetallic catalysts would be beneficial for understanding the role of Pt and Mo in the direct deoxygenation pathway for phenolic group. The STYs for direct deoxygenation, which is one of the primary steps, can be related to catalyst characterization results, Pt-Mo bimetallic particle percentage obtained via STEM-EELS, and the distribution of surface Mo phases obtained via XPS. These results could help understand the direct deoxygenation pathway and the role of Pt and Mo. Another interesting result from Chapter 5, showed the dependence of methoxy group C-O scission activity on the relative amount of Pt and Mo, with C_{sp3}-O bond scission being favored with the Pt only catalyst, while C_{sp2}-O scission being favored with the Pt-Mo bimetallic catalyst. A systematic study at low hydrogen pressure with a suitable model compound, p-alkyl-anisole can be proposed with the Pt-Mo series of bimetallic catalysts.

7.2.3 Fast pyrolysis studies with lignin model compounds and xylan polymer

Lignin and hemicellulose have not been studied extensively due to their heterogeneous structure and lack of representative, pure standards. However, in Chapter 4, lignin pyrolysis studies were performed with synthetic model oligomers made from guaiacyl monomers linked via β -O-4 bonds. In future these studies can be extended to include other types of commonly occurring linkages in the native lignin polymer, like the β -5 and α -O-4 linkages. These studies in collaboration with Py-MS studies would be instrumental in understanding the complete network of mechanistic pathways during fast pyrolysis of

lignin. Additionally, decreasing the char yield from lignin is important since it accounts for a substantial increase in the amount of char formation from biomass (~30 carbon wt%) when compared with cellulose and xylan (~17 carbon wt%). The causes for char formation have been outlined in Chapter 5, and there can be further studies to investigate other factors and search for a remedy for reducing the amount of char formed from lignin. Studies based on lignin impregnation with a suitable hydrogenation catalyst, or pretreatment for functionalization of the -OH groups in the lignin polymer could be proposed. Additionally, lignin can be extracted by processes like catalytic depolymerization of lignin (CDL)¹² and the residue can be tested to see if reduced lignin content may reduce the amount of char formed. A shortcoming of the CDL process is the extraction of hemicellulose from biomass into the solvent, which needs to be removed and processed separately. Xylan (~95% pure, Chapter 6) can be used as a good surrogate for study of fast-pyrolysis of hemicellulose to offer insights into the product distribution from xylan fraction of hemicellulose which has not been extensively studied in literature.

LIST OF REFERENCES

LIST OF REFERENCES

1. US share of primary energy. *International energy agency* at <<http://www.iea.org/stats/WebGraphs/USA4.pdf>>
2. Monthly energy review. *US Energy Information Administration* (2012). at <<http://www.eia.gov/totalenergy/data/monthly/pdf/mer.pdf>>
3. Agrawal, R. & Singh, N. R. Solar Energy to Biofuels. *Annu. Rev. Chem. Biomol. Eng.* **1**, 343–364 (2010).
4. National transportation statistics. *Research and innovative technology administration, Bureau of transportation statistics* at <http://www.rita.dot.gov/bts/sites/rita.dot.gov/bts/files/publications/national_transportation_statistics/html/table_04_04.html>
5. Use of Energy in the United States. *U.S. Energy Information Administration* at <http://www.eia.gov/energyexplained/index.cfm?page=us_energy_transportation#table1>
6. Annual Energy Outlook 2014. (2014).
7. Agrawal, R., Singh, N. R., Ribeiro, F. H. & Delgass, W. N. Sustainable fuel for the transportation sector. *Proc. Natl. Acad. Sci.* **104**, 4828–4833 (2007).
8. Serrano-Ruiz, J. C. & Dumesic, J. A. Catalytic routes for the conversion of biomass into liquid hydrocarbon transportation fuels. *Energy Environ. Sci.* **4**, 83–99 (2010).
9. Huber, G. W., Iborra, S. & Corma, A. Synthesis of Transportation Fuels from Biomass: Chemistry, Catalysts, and Engineering. *Chem. Rev.* **106**, 4044–4098 (2006).
10. Regalbuto, J. An NSF perspective on next generation hydrocarbon biorefineries. *Comput. Chem. Eng.* **34**, 1393–1396 (2010).
11. Bridgwater, A. V. Renewable fuels and chemicals by thermal processing of biomass. *Chem. Eng. J.* **91**, 87–102 (2003).
12. Parsell, T. *et al.* A synergistic biorefinery based on catalytic conversion of lignin prior to cellulose starting from lignocellulosic biomass. *Green Chem* (2014). doi:10.1039/C4GC01911C
13. Agrawal, R. *et al.* Synergy in the hybrid thermochemical–biological processes for liquid fuel production. *Comput. Chem. Eng.* **33**, 2012–2017 (2009).
14. Anex, R. P. *et al.* Techno-economic comparison of biomass-to-transportation fuels via pyrolysis, gasification, and biochemical pathways. *Fuel* **89**, Supplement 1, S29–S35 (2010).
15. Mettler, M. S., Vlachos, D. G. & Dauenhauer, P. J. Top ten fundamental challenges of biomass pyrolysis for biofuels. *Energy Environ. Sci.* **5**, 7797–7809 (2012).

16. Singh, N. R., Mallapragada, D. S., Agrawal, R. & Tyner, W. E. Economic analysis of novel synergistic biofuel (H2Bioil) processes. *Biomass Convers. Biorefinery* **2**, 141–148 (2012).
17. Thilakaratne, R., Brown, T., Li, Y., Hu, G. & Brown, R. Mild catalytic pyrolysis of biomass for production of transportation fuels: a techno-economic analysis. *Green Chem.* **16**, 627–636 (2014).
18. Wright, M. M., Daugaard, D. E., Satrio, J. A. & Brown, R. C. Techno-economic analysis of biomass fast pyrolysis to transportation fuels. *Fuel* **89**, Supplement 1, S2–S10 (2010).
19. Mohan, D., Pittman, Charles U. & Steele, P. H. Pyrolysis of Wood/Biomass for Bio-oil: A Critical Review. *Energy Fuels* **20**, 848–889 (2006).
20. Bridgwater, A. V., Meier, D. & Radlein, D. An overview of fast pyrolysis of biomass. *Org. Geochem.* **30**, 1479–1493 (1999).
21. Centi, G. & Santen, R. A. van. *Catalysis for Renewables: From Feedstock to Energy Production*. (John Wiley & Sons, 2008).
22. Bridgwater, A. V. Review of fast pyrolysis of biomass and product upgrading. *Biomass Bioenergy* **38**, 68–94 (2012).
23. Bridgwater, A. V. & Peacocke, G. V. C. Fast pyrolysis processes for biomass. *Renew. Sustain. Energy Rev.* **4**, 1–73 (2000).
24. Agrawal, R. & Singh, N. R. Synergistic routes to liquid fuel for a petroleum-deprived future. *AIChE J.* **55**, 1898–1905 (2009).
25. Singh, N. R., Delgass, W. N., Ribeiro, F. H. & Agrawal, R. Estimation of Liquid Fuel Yields from Biomass. *Environ. Sci. Technol.* **44**, 5298–5305 (2010).
26. Agrawal, R., Agrawal, M. & Singh, N. R. Process for producing liquid hydrocarbon by pyrolysis of biomass in presence of hydrogen from a carbon-free energy source. (2012).
27. Agrawal, R. & Singh, N. R. Producing liquid hydrocarbons from biomass via hydrolysis of biomass with a gaseous exhaust stream comprising CO₂, CO, H₂, and water formed from one of gasification and reforming of carbon containing moiety (CCM) such as natural gas; biofuels. (2012).
28. Mod, R. R., Conkerton, E. J., Ory, R. L. & Normand, F. L. Hemicellulose Composition of Dietary Fiber of Milled Rice and Rice Bran. *J. Agric. Food Chem.* **26**, 1031–1035 (1978).
29. Rinaldi, R. & Schüth, F. Design of solid catalysts for the conversion of biomass. *Energy Environ. Sci.* **2**, 610–626 (2009).
30. Humphreys, J. M. & Chapple, C. Rewriting the lignin roadmap. *Curr. Opin. Plant Biol.* **5**, 224–229 (2002).
31. Demirbaş, A. Effect of lignin content on aqueous liquefaction products of biomass. *Energy Convers. Manag.* **41**, 1601–1607 (2000).
32. Li, X., Weng, J.-K. & Chapple, C. Improvement of biomass through lignin modification. *Plant J.* **54**, 569–581 (2008).
33. Thangalazhy-Gopakumar, S., Adhikari, S., Gupta, R. B. & Fernando, S. D. Influence of Pyrolysis Operating Conditions on Bio-Oil Components: A Microscale Study in a Pyroprobe. *Energy Fuels* **25**, 1191–1199 (2011).

34. Thangalazhy-Gopakumar, S., Adhikari, S., Gupta, R. B., Tu, M. & Taylor, S. Production of hydrocarbon fuels from biomass using catalytic pyrolysis under helium and hydrogen environments. *Bioresour. Technol.* **102**, 6742–6749 (2011).
35. Thangalazhy-Gopakumar, S., Adhikari, S. & Gupta, R. B. Catalytic Pyrolysis of Biomass over H+ZSM-5 under Hydrogen Pressure. *Energy Fuels* **26**, 5300–5306 (2012).
36. Hoekstra, E. *et al.* Heterogeneous and homogeneous reactions of pyrolysis vapors from pine wood. *AIChE J.* **58**, 2830–2842 (2012).
37. Patwardhan, P. R., Brown, R. C. & Shanks, B. H. Understanding the Fast Pyrolysis of Lignin. *ChemSusChem* **4**, 1629–1636 (2011).
38. Cyprès, R. & Furfari, S. Direct post-cracking of volatiles from coal hydrolysis: 1. Influence of post-cracking temperature. *Fuel* **64**, 33–39 (1985).
39. Zacher, A. H., Olarte, M. V., Santosa, D. M., Elliott, D. C. & Jones, S. B. A review and perspective of recent bio-oil hydrotreating research. *Green Chem.* **16**, 491–515 (2014).
40. Pyroprobe 5200 high pressure reactor w/built-in trap. *CDS Analytical* at <http://www.cdsanalytical.com/instruments/pyrolysis/pyroprobe_5200_hp.html>
41. GC Solutions #5: Hot Split Injections – Part 1 - Separation Science :: Premier Learning for Analytical Chemists. at <<http://www.sepscience.com/Techniques/GC/Articles/832-/GC-Solutions-5-Hot-Split-Injections--Part-1>>
42. Kinne, M. *et al.* Oxidative cleavage of non-phenolic β -O-4 lignin model dimers by an extracellular aromatic peroxygenase. (2011).
43. Czernik, S. & Bridgwater, A. V. Overview of Applications of Biomass Fast Pyrolysis Oil. *Energy Fuels* **18**, 590–598 (2004).
44. Bridgwater, A. V. Catalysis in thermal biomass conversion. *Appl. Catal. Gen.* **116**, 5–47 (1994).
45. Bridgwater, A. V. Production of high grade fuels and chemicals from catalytic pyrolysis of biomass. *Catal. Today* **29**, 285–295 (1996).
46. Elliott, D. C. Historical Developments in Hydroprocessing Bio-oils. *Energy Fuels* **21**, 1792–1815 (2007).
47. Singh, N. R., Mallapragada, D. S., Agrawal, R. & Tyner, W. E. Economic analysis of novel synergistic biofuel (H2Bioil) processes. *Biomass Convers. Biorefinery* **2**, 141–148 (2012).
48. Lédé, J. Cellulose pyrolysis kinetics: An historical review on the existence and role of intermediate active cellulose. *J. Anal. Appl. Pyrolysis* **94**, 17–32 (2012).
49. Alves, S. S. & Figueiredo, J. L. Kinetics of cellulose pyrolysis modelled by three consecutive first-order reactions. *J. Anal. Appl. Pyrolysis* **17**, 37–46 (1989).
50. Lu, Q. *et al.* Influence of pyrolysis temperature and time on the cellulose fast pyrolysis products: Analytical Py-GC/MS study. *J. Anal. Appl. Pyrolysis* **92**, 430–438 (2011).
51. Cho, J., Davis, J. M. & Huber, G. W. The Intrinsic Kinetics and Heats of Reactions for Cellulose Pyrolysis and Char Formation. *ChemSusChem* **3**, 1162–1165 (2010).

52. Du, S., Valla, J. A. & Bollas, G. M. Characteristics and origin of char and coke from fast and slow, catalytic and thermal pyrolysis of biomass and relevant model compounds. *Green Chem.* **15**, 3214–3229 (2013).
53. Lin, Y.-C., Cho, J., Tompsett, G. A., Westmoreland, P. R. & Huber, G. W. Kinetics and Mechanism of Cellulose Pyrolysis. *J. Phys. Chem. C* **113**, 20097–20107 (2009).
54. Wang, S., Guo, X., Liang, T., Zhou, Y. & Luo, Z. Mechanism research on cellulose pyrolysis by Py-GC/MS and subsequent density functional theory studies. *Bioresour. Technol.* **104**, 722–728 (2012).
55. Bradbury, A. G. W., Sakai, Y. & Shafizadeh, F. A kinetic model for pyrolysis of cellulose. *J. Appl. Polym. Sci.* **23**, 3271–3280 (1979).
56. Diebold, J. P. A unified, global model for the pyrolysis of cellulose. *Biomass Bioenergy* **7**, 75–85 (1994).
57. Di Blasi, C. & Branca, C. Kinetics of Primary Product Formation from Wood Pyrolysis. *Ind. Eng. Chem. Res.* **40**, 5547–5556 (2001).
58. Šimon, P. Considerations on the single-step kinetics approximation. *J. Therm. Anal. Calorim.* **82**, 651–657 (2005).
59. Șerbănescu, C. Kinetic analysis of cellulose pyrolysis: a short review. *Chem. Pap.* **68**, 847–860 (2014).
60. Vinu, R. & Broadbelt, L. J. A mechanistic model of fast pyrolysis of glucose-based carbohydrates to predict bio-oil composition. *Energy Environ. Sci.* **5**, 9808–9826 (2012).
61. Agarwal, V., Dauenhauer, P. J., Huber, G. W. & Auerbach, S. M. Ab Initio Dynamics of Cellulose Pyrolysis: Nascent Decomposition Pathways at 327 and 600 °C. *J. Am. Chem. Soc.* **134**, 14958–14972 (2012).
62. Degenstein, J. C. *et al.* Fast Pyrolysis of ¹³C-Labeled Cellobioses: Gaining Insights into the Mechanisms of Fast Pyrolysis of Carbohydrates. *J. Org. Chem.* **80**, 1909–1914 (2015).
63. Hurt, M. R. *et al.* On-Line Mass Spectrometric Methods for the Determination of the Primary Products of Fast Pyrolysis of Carbohydrates and for Their Gas-Phase Manipulation. *Anal. Chem.* **85**, 10927–10934 (2013).
64. Mayes, H. B. & Broadbelt, L. J. Unraveling the Reactions that Unravel Cellulose. *J. Phys. Chem. A* **116**, 7098–7106 (2012).
65. Zhou, X., Nolte, M. W., Shanks, B. H. & Broadbelt, L. J. Experimental and Mechanistic Modeling of Fast Pyrolysis of Neat Glucose-Based Carbohydrates. 2. Validation and Evaluation of the Mechanistic Model. *Ind. Eng. Chem. Res.* **53**, 13290–13301 (2014).
66. Mettler, M. S., Paulsen, A. D., Vlachos, D. G. & Dauenhauer, P. J. The chain length effect in pyrolysis: bridging the gap between glucose and cellulose. *Green Chem.* **14**, 1284–1288 (2012).
67. Mettler, M. S. *et al.* Revealing pyrolysis chemistry for biofuels production: Conversion of cellulose to furans and small oxygenates. *Energy Environ. Sci.* **5**, 5414–5424 (2012).
68. Patwardhan, P. R., Dalluge, D. L., Shanks, B. H. & Brown, R. C. Distinguishing primary and secondary reactions of cellulose pyrolysis. *Bioresour. Technol.* **102**, 5265–5269 (2011).

69. Venkatakrisnan, V. K. *et al.* High-pressure fast-pyrolysis, fast-hydropyrolysis and catalytic hydrodeoxygenation of cellulose: production of liquid fuel from biomass. *Green Chem.* **16**, 792–802 (2014).
70. Mehta, D. D. Kinetic studies of model reactions to transform biomass into fuels. (Purdue University, 2014).
71. Patwardhan, P. R., Satrio, J. A., Brown, R. C. & Shanks, B. H. Product distribution from fast pyrolysis of glucose-based carbohydrates. *J. Anal. Appl. Pyrolysis* **86**, 323–330 (2009).
72. Teixeira, A. R. *et al.* Aerosol generation by reactive boiling ejection of molten cellulose. *Energy Environ. Sci.* **4**, 4306–4321 (2011).
73. Radlein, D. S. T. A. G., Grinshpun, A., Piskorz, J. & Scott, D. S. On the presence of anhydro-oligosaccharides in the sirups from the fast pyrolysis of cellulose. *J. Anal. Appl. Pyrolysis* **12**, 39–49 (1987).
74. Zhang, J., Nolte, M. W. & Shanks, B. H. Investigation of Primary Reactions and Secondary Effects from the Pyrolysis of Different Celluloses. *ACS Sustain. Chem. Eng.* **2**, 2820–2830 (2014).
75. Hajaligol, M. R., Howard, J. B., Longwell, J. P. & Peters, W. A. Product compositions and kinetics for rapid pyrolysis of cellulose. *Ind. Eng. Chem. Process Des. Dev.* **21**, 457–465 (1982).
76. Bai, X., Johnston, P. & Brown, R. C. An experimental study of the competing processes of evaporation and polymerization of levoglucosan in cellulose pyrolysis. *J. Anal. Appl. Pyrolysis* **99**, 130–136 (2013).
77. Zhang, Q., Chang, J., Wang, T. & Xu, Y. Review of biomass pyrolysis oil properties and upgrading research. *Energy Convers. Manag.* **48**, 87–92 (2007).
78. Gawecki, P. Fundamental studies of biomass fast pyrolysis for the direct production of molecules in the fuel range. (Purdue University, 2013).
79. Paulsen, A. D., Mettler, M. S. & Dauenhauer, P. J. The Role of Sample Dimension and Temperature in Cellulose Pyrolysis. *Energy Fuels* **27**, 2126–2134 (2013).
80. Degenstein, J. C. *et al.* Cellotriosan is a key intermediate during fast pyrolysis of cellulose. (*unpublished*)
81. Neumann, G. T., Pimentel, B. R., Rensel, D. J. & Hicks, J. C. Correlating lignin structure to aromatic products in the catalytic fast pyrolysis of lignin model compounds containing β -O-4 linkages. *Catal. Sci. Technol.* **4**, 3953–3963 (2014).
82. Glasser, W. G. in *Fundamentals of Thermochemical Biomass Conversion* (eds. Overend, R. P., Milne, T. A. & Mudge, L. K.) 61–76 (Springer Netherlands, 1985).
83. De Wild, P. J., Huijgen, W. J. J. & Heeres, H. J. Pyrolysis of wheat straw-derived organosolv lignin. *J. Anal. Appl. Pyrolysis* **93**, 95–103 (2012).
84. Zakzeski, J., Bruijninx, P. C. A., Jongerijs, A. L. & Weckhuysen, B. M. The Catalytic Valorization of Lignin for the Production of Renewable Chemicals. *Chem. Rev.* **110**, 3552–3599 (2010).
85. Jiang, G., Nowakowski, D. J. & Bridgwater, A. V. A systematic study of the kinetics of lignin pyrolysis. *Thermochim. Acta* **498**, 61–66 (2010).
86. Sharma, R. K. *et al.* Characterization of chars from pyrolysis of lignin. *Fuel* **83**, 1469–1482 (2004).
87. Beis, S. H. *et al.* Fast Pyrolysis of Lignins. *BioResources* **5**, 1408–1424 (2010).

88. Trinh, T. N. *et al.* Fast Pyrolysis of Lignin Using a Pyrolysis Centrifuge Reactor. *Energy Fuels* **27**, 3802–3810 (2013).
89. Nowakowski, D. J., Bridgwater, A. V., Elliott, D. C., Meier, D. & de Wild, P. Lignin fast pyrolysis: Results from an international collaboration. *J. Anal. Appl. Pyrolysis* **88**, 53–72 (2010).
90. Nunn, T. R., Howard, J. B., Longwell, J. P. & Peters, W. A. Product compositions and kinetics in the rapid pyrolysis of milled wood lignin. *Ind. Eng. Chem. Process Des. Dev.* **24**, 844–852 (1985).
91. Chu, S., Subrahmanyam, A. V. & Huber, G. W. The pyrolysis chemistry of a β -O-4 type oligomeric lignin model compound. *Green Chem.* **15**, 125–136 (2012).
92. Zhou, S. *et al.* Effect of the Fast Pyrolysis Temperature on the Primary and Secondary Products of Lignin. *Energy Fuels* **27**, 5867–5877 (2013).
93. Scholze, B., Hanser, C. & Meier, D. Characterization of the water-insoluble fraction from fast pyrolysis liquids (pyrolytic lignin): Part II. GPC, carbonyl groups, and ^{13}C -NMR. *J. Anal. Appl. Pyrolysis* **58–59**, 387–400 (2001).
94. Bayerbach, R., Nguyen, V. D., Schurr, U. & Meier, D. Characterization of the water-insoluble fraction from fast pyrolysis liquids (pyrolytic lignin): Part III. Molar mass characteristics by SEC, MALDI-TOF-MS, LDI-TOF-MS, and Py-FIMS. *J. Anal. Appl. Pyrolysis* **77**, 95–101 (2006).
95. Scholze, B. & Meier, D. Characterization of the water-insoluble fraction from pyrolysis oil (pyrolytic lignin). Part I. PY-GC/MS, FTIR, and functional groups. *J. Anal. Appl. Pyrolysis* **60**, 41–54 (2001).
96. Evans, R. J., Milne, T. A. & Soltys, M. N. Direct mass-spectrometric studies of the pyrolysis of carbonaceous fuels: III. Primary pyrolysis of lignin. *J. Anal. Appl. Pyrolysis* **9**, 207–236 (1986).
97. Bai, X. *et al.* Formation of phenolic oligomers during fast pyrolysis of lignin. *Fuel* **128**, 170–179 (2014).
98. Mu, W., Ben, H., Ragauskas, A. & Deng, Y. Lignin Pyrolysis Components and Upgrading—Technology Review. *BioEnergy Res.* **6**, 1183–1204 (2013).
99. Van der Hage, E. R. E., Mulder, M. M. & Boon, J. J. Structural characterization of lignin polymers by temperature-resolved in-source pyrolysis—mass spectrometry and Curie-point pyrolysis—gas chromatography/mass spectrometry. *J. Anal. Appl. Pyrolysis* **25**, 149–183 (1993).
100. Jiang-Yan Liu, Shu-Bin Wu & Rui Lou. Chemical structure and pyrolysis response of β -O-4 lignin model polymer. *BioResources* **6**, 1079–1093 (2011).
101. Jiang, G., Nowakowski, D. J. & Bridgwater, A. V. Effect of the Temperature on the Composition of Lignin Pyrolysis Products. *Energy Fuels* **24**, 4470–4475 (2010).
102. Guillén, M. D. & Ibargoitia, M. L. GC/MS analysis of lignin monomers, dimers and trimers in liquid smoke flavourings. *J. Sci. Food Agric.* **79**, 1889–1903 (1999).
103. Jarrell, T. M. *et al.* Characterization of organosolv switchgrass lignin by using high performance liquid chromatography/high resolution tandem mass spectrometry using hydroxide-doped negative-ion mode electrospray ionization. *Green Chem.* **16**, 2713–2727 (2014).
104. Jarvis, M. W. *et al.* Direct Detection of Products from the Pyrolysis of 2-Phenethyl Phenyl Ether. *J. Phys. Chem. A* **115**, 428–438 (2011).

105. Nakamura, T., Kawamoto, H. & Saka, S. Pyrolysis behavior of Japanese cedar wood lignin studied with various model dimers. *J. Anal. Appl. Pyrolysis* **81**, 173–182 (2008).
106. Britt, P. F., Buchanan III, A. C., Thomas, K. B. & Lee, S.-K. Pyrolysis mechanisms of lignin: surface-immobilized model compound investigation of acid-catalyzed and free-radical reaction pathways. *J. Anal. Appl. Pyrolysis* **33**, 1–19 (1995).
107. Kim, K. H., Bai, X. & Brown, R. C. Pyrolysis mechanisms of methoxy substituted α -O-4 lignin dimeric model compounds and detection of free radicals using electron paramagnetic resonance analysis. *J. Anal. Appl. Pyrolysis* **110**, 254–263 (2014).
108. Kawamoto, H., Horigoshi, S. & Saka, S. Pyrolysis reactions of various lignin model dimers. *J. Wood Sci.* **53**, 168–174 (2007).
109. Amen-Chen, C., Pakdel, H. & Roy, C. Production of monomeric phenols by thermochemical conversion of biomass: a review. *Bioresour. Technol.* **79**, 277–299 (2001).
110. Klein, M. T. & Virk, P. S. Model pathways in lignin thermolysis. 1. Phenethyl phenyl ether. *Ind. Eng. Chem. Fundam.* **22**, 35–45 (1983).
111. Sheng, H. Mass spectrometric studies on lignin sequencing and fast pyrolysis, functional-group selective ion-molecule reactions and reactivity of bi- and triradicals. (Purdue University, 2014).
112. Kawamoto, H., Ryoritani, M. & Saka, S. Different pyrolytic cleavage mechanisms of β -ether bond depending on the side-chain structure of lignin dimers. *J. Anal. Appl. Pyrolysis* **81**, 88–94 (2008).
113. Kawamoto, H., Horigoshi, S. & Saka, S. Effects of side-chain hydroxyl groups on pyrolytic β -ether cleavage of phenolic lignin model dimer. *J. Wood Sci.* **53**, 268–271 (2007).
114. Kishimoto, T., Uraki, Y. & Ubukata, M. Chemical synthesis of β -O-4 type artificial lignin. *Org. Biomol. Chem.* **4**, 1343–1347 (2006).
115. Kotake, T., Kawamoto, H. & Saka, S. Pyrolysis reactions of coniferyl alcohol as a model of the primary structure formed during lignin pyrolysis. *J. Anal. Appl. Pyrolysis* **104**, 573–584 (2013).
116. Kotake, T., Kawamoto, H. & Saka, S. Mechanisms for the formation of monomers and oligomers during the pyrolysis of a softwood lignin. *J. Anal. Appl. Pyrolysis* **105**, 309–316 (2014).
117. Nakamura, T., Kawamoto, H. & Saka, S. Condensation Reactions of Some Lignin Related Compounds at Relatively Low Pyrolysis Temperature. *J. Wood Chem. Technol.* **27**, 121–133 (2007).
118. Masuku, C. P. Thermolytic decomposition of coniferyl alcohol. *J. Anal. Appl. Pyrolysis* **23**, 195–208 (1992).
119. Bridgwater, A. V. A survey of thermochemical biomass processing activities. *Biomass* **22**, 279–292 (1990).
120. Daoutidis, P., Marvin, W. A., Rangarajan, S. & Torres, A. I. Engineering Biomass Conversion Processes: A Systems Perspective. *AIChE J.* **59**, 3–18 (2013).
121. Bu, Q. *et al.* A review of catalytic hydrodeoxygenation of lignin-derived phenols from biomass pyrolysis. *Bioresour. Technol.* **124**, 470–477 (2012).

122. Parsell, T. H. *et al.* Cleavage and hydrodeoxygenation (HDO) of C–O bonds relevant to lignin conversion using Pd/Zn synergistic catalysis. *Chem. Sci.* **4**, 806–813 (2013).
123. Furimsky, E. Catalytic hydrodeoxygenation. *Appl. Catal. Gen.* **199**, 147–190 (2000).
124. Hicks, J. C. Advances in C–O Bond Transformations in Lignin-Derived Compounds for Biofuels Production. *J. Phys. Chem. Lett.* **2**, 2280–2287 (2011).
125. Wang, H., Male, J. & Wang, Y. Recent Advances in Hydrotreating of Pyrolysis Bio-Oil and Its Oxygen-Containing Model Compounds. *ACS Catal.* **3**, 1047–1070 (2013).
126. Sun, J. *et al.* Carbon-supported bimetallic Pd–Fe catalysts for vapor-phase hydrodeoxygenation of guaiacol. *J. Catal.* **306**, 47–57 (2013).
127. Zhao, C., Kou, Y., Lemonidou, A. A., Li, X. & Lercher, J. A. Highly Selective Catalytic Conversion of Phenolic Bio-Oil to Alkanes. *Angew. Chem. Int. Ed.* **48**, 3987–3990 (2009).
128. Zhao, C., Camaioni, D. M. & Lercher, J. A. Selective catalytic hydroalkylation and deoxygenation of substituted phenols to bicycloalkanes. *J. Catal.* **288**, 92–103 (2012).
129. Foster, A. J., Do, P. T. M. & Lobo, R. F. The Synergy of the Support Acid Function and the Metal Function in the Catalytic Hydrodeoxygenation of m-Cresol. *Top. Catal.* **55**, 118–128 (2012).
130. Zhao, C., He, J., Lemonidou, A. A., Li, X. & Lercher, J. A. Aqueous-phase hydrodeoxygenation of bio-derived phenols to cycloalkanes. *J. Catal.* **280**, 8–16 (2011).
131. Zhu, X., Lobban, L. L., Mallinson, R. G. & Resasco, D. E. Bifunctional transalkylation and hydrodeoxygenation of anisole over a Pt/HBeta catalyst. *J. Catal.* **281**, 21–29 (2011).
132. Do, P. T. M., Foster, A. J., Chen, J. & Lobo, R. F. Bimetallic effects in the hydrodeoxygenation of meta-cresol on γ -Al₂O₃ supported Pt–Ni and Pt–Co catalysts. *Green Chem.* **14**, 1388–1397 (2012).
133. Nie, L. & Resasco, D. E. Kinetics and mechanism of m-cresol hydrodeoxygenation on a Pt/SiO₂ catalyst. *J. Catal.* **317**, 22–29 (2014).
134. Dietrich, P. J. *et al.* Structural and catalytic differences in the effect of Co and Mo as promoters for Pt-based aqueous phase reforming catalysts. *Appl. Catal. B Environ.* **156–157**, 236–248 (2014).
135. Dietrich, P. J. *et al.* Aqueous Phase Glycerol Reforming with Pt and PtMo Bimetallic Nanoparticle Catalysts: The Role of the Mo Promoter. *Top. Catal.* **56**, 1814–1828 (2013).
136. Prasomsri, T., Nimmanwudipong, T. & Román-Leshkov, Y. Effective hydrodeoxygenation of biomass-derived oxygenates into unsaturated hydrocarbons by MoO₃ using low H₂ pressures. *Energy Environ. Sci.* **6**, 1732–1738 (2013).
137. Xiong, K., Lee, W.-S., Bhan, A. & Chen, J. G. Molybdenum Carbide as a Highly Selective Deoxygenation Catalyst for Converting Furfural to 2-Methylfuran. *ChemSusChem* **7**, 2146–2149 (2014).

138. Xiong, K., Yu, W. & Chen, J. G. Selective deoxygenation of aldehydes and alcohols on molybdenum carbide (Mo₂C) surfaces. *Appl. Surf. Sci.* **323**, 88–95 (2014).
139. Lee, W.-S., Wang, Z., Wu, R. J. & Bhan, A. Selective vapor-phase hydrodeoxygenation of anisole to benzene on molybdenum carbide catalysts. *J. Catal.* **319**, 44–53 (2014).
140. Saidi, M. *et al.* Upgrading of lignin-derived bio-oils by catalytic hydrodeoxygenation. *Energy Environ. Sci.* **7**, 103–129 (2013).
141. Boonyasuwat, S., Omotoso, T., Resasco, D. E. & Crossley, S. P. Conversion of Guaiacol over Supported Ru Catalysts. *Catal. Lett.* **143**, 783–791 (2013).
142. González-Borja, M. Á. & Resasco, D. E. Anisole and Guaiacol Hydrodeoxygenation over Monolithic Pt–Sn Catalysts. *Energy Fuels* **25**, 4155–4162 (2011).
143. Elliott, D. C. & Hart, T. R. Catalytic Hydroprocessing of Chemical Models for Bio-oil. *Energy Fuels* **23**, 631–637 (2009).
144. Gutierrez, A., Kaila, R. K., Honkela, M. L., Slioor, R. & Krause, A. O. I. Hydrodeoxygenation of guaiacol on noble metal catalysts. *Catal. Today* **147**, 239–246 (2009).
145. Fisk, C. A. *et al.* Bio-oil upgrading over platinum catalysts using in situ generated hydrogen. *Appl. Catal. Gen.* **358**, 150–156 (2009).
146. Yohe, S. High-pressure vapor-phase catalytic hydrodeoxygenation of lignin-derived compounds to hydrocarbons on bimetallic catalysts in the range of 0.2–2.4 mpa. (Purdue University, 2013).
147. Williams, W. D., Bollmann, L., Miller, J. T., Delgass, W. N. & Ribeiro, F. H. Effect of molybdenum addition on supported platinum catalysts for the water–gas shift reaction. *Appl. Catal. B Environ.* **125**, 206–214 (2012).
148. Hibbitts, D., Tan, Q. & Neurock, M. Acid strength and bifunctional catalytic behavior of alloys comprised of noble metals and oxophilic metal promoters. *J. Catal.* **315**, 48–58 (2014).
149. Chia, M. *et al.* Selective Hydrogenolysis of Polyols and Cyclic Ethers over Bifunctional Surface Sites on Rhodium–Rhenium Catalysts. *J. Am. Chem. Soc.* **133**, 12675–12689 (2011).
150. Nie, L. *et al.* Selective conversion of m-cresol to toluene over bimetallic Ni–Fe catalysts. *J. Mol. Catal. Chem.* **388–389**, 47–55 (2014).
151. Ancheyta, J. & Speight, J. G. *Hydroprocessing of Heavy Oils and Residua*. (CRC Press, 2007).
152. Bartholomew, C. H. Mechanisms of catalyst deactivation. *Appl. Catal. Gen.* **212**, 17–60 (2001).
153. Forzatti, P. & Lietti, L. Catalyst deactivation. *Catal. Today* **52**, 165–181 (1999).
154. Furimsky, E. & Massoth, F. E. Deactivation of hydroprocessing catalysts. *Catal. Today* **52**, 381–495 (1999).
155. Moulijn, J. A., van Diepen, A. E. & Kapteijn, F. Catalyst deactivation: is it predictable?: What to do? *Appl. Catal. Gen.* **212**, 3–16 (2001).
156. Lee, W.-S., Wang, Z., Zheng, W., Vlachos, D. G. & Bhan, A. Vapor phase hydrodeoxygenation of furfural to 2-methylfuran on molybdenum carbide catalysts. *Catal. Sci. Technol.* **4**, 2340–2352 (2014).

157. Ruddy, D. A. *et al.* Recent advances in heterogeneous catalysts for bio-oil upgrading via 'ex situ catalytic fast pyrolysis': catalyst development through the study of model compounds. *Green Chem.* **16**, 454–490 (2014).
158. Sanna, A., Vispute, T. P. & Huber, G. W. Hydrodeoxygenation of the aqueous fraction of bio-oil with Ru/C and Pt/C catalysts. *Appl. Catal. B Environ.* **165**, 446–456 (2015).
159. Gualda, G. & Kasztelan, S. Initial Deactivation of Residue Hydrodemetallization Catalysts. *J. Catal.* **161**, 319–337 (1996).
160. Liu, C., Wang, H., Karim, A. M., Sun, J. & Wang, Y. Catalytic fast pyrolysis of lignocellulosic biomass. *Chem. Soc. Rev.* **43**, 7594–7623 (2014).
161. Carlson, T. R., Tompsett, G. A., Conner, W. C. & Huber, G. W. Aromatic Production from Catalytic Fast Pyrolysis of Biomass-Derived Feedstocks. *Top. Catal.* **52**, 241–252 (2009).
162. Jae, J. *et al.* Investigation into the shape selectivity of zeolite catalysts for biomass conversion. *J. Catal.* **279**, 257–268 (2011).
163. Wang, K., Kim, K. H. & Brown, R. C. Catalytic pyrolysis of individual components of lignocellulosic biomass. *Green Chem.* **16**, 727–735 (2014).
164. Carlson, T. R., Cheng, Y.-T., Jae, J. & Huber, G. W. Production of green aromatics and olefins by catalytic fast pyrolysis of wood sawdust. *Energy Environ. Sci.* **4**, 145–161 (2010).
165. Carlson, T. R., Vispute, T. P. & Huber, G. W. Green Gasoline by Catalytic Fast Pyrolysis of Solid Biomass Derived Compounds. *ChemSusChem* **1**, 397–400 (2008).
166. Venkatakrishnan, V. K., Delgass, W. N., Ribeiro, F. H. & Agrawal, R. Oxygen removal from intact biomass to produce liquid fuel range hydrocarbons via fast-hydropyrolysis and vapor-phase catalytic hydrodeoxygenation. *Green Chem.* (2014). doi:10.1039/C4GC01746C
167. Kunkes, E. L. *et al.* Catalytic Conversion of Biomass to Monofunctional Hydrocarbons and Targeted Liquid-Fuel Classes. *Science* **322**, 417–421 (2008).
168. Beeck, B. O. de *et al.* Direct catalytic conversion of cellulose to liquid straight-chain alkanes. *Energy Environ. Sci.* **8**, 230–240 (2014).
169. Chheda, J. N., Huber, G. W. & Dumesic, J. A. Liquid-Phase Catalytic Processing of Biomass-Derived Oxygenated Hydrocarbons to Fuels and Chemicals. *Angew. Chem. Int. Ed.* **46**, 7164–7183 (2007).
170. Liu, S., Tamura, M., Nakagawa, Y. & Tomishige, K. One-Pot Conversion of Cellulose into n-Hexane over the Ir-ReO_x/SiO₂ Catalyst Combined with HZSM-5. *ACS Sustain. Chem. Eng.* **2**, 1819–1827 (2014).
171. Ruppert, A. M., Weinberg, K. & Palkovits, R. Hydrogenolysis Goes Bio: From Carbohydrates and Sugar Alcohols to Platform Chemicals. *Angew. Chem. Int. Ed.* **51**, 2564–2601 (2012).
172. Sitthisa, S. & Resasco, D. E. Hydrodeoxygenation of Furfural Over Supported Metal Catalysts: A Comparative Study of Cu, Pd and Ni. *Catal. Lett.* **141**, 784–791 (2011).
173. Sitthisa, S. *et al.* Conversion of furfural and 2-methylpentanal on Pd/SiO₂ and Pd-Cu/SiO₂ catalysts. *J. Catal.* **280**, 17–27 (2011).

174. Sitthisa, S., An, W. & Resasco, D. E. Selective conversion of furfural to methylfuran over silica-supported NiFe bimetallic catalysts. *J. Catal.* **284**, 90–101 (2011).
175. Dayton, D. C., Carpenter, J., Farmer, J., Turk, B. & Gupta, R. Biomass Hydropyrolysis in a Pressurized Fluidized Bed Reactor. *Energy Fuels* **27**, 3778–3785 (2013).
176. Marker, T. L., Felix, L. G., Linck, M. B. & Roberts, M. J. Integrated hydropyrolysis and hydroconversion (IH₂) for the direct production of gasoline and diesel fuels or blending components from biomass, part 1: Proof of principle testing. *Environ. Prog. Sustain. Energy* **31**, 191–199 (2012).
177. Penning, B. W. *et al.* Validation of PyMBMS as a High-throughput Screen for Lignin Abundance in Lignocellulosic Biomass of Grasses. *BioEnergy Res.* **7**, 899–908 (2014).
178. Davda, R. R., Shabaker, J. W., Huber, G. W., Cortright, R. D. & Dumesic, J. A. Aqueous-phase reforming of ethylene glycol on silica-supported metal catalysts. *Appl. Catal. B Environ.* **43**, 13–26 (2003).
179. Huber, G. W., Cortright, R. D. & Dumesic, J. A. Renewable Alkanes by Aqueous-Phase Reforming of Biomass-Derived Oxygenates. *Angew. Chem. Int. Ed.* **43**, 1549–1551 (2004).
180. Hanna, D. G. *et al.* Experimental and Theoretical Study of n-Butanal Self-Condensation over Ti Species Supported on Silica. *ACS Catal.* **4**, 2908–2916 (2014).
181. West, R. M., Liu, Z. Y., Peter, M., Gärtner, C. A. & Dumesic, J. A. Carbon–carbon bond formation for biomass-derived furfurals and ketones by aldol condensation in a biphasic system. *J. Mol. Catal. Chem.* **296**, 18–27 (2008).
182. Hakim, S. H., Shanks, B. H. & Dumesic, J. A. Catalytic upgrading of the light fraction of a simulated bio-oil over CeZrOx catalyst. *Appl. Catal. B Environ.* **142–143**, 368–376 (2013).
183. Gangadharan, A., Shen, M., Sooknoi, T., Resasco, D. E. & Mallinson, R. G. Condensation reactions of propanal over CexZr1-xO2 mixed oxide catalysts. *Appl. Catal. Gen.* **385**, 80–91 (2010).
184. Wan, S. *et al.* Direct catalytic upgrading of biomass pyrolysis vapors by a dual function Ru/TiO₂ catalyst. *AIChE J.* **59**, 2275–2285 (2013).
185. Sad, M. E., Neurock, M. & Iglesia, E. Formation of C–C and C–O Bonds and Oxygen Removal in Reactions of Alkanediols, Alkanols, and Alkanals on Copper Catalysts. *J. Am. Chem. Soc.* **133**, 20384–20398 (2011).
186. Faba, L., Díaz, E. & Ordóñez, S. One-pot Aldol Condensation and Hydrodeoxygenation of Biomass-derived Carbonyl Compounds for Biodiesel Synthesis. *ChemSusChem* **7**, 2816–2820 (2014).
187. Ji, W., Chen, Y. & Kung, H. H. Vapor phase aldol condensation of acetaldehyde on metal oxide catalysts. *Appl. Catal. Gen.* **161**, 93–104 (1997).
188. Rekoske, J. E. & Barteau, M. A. Kinetics, Selectivity, and Deactivation in the Aldol Condensation of Acetaldehyde on Anatase Titanium Dioxide. *Ind. Eng. Chem. Res.* **50**, 41–51 (2011).

189. Climent, M. J., Corma, A., Fornés, V., Guil-Lopez, R. & Iborra, S. Aldol Condensations on Solid Catalysts: A Cooperative Effect between Weak Acid and Base Sites. *Adv. Synth. Catal.* **344**, 1090–1096 (2002).
190. Kikhtyanin, O., Kelbichová, V., Vitvarová, D., Kubů, M. & Kubička, D. Aldol condensation of furfural and acetone on zeolites. *Catal. Today* **227**, 154–162 (2014).
191. Kikhtyanin, O., Kubička, D. & Čejka, J. Toward understanding of the role of Lewis acidity in aldol condensation of acetone and furfural using MOF and zeolite catalysts. *Catal. Today* **243**, 158–162 (2015).
192. Stein, S. E. & Brown, R. L. Estimation of normal boiling points from group contributions. *J. Chem. Inf. Comput. Sci.* **34**, 581–587 (1994).

APPENDICES

Appendix A Supplementary information for Chapter 2

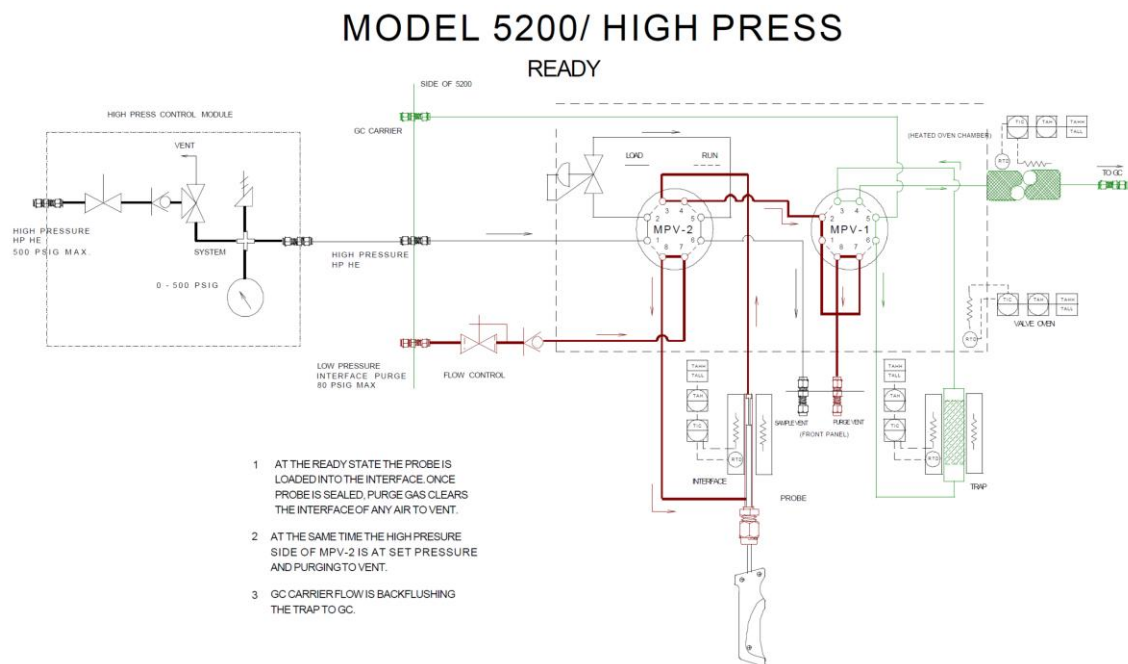


Figure A. 1 Schematic of the CDS pyroprobe 5200 high pressure reactor during the sample loading phase.

MODEL 5200/ HIGH PRESS MPV-2 ROTATED TO THE RUN POSITION

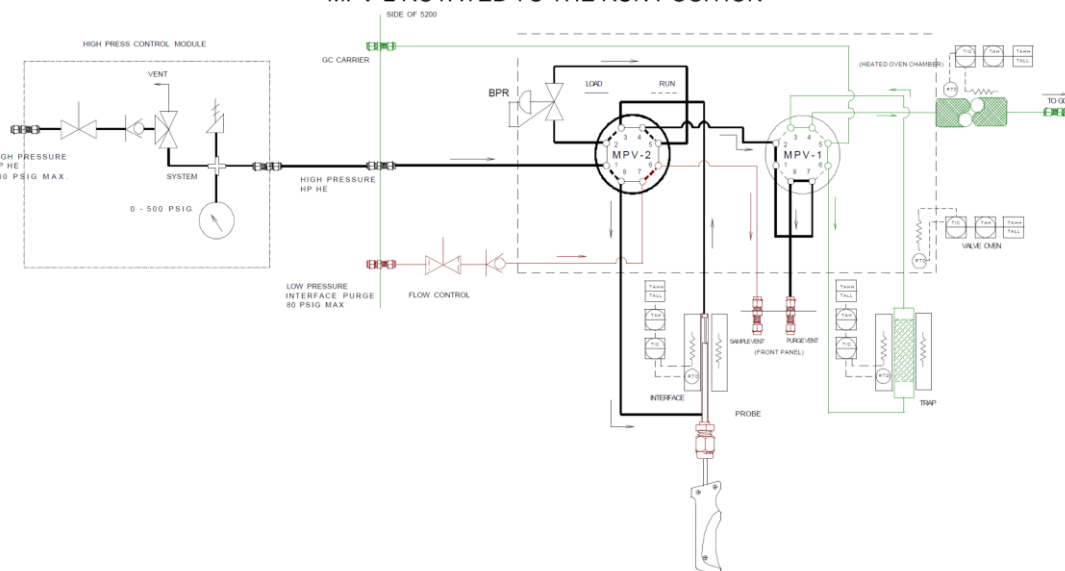


Figure A. 2 Schematic of the CDS pyroprobe 5200 high pressure reactor during the running phase.

MODEL 5200/ HIGH PRESS SAMPLING

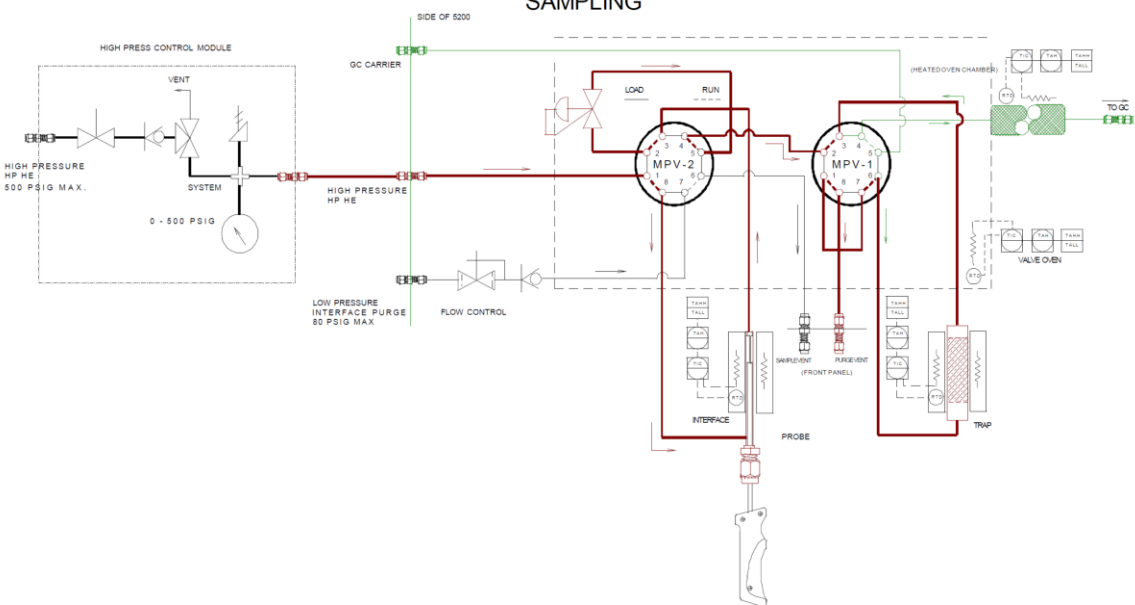


Figure A. 3 Schematic of the CDS pyroprobe 5200 high pressure reactor during the sampling phase.

Appendix B Supplementary information for Chapter 3

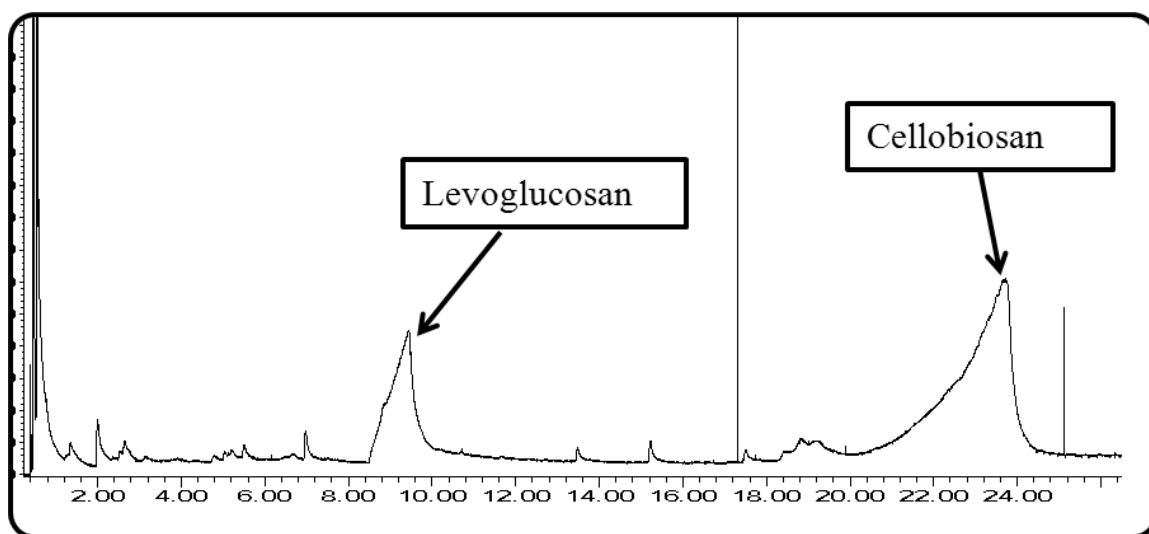


Figure B. 1 GC chromatogram (Signal: FID) for direct injection of cellobiosan solution in water, with column 4, showing peaks for cellobiosan and levoglucosan.

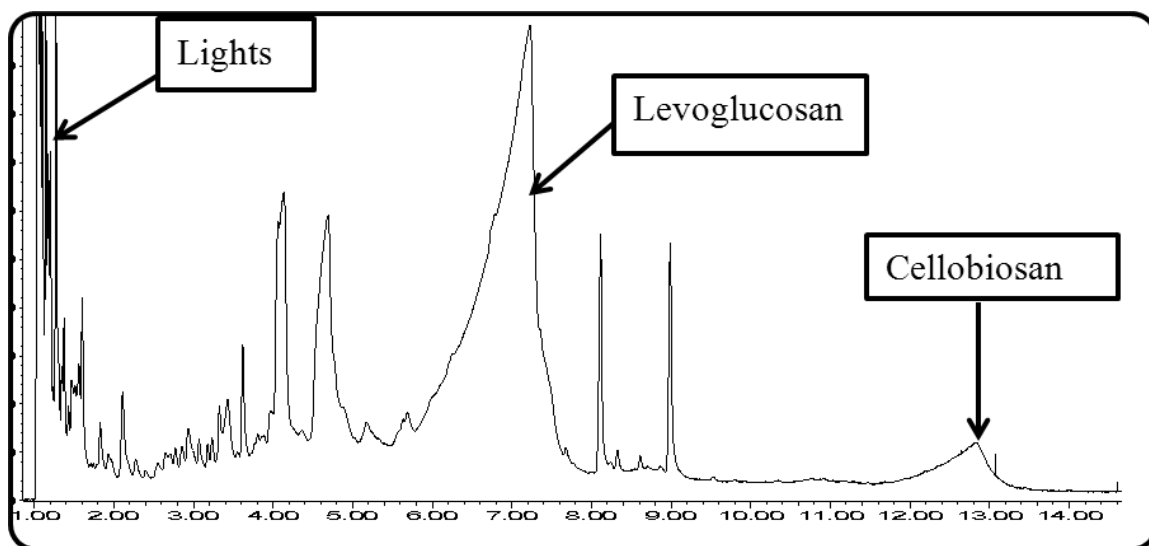


Figure B. 2 GC chromatogram (Signal: FID) for analysis of cellulose pyrolysis products, with column 4, showing peaks for cellobiosan (minor), and levoglucosan. The lights were not resolved completely as shown by amalgamation of peaks in the initial (1-2 mins) part of the chromatogram. Cellulose pyrolysis conditions were, 500°C temperature, and the vapor phase residence time was ~0.5s.

Appendix C Supplementary information for Chapter 4

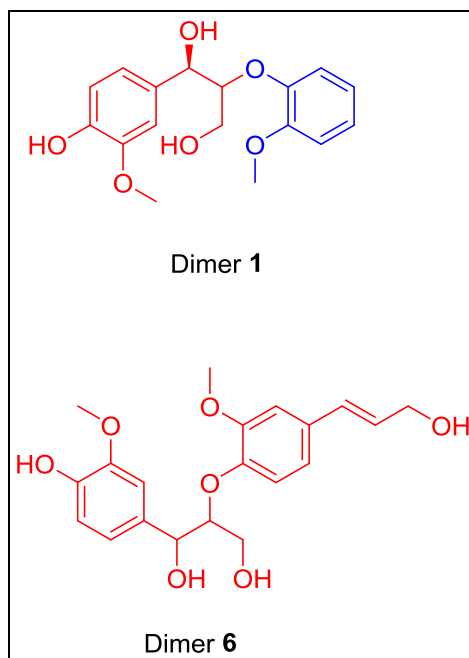


Figure C. 1 Structure of lignin model compound Dimer 1 and predicted lignin fragment Dimer 6.

Table C. 1 Predicted boiling point of the lignin model compounds – aim to show the relative volatility of the model compounds. Boiling point predicted via Joback fragmentation method modified by S.E. Stein.¹⁹²

Lignin Model compound	°C
Dimer 1	469
Trimer 2	693
Tetramer 3	917
Trimer 4	804
Dimer 6	551

Table C. 2 Weight percentage of monomeric species based on the number of carbon atoms in the molecule.

Compounds	Dimer 1	Trimer 2	Tetramer 3	Trimer 4	Polymer 5
C ₇ -C ₉ monomers	10.7	10.7	13.2	13.8	14.7
C ₁₀ monomers	89.3	89.3	86.8	86.2	85.3

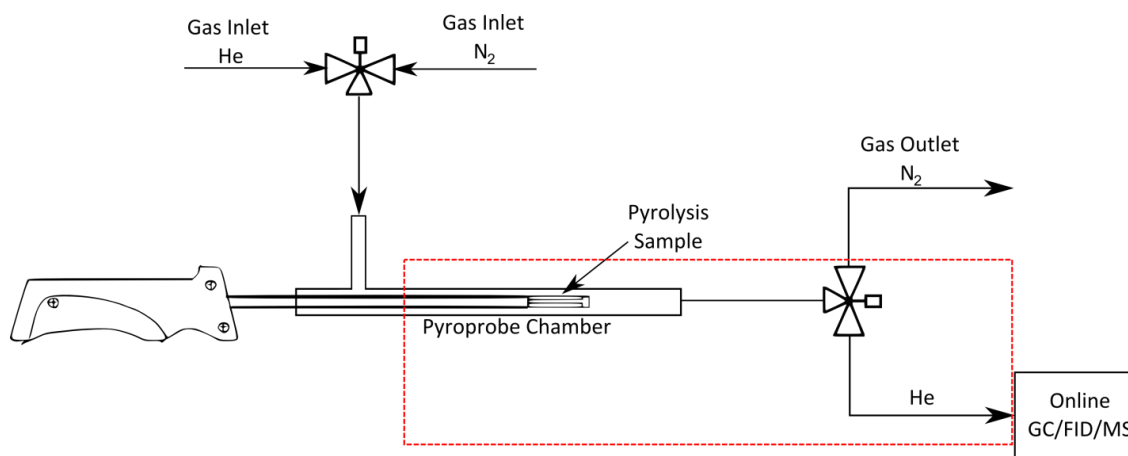


Figure C. 2 Schematic of experimental setup (Py-GC/MS) for pyrolysis studies with Lignin model compounds. Red box indicates the heated zone ($T=300^{\circ}\text{C}$).

Table C. 3 Elution time for dimer 1 for each of the different columns tested.

Column #	Solid phase volume / mm^3	Dimer 1 elution time / min
Column 1	37.4	35.0
Column 2	3.8	40.0
Column 4	0.3	23.0

Table C. 4 Quantified lumped pyrolysis product distribution from coniferyl alcohol in wt% of the reactant.

	Wt% of starting model compound
Lights	3.1
Monomers	58.5
Other Dimers	27.3
Char	10.0
Total	98.9

Estimation of Lights, CO, and CO₂

It was not possible to estimate CO and CO₂, since it was not detected in the FID. The column used for analysis of lignin pyrolysis products was a shortened HP-5ms column and as a result was not suitable for separating the light molecules. As a consequence, it was not possible to achieve baseline separation for the peaks of formaldehyde, acetaldehyde and other minor lights which are expected from pyrolysis of the lignin model compounds. Additionally CO and CO₂ also eluted along with the broad lights peaks, however their contribution to the FID signal can be considered negligible since CO has a very low response factor and CO₂ cannot be detected. Additionally, in the mass spectrometer, the major ion fragments from CO₂ and acetaldehyde overlap making it difficult to estimate CO₂ by calibrating the m/z 44 signal in the mass spectrometer for CO₂. Preliminary estimations from m/z 44 and m/z 28, however, indicate no more than 1% of the contribution from CO and CO₂.

Estimation of Water

Estimation of water was performed taking into account the amount of oxygen lost from the monomeric species (depending the structures identified) as compared to their precursors in the model compound. For polymer **5** and trimer **4** it was estimated to be 4-5% depending on the residence time. For all other model compounds it was <4%.

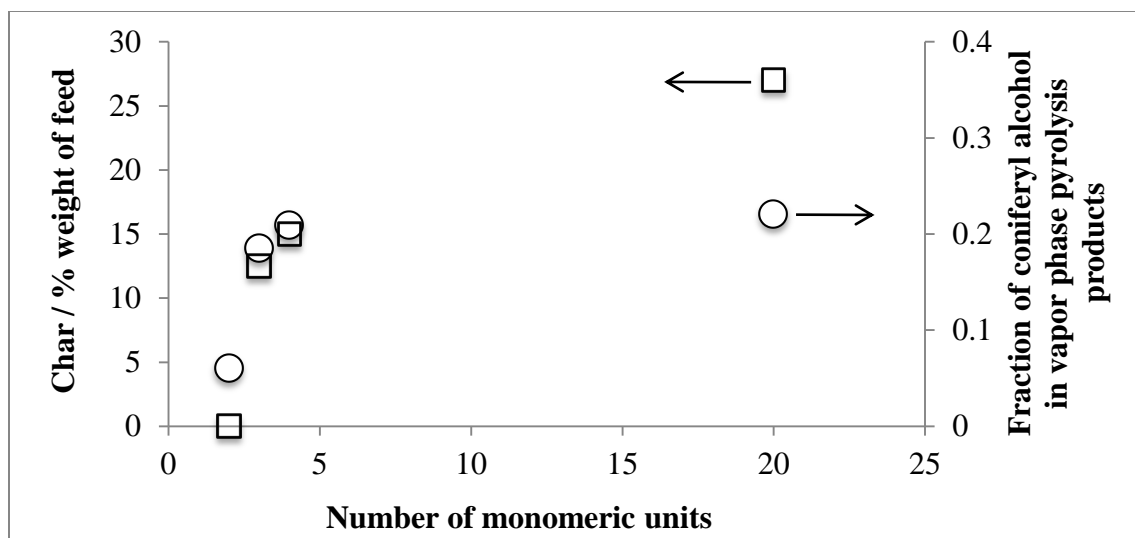


Figure C. 3 Char yield and coniferyl alcohol fraction in the vapor phase pyrolysis products as a function of the degree of polymerization of the lignin model compounds.

Figure C. 3 shows the char yield and the coniferyl alcohol fraction in vapor phase pyrolysis products as a function of the degree of polymerization. Coniferyl alcohol was used since it was the most abundant monomeric species bearing a $C\alpha=C\beta$ bond, however it was not the only compound with a $C\alpha=C\beta$ bond in the product distribution. Other species having $C\alpha=C\beta$ bonds are expected to be a part of the dimer fraction (i.e. dimer **6**), but they could not be identified due to experimental limitations. These species are expected to be a part of polymer **5** to a greater extent as compared to model compounds **1-3** due to nature of end group, and hence a higher proportion of aromatic rings with alkyl substituents. It should be kept in mind that although $C\alpha=C\beta$ bond bearing molecules have been shown to be prone to char formation via condensation reactions, it is not the only factor contributing to char formation. The fact that coniferyl alcohol pyrolysis produced less char than tetramer **3**, trimer **4**, and polymer **5** also indicated presence of other contributing factors which have been mentioned previously.

Table C. 5 Quantified pyrolysis product distribution from dimer **1** as a function of the vapor phase residence time in wt% of the reactant.

Residence time / s	0.5	1.6	3.1
Lights	2.5	2.6	3.3
Monomers	26.6	41.2	51.5
Dimer	61.3	43.9	23.5
Other Dimers	7.6	10.3	16.9
Char	n.d	n.d	n.d
Total	98.0	98.1	95.2

Table C. 6 Quantified pyrolysis product distribution from polymer **5** as a function of the vapor phase residence time in wt% of the reactant.

Residence time / s	0.5	1.6
Lights	7.5	7.7
Monomers	40.1	46.9
Other Dimers	18.8	13.5
Char	26.0	24.3
Total	92.4	92.5
Water *	4.1	4.92
Total	96.5	97.4

* Water is estimated based on the total moles of oxygen lost from the observed monomeric species

Appendix D Supplementary information for Chapter 5

Table D. 1 Yield of products from the model compounds 4-isopropylcyclohexanol and 4-propylcyclohexanone over the 2.46%Mo/MWCNT catalyst at 300 °C and 350 PSIG hydrogen total pressure in the high-pressure pulse reactor.

Products	Model Compounds	
	4-Isopropylcyclohexanol	4-propylcyclohexanone
(Iso/n)propylcyclohexane	90.6	89.4
(Iso/n)propylbenzene	3.3	2.9
(Iso/n)propylcyclohexene	3.4	3.9
Methyl- (iso/n)propylcyclopentane	0.6	0.3
4-(iso/n)propylcyclohexanol	0.4	3.1
4-(iso/n)propylcyclohexanone	0.2	0.4
Other Products	1.5	0.1

Table D. 2 Yield of products from the model compounds 4-isopropylcyclohexanol and 4-propylcyclohexanone over the 2.46%Mo/MWCNT catalyst at 300 °C and 25 PSIG helium total pressure in the high-pressure pulse reactor.

Products	Model Compounds	
	4-Isopropylcyclohexanol	4-propylcyclohexanone
(Iso/n)propylcyclohexane	0.7	0.1
(Iso/n)propylbenzene	2.9	0.4
(Iso/n)propylcyclohexene	91.0	2.0
Methyl-(iso/n)propyl cyclopentane	1.2	0.0
4-(iso/n)propylcyclohexanol	0.3	0.2
4-(iso/n)propylcyclohexanone	3.1	97.0
Other Products	0.9	0.3

Appendix E Supplementary information for Chapter 6

Table E. 1 Compositional analysis of the biomass feedstocks, % wt (dry basis).

	Poplar	Pine	Maize
Cellulose	44.5	39.5	36.0
Xylan	14	6.9	25.1
Arabinan	0.2	-	1.6
Galactan	1.1	2.5	0.6
Mannan	2.6	14.5	0.3
Hemicellulose (total)	17.9	23.9	29.7
Lignin	26.3	31.3	30.4
Extractives	3.1	4.4	-
Acetate	3.6	1.5	-
Total	95.4	100.5	96.1

Table E. 2 Ultimate and proximate analysis of cellulose and biomass feedstocks.

Ultimate analysis	Poplar	Pine	Maize	Cellulose
Carbon / %wt (dry)	50.72	52.23	49.42	44.7
Hydrogen / %wt (dry)	5.88	6.19	5.5	6.31
Nitrogen / %wt (dry)	0.14	0.17	1.04	0.19
Sulfur / %wt (dry)	<0.01	<0.01	0.08	<0.01
Ash / %wt (dry)	1.89	0.39	2.83	0.04
Oxygen / %wt (dry), by difference	41.37	41.01	40.78	48.76
Proximate analysis	Poplar	Pine	Maize	Cellulose
Moisture / %wt as used	3.32	n/a	4.16	0.94
Volatile matter / %wt (dry)	88.63	84.84	78.4	98.24
Fixed carbon / %wt (dry)	9.48	14.77	14.73	1.72
HHV /BTU lb-1	8153	8713.99	7417	6963

Table E. 3 Hydrocarbon products observed within the each hydrocarbon fraction classified on the basis of number of carbon atoms per molecule.

Groups	Identified Products
C₁	Methane
C₂	Ethane
C₃	Propane
C₄	Butane, Isobutane
C₅	Cyclopentane, 2-Methylbutane, n-Pentane
C₆	Methylcyclopentane, Cyclohexane, 2-Methylpentane, 3-Methylpentane, Hexane, Benzene
C₇*	Methylcyclohexane, Ethylcyclopentane, 3-Methylhexane (and isomers), Heptane, Toluene
C₈*	Ethyl cyclohexane, branched C ₈ alkanes, Octane, Ethyl benzene, Xylene
C₉*	Propyl cyclohexane, Nonane, Propyl benzene (and isomers)

*unidentified isomers of cycloalkanes and branched alkanes observed.

Table E. 4 Quantified pyrolysis product distribution from dimer **1** as a function of hydrogen pressure in wt% of the reactant.

Hydrogen pressure / bar	2.5	25
Lights	2.9	2.6
Monomeric species	41.6	45.7
Dimer 1	42.8	40.5
Other dimeric species	11.3	9.6
Char	0.0	0.0
Total	98.6	98.5

Table E. 5 Quantified pyrolysis product distribution from polymer **2** as a function of hydrogen pressure in wt% of the reactant.

Hydrogen pressure / bar	2.5	25
Lights	7.5	9.2
Monomeric species	40.1	40.8
Dimeric species	18.8	19.7
Char	26.0	25.0
Total	92.4	94.8

Table E. 6 Detailed product distribution from cellulose as a function of the Mo:Pt ratio of the catalysts tested quantified by carbon wt% of the reactant.

(Mo:Pt) ratio / mol Mo: mol Pt	(1:0)	(1:0.5)	(1:1)	(1:2)	(0:1)
Products yields / % carbon of feed					
Permanent gases					
CO	28.8	8.5	2.7	2.3	5.1
CO₂	3.3	n/a	0.5	n/a	n/a
Hydrocarbons					
C1	6.1	5.6	6.6	9.3	2.9
C2	3.3	11.8	11.2	11.3	10.9
C3	3.2	10.0	6.4	8.1	8.5
C4	3.9	10.8	7.3	7.8	8.3
C5	3.4	13.7	12.6	11.0	11.4
C6	2.2	12.7	22.9	21.3	27.1
C7	0.9	2.9	2.9	3.2	3.1
C8	0.7	2.6	2.6	2.6	3.0
C9	n.d.	1.9	1.6	1.4	2.2
C9+					
Char	18.5	18.0	17.0	17.0	16.0
Total	74.3	98.5	94.4	95.2	98.5
Hydrocarbons					
C1-C3 range	12.7	27.4	24.2	28.8	22.3
C4+ range	11.0	44.6	50.0	47.1	55.1
Total hydrocarbons	23.7	72.0	74.2	75.9	77.4

Table E. 7 Detailed product distribution from levoglucosan as a function of the Mo:Pt ratio of the catalysts tested quantified by carbon wt% of the reactant.

(Mo:Pt) ratio / mol Mo: mol Pt	(1:0)	(1:0.5)	(1:1)	(1:2)	(0:1)
Products yields / % carbon of feed					
Permanent gases					
CO	26.5	12.5	1.8	1.4	3.5
CO₂	1.3	n/a	0.4	n/a	n/a
Hydrocarbons					
C1	16.0	6.1	7.7	5.2	2.1
C2	4.6	14.5	9.2	9.5	7.1
C3	4.6	11.7	4.7	6.5	5.9
C4	7.6	13.7	7.0	7.1	8.7
C5	6.4	17.6	15.8	15.1	12.7
C6	3.6	18.0	47.1	46.6	52.4
C7	n/a	1.7	0.9	2.3	0.9
C8	n/a	1.6	0.8	1.7	1.0
C9	n/a	1.5	0.5	0.6	0.7
C9+					
Char	n.d	n.d	n.d	n.d	n.d
Total	70.7	99.0	95.9	96.1	95.1
Hydrocarbons					
C1-C3 range	25.3	32.3	21.7	21.2	15.2
C4+ range	17.7	54.1	72.1	73.5	76.4
Total hydrocarbons	43.0	86.5	93.7	94.7	91.7

Table E. 8 CO uptake results obtained via chemisorption of the Pt-Mo series of bimetallic catalysts as a function of the Mo:Pt ratio.

Catalyst	Mo:Pt ratio / moles:moles	CO uptake / $\mu\text{mol g}^{-1}$
5%Pt/MWCNT	0	55.4
5%Pt 1.2%Mo/MWCNT	0.5	49
5%Pt 2.5%Mo/MWCNT	1	21.1
2.5%Pt 2.5%Mo/MWCNT	2	8.2
2.5%Mo/MWCNT	∞	0

Table E. 9 Detailed product distribution from cellulose as a function of the hydrogen pressure of the catalysts tested quantified by carbon wt% of the reactant.

Hydrogen pressure / bar	25	7	2.4	1
Products yields / % carbon of feed				
Permanent gases				
CO	2.7	8.2	13.7	15.2
CO₂	0.5	1.1	2.4	7.7
Hydrocarbons				
C1	6.6	3.5	2.1	2.3
C2	11.2	9.7	7.5	12.5
C3	6.4	5.8	9.4	6.5
C4	7.3	8.0	11.5	10.3
C5	12.6	14.9	15.9	13.6
C6	22.9	19.6	14.4	10.1
C7	2.9	2.8	1.4	1.8
C8	2.6	2.5	0.9	0.4
C9	1.6	1.8	0.6	0.1
C9+	n.d	n.d	n.d	n.d
Char	17.0	16.0	16.5	16.5
Total	94.4	94.0	96.3	97.1
Hydrocarbons				
C1-C3 range	24.2	19.0	19.1	21.3
C4+ range	50.0	49.7	44.7	36.3
Total hydrocarbons	74.2	68.7	63.8	57.6
Aromatic hydrocarbons				
C6	n.d	0.20	1.05	1.69
C7	n.d	n.d	0.48	0.86
C8	n.d	n.d	0.18	0.04
C9	n.d	n.d	0.12	0.01
Total aromatic hydrocarbons	0.0	0.2	1.8	2.6

Table E. 10 Detailed product distribution from levoglucosan as a function of the hydrogen pressure of the catalysts tested quantified by carbon wt% of the reactant.

Hydrogen pressure / bar	25	7	2.4	1
Products yields / % carbon of feed				
Permanent gases				
CO	1.8	6.0	10.0	17.5
CO₂	0.4	0.8	1.7	2.2
Hydrocarbons				
C1	6.6	3.8	1.9	20.7*
C2	9.2	10.3	9.1	0.0
C3	4.7	4.7	7.9	0.0
C4	7.0	10.7	15.0	16.6
C5	15.8	22.9	24.6	21.7
C6	47.1	36.5	24.7	15.8
C7	0.9	1.4	0.8	0.4
C8	0.8	1.1	0.3	0.1
C9	0.5	0.5	0.1	n.d
C9+	n.d	n.d	n.d	n.d
Char	n.d	n.d	n.d	n.d
Total	94.8	98.8	96.0	94.9
Hydrocarbons				
C1-C3 range	20.6	18.9	18.9	20.7
C4+ range	72.1	73.1	65.5	54.5
Total hydrocarbons	92.6	92.0	84.3	75.2
Aromatic hydrocarbons				
C6	n.d	0.1	1.2	1.6
C7	n.d	0.2	0.2	0.2
C8	n.d	n.d	n.d	n.d
C9	n.d	n.d	n.d	n.d
Total aromatic hydrocarbons	0.0	0.3	1.4	1.8

* Includes C₁-C₃ product distribution, which could not be resolved into individual fractions.

Table E. 11 Detailed product distribution from xylan as a function of the hydrogen pressure of the catalysts tested quantified by carbon wt% of the reactant.

Hydrogen pressure / bar	25	1
Products yields / % carbon of feed		
Permanent gases		
CO	7.1	18.0
CO₂	1.4	7.5
Hydrocarbons		
C1	7.3	2.8
C2	9.9	12.4
C3	10.9	9.2
C4	9.6	11.0
C5	22.5	14.0
C6	7.7	4.4
C7	3.2	2.5
C8	2.8	1.3
C9	2.2	0.3
C9+	1.8	n.d
Char	18.0	17.0
Total	104.5	100.3
Hydrocarbons		
C1-C3 range	28.1	24.4
C4+ range	49.9	33.4
Total hydrocarbons	78.0	57.8
Aromatic hydrocarbons		
C6	n.d	1.2
C7	n.d	0.8
C8	n.d	0.3
C9	n.d	0.0
Total aromatic hydrocarbons	0.0	2.3

Table E. 12 Detailed product distribution from dimer **1** as a function of the hydrogen pressure of the catalysts tested quantified by carbon wt% of the reactant.

Hydrogen pressure / bar	25	7	1
Products yields / % carbon of feed			
Permanent gases			
CO	0.6	3.1	6.3
CO₂	n/a	0.5	1.2
Hydrocarbons			
C1	15.7	13.3	9.8
C2	0.0	0.4	0.5
C3	0.0	0.1	0.1
C4	0.0	0.1	0.6
C5	0.0	0.7	1.2
C6	36.1	35.9	36.0
C7	6.4	8.8	11.0
C8	20.0	22.4	20.2
C9	18.5	12.7	10.0
C9+	1.2	0.2	0.2
Char	n.d	n.d	n.d
Total	98.4	98.1	97.4
Hydrocarbons			
C1-C3 range	15.7	13.8	10.5
C4+ range	82.1	80.7	79.3
Total hydrocarbons	97.8	94.5	89.8
Aromatic hydrocarbons			
C6	n.d	1.7	28.9
C7	n.d	0.9	9.9
C8	n.d	2.0	18.6
C9	n.d	1.2	9.4
Total aromatic hydrocarbons	0.0	5.7	66.8

Table E. 13 Detailed product distribution from polymer **2** as a function of the hydrogen pressure of the catalysts tested quantified by carbon wt% of the reactant.

Hydrogen pressure / bar	25	7	1
Products yields / % carbon of feed			
Permanent gases			
CO	1.6	3.8	6.4
CO₂	0.3	1.5	3.3
Hydrocarbons			
C1	12.0	9.5	7.8
C2	0.0	1.1	1.0
C3	0.0	0.1	0.1
C4	2.2	0.1	0.1
C5	0.0	1.0	0.8
C6	5.5	8.4	13.0
C7	10.3	11.4	10.8
C8	13.6	17.1	13.8
C9	14.3	9.8	7.7
C9+	2.2	0.4	0.6
Char	32.0	31.2	30.2
Total	94.0	95.3	95.7
Hydrocarbons			
C1-C3 range	12.0	10.7	8.9
C4+ range	48.2	48.2	47.0
Total hydrocarbons	60.2	58.9	55.9
Aromatic hydrocarbons			
C6	n.d	0.4	10.1
C7	n.d	0.9	9.6
C8	n.d	2.4	12.6
C9	n.d	1.2	7.2
Total aromatic hydrocarbons	0.0	4.9	39.5

Table E. 14 Detailed product distribution from poplar as a function of the hydrogen pressure of the catalysts tested quantified by carbon wt% of the reactant.

Hydrogen pressure / bar	25	2.4	1
Products yields / % carbon of feed			
Permanent gases			
CO	1.8	9.9	13.7
CO₂	n/a	4.2	7.9
Hydrocarbons			
C1	13.8	3.6	3.5
C2	8.2	7.9	8.5
C3	4.7	6.2	6.0
C4	3.3	5.9	4.9
C5	3.5	6.5	5.9
C6	6.0	6.7	5.9
C7	7.1	6.3	5.7
C8	11.3	6.4	4.5
C9	9.8	4.5	3.5
C9+	3.4	2.3	1.0
Char	26.0	28.0	26.5
Total	99.1	98.5	97.4
Hydrocarbons			
C1-C3 range	26.8	17.7	18.0
C4+ range	44.4	38.7	31.3
Total hydrocarbons	71.3	56.3	49.2
Aromatic hydrocarbons			
C6	n.d	1.6	2.8
C7	n.d	3.3	4.4
C8	n.d	3.9	3.6
C9	n.d	2.4	3.2
Total aromatic hydrocarbons	0.0	11.2	14.0

Table E. 15 Detailed product distribution from pine as a function of the hydrogen pressure of the catalysts tested quantified by carbon wt% of the reactant.

Hydrogen pressure / bar	25	7	2.4	1
Products yields / % carbon of feed				
Permanent gases				
CO	4.0	5.9	8.0	14.5
CO₂	n/a	2.0	3.9	6.9
Hydrocarbons				
C1	11.6	5.3	4.0	3.2
C2	8.9	6.8	7.8	8.1
C3	6.4	5.2	7.7	5.4
C4	4.4	4.9	6.8	5.5
C5	4.9	6.0	8.2	7.2
C6	8.0	7.3	7.7	6.6
C7	6.8	6.3	7.6	6.1
C8	6.9	7.8	5.1	4.8
C9	6.8	4.9	2.5	3.5
C9+	4.1	4.7	1.3	1.4
Char	25.5	30.0	26.0	27.2
Total	98.3	97.1	96.5	100.3
Hydrocarbons				
C1-C3 range	26.9	17.3	19.5	16.7
C4+ range	42.0	41.9	39.1	35.0
Total hydrocarbons	68.8	59.2	58.6	51.7
Aromatic hydrocarbons				
C6	n.d	0.2	1.7	2.2
C7	n.d	0.7	4.7	4.4
C8	n.d	1.8	3.2	3.7
C9	n.d	0.6	1.4	2.9
Total aromatic hydrocarbons	0.0	3.2	11.0	13.1

Table E. 16 Detailed product distribution from maize as a function of the hydrogen pressure of the catalysts tested quantified by carbon wt% of the reactant.

Hydrogen pressure / bar	25	7	2.4	1
Products yields / % carbon of feed				
Permanent gases				
CO	2.2	5.9	8.9	12.2
CO₂	n/a	3.9	6.2	10.9
Hydrocarbons				
C1	10.0	3.5	3.6	3.3
C2	6.0	7.4	7.8	8.1
C3	4.4	5.1	7.0	6.0
C4	3.3	4.0	6.3	5.1
C5	3.2	5.6	6.7	6.0
C6	4.5	7.4	6.3	5.6
C7	6.4	7.1	5.7	5.1
C8	13.1	10.3	6.7	5.1
C9	9.7	4.6	2.6	2.0
C9+	3.4	3.6	1.5	1.0
Char	31.5	30.0	32.0	29.5
Total	97.7	98.3	101.4	99.9
Hydrocarbons				
C1-C3 range	20.3	16.0	18.4	17.4
C4+ range	43.7	42.6	35.9	29.8
Total hydrocarbons	64.0	58.5	54.3	47.3
Aromatic hydrocarbons				
C6	n.d	0.4	1.4	2.0
C7	n.d	0.6	2.9	3.5
C8	n.d	1.5	4.2	3.8
C9	n.d	0.4	1.1	1.2
Total aromatic hydrocarbons	0.0	3.0	9.7	10.5

Table E. 17 Percent of Pt monometallic, PtMo coordinated particles, and PtMo alloy particles as determined via STEM-EELS line-scans as a function of the Mo:Pt ratio (1:0.5, 1:1, and 1:2) for the series of PtMo /MWCNT catalysts.¹⁴⁶

	Pt Only	Pt-Mo Coordinated	Pt-Mo Alloy	Total Pt-Mo bimetallic particles
	Percentage of Total Particles / %			
5% Pt/MWCNT	100.0	0	0	0
5%Pt 1.2%Mo/MWCNT	50.0	45.0	5.0	50.0
5%Pt 2.5%Mo/MWCNT	22.9	54.3	22.9	77.4
2.5%Pt 2.5%Mo/MWCNT	25.0	60.0	15.0	75.0

Table E. 18 XPS Binding Energies and Component Percents for the Pt, Mo and PtMo catalysts.¹⁴⁶

Component	BE / eV					Mo Component Percent			
	Mo ⁶⁺		Mo ⁴⁺		Pt	Mo ⁶⁺		Mo ⁴⁺	
	3d _{5/2}	3d _{5/2}	3d _{5/2}	3d _{5/2}	4f _{7/2}	3d _{5/2}	3d _{5/2}	3d _{5/2}	3d _{5/2}
5%Pt/MWCNT	--	--	--	--	71.4	--	--	--	--
5%Pt 1.2%Mo/MWCNT	232.5	230.2	228.9	228.3	71.7	20	24	27	29
5%Pt 2.5%Mo/MWCNT	232.6	230.6	229.0	228.3	71.8	18	18	38	26
2.5%Pt 2.5%Mo/MWCNT	232.6	230.6	228.8	228.2	71.8	16	15	45	24
2%Pt 5%Mo/MWCNT	232.3	230.0	228.9	228.2	71.8	25	17	41	17
2.5%Mo/MWCNT	232.4	230.0	229.0	228.2	--	26	26	43	5

Table E. 19 Detailed product distribution from cellulose quantified by carbon wt% of the reactant.

Catalyst	5%Pt2.5%Mo/ MWCNT	5%Pt/MWCNT, Mo/MWCNT physical mixture
Products yields / % carbon of feed		
Permanent gases		
CO	2.7	6.6
CO ₂	0.5	2.7
Hydrocarbons		
C1	6.6	4.4
C2	11.2	11.6
C3	6.4	13.4
C4	7.3	9.8
C5	12.6	11.9
C6	22.9	11.5
C7	2.9	3.2
C8	2.6	3.7
C9	1.6	2.0
C9+		
Char	17.0	16.0
Total	94.4	96.7
Hydrocarbons		
C1-C3 range	24.2	29.4
C4+ range	50.0	42.1
Total hydrocarbons	74.2	71.5

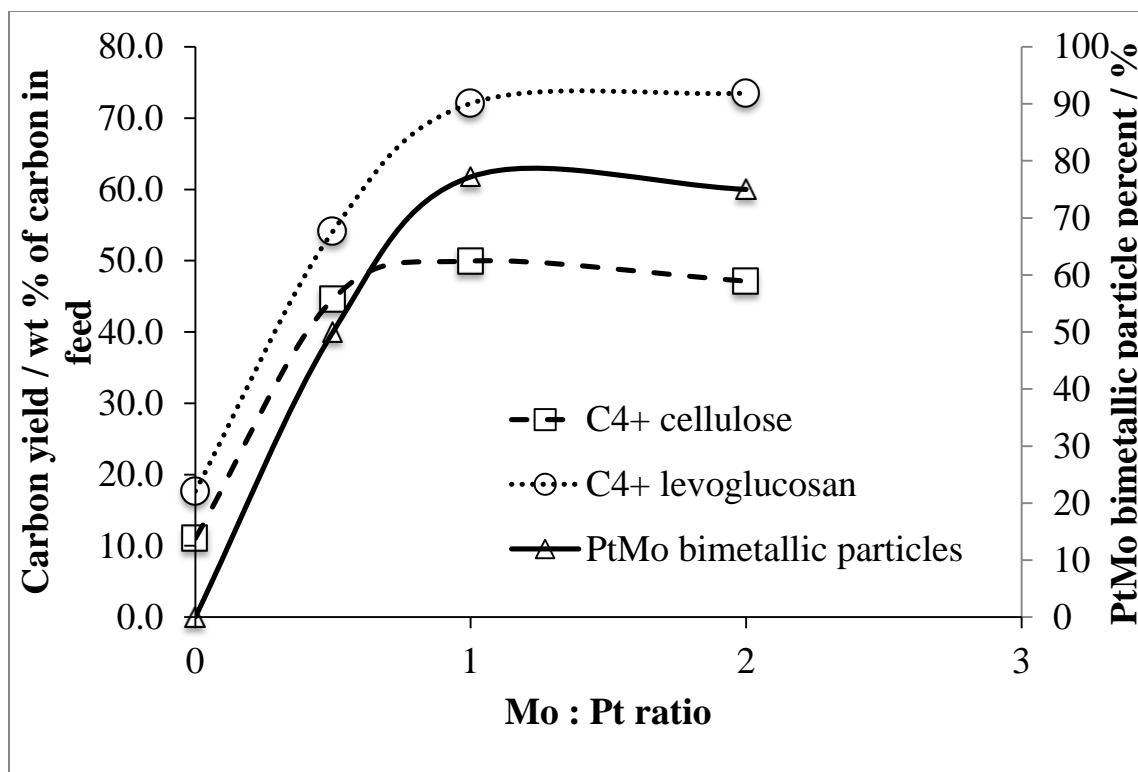


Figure E. 1 Percentage carbon yield of liquid fuel range hydrocarbon fraction (C_{4+}) from hydrodeoxygenation of cellulose pyrolysis products and levoglucosan as a function of the Mo:Pt ratio. (squares) cellulose, (circles) levoglucosan. (Triangles) Percent of PtMo bimetallic particles as determined via STEM-EELS line-scans as a function of the Mo:Pt ratio (1:0.5, 1:1, and 1:2) for the series of PtMo /MWNCT catalysts.

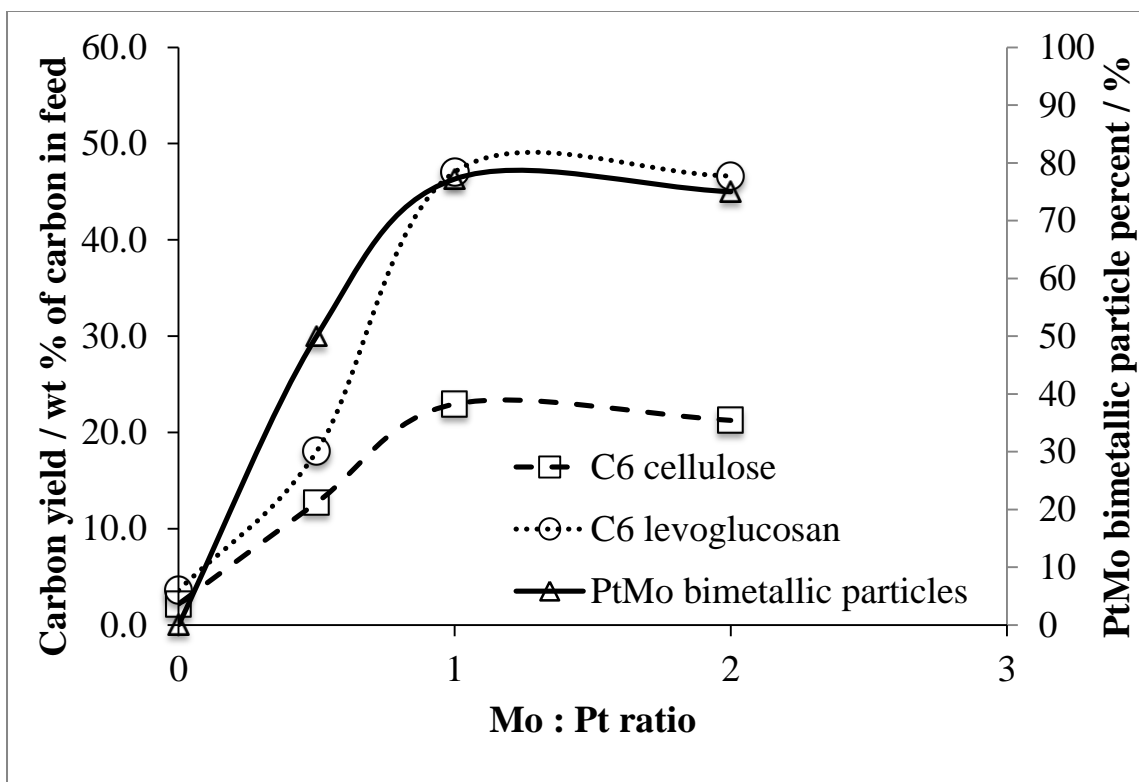


Figure E. 2 Percentage carbon yield of C₆ hydrocarbon fraction from hydrodeoxygenation of cellulose pyrolysis products and levoglucosan as a function of the Mo:Pt ratio. (squares) cellulose, (circles) levoglucosan. (Triangles) Percent of PtMo bimetallic particles as determined via STEM-EELS line-scans as a function of the Mo:Pt ratio (1:0.5, 1:1, and 1:2) for the series of PtMo /MWNCT catalysts.

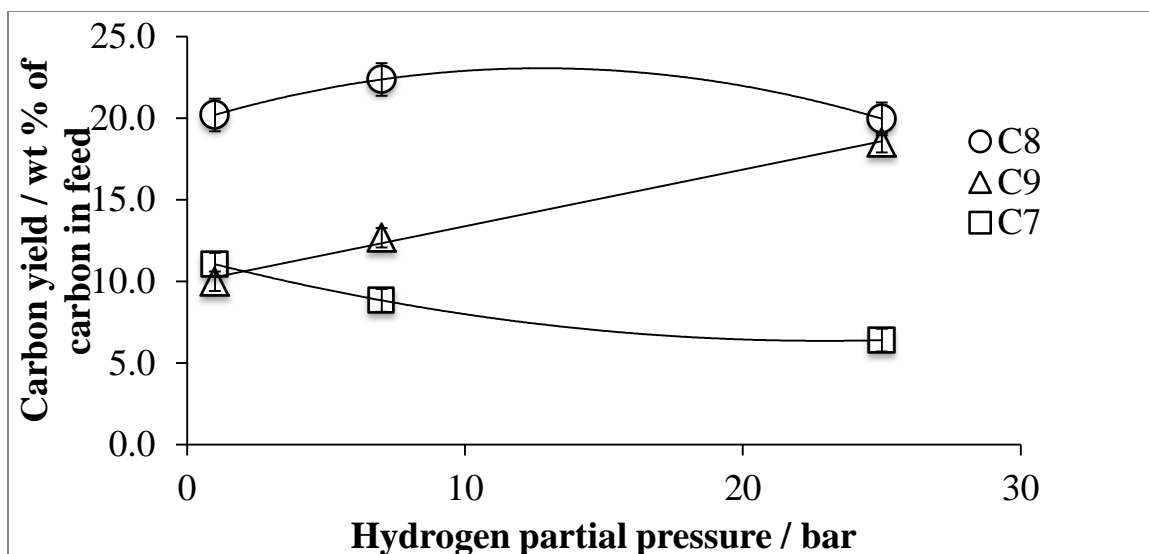


Figure E. 3 Percentage carbon yield of product fractions from hydrodeoxygenation of fast hydropyrolysis products of lignin model compound, dimer **1** as a function of the hydrogen pressure over the 5%Pt2.5%Mo/MWCNT catalyst. (squares) C₇ hydrocarbon fraction, (circles) C₈ hydrocarbon fraction, and (triangles) C₉ hydrocarbon fraction.

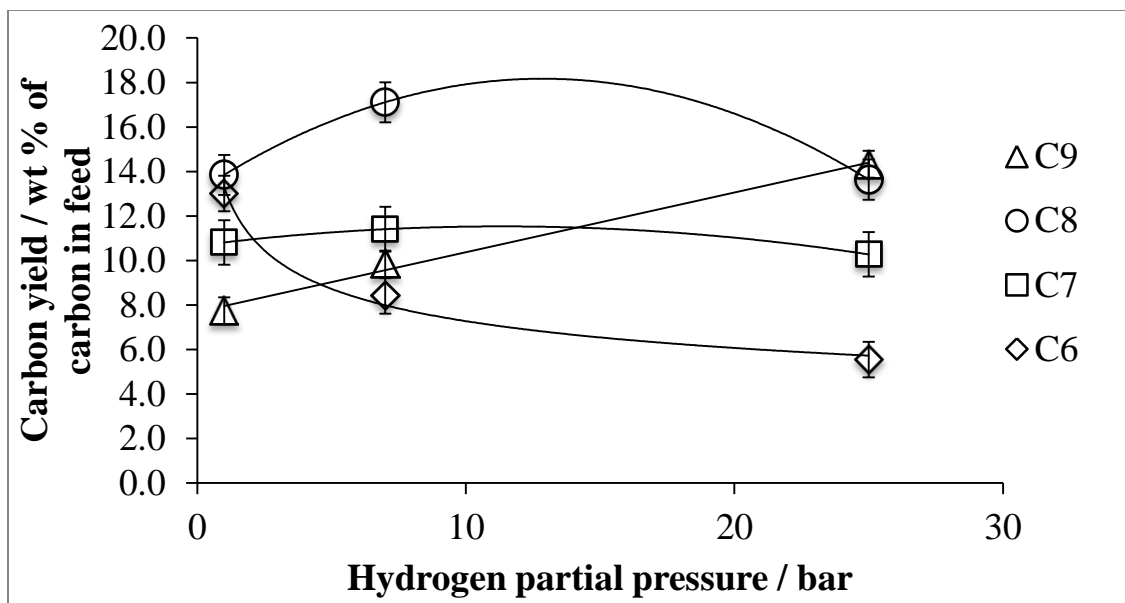


Figure E. 4 Percentage carbon yield of product fractions from hydrodeoxygenation of fast hydropyrolysis products of lignin model compound, polymer **2** as a function of the hydrogen pressure over the 5%Pt2.5%Mo/MWCNT catalyst. (diamonds) C₆ hydrocarbon fraction, (squares) C₇ hydrocarbon fraction, (circles) C₈ hydrocarbon fraction, and (triangles) C₉ hydrocarbon fraction.

Table E. 20 Equilibrium ratio of aldehyde to alcohol at 300°C at two different hydrogen partial pressure conditions as estimated by ASPEN.

Hydrogen pressure		25 bar	1 bar
Aldehyde	Alcohol	Equilibrium molar ratio aldehyde : alcohol	
Ethanal	Ethanol	1.1E-04	1.8E+00
Propanal	1-propanol	3.1E-05	4.9E-01
butanal	1-butanol	3.0E-05	4.7E-01

Table E. 21 Percentage contribution of different types of alkanes based on the structure towards the total hydrocarbon product distribution from fast hydrolysis and catalytic hydrodeoxygenation of cellulose and lignin polymer 2 at 1 bar hydrogen partial pressure and 300°C.

Feed	Percentage of total hydrocarbons observed / %	
	Cellulose	Lignin Polymer 2
Aliphatic alkanes	83	20
C ₁ -C ₄	55	17
C ₅ -C ₁₀	28	3*
Cycloalkanes +	17	80*
Aromatics		

*From Table E. 21, 80% of the hydrocarbons from lignin polymer 2 were cycloalkanes and aromatic hydrocarbons along with of the 20% aliphatic hydrocarbons, 17% of which were in the C₁-C₄ range and were obtained from methoxy group deoxygenation as well as C-C scission of the alkyl side chain. Therefore, if we were to look at the C₆₊ range of hydrocarbons from polymer 2, >95% are cyclic hydrocarbons bearing C₆ rings. This shows that there was a small degree of ring opening activity over the catalyst and majority of the C₆ rings maintained their structure. The alkyl side chain on the aromatic rings was however subjected to C-C scission.

VITA

VITA

Harshavardhan Choudhari

Purdue University

Education

Bachelor of Chemical Engineering, Institute of Chemical Technology, Mumbai, India.
May 2009

Doctor of Philosophy, Chemical Engineering, Purdue University, West Lafayette, IN.
August 2015.

Experience**Graduate Research**

- Kinetic studies - hydrodeoxygenation of lignin model compounds over Pt based catalysts at elevated hydrogen pressure (range 1-25 bar) in a continuous steady state fixed bed reactor.
- Identification of reaction pathways and active sites over Pt based bimetallic catalysts for biomass model compounds with high pressure (25 bar) pulse studies.
- Identified candidate catalysts with ~50% biomass carbon recovery to C4+ hydrocarbons (fuel grade molecules) via catalyst hydrodeoxygenation of biomass (and cellulose) pyrolysis vapors.
- Developed rapid catalyst screening capability for high pressure hydrodeoxygenation of biomass pyrolysis products and model compounds for conversion to fuel range molecules.
- Developed a novel method for online vapor phase analysis of fast-hydrolysis products in a GC-MS from a high pressure semi-batch reactor, leading to enhanced mass balance.
- Residence time studies of fast hydrolysis products of cellulose and lignin oligomers to gain insight into the mechanistic aspects of biomass fast hydrolysis.

- Studied biomass pyrolysis product distribution as a function of structural composition of the genetically modified biomass (collaboration with plant biologists). Identified descriptors linking products to the structural features of lignin polymer.

Internship

Summer Intern, NOCIL Rubber Chemicals Ltd, Navi Mumbai, India. 2008

Generated VLE data for cyclohexylamine-water system using the NRTL and UNIQUAC methods. Designed a distillation column for the separation of cyclohexylamine from water.

Teaching

Teaching assistantship, Fall 2010 and Spring 2012

ChE 434: Chemical Engineering Laboratory I – Trained and advised students in design of experiments, data analysis, data interpretation and safe lab practices.

ChE 348: Chemical Reaction Engineering – Teaching experience was obtained through recitation sessions and lab sessions, also conducted office hours and graded examinations.

Conference Presentations and Posters

H. J. Choudhari, W. N. Delgass, F. H. Ribeiro, R. Agrawal, 2013, AIChE annual meeting, “*Fast Hydropyrolysis and Catalytic Hydrodeoxygenation of Cellulose in a Micro-Scale Batch Reactor*”, San Francisco, CA.

H. J. Choudhari, D. D. Mehta, W. N. Delgass, F. H. Ribeiro, R. Agrawal, 2014, Catalysis Club of Chicago Spring Symposium, “*Fast Hydropyrolysis and Catalytic Hydrodeoxygenation of Biomass in a Micro-Scale Batch Reactor*”, Naperville, IL.

H. J. Choudhari, D. D. Mehta, W. N. Delgass, F. H. Ribeiro, R. Agrawal, 2014, Michigan Catalysis Society Spring Symposium, “*Selective C-O scission during hydrodeoxygenation of biomass pyrolysis vapors and model compounds over supported PtMo catalysts*”, Warren, MI.

H. J. Choudhari, S. Yohe, D. Mallapragada, P. Gawecki, P. Dietrich, V. Venkatakrishnan, D. Mehta, F. H. Ribeiro, W. N. Delgass, R. Agrawal, 2011, Graduate Research Symposium, “*Multidisciplinary Experimental Research for Converting Biomass to Liquid Fuel via Fast-hydropyrolysis and Hydrodeoxygenation*”, Purdue University, IN

Awards

- Outstanding Oral Presentation Award (3rd Place), 2014, Purdue GSO Symposium West Lafayette, IN.

- Outstanding Poster Presentation Award, 2014, Michigan Catalysis Society Spring Symposium Warren, MI.
- Ambuja's best design project/ home paper award for an undergraduate chemical engineering student by Indian Institute of Chemical Engineers (2009) for undergraduate design project (Manufacture of 1000 tons per year of 2,6-xylidine).
- Awarded the Eastman travel grant for conference travel in 2013.